Integrated Concept Development of
Next-Step Helical-Axis Advanced Stellarators

vorgelegt von

Felix Warmer

Master of Science in Physics, geboren in Leisnig, 1988

von der Fakultät II – Mathematik und Naturwissenschaften
der Technischen Universität Berlin
zur Erlangung des akademischen Grades

Doktor der Naturwissenschaften
– Dr. rer. nat. –

genehmigte Dissertation

Promotionsausschuss:

Vorsitzender: Prof. Dr. rer. nat. Holger Stark

Erster Gutachter: Prof. Dr. rer. nat. Dieter Breitschwerdt

Zweiter Gutachter: Prof. Dr. rer. nat. Robert Wolf

Dritter Gutachter: Prof. Dr. rer. nat. Hartmut Zohm

Tag der Wissenschaftlichen Aussprache: 13. April 2016

Berlin, 2016

Abstract

With the increasing energy demand of mankind and the transformation of our society towards sustainability, nuclear fusion by magnetic confinement is a promising option for the sustainable electricity supply in the future. In view of these prospects this thesis focuses on the concept development of next-step helical-axis advanced stellarator (HELIAS) burning-plasma devices. The HELIAS-line is the continued development of the prototype optimised stellarator Wendelstein 7-X which started operation in 2015. For the integrated concept development of such devices, the approach taken in this work encompasses detailed physics and engineering considerations while also including economic aspects.

Starting with physics considerations, the properties of plasma transport and confinement of 3D stellarator configurations are discussed due to their critical importance for the device design. It becomes clear that current empirical confinement time scalings are not sufficient to predict the confinement in future stellarator devices. Therefore, detailed 1D transport simulations are carried out to reduce the uncertainties regarding confinement. Beyond the well-validated neoclassical approach, first attempts are made to include results from state-of-the-art turbulence simulations into the 1D transport simulations to further enhance the predictive capabilities.

Next, for the systematic development of consistent design points, stellarator-specific models are developed and implemented in the well-established European systems code PROCESS. This allows a consistent description of an entire HELIAS fusion power plant including physics, engineering, and economic considerations. With the confidence obtained from a verification study, systems studies are for the first time applied for a HELIAS power-plant which shows that the available design window is constrained by the beta-limit. Furthermore, an economic comparison of an exemplary design point to an 'equivalent' tokamak shows that the total construction costs are of the same order for both concepts.

One main goal of this work – consolidating the aforementioned aspects – is the assessment of the physics and engineering dimensions of an intermediate-step burning-plasma stellarator which may be desired to mitigate development risks on the way to commercial fusion. Therefore, two boundary cases for such a device are presented. A small fast-track option using mostly today's technology and a technologically more sophisticated DEMO-like device. There is about a factor two difference in the construction costs between those two boundary cases.

Zusammenfassung

Im Hinblick auf den steigenden Energiebedarf der Menschheit und dem Wandel unserer Gesellschaft hin zu Nachhaltigkeit, erscheint die Energiegewinnung durch Kernfusion mittels magnetischen Einschluss eine vielversprechende Option für eine nachhaltige Energieversorgung in der Zukunft. Angesichts dieser Perspektiven konzentriert sich diese Arbeit auf die Konzept-Entwicklung zukunftsweisender, hochmoderner Stellaratoren mit helikaler Achse (HELIAS) und einem brennenden Plasma. Das HELIAS-Konzept ist die Weiterentwicklung des Prototyps Wendelstein 7-X, ein optimierter Stellarator, der 2015 in Betrieb gegangen ist. Zur Umsetzung einer integrierten Konzept-Entwicklung für solche Anlagen wird in dieser Arbeit auf einen Ansatz zurück gegriffen, welcher detaillierte physikalische und technische Überlegungen, aber auch ökonomische Aspekte, einschließt.

Ausgehend von Physik-Überlegungen werden Eigenschaften des Plasma-Transports und des Plasma-Einschlusses in 3D Stellarator Konfigurationen diskutiert, insbesondere aufgrund ihrer weitreichenden Bedeutung für den Entwurf solcher Anlagen. Es wird deutlich, dass die aktuellen empirischen Einschlusszeit-Skalierungen nicht ausreichen, um den Einschluss in zukünftigen Stellaratoren vorherzusagen. Aus diesem Grund wurden detaillierte 1D Transport Simulationen durchgeführt um die Ungewissheiten bezüglich des Einschlusses zu reduzieren. Über den verwendeten, gut validierten neoklassischen Ansatz hinaus werden erste Versuche unternommen, Ergebnisse von hochmodernen Turbulenz Rechnungen in die 1D Transport Simulationen zu integrieren mit dem Ziel, die prädiktiven Rechnungen zu verbessern.

Im nächsten Schritt wurden für die systematische Entwicklung von konsistenten Design-Studien Stellarator-spezifische Modelle entwickelt und in den etablierten europäischen System-Code PROCESS implementiert. Dies ermöglicht eine konsistente Beschreibung eines kompletten HELIAS-Fusionskraftwerks im Bezug auf Physik, Technik und Wirtschaftlichkeit. Innerhalb einer Teststudie wurden die entwickelten Modelle validiert. Somit konnten System-Studien zum ersten Mal für ein Kraftwerk des Typs HELIAS angewendet werden. Es hat sich dabei heraus gestellt, dass das Design-Fenster von den Grenzen des thermischen Beta limitiert ist. Der Vergleich eines exemplarischen Design-Punktes mit einem gleichwertigen Tokamak hat dabei ergeben, dass die gesamten Baukosten für beide Konzepte in der gleichen Größenordnung liegen.

Ein Hauptziel dieser Arbeit – alle vorangegangenen Aspekte zusammenführend – ist die Bewertung der physikalischen und technischen Größen eines Zwischenschritt-Stellarators mit brennendem Plasma. Solch eine Anlage erweist sich als nützlich, um Entwicklungsrisiken auf dem Weg zur kommerziellen Fusion abzumildern. Zwei Grenzfälle einer solchen Anlage wurden in dieser Arbeit untersucht. Zum einen eine kleine, zeitnah verfügbare Maschine basierend auf heutiger Technologie und eine technologisch weiterentwickelte Anlage ähnlich einem Tokamak-DEMO. Der Unterschied in den Baukosten zwischen diesen Grenzfällen beträgt in etwa ein Faktor zwei.

As already stated by *Martin Luther King Jr*, our modern society seems to face 'a poverty of the spirit albeit our scientific and technological abundance'. In particular with the further advancement of technology and research – to which this work contributes – we have to remind ourselves, that the 'value' of such progress depends on the way we utilise it. Scientific progress requires consequently also always an improvement of our mindset and ethics. It is for this reason, that I want to dedicate this work to the principles of Humanism, whose governing ideas – concisely expressed by the following quote – I support.

Nous ne pouvons pas espérer construire un monde meilleur sans améliorer les individus. Dans ce but, chacun de nous doit travailler à son propre perfectionnement, tout en acceptant dans la vie générale de l'Humanité sa part de responsabilité – notre devoir particulier étant d'aider ceux à qui nous pouvons être le plus utile.[1]

– *Marie Skłodowska Curie*

---

[1] In English: You cannot hope to build a better world without improving the individuals. To that end, each of us must work for our own improvement and, at the same time, share a general responsibility for all humanity, our particular duty being to aid those to whom we think we can be most useful.

Contents

Preface

Important results which originated from this doctoral project have been published as articles in internationally recognised scientific journals with peer-review system. This doctoral thesis is composed of these articles which are listed below followed by a description of the contributions provided by the co-authors and by myself. The articles are ordered according to the main topics investigated in this thesis and in chronological order therein. The articles where I have been co-author are placed at the end.

Magnetic Confinement and Plasma Transport

- **Article I**

  Limits of Confinement Enhancement for Stellarators
  F. Warmer, C.D. Beidler, A. Dinklage, Y. Turkin, R. Wolf
  Fusion Science and Technology, **68** (2015), p. 727
  http://dx.doi.org/10.13182/FST15-131

- **Article II**

  On the Characterisation of the Edge Ion Heat-Flux in Advanced Stellarators
  F. Warmer, P. Xanthopoulos, C.D. Beidler, H. Maaßberg, R. Wolf
  submitted to Nuclear Fusion, (03.11.2015)
  [under revision after assessment from referees]

Design of next-step Stellarator Devices

- **Article III**

  HELIAS Module Development for Systems Codes
  F. Warmer, C.D. Beidler, A. Dinklage, K. Egorov, Y. Feng, J. Geiger, F. Schauer, Y. Turkin, R. Wolf, and P. Xanthopoulos
  Fusion Engineering and Design, **91** (2015), p. 60
  http://dx.doi.org/10.1016/j.fusengdes.2014.12.028

- **Article IV**

  Implementation and Verification of a HELIAS Module for the Systems Code PROCESS
  F. Warmer, C.D. Beidler, A. Dinklage, K. Egorov, Y. Feng, J. Geiger, R. Kemp, P. Knight, F. Schauer, Y. Turkin, D. Ward, R. Wolf, and P. Xanthopoulos
  Fusion Engineering and Design, **98-99** (2015), p. 2227
  Proceedings of the 28th Symposium on Fusion Technology (SOFT-28)
  http://dx.doi.org/10.1016/j.fusengdes.2014.12.021

- **Article V**

  Systems Code Analysis of HELIAS-Type Fusion Reactor and Economic Comparison to Tokamaks
  F. Warmer, S.B. Torrisi, C.D. Beidler, A. Dinklage, Y. Feng, J. Geiger, R. Kemp, P. Knight, H. Lux, F. Schauer, D. Ward, R. Wolf
  submitted to IEEE Transactions on Plasma Science, (20.07.2015), [accepted 15.03.2016]
  http://dx.doi.org/10.1109/TPS.2016.2545868

- **Article VI**

  From W7-X to a HELIAS Fusion Power Plant: Motivation and Options for an Intermediate-Step Burning-Plasma Stellarator
  F. Warmer, C.D. Beidler, A. Dinklage, R. Wolf
  submitted to Plasma Physics and Controlled Fusion, (28.01.2016), [accepted 27.04.2016]

- **Article VII**

  Neutronics source modeling for stellarator power reactors of the HELIAS-type
  A. Häußler, U. Fischer, F. Warmer
  submitted to Annual Meeting on Nuclear Technology, (04.11.2015)

- **Article VIII**

  Wendelstein 7-X Programme – Demonstration of a Stellarator Option for Fusion Energy –
  R. Wolf, C.D. Beidler, A. Dinklage, P. Helander, H.P. Laqua, T. Pedersen, F. Schauer, F. Warmer
  submitted to IEEE Transactions on Plasma Science, (31.07.2015), [accepted 28.04.2016]

Contributions by Co-Authors and by myself

- **Article I**
  The paper was written completely by myself and I have also done all simulations and calculations. Y. Turkin provided the 1D code employed for the transport simulations as well as helpful instructions. All co-authors are IPP colleagues who contributed by constructive discussions and proof-reading.

- **Article II**
  The paper was written completely by myself following the strategy already conceptually proposed in Article III. I have also re-evaluated the W7-AS data, proposed the basic critical gradient model and done all the 1D transport simulations. P. Xanthopoulos provided the results from the GENE simulations, Y. Turkin the 1-D transport code and H. Maaßberg the W7-AS data. C.D. Beidler and R. Wolf contributed by constructive discussions and proof-reading.

- **Article III**
  The paper was written completely by myself. I have reviewed PROCESS and identified and developed stellarator-specific models. K. Egorov helped with the scaling of the mass of support structure as a function of stored magnetic energy. Y. Feng, J. Geiger, and F. Schauer consulted as experts on the development of the models. P. Xanthopoulos provided the results from the GENE simulations of Fig. 5. Y. Turkin provided the 1D transport code. C.D. Beidler, A. Dinklage and R. Wolf contributed by constructive discussions and proof-reading.

- **Article IV**
  The paper was written completely by myself and I have also done the verification study. Y. Feng provided the EMC3-Eirene result seen in Fig. 1. P. Knight helped to implement the stellarator modules into the systems code PROCESS. R. Kemp and D. Ward gave helpful instructions regarding PROCESS. All other co-authors contributed by constructive discussions and proof-reading.

- **Article V**
  The paper was written completely by myself and I have also done all simulations and calculations. S.B. Torrisi was a student of mine who I supervised for three months and who developed under my guidance a Python tool to do parameter scans with PROCESS in several dimensions. R. Kemp, P. Knight, H. Lux and D. Ward maintain the PROCESS code at CCFE. All other co-authors contributed by constructive discussions and proof-reading.

- **Article VI**
  The paper was written mainly by myself. Prof. Wolf provided the overview given in section 2 up until the caption 'Step-Ladder Approach'. A. Dinklage provided Fig. 1 and equations (2) – (4) with some general instructions to the description. I have done all other simulations and calculations. C.D. Beidler contributed by constructive discussions and proof-reading.

- **Article VII**
  The paper has been written by A. Häußler. I contributed by carrying out 1D trans-

port simulations to obtain the relevant plasma parameters. Based on these inputs, I developed a 3D neutron source which provides a volumetric emission probability for neutrons under the consideration of the details of the 3D magnetic field. I benchmarked the neutron source with results available from ITER which showed good agreement. Further, I contributed by proof-reading and corrections to the manuscript.

- **Article VIII**
  The paper has been written by R. Wolf. I contributed with my overall work and results to the discussions in the section 'Extrapolation to a Power Plant'. Further, I contributed by proof-reading and corrections to the manuscript.

In order to put the publications listed above in context with the overall research field of magnetic fusion and plasma physics and further to elucidate their importance for the advancement of these fields, the following chapters will first give a general introduction and motivation regarding these topics and some brief historical context. On this basis the reader is introduced to the underlying theoretical concepts which build the foundation of the current understanding of the physics of high-temperature fusion plasmas. Furthermore, engineering concepts and limitations are introduced which are important to characterise a stellarator fusion power plant. The results of the publications listed above are continuously interwoven at appropriate places in the following chapters and summarised in their entirety again at the end.

Full List of Publications and Conference Contributions

Publications

Book contributions

- _F. Warmer_, _C.D. Beidler_, _R. Wolf_, Magnetic Fusion Energy: From Experiments to Power Plants, Chapter 25: Stellarator fusion power plants. (2015, A volume in the Woodhead Publishing Series in Energy)

Publications without Peer-Review

- _F. Warmer_, Benchmark and Application of the PROCESS Stellarator Module (continuation). EUROfusion Report WP15-S2.D10.1 (2015)

- _F. Warmer_, _U. Fischer_, Requirements of stellarator-specific breeder blanket and neutronic calculations. EUROfusion Report WP15-S2.D11.1 (2015)

- _F. Warmer_, Benchmark and Application of the PROCESS Stellarator Module. EUROfusion Report WP14-S2.D3.1 (2014)

- _F. Warmer_, _U. Fischer_, Design of Stellarator-Specific Breeder Blanket and Neutronic Calculations. EUROfusion Report WP14-S2.D3.2 (2014)

- _F. Warmer_, _C.D. Beidler_, _A. Dinklage_, _Y. Feng_, _J. Geiger_, _R. Kemp_, _P. Knight_, _F. Schauer_, _Y. Turkin_, _D. Ward_, _R. Wolf_, _and P. Xanthopoulos_, Systems Code Approach for Burning Plasma Stellarator Devices. Stellarator News, Issue 143 (2014)

- _S.B. Torrisi_, _F. Warmer_, Design of an N-Dimensional Parameter Scanner for the Systems Code PROCESS. IPP Report No. 13/23 (2014)

- _F. Warmer_, System Code Stellarator Module Review and Improvement. EFDA Report WP13-DAS09-T03 (2013)

- <u>*F. Warmer*</u>, Intermediate Device Requirements Exploration. EFDA Report WP13-DAS09-T04 (2013)

- <u>*F. Warmer*</u>, Reactor Extrapolation of Wendelstein 7-X. IPP Report No. 13/21 (2013)

Conference Contributions

Invited Talks

- 20th International Stellarator-Heliotron Workshop, Greifswald, Germany (October 2015)
  R.C. Wolf, F. Warmer, C.D. Beidler, S. Bozhenkov, V. Bykov, W. A. Cooper, A. Dinklage, M. Drevlak, V. Erckmann, J.M. Faustin, U. Fischer, J. Geiger, J.P. Graves,D. Hartmann, A. Häußler, P. Helander, W. Kasparek, R. Kemp, P. Knight, H. P. Laqua, H. Lux, C. Lechte, H. Maaßberg, D. Pfefferlé, B. Plaum, F. Schauer, T. Stange, D. Ward, P. Xanthopoulos, W7-X to HELIAS: Strategy and Progress towards a Stellarator Power Plant

- 26th Symposium on Fusion Engineering, Austin, USA (June 2015)
  F. Warmer, S.B. Torrisi, C.D. Beidler, A. Dinklage, Y. Feng, J. Geiger, R. Kemp, P. Knight, F. Schauer, D. Ward, R. Wolf, Systems Code Analysis of HELIAS Power Plants

Contributed Talks

- German DEMO Working Group Meeting, KIT, Karlsruhe, Germany (January 2016)
  F. Warmer, Status Update on HELIAS reactor studies

- 14th Coordinated Working Group Meeting, Warsaw, Poland (June 2015)
  F. Warmer for the members of the ISHCDB, Recent updates of the International Stellarator-Heliotron Confinement and Profile Database

- German DEMO Working Group Meeting, FZJ, Jülich, Germany (April 2015)
  F. Warmer, Progress on Stellarator Reactor Studies

- DPG Spring Meeting for Plasma Physics / HEPP Colloquium, Bochum, Germany (March 2015)
  F. Warmer, Progress on HELIAS Systems Studies
  Received Promotional Stipend from the Wilhem and Else Heraeus Foundation

- Research Stay at the National Institute for Fusion Science, Toki, Japan (January/February 2015)
  F. Warmer, Past, Present, and Future of HELIAS Power Plant Studies

- DPG Advanced School: The Physics of ITER, DPG, Bad Honnef, Germany (September 2014)

F. Warmer, _H. Zohm_, Stellarators

- Workshop On Systems Codes, IPP, Garching, Germany (September 2014)
  F. Warmer, The Way to Systems Studies of HELIAS Burning Plasma Devices

- German DEMO Working Group Meeting, IPP, Garching, Germany (September 2014)
  F. Warmer, Preliminary Approach to Tokamak / HELIAS Comparison within the Systems Code PROCESS

- DPG Spring Meeting for Plasma Physics / HEPP Colloquium, Berlin, Germany (March 2014)
  F. Warmer, Stellarator-specific Developments for the Systems Code PROCESS

- 13th Coordinated Working Group Meeting, Japan (February 2014)
  F. Warmer, Stellarator-specific Developments for the Systems Code PROCESS

- German DEMO Working Group Meeting, KIT, Karlsruhe, Germany (November 2013)
  F. Warmer, Stellarator-specific Developments for the Systems Code PROCESS

- 11th Coordinated Working Group Meeting, CIEMAT, Madrid, Spain (March 2013)
  F. Warmer, Reactor Extrapolations of Wendelstein 7-X

Contributed Posters

- 20th International Stellarator-Heliotron Workshop 2015, Greifswald, Germany (October 2015)
  F. Warmer, Options for an Intermediate-Step Burning-plasma Stellarator

- Symposium on Fusion Technology 2014, San Sebastian, Spain (September/October 2014)
  F. Warmer, Stellarator-specific Developments for the Systems Code PROCESS

- Programme Oriented Funding: Evaluation 2014, Nuclear Fusion, IPP, Greifswald, Germany (March 2014)
  F. Warmer, Stellarator-specific Developments for the Systems Code PROCESS

- 2nd IAEA DEMO Programme Workshop, IAEA Headquarters, Vienna, Aus-

tria (December 2013)
F. Warmer, Stellarator-specific Developments for the Systems Code PROCESS

- Joint 19th ISHW and 16th IEA-RFP Workshop, Padova, Italy (September 2013)
F. Warmer, Reactor Extrapolation of Wendelstein 7-X

- 531st Wilhelm and Else Heraeus Seminar: 3D versus 2D in Hot Plasmas, DPG, Bad Honnef, Germany (Mai 2013)
F. Warmer, Reactor Extrapolation of Wendelstein 7-X

Conference Attendance without Contribution

- 597th Wilhelm and Else Heraeus Seminar: Stochasticity in Fusion Plasmas, Bad Honnef, Germany (September 2015)

- Joint EPS-SIF International School on Energy 2014: basic concepts and forefront ideas, Villa Monastero, Varenna, Italy (July 2013)
Received a full scholarship from the Societa Italiana di Fisica / Europeen Physical Society

- LHD and W7-X Collaboration Meeting, IPP, Greifswald, Germany (June 2014)

- PROCESS Working Group Meeting, CCFE, Oxford, Great Britan (November 2013)

- German DEMO Working Group Meeting, FZJ, Jülich, Germany (April 2013)

- PROCESS Systems Code Training workshop, CCFE, Oxford, Great Britian (January 2013)

Introduction

Throughout the history of mankind, the human desire for 'prosperity' has led to incredible innovations with the purpose of easing physical work and multiplying the human workforce thereby increasing the productivity and efficiency of societies. However, these new technologies – like the steam engine which introduced the age of industrialisation – required a substitutional energy source to be powered. Amplified by the introduction of electricity and its various applications mankind developed an ever increasing demand for energy. It appears to be evident that a sufficient supply and availability of energy is a necessary condition for the development of societies [1]. Figure A shows an attempt to quantify this statement, where the power consumption per capita is shown as function of the productivity per capita in terms of the gross domestic product (GDP). This empirical relationship indicates that highly developed nations with a high productivity also have a higher per capita energy consumption. It is very likely and from a humanistic viewpoint also desirable that, in the future nations in the lower left corner will increase their GDP and thereby also increasing their energy consumption. While more efficient technologies may reduce the speed at which developed nations increase their energy consumption, future, not yet foreseeable innovations, may lead to further energy needs, requiring in turn further energy sources.
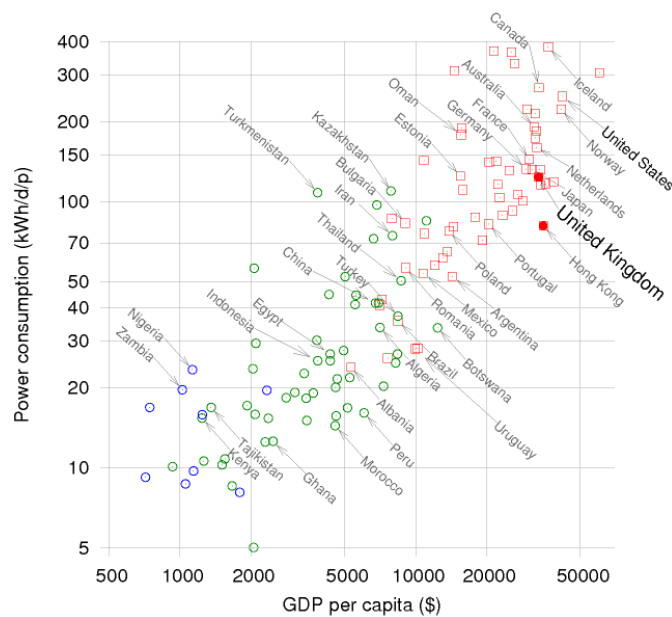
Figure A: *Power consumption per capita versus gross domestic product per capita, in US dollars. Data from Human Development Report [1]. Figure from [2].*

In the past mankind first utilised wood, then coal and oil, and finally also nuclear power to satisfy the increasing energy demand. In particular the carbon-based sources are limited by their finite availability on Earth. Given the technological possibilities of today (excluding fast breeders and transmutation), in the long term, energy demand could only be stilled by coal [3] having the highest identified resources left. However, considering the current state of our atmosphere and the level of greenhouse gas pollution [4], a further exhaust of huge amounts of carbon dioxide may have significant consequences for the climate on Earth. Although a full understanding of the impact of CO_2 concentration in the atmosphere on the global temperature increase is lacking, there is clear evidence of a strong correlation between temperature and CO_2 concentration. Consequently, based on the outlined scenario current climate models predict a global temperature increase and climate change in the next hundred years [5].

Confronted with these facts, the United Nations have started to take actions to reduce the emission of greenhouse gases, e.g. through the Kyoto Protocol. Associated with the climate problem is the concept of *sustainable development* as baseline for future national and international policies [3]. In fact, in recent years several societies have become increasingly aware of the concept of sustainability with the most famous example being the German 'Energiewende' which has the ambitious goal to replace fossil fuels and nuclear power by sustainable energy sources. One could argue that sustainability has evolved from a pragmatic approach towards a governing philosophy very much in line with our humanistic principles.

Nevertheless, especially the energy sector with its mainly conventional hydrocarbon sources is by nature in contradiction with sustainable development and therefore sustainable energy poses one of the greatest challenges for mankind. In this discussion, *Nuclear Fusion* can be regarded as an option for a possible future energy source with virtually unlimited supply of fuel, namely deuterium and lithium, making it one of the few sustainable energy sources [6]. Although a short-term (< 20 years) impact of fusion power on the energy supply cannot be expected, the significance of the energy problem requires investigation of all options for sustainable energy sources. The current European roadmap for the realisation of commercial fusion aims at a first demonstration power plant by 2050 [7]. By this time, it is expected that other renewables like wind and solar will significantly contribute to the electricity supply. However, the fluctuating nature of these sources requires large-scale energy storage and back-up solutions to which fusion can contribute [8].

The advantage of electricity production by nuclear fusion over nuclear fission is the fact that the fusion process itself does not leave long-lived radioactive products, and the issue of radioactive-waste disposal is therefore much less severe. From a safety perspective, the fusion process stops itself in case of an accident, quite in contrast to the chain-reactions which can continue in fission plants if safety systems fail.

Interestingly enough, nuclear fusion is what made life on Earth possible being the power source of the sun. The sun consists of a very dense and hot gas, i.e. 15 million Kelvin. At these temperatures every gas is completely ionised. The ions and

electrons are thus separated, but exhibit collective behaviour. Such a state is called *plasma*. At such high temperature and densities, the ionised hydrogen, i.e. protons have a chance to fuse. As this is an exothermic reaction, energy is released. The proton-proton (pp) reaction in the core of the sun provides a steady energy source over billions of years due to the very low cross-section of this reaction. In general, the cross-section of a fusion reaction can be described by three factors, namely the geometry, the Gamow factor (i.e. the transparency of the Coulomb barrier due to the quantum mechanical tunneling effect), and the 'astrophysical' S factor which contains the nuclear physics of each reaction. The pp-reaction is somewhat unusual compared to other fusion reactions as the protons have to experience a β^+ decay in order to fuse. As this process is governed by the weak interaction, the probability is very low and consequently, the fusion cross-section is 25 orders of magnitude smaller than, e.g. for the D-T reaction. The energy released by the pp-reaction is lost to a small part due to weakly interacting neutrinos. The rest of the energy is deposited in Gamma rays, but as the mean-free-path of a photon in the centre of the sun is only about 2 cm, the photons experience a random-walk-like scattering thus transferring a great part of their energy to the background plasma. This ensures that the energy of the plasma in the core of the sun is well confined before it is lost over a broad energy spectrum, including visible light. But not only the energy is well confined in the sun, but also the plasma itself as the kinetic force of the plasma is balanced by the gravitational force of the sun. With this knowledge the immediate questions arises, if one is able to harness this energy source in a controlled way on Earth with the potential to solve the future energy demand of mankind.

The most suitable fusion reaction is that of deuterium and tritium which has in the range of $10\ldots100$ keV a cross-section which is about a factor 100 higher than that of any other fusion reaction. The reason lies again in the nuclear physics of the reaction. The intermediate compound formed by D-T has a broad resonance with the excited level of the unstable ^{5}He at 64 keV. At such a resonance, the probability for a reaction is greatly increased explaining the high cross-section of the D-T fusion reaction in the considered energy range. Also the energy output per reaction is with a total of 17.6 MeV fairly high where about 1/5 is deposited in the resulting charged alpha particle and the rest of the energy in a neutron.

$$\text{D} + \text{T} \longrightarrow \text{n (14.1 MeV)} + \alpha \text{ (3.5 MeV)}$$

The split of energy between a charged and an uncharged particle is another advantage of the D-T reaction. The energy of the charged particle helps to maintain the temperature of the background plasma by collisions. On the other hand, the energy stored in the uncharged particle can escape the plasma and thus be utilised for electricity generation without the need to directly tap the energy of the plasma. However, a negative aspect of the D-T reaction is the fact, that the uncharged particle is a neutron, which causes some radioactive activation in the surrounding material.

From the above description follows, that, in order to maximise the fusion output, high temperatures on the order of ~ 10 keV are required. However, at such

temperatures any gas is completely ionised, i.e. one has to consider the properties of a plasma. Most importantly, a plasma is quasi-neutral, i.e. electric potentials are shielded out reducing the long-range interaction of the Coulomb force. Still, the effective fusion cross-section of the D-T reaction is some orders of magnitude smaller in comparison to the cross-section of the Coulomb scattering. Consequently, the need arises to *confine*, i.e. avoid losses of, both the particles and their energy for a sufficient amount of time such that the particles can undergo fusion reactions. Similar to the sun, a force is required to balance the kinetic pressure of the plasma.

One of the most promising concepts to achieve this is magnetic confinement. In this concept, the charged particles are bound to the magnetic field lines by the Lorentz force. The magnetic field lines are toroidally closed to effectively confine the particles and their energy. As will be explained in section 2, this does not suffice to confine a plasma. In addition to the toroidal magnetic field component, a poloidal component is required to circumvent arising particle drifts.

Before the concept of magnetic confinement is explored in more detail, first a consistency check is done to see if magnetic confinement is realistic at all and to familiarise the reader with important parameters and their order of magnitude.

Consider a toroidally closed magnetic field with a magnetic field strength on the order of 5 T, which can be realised by currently available low-temperature-superconductor (LTS) technology. Let this closed domain be filled with a hot D-T plasma with a Maxwellian averaged particle energy in the range 10–20 keV. The magnetic field pressure must balance the plasma pressure. A measure for this is the so-called dimensionless plasma $\beta = 2\mu_0 p / B^2$ and in today's experiments values of up to $\beta = 5\%$ can be achieved before detrimental effects occur. With the definition of β and the magnetic field one obtains the roughly achievable plasma pressure as $p \approx 1$ bar. As the 'temperature' was already set, it follows that the deuterium / tritium density must be on the order of $n \approx 10^{20}$ m^{-3}. The internal energy of the plasma is defined by $W = 3/2 \int p \, \mathrm{dV}$ and the produced fusion power by $P_{fus} = E \int n_D n_T \langle \sigma \nu \rangle \, \mathrm{dV}$ where $E = 17.6$ MeV is the total energy output of one fusion reaction and $\langle \sigma \nu \rangle$ the fusion rate coefficient, which can be approximated by $\langle \sigma \nu \rangle \sim T^2$ in the considered temperature range. A global measure for the quality of the confinement of energy in the plasma volume is the *energy confinement time* defined by

$$\tau_\mathrm{E} = \frac{W}{P}$$

where, in steady-state, P is equal to the total input power to the plasma. The plasma is heated intrinsically by the produced alpha particles which carry 1/5 of the total fusion power and ensure a self-sustained burn condition. Assuming that the alpha heating power is much larger than any power loss, such as radiation, and in addition neglecting profile factors, the required energy confinement time turns out to be on the order of a few seconds $\tau_\mathrm{E} \approx \mathrm{const} \cdot (p \cdot V)/(E \cdot p^2 \cdot V) \approx 1 \ldots 3$ s. If fusion is to provide a base load electricity supply in the future aiming at a typical net electric power output of 1 GW (with a conservative heat conversion efficiency of about $\eta_{th} = 30\%$) one realises that such a plant must have a plasma volume on

the order of 1000 m^3.

From this 'back-of-the-envelope' assessment one is able to gain a first insight into the dimensions of important parameters. It can be realised that fusion by magnetic confinement is potentially possible simplifying here any physics and engineering issues which will be discussed later in more detail.

Indeed, this has already been realised over 50 years ago when research on fusion by magnetic confinement started. However, many physics and engineering challenges have been encountered during this time. Although commercial fusion has not yet been realised, tremendous progress has been made over the course of the past decades. For this reason, some historical context is given in the next chapter. The focus is thereby put on the so-called *stellarator* concept. In the field of magnetic confinement different concepts are investigated, e.g. the *tokamak* and the *stellarator*. The difference between these concepts concerns how the poloidal component of the magnetic field is created as will be discussed in the next section.

1 Historical Overview[1]

The invention of the stellarator concept goes back to Lyman Spitzer who realized in 1951 [9] – even before the idea of the tokamak concept appeared in 1952 [10] – that there are different ways to provide a rotational transform of the field lines for a magnetic field which is toroidally closed. Aside from driving a toroidal current, it is possible to achieve a twist of the magnetic field by creating a non-planar magnetic axis or by elongating the flux surfaces and letting them rotate poloidally while going in the toroidal direction [11]. These ideas were later proven mathematically by Mercier [12], and the last two may be considered the basis for the stellarator concept, where the term stellarator is used here in its broadest sense to include 'helical devices' of all types (e.g. heliotrons, torsatrons, heliacs).

Applying these ideas, it becomes clear that the common feature of all stellarators is that they provide a rotational transform of field lines without the necessity of plasma current. This means that, in contrast to tokamaks, the magnetic flux surfaces of helical devices already exist in vacuum. This is a great advantage as it signifies that stellarators inherently offer the prospect of steady-state operation with an externally produced magnetic field. As there is no need to drive a toroidal current in a helical device, the second great advantage of the stellarator is the absence of current-related instabilities. In particular, disruptions do not occur, well known from tokamaks when operational limits are reached [13]. For reactor-sized devices, disruptions pose a risk, both with regard to the forces acting on the machine as well as the possibility of generating runaway electrons [14]. Generally, magnetohydrodynamic (MHD) instabilities in stellarators are far less important than in tokamaks. For example, the neoclassical tearing modes which can strongly limit the achievable plasma performance in tokamaks [15] are non-linearly stable in some stellarators where the magnetic shear (t') has the opposite sign compared to tokamaks. In a stellarator, the appearance of a magnetic island which flattens the pressure profile reduces the bootstrap current and consequently causes the island to shrink rather

---

[1]Parts of this chapter have been published in similar form as part of a chapter in the book 'Magnetic Fusion Energy: From Experiments to Power Plants'. Only the general points from the book chapter have been taken and summarised here. The author here was also the first author for the chapter in question.

than to grow [16]. For example, in W7-A, disruptive instabilities could be avoided by introducing an external component of the rotational transform of $\iota > 0.14$ [17].

The advantages of helical concepts unfortunately come at a price. A stellarator cannot be axissymmetric as both rotating elongated flux surfaces as well as a non-planar axis require the magnetic field to be helically shaped. Consequently, stellarators exhibit fully three-dimensional fields with a helically structured plasma topology. The three-dimensionality of the concept leads to a very large configuration space. This can also be regarded as positive, as it allows optimisation of suitable configurations with respect to a multitude of criteria. This is important, as in an arbitrary helical configuration, the trajectories of collisionless particles are not necessarily confined in all regions of phase-space, with the consequence of direct fast-particle losses as well as large 'neoclassical' transport [18]. Consequently, the choice of a suitable helical configuration and its optimisation are critical aspects of stellarator research, which conceptually may turn out to be an advantage. While for a given tokamak experiment, the plasma configuration is very flexible, e.g. the magnetic shear can be modified in dedicated scenarios, the overall configuration space is limited due to the two-dimensional restriction caused by axisymmetry. Stellarator experiments in contrast are not very flexible for a certain experimental design. The rotational transform can be modified only within certain limits by changing the currents in the external field coils. But due to the intrinsic 3D topology, the overall configuration space of possible stellarator designs is very large and in fact the search for realistic 3D configurations with favourable properties is an important topic within the field of stellarator research.

In comparison to their axissymmetric cousins, early helical experiments were not very successful. The initial results of the American Model-C stellarator were disappointing, and the experiments were abandoned after the Russian T3 tokamak results became known in 1968, which in comparison, were much more promising. Later it turned out that field errors resulting from coil misalignment during construction of Model-C were so large that the plasma volume in which nested flux surfaces existed was only a small fraction of that designed for [19]. The 3D engineering and construction accuracy needed for a stellarator had been underestimated. After this setback new and more accurately constructed devices such as W7-A [20] and Heliotron-E [21] began operation and showed comparable confinement results to tokamaks of similar size. Nonetheless, it was observed that the particle losses strongly increased with increasing temperature attributed to the direct losses from particles trapped in local minima of the complex 3D magnetic field. This general drawback had the effect that fusion research mainly focused on the development of the tokamak concept while the stellarator community concentrated on the understanding and mitigation of the so-called neoclassical transport. This delay in development and the early success of tokamaks, is the reason why the stellarator community is comparatively small with only a few experimental devices. Additionally, the freedom of the large 3D configuration space led to the exploration of different helical concepts, and so far no conclusion has been reached in the community as to which configuration is the 'best'.

The stellarator concept followed in Europe is the so-called 'Helical-axis advanced stellarator' (HELIAS) line. Its prime example is the stellarator experiment Wendelstein 7-X (W7-X) [22] being the first of its type, where several optimisation criteria have been used to obtain a suitable reactor-relevant magnetic configuration, which is realised by a modular coil set only. After the successful construction and commissioning of W7-X, the first operation phase and experiments have recently started.

The extrapolation of the W7-X stellarator concept to reactor conditions is here referred to as 'HELIAS'. Historically, this is somewhat ambiguous as this term has originally been used to refer to finite-beta magnetic configurations with high aspect ratio being stable with respect to different MHD modes [23]. Further and more systematic studies resulted in configurations where the trapped particles are bound to poloidally closed drift orbits providing good confinement. In view of the movement of the particles these magnetic configurations are called 'quasi-isodynamic' and are today's basis of the HELIAS concept [24]. The prospects and systematic study of the HELIAS line as potential fusion power plants are the subject of this work.

In a HELIAS, the rotational transform is provided by a non-planar axis and a rotating field symmetry. This is realised by using a modular coil set. This means different classes of discrete non-planar toroidal field coils are used, which differ in shape. Due to the complex 3D shaping of the coils, the current in the coils creates both a toroidal and a poloidal magnetic field component. Thus, large poloidal field coils as used in tokamaks can be avoided with the great advantage that the corresponding large forces which would have arisen between poloidal and toroidal field coils can be avoided. But nonetheless, large forces remain between the toroidal field coils which require a strong support structure. In stellarators the force distribution is quite complex due to the 3D shaping of the coils. In contrast to tokamaks, there are forces which are directed radial inwards and outwards, but also lateral forces.

It should be noted that W7-X has a set of 20 additional inclined planar coils. These coils produce also a vertical field component and are used in W7-X to allow for some flexibility in changing the magnetic field configuration. In a HELIAS power plant such coils would not be present.

Moreover, the modular coil set itself allows realisation of a large variety of magnetic configurations as they are able to not only mimic a superposition of fields with different helicities but also a toroidal field mirror term. With this flexibility, optimised stellarator magnetic configurations can be realised. In particular, they can be optimised with respect to reactor-relevant criteria, which are briefly summarised as follows [25]:

- Good flux surfaces of the vacuum magnetic field. Nested flux surfaces are a necessary condition to reduce radial transport. In particular in a 3D magnetic configuration, small error fields can induce magnetic islands which short-circuit density and temperature gradients and thus reduce the achievable pressure.
- Low Shafranov shift. In equilibrium the force balance requires that certain currents flow in the plasma which increase with increasing plasma pressure. However, due to the toroidal bending of the equilibrium, the current is not

equally distributed such that the poloidal field contribution from the current is stronger on the inside than on the outside. This causes a radially outward shift of the magnetic axis, the so-called Shafranov shift. This introduces free energy in the plasma and is not desired in a stellarator. Moreover, the plasma configuration should not deviate too much from the optimised vacuum configuration.

- Good MHD stability up to a plasma beta of 5%. At increasing plasma pressure, small perturbations start to grow, i.e. they tap the free energy of the increasing pressure gradient and can have severe effects on the energy confinement or even disrupt the plasma as in tokamaks. A critical stability limit is usually given by the plasma beta. As the fusion power density increases with β^2, an efficient fusion reactor should operate at high beta. The increase of the beta-limit is therefore one of the key aspects of fusion research.

- Good energy confinement, i.e. small neoclassical transport losses (drift optimisation). As already outlined in the introduction and as will be discussed in the next chapter, the confinement of the energy is a key requirement in order to sustain the temperatures which are needed for a high fusion power output.

- Low bootstrap current for a stiff magnetic equilibrium. The bootstrap current is a self-generated plasma current. If not taken into account, it can reach very high values and the resulting field which is exerted by the bootstrap current may negatively affect the magnetic equilibrium. This can cause higher transport and also shift the magnetic configuration causing issues with, e.g. the power exhaust. As the divertor is fixed, such an uncontrolled change of the magnetic configuration must be avoided.

- A suitable divertor concept for controlled particle and energy exhaust (e.g. island divertor). This is realised with a divertor which acts as plasma facing component and is designed to endure high heat loads. In a 3D geometry, the divertor must be carefully placed to control the density and energy exhaust.

- Good confinement of fast particles (i.e. alpha particles in a fusion plasma). Fusion-born alphas are very energetic with 3.5 MeV. It is one of the greatest challenges of magnetic confinement to guarantee that the alpha particles stay long enough in the plasma to transfer their energy to the background. Losses of only a few percent are allowed, as otherwise the first wall would receive unacceptably high power loads.

- Feasibility of the modular coil set (low curvature, tolerable forces). The freedom in designing a 3D magnetic field is nearly endless. However, this freedom is somewhat reduced by engineering constraints. In the end, the stellarator magnetic field must be created by real coils which cannot be arbitrarily bent, nor can they allow an arbitrary variation of current density.

These criteria have already been used to optimise the Wendelstein 7-X magnetic configuration. The magnetic field exhibits a 5 field-period symmetry in which every field period is point-symmetric in itself produced by 5 different classes of modular coils totaling 50 non-planar coils. A flux surface of the W7-X magnetic configuration and the corresponding modular coils are illustrated in Fig. 1.1. The mission of W7-X
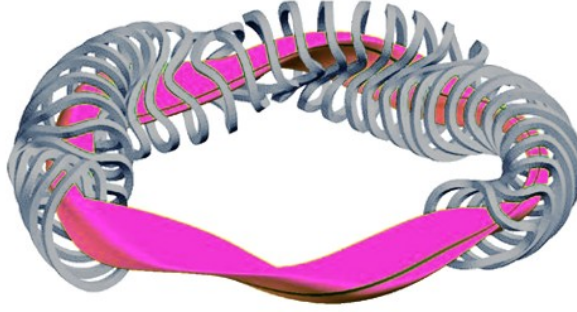
Figure 1.1: *Modular coil set of Wendelstein 7-X (grey) and a corresponding magnetic field flux surface (pink) [22].*

is to prove that the optimisation criteria indeed lead to the desired beneficial effects. This, together with quasi-steady-state operation (discharges up to 30 min) at high performance (10 MW of heating power), is of highest priority to demonstrate the reactor capability of the HELIAS concept [26].

As the idea for a modular coil set already emerged in 1972 [27] and HELIAS configurations were discussed in more detail from 1988 [23], it is not surprising that early studies for HELIAS reactors were carried out. Originally 4 field-period configurations were also investigated [28], resulting in more compact machines, but it was found that the confinement of fast particles and the reduction of bootstrap current is more difficult than in the more favourable 5 field-period configurations [29]. Thus, in this thesis, reactor studies for the HELIAS line mainly concentrate on the 5 field-period case.

In the next chapter emphasis is put on the confinement of particles and energy in a toroidal magnetic field which, as we will see, is crucial for the success of fusion power plants. In particular, focus is put on the aspects of the 3D field topology inherent to stellarators.

2 Magnetic Confinement and Plasma Transport

To effectively use fusion, the employed particles must be highly energetic in order to overcome the Coulomb barrier in sufficient number. This increases the probability for quantum tunneling, allowing nuclear attraction to overcome the electromagnetic repulsion. But even then, the fusion cross-section is some orders of magnitude smaller than the Coulomb scattering. The particles must therefore undergo many collisions before they finally fuse. In order to increase the number of reactions and fusion output, the particle density must be sufficiently high. Consequently, both the particles and their energy must be maintained over many collisions to achieve sufficient fusion reactions. This requirement is usually referred to as *confinement*, i.e. the confinement of particles and energy for a sufficient amount of time.

In order to keep plasma in thermal equilibrium, the kinetic pressure of the plasma must be balanced. Magnetic confinement exploits the electromagnetic properties of the plasma to achieve a force balance, i.e. the confinement is provided by the magnetic field.

However, this confinement is not perfect since different loss channels exist which lead to a constant loss of energy and particles. Therefore, the study and under-standing of *transport* – i.e. the effective radial flux of energy and particles – is one of the key research topics for magnetic confinement. It turns out that a multitude of different effects exist which lead to transport, i.e. diffusive processes, convection, magnetic instabilities, etc.

While in general, the energy transport should be low, the picture for particle transport is not as clear. In a burning fusion plasma, the main energy source comes from the fusion-born alpha particles, which transfer their initial energy of 3.5 MeV during the slowing down process to the background plasma and thus balance energy losses. The fast alpha particles should therefore be well confined over the time period required for slowing down. However, after they have transferred their energy, it becomes desirable to exhaust this so-called helium 'ash' rapidly. Otherwise, the cold helium would accumulate and dilute the plasma reducing the fusion output.

It is clear, that satisfying all these requirements at the same time is not achievable with arbitrary precision.

Thus, the understanding of confinement is a key aspect of fusion research, with the aim of fine-tuning, modelling, prediction and optimisation of future devices. In the following some of the most significant effects are introduced and discussed.

2.1 Particle Motion in a Magnetic Field

Drifts

The basic means for the confinement of charged particles in a magnetic field is the *Lorentz force*

$$m\frac{\mathrm{d}\mathbf{v}}{\mathrm{d}t} = q\left(\mathbf{E} + \mathbf{v} \times \mathbf{B}\right) \tag{2.1}$$

which can be derived from classical field theory [30] for the particle mass m, charge q, electric field vector $\mathbf{E}$, the magnetic flux density $\mathbf{B}$ and the velocity vector of the particle $\mathbf{v}$. This leads to a helix-like motion. Perpendicular to the magnetic field line the particles are bound to a circular motion with a distinct radius, the so-called gyro-radius[1] $r_G = mv_\perp/|q|B$, but can move freely along the field line. The axis of the circular motion is referred to as the *guiding center*.

However, any force $\mathbf{F}$ acting perpendicular to the magnetic field on the particles causes them to drift perpendicular to $\mathbf{B}$ according to

$$\mathbf{v}_F = \frac{\mathbf{F} \times \mathbf{B}}{qB^2}. \tag{2.2}$$

It is apparent, that if the force $\mathbf{F}$ does not depend linearly on q, the ions and electrons will drift in opposite directions. Indeed, as any toroidally closed magnetic field has a gradient of the magnetic field ∇B (the field is higher on the inner than on the outer side), the ∇B drift cannot be avoided. The inherent ∇B drift would therefore lead to a charge separation of the ions and electrons and consequently to a strong vertical electric field. The resulting $\mathbf{E} \times \mathbf{B}$-drift would flush the particles radially out of a toroidal field. To render these radial drift motions innocuous, a poloidal magnetic field component is necessary.

The poloidal field component 'short-circuits' the drifts as the particles now move also poloidally around the torus such that they drift inwards on one side and outwards on the other side and the mean drift balances out. However, due to the poloidal motion along the torus the particles now experience a modulation of the magnetic field, which is weaker on the outer side and stronger on the inner side of the torus. Thus particles in the appropriate region of phase-space with nearly perpendicular velocity vector become trapped in regions of weak magnetic field as

---

[1]Also called Larmor radius or gyration radius. The eigenfrequency of this motion is the cyclotron frequency $w_c = |q|B/m$.

will be discussed next.

Trapped Particles

As trapped particles may lead to considerable particle and energy losses in a stellarator, the basic principle and its mitigation are explained in the following.

It is well known from the *Noether Theorem* of classical mechanics, that every symmetry of motion implies a conserved quantity [31]. The connection with the circular motion of the gyration of particles is apparent. It follows that the action integral over one gyration must be constant, which apart from some constant yields the magnetic moment $\mu = mv_\perp^2/2B$. It should be pointed out that the magnetic moment is not strictly constant as the particle trajectories in inhomogeneous magnetic fields are not closed. However, the change of the system is small compared to the periodic motion and the variation of the conserved quantity marginal, thus the magnetic moment is here an *adiabatic invariant*.

As the magnetic moment is a conserved quantity, the perpendicular velocity of a particle which experiences an increasing magnetic field strength B along its path must increase and since also the energy of the particle is conserved (neglecting collisions for the moment), the parallel velocity must decrease. If the initial parallel velocity was already low enough, i.e. $v_\parallel^2 \leq v_0^2 \left(1 - B_{\min}/B_{\max}\right)$, the parallel velocity decreases to zero and the particle is reflected. The particle is therefore trapped in the region of low magnetic field. The trapping of charged particles is also of interest in astrophysical plasmas, as e.g. in the mirror field of the Earth's magnetosphere where trapped particles contribute to the aurora borealis.

Taking a projection of the trajectories of trapped particles in an axisymmetric tokamak to the poloidal cross-section, one sees that the trapped particles are reflected at the top and bottom of the torus. Due to their characteristic shape when projected in the poloidal plane they are referred to as 'banana' orbits. Since those particles spend equal amounts of time in the upper and lower half of the torus, the ∇B-drift averages out over time. This means, banana orbits do not cause radial transport per se. However, one has to take into account collisions with other particles. These collisions lead to a random-walk-like diffusion where the step-size is the banana-width which is much larger than the gyro-radius and consequently leads to an effective radial particle and energy transport.

In stellarators, the behaviour of trapped particles is even more complex. In contrast to tokamaks, particles in a stellartor field can get trapped *locally* leading to transport even without collisions. The local trapping interrupts the particles poloidal movement. Thus the drifts outlined above cannot cancel out any longer and consequently such particles would get lost quickly in a toroidal configuration. In a stellarator like W7-X there is a strong modulation of the field strength along a field line attributed to the 3D topology of the magnetic field. Thus, there exist numerous trapped particle orbits that normally lead to strong losses of particles and energy considerably degrading confinement. Modern stellarators like W7-X are therefore

optimised with respect to these effects. The magnetic topology has been chosen such that trapped particles precess poloidally while they are bouncing back and forth in the trapping region. Thus the vertical drifts are balanced again but on a longer time scale. In Fig. 2.1, a trajectory of a poloidally precessing trapped particle is shown which bounces forth and back in the 'straight' region of the magnetic field in W7-X.
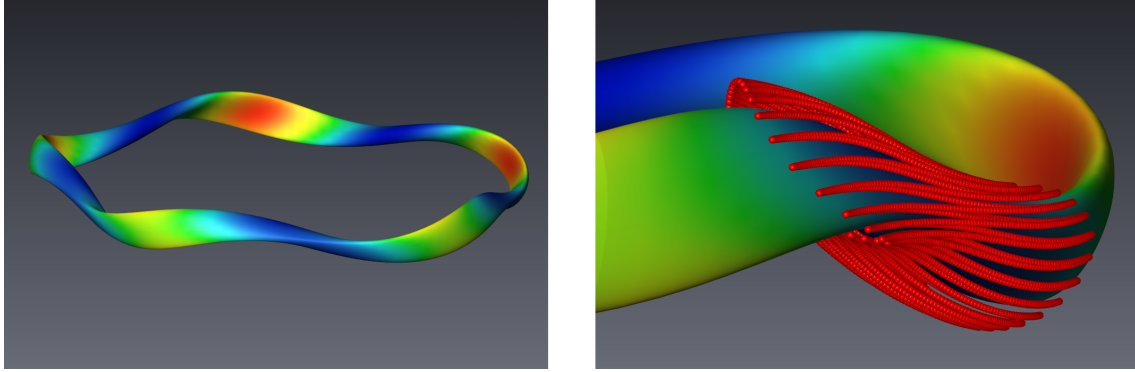
Figure 2.1: *Magnetic flux surface of Wendelstein 7-X at half toroidal flux (left) and color representing the magnetic field strength: blue – minimum, red – maximum. Zoom of a trajectory of a poloidally precessing particle trapped in the minima of the magnetic field (right). Figure was kindly provided by M. Borchardt, IPP.*

In spite of these optimisations, energetic particles are less well confined than thermal particles. The vertical drift scales with the energy. In particular for electrons, the transport increases strongly with increasing temperature. Due to the complexity of the magnetic field and the high inter-dependencies the calculation of an effective transport of particles and energy is not straightforward. In particular, Coulomb collisions must be taken into account including trapping or detrapping of particles. In fact, to calculate the transport caused by these collective effects, *kinetic theory* is required for an adequate description and is investigated in section 2.3. But before kinetic theory is considered, some general aspects of magnetic equilibria will be introduced in the next section.

2.2 Magnetic Equilibrium

Advancing from a microscopic single particle view to a collective macroscopic plasma view, the simplest model to describe a magnetised plasma is a set of equations given by *magnetohydrodynamics* (MHD). As the name states, the plasma is described as a conducting fluid in a magnetic field frame. This is motivated from the fact, that in a hot fusion plasma in thermal equilibrium, the particles are nearly Maxwell-distributed at every point and thus the plasma behaves like an ideal gas.

The MHD equations are widely used to calculate magnetic equilibria. The first main aspect of magnetic equilibria is the force balance between the plasma pressure and the magnetic field pressure. The second aspects concerns the shape of the

plasma which is determined by the currents in the external coils as well as by the currents flowing in the plasma.

A pressure gradient ∇p must exist in every finite confinement volume since the plasma must interact at some point with a cold boundary. In the picture of ideal MHD, i.e. assuming the fluid has infinite conductivity, the thermodynamic force is compensated by the electromagnetic force

$$\nabla p = \mathbf{j} \times \mathbf{B} \tag{2.3}$$

where $\mathbf{j}$ is the current density in the plasma. Here the time dependence, the viscosity as well as the inertial term have been omitted since the interest is focused on an equilibrium. This is in particular relevant for stellarators where the plasma cannot rotate toroidally due to viscous losses, i.e. the toroidal flow velocity is generally very small.

From equation (2.3) follows that $\mathbf{B}$ and $\mathbf{j}$ lie on surfaces of constant pressure and therefore

$$\mathbf{B} \cdot \nabla p = 0, \qquad \mathbf{j} \cdot \nabla p = 0. \tag{2.4}$$

Mathematically, there is only one topology fulfilling these criteria - the torus [32]. Moreover, the constant pressure surfaces lie inside each other, i.e. they are *nested*. Consequently the term *flux surface* is frequently used in fusion research. The term refers to nested surfaces of constant pressure, but flux surfaces are often also associated with their enclosed toroidal flux ψ_t.

Taking $\mathbf{B} \cdot \nabla p = 0$ as well as Ampère's law $\nabla \times \mathbf{B} = \mu_0 \mathbf{j}$ and Maxwell's equation $\nabla \cdot \mathbf{B} = 0$ one can express the magnetic field in its symplectic form [32, 33, 34] as

$$\mathbf{B} = \nabla \psi_t \times \nabla \theta + \nabla \phi \times \nabla \psi_p \tag{2.5}$$

where ϕ is the toroidal angle, θ the poloidal angle, and ψ_t, ψ_p the toroidal and poloidal flux respectively. The magnetic flux passing through a poloidal cross section, i.e. constant ϕ, is simply calculated by the surface integral

$$\int_{\phi=\text{const.}} \mathbf{B} \cdot d\mathbf{S} = 2\pi \psi_t \tag{2.6}$$

and vice versa for constant θ. In this representation the *rotational transform* which describes the number of poloidal turns of a field line per toroidal turn is given by

$$\iota = \frac{d\psi_p}{d\psi_t}. \tag{2.7}$$

It should be noted that the MHD equations require that certain currents flow in the plasma which have impact on the magnetic equilibrium. Due to the toroidal bending of the plasma, a pressure force arises which is directed radially outward. This force is compensated by intrinsic plasma currents which have both a perpendicular and a parallel component. The parallel current is known as Pfirsch-Schlüter current which

has an impact on diffusive transport at high collisionality. Although these currents do not result in a net current, they lead to a radial outward shift of the magnetic axis known as Shafranov-shift. A main aspect of stellarator optimisation is the minimisation of these currents as such a shift changes the magnetic field spectrum and leads to degradation of confinement.

In order to calculate a magnetic equilibrium, the MHD equations must be solved. For an axissymmetric toroidal field, an analytic formula can be derived which allows a basic description of a 2D equilibrium which is known as the Grad-Shafranov equation. In 3D geometry, however, dedicated codes are required to solve the set of MHD equations to obtain an equilibrium. The most widely used tool for this purpose is the VMEC code [35]. VMEC solves the MHD force balance equations in combination with the total plasma potential energy

$$W = \int \left(\frac{p}{\gamma - 1} + \frac{B^2}{2\mu_0} \right) dV \tag{2.8}$$

where γ is the adiabatic index. In this ansatz a variational principle [36] is employed to find solutions which are states of minimum MHD energy. From this follows also that a three-dimensional magnetic equilibrium is completely determined by the shape of the outermost flux surface and two radial profile functions, e.g. $p(\psi_t)$ and $\iota(\psi_t)$. However, in the VMEC approach it is assumed that nested flux surfaces exist in the whole toroidal plasma. While it can be proven mathematically, that flux surfaces exist in 2D geometry, it is still under debate under what conditions nested flux surfaces exist in 3D geometry and how they can be adequately computed. Numerically, flux surfaces can be found using a Poincaré mapping of a straightforward Biot-Savart approach when the coil currents are provided.

A particular drawback of VMEC is that it is not able to treat magnetic islands. At rational surfaces ($\iota = d\psi_p/d\psi_t \in \mathbb{Q}$), the VMEC approach leads to singularities in the current density on the surface. In reality, the current is dissipated by resistivity causing magnetic islands. Apart from plasma related islands, in a stellarator magnetic islands also appear in vacuum. For example in W7-X, the rotational transform is $\iota = 5/5$ at the edge and together with the low shear and the 3D field results in naturally occurring vacuum magnetic islands.

In order to treat magnetic islands and stochasticity of magnetic fields other codes have been developed. One example is the SIESTA code [37] which uses nearly the same approach as VMEC, but with the small modifications that in some iterations resistivity is included allowing the flux surfaces to break up and form islands. Another widely used code is HINT [38] which does not minimise the MHD energy, but rather solves the resistive MHD equations using an initial value approach. Still, some problems remain and the improvement of equilibrium codes for stellarators remains a research topic.

Although stellarators are not axisymmetric, one can still find certain 'quasi-symmetries'. However, to describe the properties of quasi-isodynamic configurations (like W7-X) or maximum-J configuration (as envisaged for HELIAS power plants)

tedious mathematical elaborations are required. The reader is therefore referred to the broad overview given in [34].

It should be noted that in the collective MHD picture one finds also a diamagnetic drift not covered by the single particle view. Moreover, MHD is widely used to study stability of equilibria and propagation of plasma waves. Beyond its fusion applications, MHD theory is also widely used in astrophysics. E.g. the Weibel instability is an example of an electromagnetic instability studied in both fields.

2.3 Kinetic Theory

In fusion research kinetic theory is generally applied to calculate the effective plasma transport, i.e. the particle and heat flux densities $\mathbf{\Gamma}$ and $\mathbf{q}$ directed radially outwards, and thus the quality of confinement. These fluxes are driven by the thermodynamic forces present in the plasma including the temperature gradient, density gradient as well as the radial electric field. In particular for stellarators, also the details of the 3D magnetic configuration play an important role for the determination of the fluxes.

In order to relate the fluxes to the thermodynamic forces in a non-equilibrium state – e.g. according to the general concept of the Onsager reciprocal relations – thermal transport coefficients [39] must be calculated which are dependent on the *local* plasma parameters. Consequently, kinetic theory is required, which is used to connect the local microscopic behaviour of particles to effective macroscopic quantities in space and time. For the description of a magnetised plasma often the *Vlasov equation* (i.e. the collisionless Boltzmann equation) is employed which comprises the particle balance in phase-space and electromagnetic forces [40]. However, this equation is not adequate for the description of a plasma confined in a stellarator as collisions are neglected. The inclusion of collisions is mandatory since, in a stellarator, they can lead to trapping or detrapping of particles which strongly impacts particle and energy losses.

Reordering of the Vlasov equation with respect to small Larmor radius and large gyrofrequency, and taking collisions into account yields the so-called *drift kinetic equation* [41, 42] (DKE)

$$\frac{\partial f_a}{\partial t} + \left(v_\parallel \mathbf{b} + \mathbf{v}_D\right) \cdot \nabla f_a = C_a\left(f_a\right) \tag{2.9}$$

where f_a is the distribution function of each particle species, $\mathbf{b}$ the normalised field strength, $\mathbf{v}_D$ the drift velocity and $C_a\left(f_a\right)$ the linearised collision operator. The exact form of this equation depends highly on the applied ordering and the magnitude of the electric field and can thus, depending on the specific application, take different forms [34, 43]. Solving this equation to obtain local transport coefficients is the aim of the so-called *neoclassical transport theory* which is briefly discussed in the next section.

2.3.1 Neoclassical Transport

A number of different methods and codes have been developed over time to solve the drift kinetic equation for 3D magnetic fields. A broad overview and detailed benchmark with respect to stellarator magnetic configurations is given in [44]. Here, the focus is set on the *Drift Kinetic Equation Solver* (DKES) [45, 46] which has been employed to provide the neoclassical thermal transport coefficients used in this thesis.

Without simplifications or constraints the DKE must be solved in six dimensions, three in space, two in momentum (gyro-average) and one in time. But as computational requirements grow with the dimension of the system, a full solution of the DKE in all dimensions is far too demanding to be feasible. In the DKES approach the phase-space can be reduced. For this, only small deviations from an equilibrium distribution are considered, where the background equilibrium is assumed to be Maxwellian. With such a perturbation ansatz a linearised and radially local drift equation can be obtained that depends only on three phase-space variables, namely the toroidal angle ϕ, the poloidal angle θ and the pitch angle $p = v_\parallel/v$.

In this approach the obtained solution is independent of v meaning that the integral $\int \ldots v dv$ can be dragged out and carried out later. The result is the so-called *mono-energetic* solution of the transport coefficients. Moreover, this solution depends only on three dimensionless parameters which characterise the plasma, namely the toroidal magnetic flux ψ_t, the collisionality $\nu^* = \nu R_0/v\iota$ and the normalised $\mathbf{E} \times \mathbf{B}$ drift velocity $v_E^* = E_r/vB_0$. In order to describe an arbitrary plasma, it is therefore necessary to create a database of mono-energetic transport coefficients covering the range of these parameters. For any plasma in the considered magnetic equilibrium, the effective thermal transport coefficients can then be straightforwardly obtained by an energy convolution of the appropriate mono-energetic solution with the local Maxwell distribution.

However, already the solution of the mono-energetic transport coefficients within the reduced phase-space of the linearised DKE allows great insight into the transport properties of a stellarator device. As an example, the normalised mono-energetic diffusion coefficient of the W7-X standard configuration is shown in Fig. 2.2 as function of the collisionality. For comparison, and to stress the importance of neoclassical transport in stellarators, a tokamak case is shown. Several distinct transport regimes can be identified. In order from higher to lower collisionality, these are the *Pfirsch-Schlüter-*, *plateau-*, $1/\nu$- and $\sqrt{\nu}$-regime.

The parameter regime most relevant for a stellarator power plant is at high temperature which means low collisionality since $\nu^* \propto 1/T^2$. Of greatest interest are, therefore, the $1/\nu$- and $\sqrt{\nu}$-regime. In Fig. 2.2 the importance of these regimes become clear since the transport coefficients are much higher in those regimes. In the $1/\nu$-regime, trapped particles are less frequently detrapped at decreasing collisionality. As the trapped particles are less well confined than passing particles, the effective loss of particles and energy increases. In a tokamak the picture is reversed.
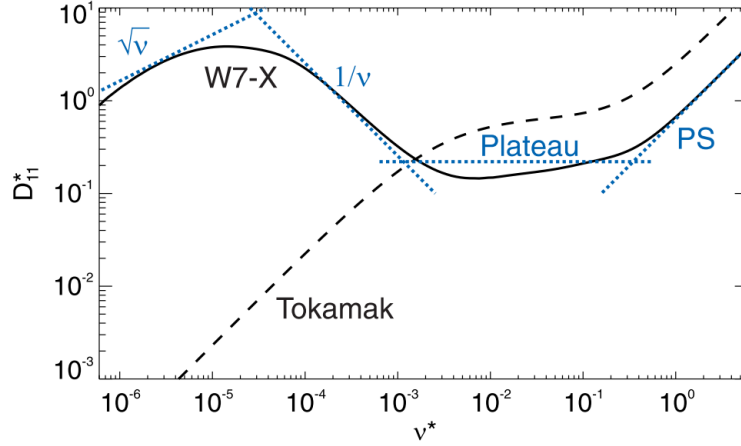
Figure 2.2: *The so-called 'mono-energetic' diffusion coefficient versus mono-energetic collisionality ν^* in the standard configuration of W7-X (bold) and a tokamak (dashed) with similar aspect ratios at finite electric field. The asymptotic regimes are indicated by dotted straight lines. The diffusivity has been normalized to the plateau value in a circular tokamak. The figure was kindly provided by C.D. Beidler, IPP.*

As the orbits of trapped particles are well confined in a tokamak, the reduction of collisions reduces the effective transport. Generally, the transport coefficients are very sensitive to the temperature. This can be made clear by taking the analytic limit of the $1/\nu$-regime [47] for the mono-energetic diffusion coefficient

$$D_{1/\nu} = \frac{4}{9\pi} v_D^2 \frac{(2\,\epsilon_{\mathrm{eff}})^{3/2}}{\nu} \propto \epsilon_{\mathrm{eff}}^{3/2} \frac{T^{7/2}}{nB^2R^2} \qquad (2.10)$$

where ϵ_{eff} is the effective helical ripple of the magnetic configuration. It is apparent from Eq. (2.10), that a high magnetic field strength and a large major radius is desired to reduce the neoclassical transport. Further, plasma operation favours high density and low temperature for optimal confinement. The effective helical ripple, however, is dependent on the details of the magnetic configuration and serves as a figure of merit for the number of trapped particles and their average radial drifts. Here, the optimisation of stellarator magnetic configurations comes into play, where one criterium is the minimisation of ϵ_{eff} to reduce the neoclassical transport by appropriately shaping the magnetic geometry.

It should be noted that the neoclassical transport is not intrinsically ambipolar such that the ambipolarity constraint on the plasma leads to a radial electric field E_r. The radial electric field, however, is in turn interconnected to the transport coefficients, especially for the $\sqrt{\nu}$-regime. In particular, at higher electric fields, the transition from the $1/\nu$ to the $\sqrt{\nu}$-regime is shifted to higher collisionality. When density and temperature are monotonically decreasing functions from the plasma centre to the edge with roughly equal values for electrons and ions, than the transport coefficients for the heavier ions are larger. Thus, ions would get lost more rapidly

31

than electrons and a negative electric field arises. A negative radial electric field ('negative' in the sense that it points inwards) reduces the ion transport coefficients due to the increasing poloidal drift. However, under certain circumstances E_r can be positive. For example, when the electron temperature is much higher than the ion temperature.

Especially the comparison of the stellarator mono-energetic diffusion coefficient to an 'equivalent' tokamak at low collisionality shows the importance of the neoclassical transport in stellarators. In the past great strides have been taken to understand and model neoclassical transport considering the numerous codes existing worldwide [44]. Consequently, the understanding of this issue led to the optimisation of magnetic configurations as discussed in chapter 1. The quality of the confinement can be assessed in terms of the confinement time τ_E and by comparing it to other helical devices employing for example an empirical scaling of the confinement time.

Empirical confinement time scalings have been widely used in the fusion community to assess and predict the confinement time τ_E in terms of global physics and engineering parameters. Such a scaling is obtained by performing a regression over a dataset of experimental results covering devices worldwide. The most recent scaling for the stellarator concept is the ISS04-scaling [48] obtained from the international stellarator-heliotron confinement database (ISHCDB)

$$\tau_E^{\text{ISS04}} = 0.465 \, a^{2.28} R^{0.64} P^{-0.61} \bar{n}_e^{0.54} B_t^{0.84} \iota_{2/3}^{0.41} \tag{2.11}$$

where a is the minor radius in m, R major radius in m, P heating power in MW, $\bar{n}_e$ the line-averaged density in 10^{20} m^{-3}, B_t the magnetic field strength on axis in T and ι the rotational transform at 2/3 of the minor radius. Fig. 2.3 shows the experimental data in relation to the ISS04-scaling.

Although modern stellarators, like W7-X, are optimised for reduced neoclassical transport, the improvement of the global confinement by such measures remains to be proven. First indications, however, could be obtained by analysing the dataset of the ISS04 scaling. Different magnetic configurations as represented by different devices seem to deviate somewhat from the overall regression. Indeed, different clusters have been identified within the dataset used for the ISS04 scaling [49]. Consequently, a configuration-dependent factor, f_{ren}, has been introduced to account for a general improvement or degradation with respect to the reference scaling which is defined as

$$\tau_E = f_{\text{ren}} \cdot \tau_E^{\text{ISS04}}. \tag{2.12}$$

One of the main goals of W7-X is to prove the concept of optimisation and its impact on the confinement time. The renormalisation factor f_{ren} can thus serve as a measure for the optimisation of the magnetic configuration. Apart from experimental investigations, transport codes can be employed to calculate the neoclassical transport for a specific magnetic configuration to obtain a predictive confinement time [50]. Comparing the confinement time obtained from such simulations to the value given by the direct extrapolation of the ISS04-scaling allows one to obtain a predictive confinement enhancement factor. For example, the prediction for the
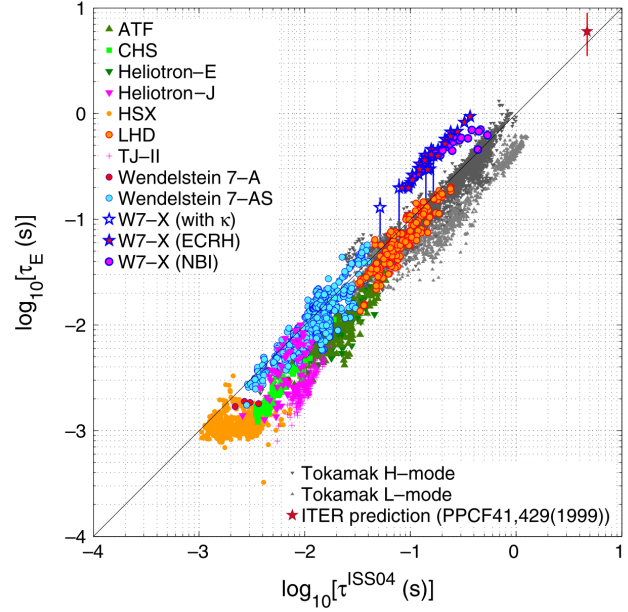
Figure 2.3: *Experimentally obtained energy confinement times versus the ISS04 scaling. The W7-X values stem from neoclassical transport predictions. For the representation of the the tokamak values the plasma current was rephrased as rotational transform. Figure from [49].*

confinement improvement of W7-X is expressed via the renormalisation factor as $f_{\rm ren} \approx 2$. This means, that the energy confinement time of W7-X should be two times higher than an extrapolation of the ISS04-scaling would suggest, see Fig. 2.3.

The concept of an empirical confinement time scaling is a practical tool and can straightforwardly be employed to estimate the expected confinement time scaling in a fusion power plant – an approach which has been used in many previous fusion reactor studies. Considering that the predictions for W7-X foresee a confinement improvement by a factor two with respect to the ISS04 scaling, a direct extrapolation to a HELIAS power plant would be very promising. Consequently, the question arises – especially in view of the different transport regimes at lower collisionality – if the promising confinement improvement as predicted for W7-X holds for a power-plant-sized device.

This question has been studied in detail in **Article I** of this thesis, see page 70. With a power balance model it has been shown that only slight variations of the confinement improvement with respect to the reference scaling (in terms of the renormalisation factor) have great impact on the size of a stellarator power plant. This approach also demonstrated that there are certain limits associated with the confinement. It has been found that a lower limit with $f_{\rm ren} = 0.5$ exists below which no stellarator power plant of reasonable size can be built. But there exist also upper limits at which a further confinement improvement is of not additional benefit in reducing the size of the machine. This is in the range of $f_{\rm ren} = 1.5 \ldots 1.7$ where the plasma reaches its β-limit and the plasma volume shrinks as parts of the flux

surfaces become stochastic.

Further in **Article I**, in order to estimate the confinement improvement for the reactor case, for the first time a neoclassical transport model has been thoroughly applied to a reactor-relevant magnetic configuration. For this purpose a database of mono-energetic transport coefficients was prepared for a reactor-relevant magnetic configuration using the DKES code. Then, the 1D transport code is able to solve the power balance for the electrons and ions. The neoclassical transport (in terms of energy fluxes) is obtained by a convolution of interpolated transport coefficients with the local plasma parameters taking into account all thermodynamic forces. In addition, an 'anomalous' energy flux is used to take into account other transport channels such as turbulence. For this 'anomalous' transport, an empirical description has been used which was derived from W7-AS experimental data, the predecessor of W7-X. In this model the anomalous energy diffusivity scales inversely with the density, $\chi^{\mathrm{ano}} \propto 1/n$ [51, 52].

It turns out that the renormalisation factor is continuously decreasing for an upscaling from W7-X to reactor-relevant sizes and reaches values around $f_{\mathrm{ren}} = 1.2\ldots1.3$. The most important conclusion is, that empirical confinement time scalings cannot be used to predict the confinement in stellarator power plants. While it is true that the transport regimes change, a sensitivity study of additional 'anomalous' transport at the edge showed, that the decrease of the renormalisation factor is rather robust. This is because the scaling approach itself is not valid. In scalings from today's experiments the heating power P is an independent external parameter. However, under reactor-relevant conditions this parameter is determined by the engineering and physics parameters and thus ceases to be independent. This change of paradigm is to a high degree responsible for the deviation of the renormalisation factor under reactor conditions from the values predicted for W7-X.

While the treatment of neoclassical transport is well understood and validated, other loss channels exist in a magnetised plasma which cause additional radial energy and particle fluxes, in particular turbulence. The nature of this transport and attempts at better modelling are introduced below.

2.3.2 Turbulent Transport

In stellarators, neoclassical transport is dominant in the plasma core due to the higher temperatures found there. At the plasma edge, however, the heat and particle fluxes are usually much higher than predicted by neoclassical theory. This additional transport is refereed to as anomalous transport, which especially in tokamaks is the dominating transport channel throughout the plasma cross-section. Many aspects of the anomalous transport are to date un-resolved but it is widely accepted that the anomalous transport originates from plasma *turbulence* which is driven by *microinstabilities* which tap the free energy of the plasma [53].

The general mechanism of microinstabilities can be explained by means of the electrostatic drift wave picture as illustrated in Fig. 2.4. Considering a magnetised

plasma with density gradient ∇n, small fluctuations of the density $\tilde{n}$ may continuously occur. Due to the high mobility of the electrons which directly react to such a perturbation, an electric potential of the form

$$\Phi = \frac{\tilde{n}}{n} \cdot \frac{e}{T} \tag{2.13}$$

arises according to the Boltzman distribution. The resulting electric field $\mathbf{E}$ associated with this potential is pointing from the region of increased electron density to the region of decreased density. If $\mathbf{E}$ has a component perpendicular to $\mathbf{B}$, the associated $\mathbf{E} \times \mathbf{B}$ drift will cause a density advection in direction of the density gradient. If the density and electric field are in phase, the net plasma transport is zero and the wave simply propagates through the plasma. However, if the perturbations are out of phase the particles are transported to the positive density perturbation essentially amplifying the wave, i.e. the drift wave becomes unstable.
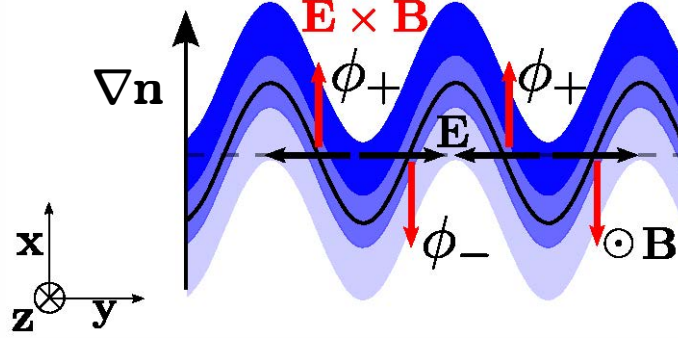
Figure 2.4: *Conceptual sketch of a drift wave in a magnetised plasma. The figure was kindly provided by J.H.E. Proll, IPP.*

There exist a number of conceptually similar instabilities which are driven unstable due to different mechanisms. Some of those which have been identified to contribute strongly to transport are e.g. *ion-temperature-gradient* instability (ITG), *electron-temperature-gradient* instability (ETG), or *trapped-particle-modes* (TPM).

Similar to the approach for neoclassical transport, a kinetic description can be found to treat the small-scale fluctuations which lead to turbulent transport. Starting from the general Boltzman equation one has to keep an ordering for fluctuations on the scale of the gyroradius and time derivatives on the scale of the gyrofrequency. Writing the distribution function as $f_a = f_{a0} + g_a$ and introducing the gyro-average at fixed guiding centre position $\langle \cdots \rangle_{\mathbf{R}}$, the *gyrokinetic equation* (GKE) can be derived

$$\frac{\partial g_a}{\partial t} + \left(v_\parallel \mathbf{b} + \mathbf{v}_D + \delta \mathbf{v}_D \right) \cdot \nabla \left(f_{a0} + g_a \right) - \frac{e}{T_a} \frac{\partial \langle \chi \rangle_{\mathbf{R}}}{\partial t} f_{a0} = \langle C_a(g_a) \rangle_{\mathbf{R}} \tag{2.14}$$

where $\chi = \delta \Phi - \mathbf{v} \cdot \delta \mathbf{A}$ is the gyrokinetic potential including electric and magnetic fluctuations.

A focal point of modern turbulent transport theory of magnetised plasmas is to solve the gyrokinetic equation. Several codes have been developed in recent

years taking up this task. However, to calculate macroscopic quantities from such simulations while maintaining the fine scales of the gyro-kinetic approach requires tremendous computational effort on the peta-flop scale. This is aggravated by the 3D geometry of stellarators which results in additional complexity compared to the axisymmetry of tokamaks. While linear and flux-tube simulations have been studied for some time, non-linear full-flux surface simulations are only now becoming possible [54, 55].

While the gyrokinetic approach in stellarators has so far been used to investigate the behaviour and characteristics of turbulence, the ultimate goal is not only to understand turbulent transport, but also to develop the capability to predict it. In particular, with the envisaged reduction of neoclassical transport in optimised stellarators, turbulence induced transport will play a significant role. However, in predictive transport simulations, as described above for **Article I**, anomalous transport has so far been treated superficially relying on a simple empirical regression. Although a stellarator gyrokinetic treatment is available, the required computational resources on the peta-flop scale are too demanding and unpractical to be integrated in transport simulations. Since transport simulations are an integral part of preparing and assessing experimental scenarios (e.g. for W7-X) and for predicting the performance of power plants, other means must be found to integrate gyrokinetic results in transport simulations.

A general way to achieve this, is by developing basic 1D models which capture the 3D features and characteristics of the turbulence. In other words, 3D results are parametrized in a physically meaningful way. Such an approach is common in the tokomak community. For the advanced stellarator line, this has been studied in **Article II**, page 81, for the first time. For this purpose, a set of stellarator gyrokinetic simulations were carried out and the results compared to experimental experience from W7-AS. Focus was thereby put on the ITG mode which is anticipated to be a main driver of heat flux in advanced stellarators [56]. For the study of the ITG mode, results have been used which stem from the 3D version of the widely employed GENE code [57, 58]. However, due to the computational limitations several effects were neglected by treating electrons adiabatically. Further, density gradient, electron temperature gradient, radial electric field and its shear were neglected.

In an attempt to judge the results obtained from non-linear full-flux surface simulations of W7-X, similar simulations have been carried out for the predecessor experiment W7-AS. The obtained heat flux is normalised to the gyro-Bohm value which represents diffusive transport based on the scale length of the ion gyroradius. Interestingly, it turned out that the heat flux density scales nearly identically in both devices as function of the normalised temperature gradient length $L_T = a \cdot (\nabla T/T)$. Such simulations have been carried out for W7-AS for the first time. The electrostatic potential fluctuations are rather localised on the outboard side of the device although the localisation is not as strong as in W7-X.

Both devices show the same critical gradient behaviour of the ITG heat flux, i.e. the heat flux density increases linearly with L_T above a certain threshold. The parametrisation of such a characteristic is straightforward employing two independ-

dent parameters. One parameter representing the critical threshold $(L_T)_{\text{crit}}$ and a second parameter which describes the slope at which the heat flux increases with L_T. The latter is in the tokamak community referred to as 'stiffness' since in tokamaks the heat flux increases very strongly above $(L_T)_{\text{crit}}$. Although stellarators have not such a pronounced increase of the heat flux, the terminology has been adopted here. The model itself is accordingly referred to as 'critical gradient model'. This physics motivated model was consequently implemented in the 1D transport code and integrated transport simulations of neoclassical and turbulent transport have been done based on experimental data of W7-AS. As the model is able to reproduce the W7-AS experimental values adequately it is concluded that – although a full validation is not yet possible – the model at least does not contradict the experiments.

In the next step, the critical gradient model has been employed for predictive transport simulations of W7-X. The important result from this simulation as shown in **Article II** is, that the confinement improvement for W7-X holds even for such a physics motivated turbulence model. However, a sensitivity analysis showed a strong dependence of the global confinement with respect to variations in the 'stiffness'. Finally the predictive simulations have been taken one step further for the stellarator reactor case. Even for the reactor case a suitable burn-point is found, although the critical gradient model leads to a strong reduction of the temperature in the edge region and a global confinement enhancement factor of $f_{\text{ren}} = 1.3$ is obtained.

Since the work done in **Article II** considers recent state-of-the-art gyrokinetic simulation results, not all relevant effects have been included yet, such as the density gradient and the radial electric field which are anticipated to reduce turbulent transport. It is expected that these effects will be included in the near future and experimental results of W7-X will allow a further test of the knowledge gained so far.

3 Design of next-step HELIAS Devices

The study of power generating reactor concepts has a long tradition in fusion research. This is due to the fact that fusion research is both goal- and project-oriented. Consequently, over the last 50 years, the prospects of fusion power plants, subject to a changing knowledge-base and expectations, were of great interest. In particular, reactor studies serve the purpose of revealing inconsistencies both in physics and technology assumptions. In this sense, reactor studies of fusion devices are especially important to identify and guide a critical research path including the preparation of dedicated experiments and simulations as well as the development of relevant technologies.

For the advanced stellarator line, initial reactor studies have been carried out in the nineties with focus on individual point studies. Here, a new, more systematic approach will be introduced with the aim of finding an optimal reactor design within a multi-dimensional parameter space. Moreover, this approach will not only be used for HELIAS power-plant studies, but also for an intermediate-step stellarator which may follow W7-X. Before proceeding to these studies, the functional principle and the key components of a stellarator power plant are briefly introduced which define technological constraints and boundary conditions. This illustrates also the complexity of reactor studies as, apart from physics considerations, detailed technology and engineering considerations need to be kept in mind. Consequently, a broad overview and knowledge-base is required to carry out reactor studies and the complexity of different aspects can sometimes lead to non-intuitive results.

A conceptual engineering design of a HELIAS power plant as well as a conceptual sketch of the most important technical components can be seen in Fig. 3.1. In the centre of the toroidal vessel the plasma is confined by the magnetic field. For the D-T reaction, the produced fusion power comes in form of energetic alpha particles and neutrons. The alpha particles heat the plasma and sustain the burn conditions while the neutrons directly leave the plasma and are absorbed in the blanket which surrounds the plasma vessel. The neutrons not only deposit their energy in the blanket but also fuse with lithium in order to produce tritium. This is necessary as
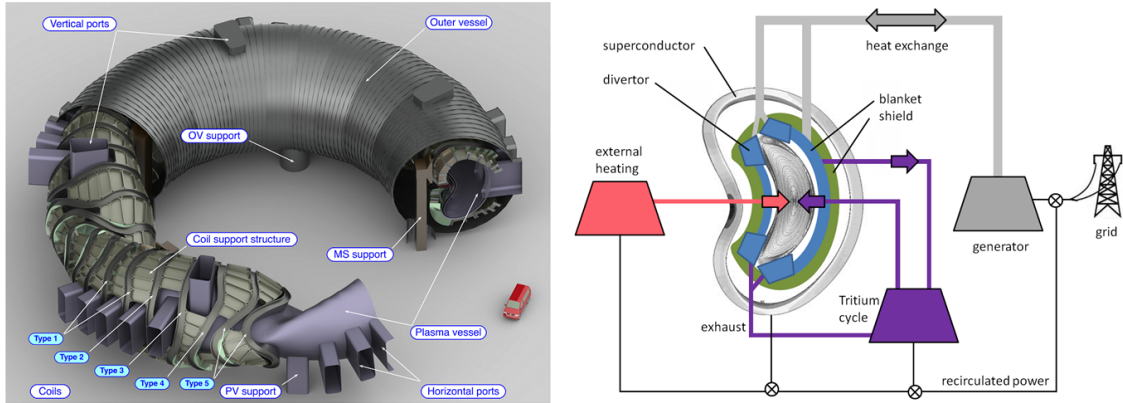
Figure 3.1: *Illustration of the HELIAS 5-B engineering study [59] (left) and conceptual sketch of the radial build of the power plant core and the main facilities required for operation (right).*

tritium has a half life of only 12.5 years and the fusion power plant must produce tritium self-sufficiently. To protect the superconducting magnets from the residual neutron flux, a shield adjacent to the blanket is required. Additionally, the divertor, a component responsible for the controlled energy and particle exhaust, is needed. With an active cooling system the heat deposited in blanket and divertor must be extracted and converted to electricity. Before the electricity can be provided to the national grid some of the electrical power needs to be recirculated in order to operate all power plant facilities. Further, due to the radioactive nature of the tritium, a closed cycle is needed that brings the tritium from the blanket and divertor to the tritium facility. This facility purifies the exhaust to streams of deuterium and tritium which can then be re-injected into the plasma as fuel. Besides that, a reactor needs an external heating source for the start-up phase of the plasma and for control. The components of the reactor are held in place by a strong support structure enclosed by the outer vessel.

3.1 Engineering Characteristics and Boundary Conditions

Modular Coils

In an advanced stellarator the rotational transform of the 3D magnetic topology is realised by a so-called modular coil set. Modular coils are discrete non-planar 'toroidal' field coils which are capable of producing magnetic fields traditionally created with various combinations of toroidal, helical and vertical field coils. In order to minimise the number of differently shaped coil types, an advanced stellarator configuration consists of identical modules which are point-symmetric in themselves. In the past, different numbers of modules have been investigated, but the current research of advanced stellarators focuses on 5-field periods. This is a compromise between the more compact 4-periodic (having poorer physics qualities) and the larger

configurations with higher aspect ratio.

Due to the complex 3D shaping of the coils, the current in the coils creates both a toroidal and a poloidal magnetic field component. Thus, large poloidal field coils as used in tokamaks can be avoided with the great advantage that the corresponding large forces which would have arisen between poloidal and toroidal field coils can be avoided. But nonetheless, large forces remain in-between the toroidal field coils which require a strong support structure. In stellarators the force distribution is quite complex due to the 3D shaping of the coils. In contrast to tokamaks, there are forces which are directed radial inwards and outwards, but also lateral forces.

Moreover, the modular coil set itself allows the realisation of a large variety of magnetic configurations as they are able not only to mimic a superposition of fields with different helicities but also a toroidal field mirror term. With this flexibility, optimised stellarator magnetic configurations can be realised. In particular, they can be optimised with respect to reactor-relevant criteria [25], which is a topic of active research.

Due to the required high field strength for the plasma confinement, the coils must maintain a large current. In order to realise this, the coils must be superconducting using low-temperature superconducting material (LTS) such as niobium-titanium (NbTi) as used in W7-X. To achieve even higher field strengths, modern niobium-tin (Nb_3Sn) can be used as for ITER. Both require cooling to 4.2K to be superconducting. Due to the large fields (up to 13 T at the surface of the coil), large forces act on the reactor structure which are on the order of several hundred MPa. Therefore, a robust support structure is required to compensate the magnetic forces. Due to their size, shape and material, the modular coils have significant impact on the total costs of a stellarator reactor. In the future, also high-temperature superconductors may play a role which have undergone a very rapid advancement in the recent years.

Blanket and Shield

The blanket and shield are critical components of a fusion reactor. In particular, the blanket must breed the hydrogen isotope tritium from lithium to serve as fuel for the power plant. Blanket and shield are situated between the first wall and the superconducting magnets. Because of the high fusion power output of a reactor, the blanket is exposed to strong radiation, both from energetic photons and neutrons. The blanket must withstand the resulting thermal stresses reliably for long time periods to ensure economic operation of a plant and at the same time fulfill three major functions. It must shield the superconducting coils outside the blanket, convert the fusion energy into heat energy and breed tritium.

In the European fusion program different blanket concepts are considered. Due to its low space requirements the Helium Cooled Pebble Bed (HCPB) [60] design is the most favourable blanket concept for a HELIAS reactor. The space between the plasma and the coils, where the blanket is located, is very limited and puts constraints on the aspect ratio and the size of a stellarator. Therefore it is necessary

to minimise the thickness of blanket and shield as much as reasonably possible. The HCPB is introduced here as reference, but a final decision on a stellarator-specific blanket concept can only made after a complete neutronic analysis and experiments, as e.g. planned for ITER. Work towards the neutronic analysis of a HELIAS has recently been started, see **Article VII**. For this purpose a 3D neutron source was developed, validated and implemented in the widely used Monte Carlo neutron transport code MCNP [61].

The HCPB has originally been developed for tokamak power reactors but it is currently anticipated that the technology can be readily adapted to stellarators. The breeding material is a Li_4SiO_4 ceramic enriched with ^6Li together with beryllium pebbles which serve as an efficient neutron multiplier providing a high tritium breeding ratio. The blanket is organised in segments with a cross-section of about 0.85 m^2.

The cooling system uses helium with an inlet temperature of about 300°C and an outlet temperature of 500°C at about 8 MPa pressure using 'EUROFER' (a ferritic martensitic steel) as structural material. With a conventional Rankine cycle, one can expect a thermal power conversion efficiency of about 40%. An independent helium purge flow loop at low pressure (about $0.1 - 0.2$ MPa) is used to extract the tritium from the ceramic breeder and from the beryllium. Due to the high aspect ratio, the average neutron wall load in a HELIAS is about half of that of a tokamak of the same fusion power. This also means that the power density in the blanket is about a factor two lower. Without changing the blanket design, the flow velocity of the coolant could be reduced, which would reduce the associated pumping power considerably. This advantage is somewhat reduced by the fact that the total blanket volume can be up to a factor two higher in a HELIAS increasing the required pumping power somewhat. This is due to the difference in aspect ratio. As the HELIAS has a higher aspect ratio, the surface area which needs to be covered by a blanket is higher. As the radial extent of the blanket is fixed, the blanket volume increases compared to a tokamak.

Similar to the modular coils, the blanket and shield are massive components consisting of high-technology parts. Consequently, they also contribute significantly to the reactor costs. Additionally, due to the use of materials like lithium and beryllium, and the radioactive activation with time, the blanket will have an impact on safety considerations.

Divertor

To ensure a steady-state operation of a fusion reactor, the accumulation of the fusion ash – helium – and first wall impurities must be prevented. This is done with a so-called divertor, which consists of special plates which intersect the plasma in a controlled way. The main function of the divertor is the removal of particles and the radial transport of heat out of the plasma chamber. The divertor plates, therefore, need to be actively cooled. Reactor-suitable pumps [62] will have to be

located behind the plates to remove the neutral particles.

For the placement of the divertor plates in a 3D stellarator, the inherent magnetic field structure is exploited. In a HELIAS configuration with low shear, i.e. small $d\iota/dr$, the rational surface at the edge with $\iota = 5/5$ produces five large magnetic islands. These islands provide an intrinsic separatrix at the edge. These naturally occurring magnetic island chains can be exploited by placing independent divertor plates symmetrically at the top and bottom of each field period [63]. These intersect the magnetic islands at the edge in order to efficiently control the particle and energy exhaust. The island divertor concept was successfully tested in Wendelstein 7-AS [64] and seems to be a promising exhaust concept for a HELIAS reactor. As such it will be further investigated in Wendelstein 7-X.

However, at finite β, plasma currents have an impact on the magnetic configuration and thus may shift or deform the islands at the edge. Therefore, these currents (e.g. bootstrap and Pfirsch-Schlüter currents) are minimised during the optimisation of the magnetic configuration. Although the island divertor concept provides a very broad flux expansion due to the very long connection lengths (an order of magnitude longer than in tokamaks), the total effective wetted area is only 2 to 3 times higher than in tokamaks due to the discontinuity of the divertor plates. If the heat load limit is strictly set to 5 MW/m^2, most of the power must be radiated before reaching the divertor, including radiation in the plasma centre and near the separatrix, meaning that (partial) detachment is required [65].

Due to the direct interaction with the plasma, the divertor must withstand very high heat loads in continuous operation. In addition, with the high neutron fluence, the divertor must be replaced on a fixed maintenance schedule. The question of suitable materials and divertor concepts is a topic of ongoing research. In fact, the issue of plasma exhaust is one of the greatest challenges in fusion research.

Plasma Heating

In a commercial fusion reactor it is envisaged that the plasma is self-sustained by the energy released from the fusion reaction for which charged alpha particles carry 3.5 MeV and thus one fifth of the released energy. The energy is transferred to the background plasma by collisions while the neutrons are unaffected by the magnetic field and go directly to the blanket. When the power generated and transferred from the alpha particles is in balance with the power losses of the plasma, the machine is in equilibrium and the plasma is regarded as 'ignited'.

A figure-of-merit for the ignition of a fusion power plant is the fusion gain which is the ratio of the produced fusion power to the externally supplied heating power

$$Q = \frac{P_{\text{fus}}}{P_{\text{heat,ex}}}. \tag{3.1}$$

The requirement for a fusion power plant is thus to operate at $Q \gg 1$, i.e. on

the order of $Q \sim 30 \ldots 50$. If the plasma is completely self-sustained by the alpha heating, Q becomes infinite.

There are two main reasons why a system for external heating is required. The first is, that for the start-up of the device external heating is required to bring a pre-filled gas to plasma conditions and finally to the temperatures where the fusion power starts and ultimately takes over. Depending on the amount and species of impurities present in the start-up phase of the plasma, heating on the order of $50 \ldots 100$ MW is required to overcome the loss channels such as radiation, for a detailed discussion see **Article V**. The second reason is that one can also envisage operation which is not completely ignited, i.e. constant external heating is provided to maintain the plasma conditions.

It should be noted that there is some difference between the heating scheme in stellarators and in tokamaks. Tokamaks require a high plasma current for operation. Thus, for tokamaks the heating system serves also as a means to drive current in the plasma. For this purpose neutral beam injection is employed which has a high efficiency in terms of how much power is required to drive a certain amount of current. But tokamaks also require micro-wave heating to control the plasma, i.e. stabilise occurring instabilities such as neoclassical tearing modes, an instability which degrades confinement and can lead to disruptions.

In a stellarator, plasma current should be avoided as discussed in the last chapter. Therefore stellarators favour electron cyclotron resonance heating (ECRH). ECRH can reach a very high power density meaning that only small openings to the plasma chamber are required. This helps also to protect the sensible components of the heating system from neutrons. In particular, a remote steering launcher is an option for a stellarator power plant. Further, ECRH is already in existence and is directly scalable to power plant scenarios.

For this purpose one uses so-called gyrotrons, which are designed to emit microwaves which resonantly couple to the electron cyclotron frequency for a specific value of the magnetic field. This provides a localised resonance in the plasma leading to a very efficient absorption of electromagnetic waves. The heated electrons are then thermalised within the plasma due to collisions, heating the ions in the process.

Current gyrotrons as employed for W7-X can produce micro-waves with a power of about 1 MW (up to 30 minutes), which can be easily scaled by combining an array of gyrotrons. Ten such gyrotrons will be installed at W7-X with the possibility for later upgrades.

Balance of Plant

Along with the main heat generating system, a fusion plant needs, like every power plant, components for power conversion and distribution, generally known as balance of plant (BOP). Often given little attention, the balance of plant plays an important role for the reliable operation of a power plant. The objectives that must be achieved

by the balance of plant are an efficient conversion of thermal power to electricity, reliable supply of electricity to the power plant components and effective operation of all auxiliary systems. To make a fusion power plant economical the balance of plant systems must work with high efficiency and availability at low construction costs. Conceptually the design of the balance of plant of a fusion power plant is similar to those of conventional power plants although the use of a different coolant leads to certain changes. Due to its better safety properties gaseous helium is foreseen as coolant for the blanket and divertor in combination with a Rankine or Brayton cycle. This requires a high amount of pumping power but at the same time provides a higher thermal conversion efficiency.

Safety

The safety of future fusion power plants has been assessed in many studies. In the European Power Plant Conceptual Study (PPCS) [66], the safety properties of four tokamak models are investigated applying different levels of extrapolation to both the assumed physics and technology properties of the plants. Important findings of the study are that a total loss of coolant would not result in a melting of components such as the plasma facing wall. Furthermore, in-plant energies are not sufficient to cause accidents which result in radiation doses to the public which would require evacuation. Finally, all activated material could be either recycled in a new power plant or regarded as non-radioactive and returned to the general materials cycle after several decades of decay. Studies for the ARIES compact stellarator come essentially to the same conclusions [67]. What up to now has not been considered in any relevant detail are the possible differences between tokamaks and stellarators with regard to the physics or technology properties. From the physics point of view, the favourable stability properties of stellarators near operational boundaries and the absence of disruptions could also turn out to be an advantage with regard to safety. From the technology point of view the more complex in-vessel geometry and the resulting blanket and neutron shield requirements have to be considered when comparing stellarators and tokamaks. First detailed studies of the distribution of neutrons in a 3D HELIAS geometry and their interaction with the blanket and shield have just recently started, see **Article VII**.

3.2 Systemic Approach for the Integrated Concept Development of next-step Stellarator Devices

As may already be grasped from the physics and engineering considerations described so far, even the conceptual design of a power-plant-like fusion device is a complex and demanding task. In the past, stellarator reactor studies considered only individual design points with focus on engineering aspects of the actual confinement device [68, 69]. While these studies are important for the investigated aspects, many physics aspects were treated only superficially. Moreover, due to the focus on individual designs, it is not possible to obtain a broader overview in particular with respect to parameter variations and uncertainties.

In order to overcome these drawbacks, this work goes a different, more systematic way, where not only specific aspects of next-step stellarator devices are examined, but rather they are treated as a complete system. Consequently, this work has the aspiration to develop concepts of next-step stellarator systems in an integrated manner, i.e. consistently combining physics, engineering and economic considerations, in order to produce conceptual designs and assess uncertainties which will guide future research.

In order to facilitate such studies, so-called 'systems codes' are often employed as valuable tools for the design process which are explained next followed by the applications to next-step stellarators.

3.2.1 Systems Codes

Systems codes, also known as design codes, are simplified yet comprehensive models of a complete fusion facility. Such codes bring together physics, engineering and economic aspects allowing development of self-consistent design points. Furthermore, the sensitivity and robustness of such design points can be tested against variations of important parameters. With this approach especially critical development directions for physics scenarios or technology advancements can be identified necessary to guide future research directions. Following this strategy, dedicated experiments in today's devices may be performed as well as state-of-the-art simulations. With the obtained results, systems codes models can be further upgraded to improve the overall modelling. This is a long-term iterative process as conceptually outlined in **Article III**, page 94, of this thesis and shown here in Fig. 3.2.

Systems codes are commonly applied in the tokamak community, especially with respect to a tokamak demonstration fusion power plant, also known as 'DEMO', for which many studies are ongoing [70]. Considering confinement concepts with a 3D topology, similar studies have been done for the heliotron concept [71]. However, so far no systems code existed capable of modelling a helical-axis advanced stellarator (HELIAS). Since the development of a systems code from scratch would take several man-years and is thus beyond the scope of a PhD-thesis, it was decided to review an existing, tokamak systems code – PROCESS [72] – and develop and implement
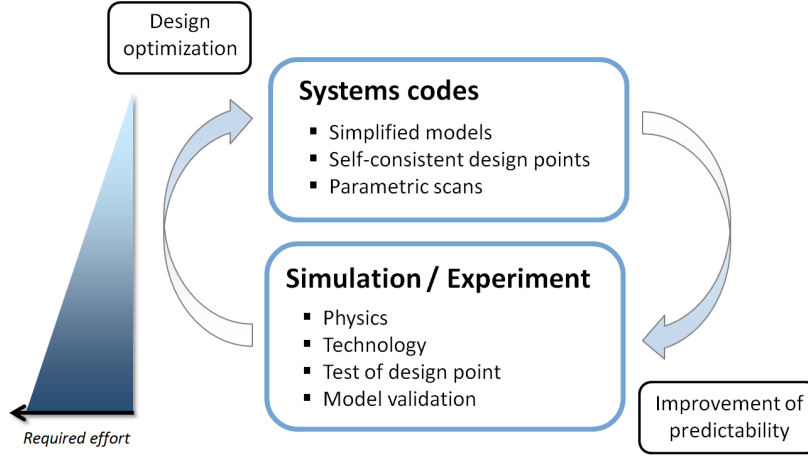
Figure 3.2: *Concept of systems codes and their interaction with detailed simulations and experiments. The left scale illustrates the required effort (in terms of complexity and time) to carry out the individual tasks.*

stellarator-specific models into this framework. This strategy had the additional advantage, that both the tokamak and stellarator concepts could be compared within a common code framework.

PROCESS is a well-established, partly modular, European tokamak systems code that gained maturity through years of development and application. A solver based on Lagrangian multipliers is employed within PROCESS to allow for design optimisation with respect to the descriptive models and constraints. This is done by minimising (or maximising) a user-defined figure-of-merit consistent with the relevant inputs (iteration variables, constraint equations, and limits). The framework of PROCESS consists of detailed, well-developed plasma physics, engineering and economic models allowing for a broad scope of application.

In a first step, the systems code PROCESS has been assessed to identify changes necessary to accommodate helical-axis advanced stellarators. Based on this assessment, HELIAS-specific models have been developed as documented in **Article III** of this thesis designed for a systems code approach consisting of three major models:

- First, a geometry model to describe the plasma shape (flux surfaces) based on Fourier coefficients. In position-space the geometry is described by cylindrical coordinates, which have been decomposed in a Fourier series allowing modelling of any arbitrary 3D toroidal surface. Such a formulation allows one to accurately calculate the important geometrical parameters such as plasma volume, surface area and cross-section which have direct impact on e.g. fusion power or neutron wall load. Moreover, it is possible to scale both the minor and major plasma radius by scaling of the corresponding Fourier coefficients making the model very flexible and suitable for a systems code approach.

- Second, a basic island divertor model for the energy exhaust is derived from

geometrical considerations, in addition assuming cross-field transport and radiation at the X-point. The model is of analytic nature and combines physics and engineering relations. From the engineering side, the length of the divertor plate is estimated by considering how a helical field line in the scrape-off layer just passes the divertor plate on the inner side but eventually hits the divertor on the outer side where the radial distance is given by the size of the magnetic island. The broadening of the heat along such a field line is estimated by assuming diffusive cross field transport where the time it takes to reach the divertor is determined by the connection length.

- And third, a coil model which calculates the maximum field at the coils, the total stored magnetic energy, and the dimensions of the winding pack has been developed based on the sophisticated HELIAS 5-B [59] reactor design. For this purpose scaling relations and analytic inductance and field calculations are employed in combination with a critical current density scaling of the superconducting material used, i.e. scalings for both NbTi and Nb_3Sn have been implemented.

It should be noted, that **Article III** represents the very first work where HELIAS-specific systems code models have been developed. Since the aim of this approach was not only to simulate individual design points but also to carry out parameter variations over wide ranges, a consequent requirement for the developed models was to retain low calculation times (in comparison to more specific codes which require hundreds of CPU-hours for single runs). A particular difficulty has therefore been the reduction of the 3D complexity of the stellarator to lower dimensions in order to shorten calculation times without sacrificing too much accuracy. Although a PROCESS run for a single stellarator design point takes a few minutes compared to a few seconds for a tokamak, this time frame is entirely sufficient for the envisaged applications.

However, the systems code PROCESS employs empirical confinement time scalings to extrapolate the confinement time, i.e. to describe the radial transport of energy in power plant sized devices. But as already discussed in chapter 2 and **Article I**, empirical confinement time scalings are not sufficient to confidently predict the confinement properties of a HELIAS power plant. Therefore, in addition to the systems code approach, a 1D transport code (as introduced in chapter 2) is employed to calculate and estimate the neoclassical and turbulent transport and thus provide a more sophisticated estimation of the confinement in the systems studies.

The transport simulations could not be directly coupled to the systems codes since the transport simulations can be very time consuming. Therefore, the transport simulations have been done for a representative design point in the envisaged engineering parameter regime. Essentially, the simulations provide an energy confinement time τ_E. But in order to use this result for the systems studies it is convenient to rephrase it as an renormalisation factor f_{ren} with respect to the ISS04 scaling. This 'offset' to the scaling can be directly implemented for the systems studies. Strictly speaking, the obtained renormalisation factor would only be valid for the simulated

design point. However, in order to be able to effectively use the systems code, the assumption has been made, that the renormalisation factor is valid in the parameter regime around this reference point. Thus, the empirical confinement time scaling could be used without the need to carry out transport simulations for every design point. Still, a few iterations back and forth between the systems studies and the transport simulations were required to arrive at a consistent design.

The models described above have been successfully implemented in the systems code PROCESS and, subsequently, a verification study has been carried out as described in detail in **Article IV**, see page 103. First, W7-X was modeled within the stellarator-representation of PROCESS and compared to the real machine parameters which showed good agreement of the important parameters within 10% deviation. Secondly, a tokamak DEMO case has been modeled by the 3D stellarator modules where the coil module has been adopted using ITER parameters as basis. Moreover, the island divertor model was modified to take into account the tokamak symmetry and continuous divertor plates. The subsequent modelling of a tokamak DEMO using the stellarator modules showed good agreement to the original PROCESS tokamak models with differences of maximum 10%.

With this tool available and given confidence from the verification exercises, stellarator systems studies have been conducted. Moreover, a direct comparison between a tokamak and a stellarator power plant design has been carried out.

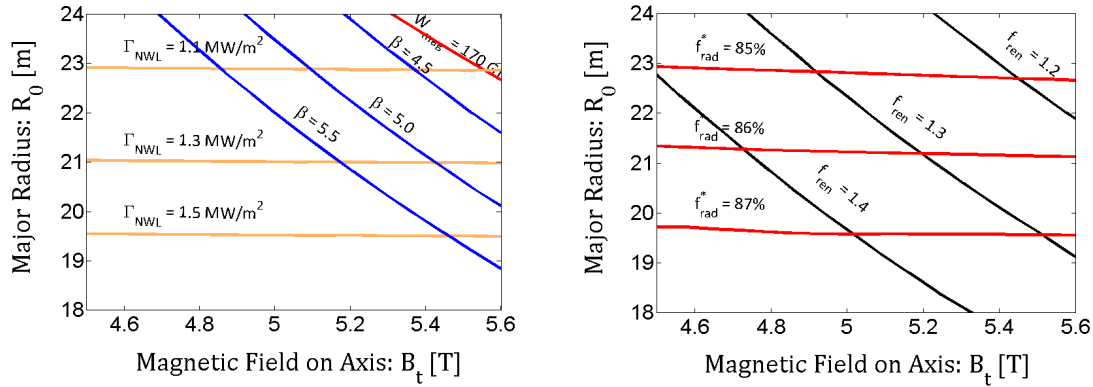### 3.2.2 Design Window for a HELIAS Power Plant

Systems Studies

In **Article V**, page 107, a systems code approach has been applied for the helical-axis advanced stellarator line with the aim of defining the accessible design window for a power-plant-sized HELIAS. For this purpose the stellarator version of PROCESS (v. 389) described above is used. However, before such a study can be undertaken, several general assumptions must be made about the constraints and goals of such a device. These are described in detail in **Article V**, but the most important shall be summarised here.

Most notably, transport simulations, as discussed in chapter 2, were carried out separately using dedicated codes to serve as input for the systems studies. In agreement with **Article I**, the confinement enhancement factor was limited to $f_{\mathrm{ren}} \leq 1.5$ and the volume-averaged temperature fixed to $\langle T_i \rangle \approx \langle T_e \rangle = 7$ keV. In order to estimate the helium 'ash' in the plasma, first a source profile has been defined by taking the alpha particle birth profile and slowing down on the flux surface (i.e. neglecting losses of alpha particles). Secondly, using the neoclassical transport approach as discussed before employing DKES, the particle flux of the helium ash is calculated and in combination with the source profile a helium density profile is obtained. This leads to a 10% concentration of helium 'ash' in the plasma which reduces the fusion power due to fuel dilution.

From the engineering side, the aspect ratio was fixed to $A = 12$ to provide enough space for blanket and shield between plasma and coils. For simplicity, the blanket has been modelled according to [73] with a blanket thickness of 0.8 m. Helium was chosen as coolant for blanket and divertor as described in the last section leading to a pumping power of $P_{\text{pump}} = 200$ MW and a thermal conversion efficiency of $\eta_{th} = 0.4$.

Although a systems code provides comprehensive modelling of a fusion power plant, such a code comprises hundreds of different parameters. Therefore, a particular difficulty lies in the creation of a suitable input file which needs to specify equations, constraints, boundary conditions and a high number of input parameters across many systems. Moreover, PROCESS intrinsically allows only a parameter scan in one dimension. In order to allow for an N-dimensional scan, a utility was developed in the course of this thesis[1].

For the engineering parameter variation, the major radius and the magnetic field strength on-axis were varied over a wide range with the fixed goal to achieve 1 GW net electric power similar to other base-load power plant concepts. The results of this systems study are shown in Fig. 3.3.

Figure 3.3: *Design window analysis for a HELIAS power plant device with 10% helium ash concentration constrained to achieve $P_{\text{net,el}} = 1$ GW = const. showing isocontours of the volume-averaged thermal plasma β (blue), the average neutron wall-load (orange), and the stored magnetic energy (red) [left]. Complementary are shown the isocontours of the confinement enhancement factor f_{ren} (black) and the radiation fraction of the power crossing the separatix to keep the peak heat load on the divertor plates at 5 MW/m^2 (red) [right].*

The accessible design window depends strongly on the envisaged beta-limit and suggest that the beta-limit should be investigated experimentally. The average neutron wall load on the other hand does not limit the design of a HELIAS device as it does not exceed 1.5 MW/m^2 even at smaller machine sizes due to the high aspect

---

[1] After successfully placing a project within the German DAAD-Rise program, I obtained funding for an American student, S.B. Torrisi, who programmed the N-dimensional parameter scanner [74] under my supervision and in collaboration with CCFE.

ratio and surface area. The required confinement enhancement factor with respect to the ISS04 scaling lies between $f_{\mathrm{ren}} = 1.2 - 1.3$ for machines of every size at high field. This is in line with results from detailed 1D transport simulations; see **Article I**. In order to control the power exhaust of such a HELIAS device, $85 - 87\%$ of the power must be radiated to protect the divertor and ensure a peak heat load limit of $5\ \mathrm{MW/m^2}$. This may be considered an upper limit as so far only bremsstrahlung and synchrotron radiation were considered in the plasma core, but additional power could potentially be radiated from the core if impurities were to be injected. Even under the most conservative assumptions with $\beta = 4.5\%$ and 10% helium ash, a feasible design window emerges around $R = 22$ m, $B_t = 5.5$ T. But if a scenario with effective helium exhaust (e.g. through a positive electric field by means of a hollow density profile [75]) can be found and/or the beta-limit can be verified to be higher, the design window drastically increases opening many more options for potential devices and robust design points.

Beyond the design-window analysis, it was shown that single design points can be further studied using plasma operation contour analysis (POPCON) [76]. Such a detailed study of a single design point allows, for example, the determination of the external heating power that is required to reach the ignition state. Furthermore, the POPCON analysis can be used for sensitivity studies. As examples, the impact of the confinement enhancement and the tungsten impurity concentration on the ignition window were additionally studied in **Article V**. It became clear that a higher confinement strongly reduces the required external heating power while increasing the available ignition window. In contrast, an intrinsic impurity concentration of tungsten would make the start-up very difficult as tungsten has a strong radiation maximum at around 2 keV while the ignition region at higher temperatures is not affected very much.

Economic Comparison to Tokamaks

In the second part of **Article V**, the stellarator has been compared to the tokamak concept. A tokamak design point was chosen with the same set of goals and assumptions and the total construction costs compared. One of the most important findings is that the costs for a stellarator power plant are on the same level as the costs for an equivalent tokamak; see Fig. 3.6 in the next section. Although the stellarator is a larger device in terms of its dimensions, the masses for the different components are comparable to those of a compact tokamak leading to similar construction costs in this analysis. A detailed cost break-down and comparison of a tokamak and stellarator design point have shown that the costs of the tokamak magnet system are higher due to the high costs for the poloidal field coil system and the transformer. The stored magnetic energy of a stellarator is only a fraction of that of a tokamak. Also, the equipment costs for the tokamak are higher than for the stellarator as the tokamak requires current drive to operate in steady-state which is more cost intensive.

3.2.3 Options for an Intermediate-Step Burning Plasma Stellarator

With the definition of the design window for a HELIAS power plant and indications for the economic viability of the concept in comparison to tokamks, the next question is: 'How close are we to such a device from today's point of view?' and 'What steps are necessary to build such a device?'

In other words, in order to advance HELIAS reactor studies, it is necessary to assess the gaps which exist in physics knowledge and available technology from today's point of view. The identification of such gaps is important in order to be able to make decisions about the focus of stellarator research in the near future. In particular, the development of a qualified research strategy depends on such an assessment and has been studied in **Article VI**, page 117, of this thesis.

Step-Ladder Approach

Indicative representations for the assessment of physics and engineering gaps are so-called 'step-ladder' plots that show the relation of today's experiments to power-plant-like devices in terms of the governing dimensionless parameters. For the definition of the leading dimensionless physics quantities which characterise a magnetised plasma, dimensional analysis [77, 78] or transformation invariance [79] can be employed. Consequently, one obtains the three commonly employed dimensionless plasma parameters which are the normalised plasma pressure β, the normalised gyroradius ρ^* and the collisionality ν^*, defined as:

$$\beta = 2\mu_0 \frac{p}{B_t^2}, \qquad \rho^* = \frac{v_i m_i}{eBa}, \qquad \nu^* = \frac{R_0 \nu_{th}}{v_{th} t}, \tag{3.2}$$

where a is the minor radius, R_0 the major radius, p the plasma pressure, v_{th} the thermal velocity and ν_{th} the thermal collision frequency.

In order to measure the reactor relevance of existing and planned magnetic confinement devices, it is convenient to rephrase the leading operation parameters of a device in so-called 'dimensionless' (omitting dimensional constants) engineering parameters $B^* \propto Ba^{5/4}$, $P^* \propto Pa^{3/4}$ and $n^* \propto na^{3/4}/B$ [80]. Considering the Kadomtsev similarity constraints [77], B^*, P^* and n^* must remain constant in differently sized devices, in order to obtain the same dimensionless plasma physics parameters. Thus, the formulation of such dimensionless engineering parameters allows one to link both the governing dimensionless physics quantities and the machine parameters. This 'link' is established using empirical scaling laws which can be expressed not only as a function $\tau_E = \tau_E(R, a, B, P, n, t)$, but also as $\tau_E = \tau_E(\nu^*, \rho^*, \beta)$.

The combined engineering-physics parameter view can be seen in Fig. 3.4, where the left side shows the step-ladder plot for ASDEX Upgrade, JET and ITER as adapted from [80]. The right side of Fig. 3.4 reflects the same approach for the HELIAS line employing the scaling law ISS04 for the energy confinement time τ_E [48].
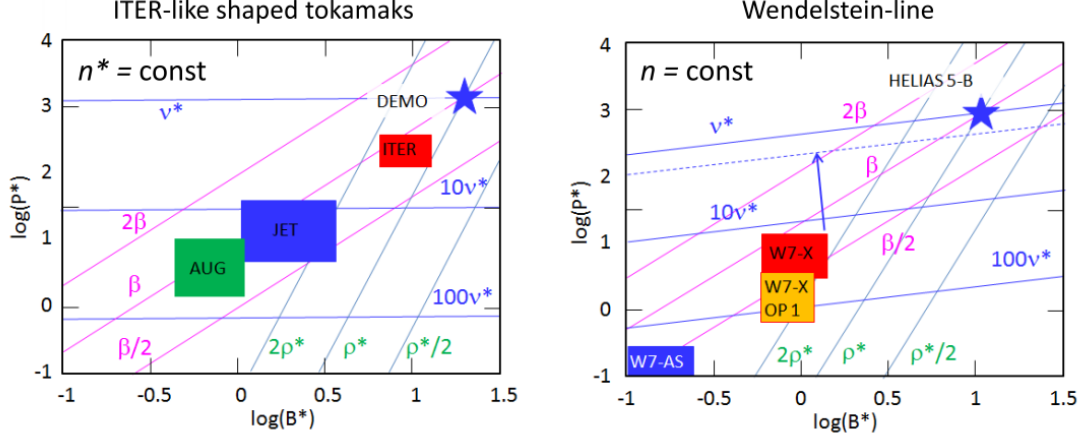
Figure 3.4: *Step-ladder plots for ITER-like tokamaks (left) and the HELIAS line (right). The left side shows operation windows of ASDEX Upgrade (AUG), JET and ITER in dimensionless engineering parameters with isocontours of dimensionless physics parameters at constant n^*. The right side shows the same for the HELIAS line. The W7-X operation windows refer to operation phase 1 (OP1) and 2 (OP2) for X2 and O2 heating, respectively, where n^* has been adapted to ECH cut-off densities and 'HELIAS 5-B' is an engineering-based reactor study [59].*

Comparing the step-ladder plot of ITER-like tokamaks with the HELIAS devices, indicates that the physics basis of advanced stellarators is less well covered than that of tokamaks. In physics dimensionless parameters, the gap from existent devices to burning plasmas is clearly evident. In comparison to tokamaks, the change both in B^*, P^* and n^* as well as in ρ^* and ν^* is more substantial for the discussed stellarators. This fact reflects, that the degree of maturity is more advanced for tokamaks. In particular, the ITER device plays a key role in the advancement of the tokamak-line.

The analysis of required control parameters in figures of dimensionless variables shows that the step from W7-X to a HELIAS reactor would be very large in the dimensionless engineering and physics quantities. In particular, simultaneous attainment of ν^*, ρ^* and β of an envisaged reactor working point cannot be achieved in W7-X.

Apart from the dimensionless physics quantities shown, other global parameters can be investigated which are not necessarily dimensionless but which can be used to characterise the step-size to reactor conditions. For example, the parameter P/R [81] which is the ratio of the power losses to the major radius of the machine, is used as a figure-of-merit in the tokamak-community to measure the extrapolation of the exhaust system [82]. It is assumed that the radial power decay length of the power flowing to the divertor does not change with size [83]. This means, the wetted area on the divertor scales only with R.

Other parameters of interest are the fusion triple product $nT\tau_E$ which characterises the fusion burn conditions and p^* which is the normalised alpha particle pressure and is a measure of the expected fraction of the energy density of high energy particles in the plasma which can act as a drive for Alfvénic instabilities. As outlined in detail in **Article VI**, considerable gaps also exist for these parameters.

Somewhat differently stated, 3D burning plasma effects which are important in a HELIAS reactor are not accessible in smaller devices. These arguments give rise to the conclusion that a direct step from W7-X to a HELIAS reactor bears high risks of not achieving the desired performance. Therefore an intermediate-step burning-plasma HELIAS device appears prudent in order to investigate the physics of 3D burning plasmas and to reduce development risks towards commercial fusion. Different options for such an intermediate-step machine are presented in the following.

Systems Studies of possible next-step Stellarators

Since the step from W7-X to a HELIAS power plant is rather large both in engineering and physics quantities, a number of different machines could be envisaged to fill this gap. In the following two boundary cases are studied. The first case represents a reasonably small device, which could be realised on a near-term time scale using mostly today's technology, in the following called 'Option A'. The second case, which can be regarded as the upper boundary, is meant to be a DEMO-like design which employs reactor-ready technology and should consequently produce a net amount of electricity. Since there are still possibilities for a design compromise between those two boundary cases, the DEMO-like concept is referred to here as 'Option C' (i.e. 'Option B' would be the in-between compromise which is not investigated in this work). It should be pointed out that a direct step from W7-X to a HELIAS power plant is not generally excluded, however the options presented here would greatly reduce the development risks.

According to the identified physics and engineering gaps as discussed above a tentative list of high-level requirements was specified in **Article VI** and serves as input for the systems studies for the Options A and C. Moreover, a number of sub-goals were defined according to the level of sophistication for each option. For example, detailed 1D transport simulations were carried out for both Option A and C which served as input to the according systems studies. For the details, the reader is referred to **Article VI**. The resulting design window analysis is shown in Fig. 3.5 for Option A (left) and C (right).

According to Fig. 3.5, it can be concluded that the beta-limit does not play a role for Option A unless one would go to very low field and small device sizes. But this would also require substantially more external heating power as the contours of beta and external heating power are nearly parallel. At 50 MW external heating power a beta of about 4.5% is reached. Although the systems studies have been iterated in alternation with detailed transport studies in order to limit the uncertainty concerning the confinement, the results remain sensitive to the achieved confinement. For
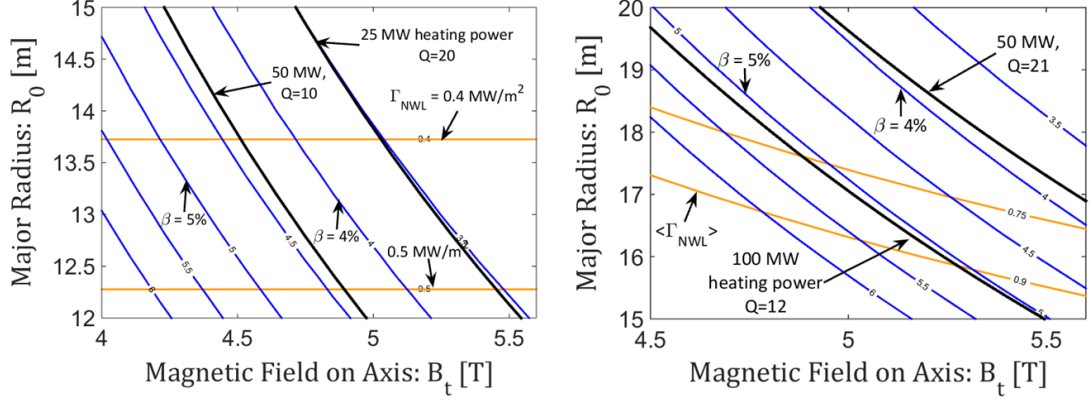
Figure 3.5: *Design window analysis for the intermediate-step HELIAS – **Left: Option A**, constrained to achieve 500 MW fusion power with a confinement enhancement factor of $f_{ren} \leq 1.8$. **Right: Option C**, constrained to achieve 200 MW net electric power. – Shown are isocontours of the volume-averaged thermal plasma $\langle \beta \rangle$ (blue), the average neutron wall-load Γ_{NWL} (orange), and external heating power (black).*

example, a reduction of the confinement by 10% from $f_{ren} = 1.8$ to 1.6 would double the required heating power. Being a stellarator, the device would be designed for steady-state operation and the average neutron wall load of $0.4 - 0.5$ MW/m^2 may open opportunities for material testing. The exhaust requirements for Option A are moderate compared with a reactor as the maximum required radiation in the SOL is only on the order of 50% even when ignoring core radiation by impurities. Although the systems studies for Option A suggest that NbTi can be used, the maximum field on the coil reaches values of $B_{max} \approx 10$ T for 4.5 T on-axis which would require super-critical helium cooling at 1.8K. However, as the NbTi scaling of W7-X is used, errors of 10% are conceivable which could make the difference between normal and super-critical cooling. A more detailed engineering study is required to assess which maximum field can be achieved on-axis using NbTi. In an older study for a 4-period HELIAS (HSR4/18i [68]) the field on the coils could be reduced by trapezoidally shaping the winding pack. These aspects should be included in a future study.

For Option C, the use of Nb$_3$Sn is envisaged from the beginning allowing higher fields with fewer constraints. But even at higher fields, the design points are not ignited, i.e. external heating power is required to sustain the plasma. Since the goal was fixed to 200 MW net electric power, the fusion power is rather low with 1100 MW and the alpha heating thus does not suffice to self-sustain the burn conditions. However, one can also view this from another perspective: in order to achieve 200 MW net electric power, a DEMO-like HELIAS does not need to be ignited.

The aspect ratio for Option C is with $A = 12$ higher than for Option A with $A = 10$. This is necessary to have enough space for the blanket, but the plasma volume is somewhat reduced. Again, the heating power contours are nearly parallel to the beta contours and the beta-limit does not seem to play a role unless very small

devices are considered. For Option C it appears favourable to go to higher fields since a higher fusion power is required at low field due to the reduced confinement. As a larger range of major radii was considered, the average neutron wall load varies between $0.5 - 1.0$ MW/m^2 and the required radiation fraction in the SOL lies between $60 - 80\%$. Also for Option C, the systems studies were iterated with detailed transport simulations in order to obtain a higher accuracy for the predicted confinement and led to $f_{\rm ren} \leq 1.5$.

Economic Comparison

As the options presented here for an intermediate-step stellarator represent boundary cases with quite a conceptual difference, an economic comparison rating the effect of the level of sophistication on the construction costs should show a significant difference.

The current version of PROCESS accommodates a basic cost-model with which it is possible to estimate the construction costs of a design point based on the total sum of material costs. In fact, the systems code PROCESS can calculate for each component of a fusion device the size. Each component is described by a material or even several materials. Based on the size of the components and the material densities the total weight for each material can be estimated. Every material in turn is associated with specific cost-per-weights which allows estimation of the costs of each component and in total the direct costs of the device as a sum of all individual components. The direct costs are complemented by indirect costs which are a flat rate of the direct costs and represent together the total construction costs. A cost penalty for the complexity of components is not yet included in the model (costs of certain components may thus be underestimated). The PROCESS cost model has been benchmarked with the dedicated cost analysis code FRESCO which showed a reasonable agreement for the total costs of a tokamak test case with about 20% difference [84]. The cost estimates will be given here as 'PROCESS currency units' (PCU) since the cost analysis is carried out for all devices in the same framework allowing a relative comparison between the individual devices while absolute values should be treated with care.

For the economic comparison, exemplary, favourable design points are selected from each design window analysis and compared in a cost-breakdown. For Option A, a medium-sized low-field machine was selected with $R = 14$ m and $B_t = 4.5$ T while for Option C, a high-field, larger machine seems to be a favourable design point with $R = 18$ m and $B_t = 5.5$ T. The total construction cost of both these design points have been broken down into their major contributions, which are the magnets, the blanket, the buildings, the equipment and indirect costs. The results are shown in Fig. 3.6. In addition to these design points, the total construction costs of a HELIAS power plant and an 'equivalent' tokamak (Model B of the European PPCS study [70]) are presented as reference which have been discussed in section 3.2.2 and **Article V**.
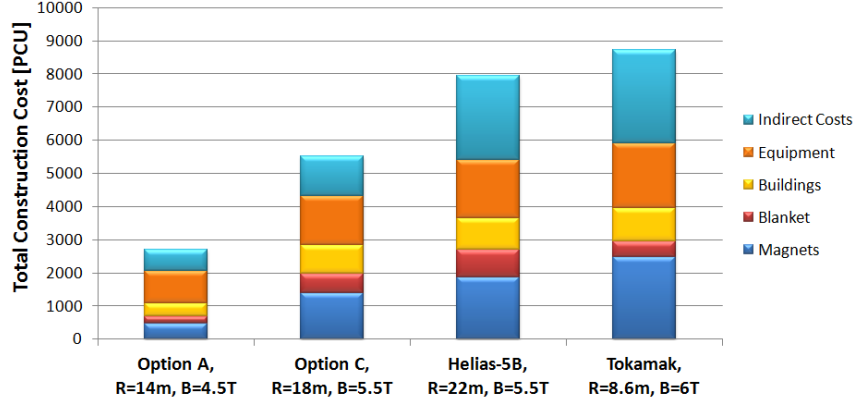
Figure 3.6: *Cost breakdown of total construction costs to major costing accounts for exemplary design points of Option A, Option C as well as for a HELIAS power plant and an 'equivalent' tokamak.*

The total magnet costs are higher for the tokamak than for the HELIAS as the massive PF coils and transformer add considerable mass of superconducting material (Nb_3Sn) and additional costs for assembly. The stored magnetic energy is lower in the stellarator since there is nearly now stray-field. This is because the HELIAS exploits the intrinsic magnetic islands as divertor while the tokamk requires the large PF coils to achieve a divertor configuration. The blanket cost on the other hand is higher for the HELIAS as the total surface area covered by the blanket is higher due to the higher aspect ratio. This in turn means also that the average neutron wall load is lower in the stellarator ensuring longer lifetime of the exposed inner components. The costs for the buildings are comparable in both the tokamak and stellarator case. The reactor building for the HELIAS must be broader but the tokamak reactor building on the other hand higher while the requirement for other buildings are similar. The equipment costs, in contrast, are higher for the tokamak as consequence of the requirement for external current drive.

A further striking result from this comparison as seen in Fig. 3.6 and discussed in **Article VI** is the fact that the cost difference between the boundary cases Option A and C is about a factor two. In particular the magnet costs contribute to this difference which are much higher for the DEMO-like device than for the near-term step. This is attributed to two reasons. First, Option C is a larger device with higher field and requires therefore a higher amount of superconducting material. Second, the costs for Nb_3Sn are considerably higher than for NbTi. This provides justification for the strategy to employ NbTi for the near-term device.

The results presented here are only a first step for the integrated concept development of next-step HELIAS devices. Systems codes and the according models which describe physics and engineering aspects are constantly improved and new models are being developed. For the HELIAS line it is expected that W7-X will improve our understanding of many physics topics in the upcoming years allowing to further ver-

ify or improve the stellarator modules. Further, efforts are undertaken at different research institutes to refine the cost models substantiating economic studies. Thus, systems studies will remain an important research topic in the upcoming years.

4 Summary & Conclusions

With the worldwide increasing energy demand and the transformation of our society towards sustainability, fusion seems to be a promising option supporting a sustainable electricity supply in the future. Great advancements have been achieved in fusion research over the last decades and the commercial application seems to be nearly in reach considering the long development times of such a complex technology. In particular with the construction of ITER and the recent start of operation of the optimised advanced stellarator – Wendelstein 7-X – renewed attention is put on the prospects of fusion power plants. However, while considerable research has been concentrated on the tokamak DEMO development, only little attention has been devoted to next-step HELIAS devices. Consequently, the approaches and techniques used in this work for the concept development of next-step helical-axis advanced stellarators are in nearly all aspects carried out for the first time. In particular, the systematic approach including considerations of plasma transport, is fundamentally new for HELIAS devices. In other words, this work builds the foundation for the concept development of any kind of advanced stellarator which may follow W7-X. A number of detailed conclusions obtained from this thesis are summarised below.

- With a power balance model it has been shown that only slight variations of the confinement improvement with respect to the reference scaling (in terms of the renormalisation factor) have great impact on the size of a stellarator power plant. This approach also demonstrated that there are certain limits associated with the confinement. It has been found that a lower limit of $f_{\mathrm{ren}} = 0.5$ exists below which no stellarator power plant of reasonable size can be built. But there exist also upper limits at which a further confinement improvement is of no benefit in reducing the size of the machine. This is in the range of $f_{\mathrm{ren}} = 1.5 \ldots 1.7$ where the plasma reaches its β-limit and the plasma volume shrinks as outer flux surfaces become stochastic. (Sec. 2.3.1; Article I)

- In order to estimate the confinement improvement for the reactor case, a neoclassical transport model has been applied to a reactor-relevant magnetic configuration. It turns out, that the renomalisation factor continuously decreases when upscaling from W7-X to reactor-relevant sizes and reaches values around

$f_{\text{ren}} = 1.2 \ldots 1.3$. The resulting important conclusion is that empirical confinement time scalings cannot be used to predict the confinement in stellarator power plants. While it is true that the transport regimes change having an impact on the confinement, a sensitivity study of additional 'anomalous' transport at the edge showed, that the decrease of the renormalisation factor is rather robust. However, the understanding of turbulent transport in stellarators is still in its infancy and progress in the understanding and modelling may provide new insights. Considering the formal scaling technique, in today's experiments the heating power P is an independent external parameter. But under reactor-relevant conditions this parameter is determined by the engineering and physics parameters and thus ceases to be independent. This change of paradigm contributes strongly to the deviation of the renormalisation factor under reactor conditions from the prediction of W7-X. (Sec. 2.3.1; Article I)

- State-of-the-art non-linear full-flux-surface GENE simulations showed that the normalised ITG heat flux is similar both in W7-AS and W7-X, i.e. the heat flux density increases linearly with L_T above a certain threshold. A basic critical gradient model has been proposed reducing the complex 3D treatment of turbulence to a computationally tractable 1D description. The model was consequently implemented in the 1D transport code for the characterisation of the turbulent transport in the plasma edge. Integrated transport simulations of neoclassical and turbulent transport have been done based on experimental data of W7-AS and the model was able to reproduce the W7-AS experimental values adequately. (Sec. 2.3.2; Article II)

- The 'stiffness', a parameter of the critical gradient model which describes the resilience of the temperature profile, has been employed for predictive transport simulations of W7-X. The important result from these simulations is that the confinement improvement for W7-X holds even for the critical gradient model. However, a sensitivity analysis showed a strong dependence of the global confinement with respect to variations in the 'stiffness'. Further, the results of such simulations are strongly dependent on the boundary condition which have been taken from basic scaling relations. Finally, the predictive simulations have been taken one step further for the stellarator reactor case. Even for the reactor case a suitable burn-point is found, although the model leads to a strong reduction of the temperature at the edge and a global confinement enhancement factor of $f_{\text{ren}} = 1.3$ is obtained. (Sec. 2.3.2; Article II)

- For the first time, HELIAS-specific systems code models have been developed capable of accurately describing the 3D properties of a stellarator while retaining small calculation times. The developed models include a geometry model to describe the plasma shape, a basic island divertor model to describe the energy exhaust and divertor heat load as well as a coil model which calculates the maximum field at the coils, the total stored magnetic energy, and the dimensions of the winding pack. (Sec. 3.2.1; Article III)

- The HELIAS models have been successfully implemented in the widely used European systems code PROCESS and verified against two test cases. First,

W7-X was modelled and the results compared to real machine parameters, second, the 3D generality of the stellarator models was exploited to model a tokamak DEMO and compared to the original tokamak models. Both test cases showed agreement within 10%. (Sec. 3.2.1; Article IV)

- For the first time, a systems code approach has been applied for the helical-axis advanced stellarator line with the aim of defining the accessible design window for a power-plant-sized HELIAS. The major radius and the magnetic field strength on axis were varied over a wide range with the fixed goal to achieve 1 GW net electric power. The results have shown that the accessible design window of a stellarator power plant depends strongly on the envisaged beta-limit and the plasma core helium dilution. This is somewhat in contrast to an intermediate-step stellarator, where the beta-limit does not play a role. Consequently, if a scenario with effective helium exhaust can be found and/or the beta-limit can be verified to be higher, the design window drastically increases opening many more options for potential devices and robust design points. Therefore, it is important that both the beta-limit and scenarios with efficient impurity exhaust are investigated in detail in the W7-X experimental campaigns. (Sec. 3.2.2; Article V)

- Although not explicitly discussed in this summary, contours of heating power were assessed as a function of temperature and density to study exemplary design points in more detail. As examples, the impact of the confinement enhancement and the tungsten impurity concentration on the ignition window were studied. It became clear that a higher confinement strongly reduces the required external heating power while increasing the available ignition window. In contrast, an intrinsic impurity concentration of tungsten would require substantially more heating power as tungsten has a strong radiation maximum at around 2 keV while the ignition region at higher temperatures is not affected very much. (Sec. 3.2.2; Article V)

- An exemplary conservative HELIAS design point has been compared to an 'equivalent' tokamak including construction costs. It is an important finding, that the costs for a stellarator power plant are on the same level as the costs for an equivalent tokamak. Although the stellarator is a larger device in terms of its dimensions, the masses for the different components are comparable to those of the more compact tokamak leading to similar construction costs in this analysis. (Sec. 3.2.2; Article V)

- In order to measure the reactor relevance of existing and planned magnetic confinement devices, the 'step-ladder' approach has been applied for the HELIAS line. Comparing the step-ladder plot of ITER-like tokamaks with the HELIAS-like devices indicates that the physics basis of advanced stellarators is less well covered than that of tokamaks. The analysis of required engineering and physics parameters in terms of dimensionless variables shows that the step from W7-X to a HELIAS reactor would be very large. In particular, simultaneous attainment of ν^*, ρ^* and β of an envisaged reactor working point cannot be achieved in W7-X. (Sec. 3.2.3; Article VI)

- The arguments stated above give rise to the conclusion that a direct step from W7-X to a HELIAS reactor has larger uncertainties. Additional risks appear for the development of physics scenarios of stellarator reactors if a burning plasma HELIAS is not available. Therefore, an intermediate-step burning-plasma HELIAS device is proposed in order to investigate the physics of 3D burning-plasmas and to reduce development risks. (Sec. 3.2.3; Article VI)

- Since the step from W7-X to a HELIAS power plant is rather large both in engineering and physics quantities, a number of different devices could be envisaged to fit the requirements of an intermediate-step machine. Consequently, two boundary cases have been investigated employing the systems code approach. Case one represents a reasonably small device which could be realised on a near-term time scale using mostly today's technology (Option A). Case two, in contrast, represents an upper boundary with a DEMO-like design employing reactor-ready technology and envisions the production of a net amount of electricity (Option C). (Sec. 3.2.3; Article VI)

- For the economic comparison, exemplary design points were selected from each design window analysis and compared in a cost-breakdown. For Option A, a medium-sized low-field machine was selected with $R = 14$ m and $B_t = 4.5$ T while for Option C, a high-field, larger machine with $R = 18$ m and $B_t = 5.5$ T was chosen. The difference in total construction costs between those two design concepts is about a factor two. (Sec. 3.2.3; Article VI)

4.1 Outlook

There are many open questions and challenges which need to be addressed in future studies. A number of important points are listed below.

- A collaboration with the Karlsruhe Institute of Technology has been started in order to carry out a complete neutronic analysis of a HELIAS power plant. As stated above a neutron source has been provided which has recently been incorporated into a widely used Monte Carlo neutron transport code (MCNP), see **Article VII**. In the next steps it is planned to integrate the 3D HELIAS geometry in the code and to simulate the detailed neutron wall load and in particular the tritium breeding ratio employing the HCPB blanket design. Ultimately this should lead to an engineering design of a stellarator-specific breeder blanket. These results may then be incorporated in a systems code to improve the blanket modelling.

- With the start of the operation of Wendelstein 7-X, many scientific results will be obtained over the coming years. Most importantly, W7-X must demonstrate the success of the optimisation of the magnetic configuration with its associated beneficial properties, in particular in view of steady-state operation. The transport must be investigated in detail in order to improve our understanding and modelling capabilities especially in terms of anomalous transport. The

resulting enhancement of predictive models then allows to further assess the expected transport properties in next-step stellarators which may have great impact on the design of such a device.

- From a theoretical point of view, upcoming work should concentrate on the investigation of the beta-limit and the finding of feasible modular coil sets for quasi-isodynamic configurations. Considering the high alpha pressure in a fusion reactor, it must be assessed to what degree fast particles can drive Alfvénic instabilities. In particular, it must be studied if a threshold exists for the fast particle pressure beyond which deleterious effects appear. While configurations with a higher beta increase the design window of HELIAS power plants, the characterisation of fast particle effects may have great impact on the design of an intermediate-step stellarator.

5 Bibliography

[1] S. Fukuda-Parr. "Human Developement Report 2003 - Millennium Developement Goals: A compact among nations to end human poverty." Palgrave Macmillan, Houndmills, Report (2003). 11

[2] D. MacKay. *Sustainable Energy - without the hot air.* UIT (2009). 11

[3] T. Hamacher and J. Sheffield. "Developement of Fusion Power: What role could fusion power play in transitional and developing countries?" IPP-Report, Max-Planck-Institut für Plasmaphysik (2004). 12

[4] J. R. Petit, J. Jouzel, D. Raynaud et al. "Climate and atmospheric history of the past 420,000 years from the Vostok ice core, Antarctica." *Nature*, vol. 399, p. 429 (1999). 12

[5] E. Roeckner, G. Brasseur, M. Giorgetta et al. "Klimaprojektionen für das 21. Jahrhundert." Max-Planck-Institut für Meteorologie (2006). 12

[6] A. M. Bradshaw, T. Hamacher and U. Fischer. "Is nuclear fusion a sustainable energy form?" *Fusion Engineering and Design*, vol. 86, p. 2770 (2010). 12

[7] F. Romanelli, L. H. Federici, R. Neu et al. "A roadmap to the realization of fusion energy." *Proc. IEEE 25th Symp. Fusion Eng*, pp. 1–4 (2013). 12

[8] F. Wagner. "Considerations for an EU-wide use of renewable energies for electricity generation." *The European Physical Journal Plus*, vol. 129, no. 10, 219 (2014). 12

[9] L. Spitzer. "Project Matterhorn Report PM-S-1 NYO-993." Tech. rep., Princeton University (1951). 17

[10] A. Sacharow and I. Tamm. Tech. rep., Kurtschatow Institute (1952). 17

[11] L. Spitzer. "The Stellarator Concept." *Physics of Fluids*, vol. 1, p. 253 (1958). 17

[12] C. Mercier. "Equilibrium and stability of a toroidal magnetohydrodynamic system in the neighbourhood of a magnetic axis." *Nuclear Fusion*, vol. 4, no. 3, p. 213 (1964). 17

[13] F. Schuller. "Disruptions in tokamaks." *Plasma Physics and Controlled Fusion*, vol. 37, no. 11A, p. A135 (1995). 17

[14] H. Smith, T. Fehér, T. Fülöp et al. "Runaway electron generation in tokamak disruptions." *Plasma Physics and Controlled Fusion*, vol. 51, no. 12, p. 124008 (2009). 17

[15] H. Zohm, G. Gantenbein, A. Gude et al. "The physics of neoclassical tearing modes and their stabilization by ECCD in ASDEX Upgrade." *Nuclear Fusion*, vol. 41, no. 2, p. 197 (2001). 17

[16] C. Hegna and J. Callen. "Stability of bootstrap current-driven magnetic islands in stellarators." *Physics of Plasmas*, vol. 1, p. 3135 (1994). 18

[17] M. Hirsch, J. Baldzuhn, C. D. Beidler et al. "Major results from the stellarator Wendelstein

7-AS." *Plasma Physics and Controlled Fusion*, vol. 50, p. 053001 (2008). 18

[18] A. A. Galeev and R. Z. Sagdeev. "Theory of Neoclassical Diffusion." *Reviews of Plasma Physics*, vol. 7, p. 257 (1979). 18

[19] J. Hosea, G. Sheffield, R. Sinclair et al. "Properties of magnetic surfaces in the Model C stellarator." *Plasma Physics*, vol. 13, no. 5, p. 365 (1971). 18

[20] G. Grieger, G. Catanei, D. Dorst et al. "Confinement of stellarator plasmas with neutral beam and RF heating in W VII-A." *Plasma Physics and Controlled Fusion*, vol. 28, no. 1A, p. 43 (1986). 18

[21] A. Iiyoshi, M. Sato, O. Motojima et al. "Confinement of a Currentless Plasma in the Heliotron-E." *Phys. Rev. Lett.*, vol. 48, pp. 745 (1982). 18

[22] G. Grieger and I. Milch. "Das Fusionsexperiment WENDELSTEIN 7-X." *Physikalische Blätter*, vol. 49, p. 1001 (1993). 19, 21

[23] J. Nührenberg and R. Zille. "Quasi-helically symmetric toroidal stellarators." *Physics Letters A*, vol. 129, no. 2, pp. 113 (1988). 19, 21

[24] J. Nührenberg. "Development of quasi-isodynamic stellarators." *Plasma Physics and Controlled Fusion*, vol. 52, no. 12, p. 124003 (2010). 19

[25] G. Grieger, W. Lotz, P. Merkel et al. "Physics optimization of stellarators." *Physics of Plasmas B*, vol. 4 (1992). 19, 41

[26] C. Beidler, G. Grieger, F. Herrnegger et al. "Physics and Engineering Design for Wendelstein VII-X." *Fusion Science and Technology*, vol. 17, p. 148 (1990). 21

[27] *W. Wobig, S. Rehker, Proc. 7th Symp. on Fusion Techn., Grenoble, France, p. 333* (1972). 21

[28] C. D. Beidler, E. Harmeyer, F. Herrnegger et al. "The Helias reactor HSR4/18." *Nuclear Fusion*, vol. 41, p. 1759 (2001). 21

[29] R. Wolf. "A stellarator reactor based on the optimization criteria of Wendelstein 7-X." *Fusion Engineering and Design*, vol. 83, no. 7–9, pp. 990 (2008). Proceedings of the Eight International Symposium of Fusion Nuclear TechnologyISFNT-8 {SI}. 21

[30] L. D. Landau and E. M. Lifschitz. *Lehrbuch der theoretischen Physik, Band 2: Klassische Feldtheorie.* Akademie-Verlag, Berlin (1992). 24

[31] F. Scheck. *Theoretische Physik 1 - Mechanik.* Springer, Berlin (2002). 25

[32] A. H. Boozer. "Physics of magnetically confined plasmas." *Reviews of Modern Physics*, vol. 76, no. 4, p. 1071 (2004). 27

[33] W. D. D'haeseleer, W. N. G. Hitchon, W. I. van Rij et al. *Flux Coordinates and Magnetic Field Structure.* Springer, New York (1991). 27

[34] P. Helander. "Theory of plasma confinement in non-axisymmetric magnetic fields." *Reports on Progress in Physics*, vol. 77, no. 8, p. 087001 (2014). 27, 29

[35] S. P. Hirshman, W. I. van Rij and P. Merkel. "Three-dimensional free boundary calculations using a spectral Green's function method." *Computer Physics Communications*, vol. 43, p. 143 (1986). 28

[36] M. Kruskal and R. Kulsrud. "Equilibrium of a Magnetically Confined Plasma in a Toroid." *Physics of Fluids*, vol. 1, p. 265 (1958). 28

[37] S. Hirshman and et al. "Proc. 35th EPS Conf. on Plasma Phys. Hersonissos, Crete, Greece, 32D, P2-058 (2008)." 28

[38] Y. Suzuki, N. Nakajima, K. Watanabe et al. "Development and application of HINT2 to helical system plasmas." *Nuclear Fusion*, vol. 46, no. 11, p. L19 (2006). 28

[39] A. V. Luikov. *Analytical Heat Diffusion Theory.* Academic Press, New York (1968). 29

[40] F. F. Chen. *Plasma Physics and Controlled Fusion.* Plenum Press, New York (1984). 29

[41] R. D. Hazeltine and J. D. Meiss. *Plasma Confinement.* Addison-Wesley, Redwood City (1992). 29

[42] R. D. Hazeltine. "Recursive derivation of drift-kinetic equation." *Plasma Physics*, vol. 15, p. 77 (1973). 29

[43] P. Helander and D. J. Sigmar. *Collisional Transport in Magnetized Plasmas.* Cambridge University Press, Cambridge (2002). 29

[44] C. D. Beidler, K. Allmaier, M. Y. Isaev et al. "Benchmarking of the mono-energetic transport coefficients - results from the International Collaboration on Neoclassical Transport in Stellarators (ICNTS)." *Nuclear Fusion*, vol. 51, p. 076001 (2011). 30, 32

[45] W. I. van Rij and S. P. Hirshman. "Variational bounds for transport coefficients in threedimensional toroidal plasmas." *Phyiscs of Fluids B: Physics of Plasmas*, vol. 1, p. 563 (1989). 30

[46] S. P. Hirshman, K. C. Shaing, W. I. van Rij et al. "Plasma transport coefficients for nonsymmetric toroidal confinement systems." *Physics of Fluids*, vol. 29, p. 2951 (1986). 30

[47] H. Maaßberg, C. D. Beidler and E. E. Simmet. "Density control problems in large stellarators with neoclassical transport." *Plasma Physics and Controlled Fusion*, vol. 41, p. 1135 (1999). 31

[48] H. Yamada, J. H. Harris, A. Dinklage et al. "Characterization of energy confinement in net-current free plasmas using the extended International Stellarator Database." *Nuclear Fusion*, vol. 45, p. 1684 (2005). 32, 52

[49] A. Dinklage, H. Maaßberg, R. Preuss et al. "Physical model assessment of the energy confinement time scaling in stellarators." *Nuclear Fusion*, vol. 47, p. 1265 (2007). 32, 33

[50] Y. Turkin, C. D. Beidler, H. Maaßberg et al. "Neoclassical transport simulations for stellarators." *Physics of Plasmas*, vol. 18, p. 022505 (2011). 32

[51] H. Maaßberg, R. Brakel, R. Burhenn et al. "Transport in stellarators." *Plasma Physics and Controlled Fusion*, vol. 35, p. B319 (1993). 34

[52] U. Stroth. "A comparative study of transport in stellarators and tokamaks." *Plasma Physics and Controlled Fusion*, vol. 40, p. 9 (1998). 34

[53] F. Ryter. "Electron heat transport studies." *Plasma Physics and Controlled Fusion*, vol. 48, p. B453 (2006). 34

[54] P. Xanthopoulos, W. A. Cooper, F. Jenko et al. "A geometry interface for gyrokinetic microturbulence investigations in toroidal configurations." *Physics of Plasmas*, vol. 16, p. 082303 (2009). 36

[55] P. Xanthopoulos, F. Merz, T. Görler et al. "Nonlinear Gyrokinetic Simulations of Ion-Temperature-Gradient Turbulence for the Optimized Wendelstein 7-X Stellarator." *Physical Review Letters*, vol. 99, p. 035002 (2007). 36

[56] P. Helander, T. Bird, F. Jenko et al. "Advances in stellarator gyrokinetics." *Nuclear Fusion*, vol. 55, no. 5, p. 053030 (2015). 36

[57] F. Jenko, W. Dorland, M. Kotschenreuther et al. "Electron temperature gradient driven turbulence." *Physics of Plasmas*, vol. 7, p. 1904 (2000). 36

[58] P. Xanthopoulos, H. Mynick, P. Helander et al. "Controlling Turbulence in Present and Future Stellarators." *Physical Review Letters*, vol. 113, p. 155001 (2014). 36

[59] F. Schauer, K. Egorov and V. Bykov. "HELIAS 5-B magnet system structure and maintenance concept." *Fusion Engineering and Design*, vol. 88, p. 1619 (2013). 40, 48, 53

[60] U. Fischer, P. Pereslavtsev and S. Hermsmeyer. "Neutronic design optimisation of modular {HCPB} blankets for fusion power reactors." *Fusion Engineering and Design*, vol. 75-79, pp.

751 (2005). Proceedings of the 23rd Symposium of Fusion TechnologySOFT 23. 41

[61] T. Goorley, M. James, T. Booth et al. "Initial MCNP6 release overview." *Nuclear Technology*, vol. 180, no. 3, pp. 298 (2012). 42

[62] T. Giegerich and C. Day. "The KALPUREX-process – A new vacuum pumping process for exhaust gases in fusion power plants." *Fusion Engineering and Design*, vol. 89, no. 7–8, pp. 1476 (2014). Proceedings of the 11th International Symposium on Fusion Nuclear Technology-11 (ISFNT-11) Barcelona, Spain, 15-20 September, 2013. 42

[63] H. Renner, J. Boscary, H. Greuner et al. "Divertor concept for the W7-X stellarator and mode of operation." *Plasma Physics and Controlled Fusion*, vol. 44, no. 6, p. 1005 (2002). 43

[64] K. McCormick, P. Grigull, R. Burhenn et al. "Island divertor experiments on the Wendelstein 7-AS stellarator." *Journal of Nuclear Materials*, vol. 313-316, pp. 1131 (2003). Plasma-Surface Interactions in Controlled Fusion Devices 15. 43

[65] Y. Feng. "Up-scaling the island divertor along the W7-stellarator line." *Journal of Nuclear Materials*, vol. 438, p. S497 (2013). 43

[66] D. Maisonnier, I. Cook, S. Pierre et al. "The European power plant conceptual study." *Fusion Engineering and Design*, vol. 75-79, pp. 1173 (2005). Proceedings of the 23rd Symposium of Fusion TechnologySOFT 23. 45

[67] B. J. Merrill, L. A. El-Guebaly, C. Martin et al. "Safety Assessment of the ARIES Compact Stellarator Design." *Fusion Science and Technology*, vol. 54, p. 838 (2008). 45

[68] H. Wobig, T. Andreeva, C. D. Beidler et al. "Concept of Helias ignition experiment." *Nuclear Fusion*, vol. 43, p. 889 (2003). 46, 55

[69] J. Kisslinger, ed. *Fusion energy Proc. 17th Int. Conf.*, vol. 4 of *1239-42*. IAEA, Vienna, Yokohama (1998). 46

[70] D. Maisonnier, D. Campbell, I. Cook et al. "Power plant conceptual studies in Europe." *Nuclear Fusion*, vol. 47, p. 1524 (2007). 46, 56

[71] T. Goto, J. Miyazawa, H. Tamura et al. "Design Window Analysis for the Helical DEMO Reactor FFHR-d1." *Plasma and Fusion Research: Regular Articles*, vol. 7, p. 2405084 (2012). 46

[72] M. Kovari, R. Kemp, H. Lux et al. "PROCESS: A systems code for fusion power plants - Part 1: Physics." *Fusion Engineering and Design*, vol. 89, p. 3054 (2014). 46

[73] A. R. Raffray, L. El-Guebaly, S. Malang et al. "Engineering Design and Analysis of the ARIES-CS Power Plant." *Fusion Science and Technology*, vol. 54, p. 725 (2008). 50

[74] S. Torrisi and F. Warmer. "Design of an N-Dimensional Parameter Scanner for the Systems Code PROCESS." Tech. Rep. Report No. 13/23, Max-Planck-Institute for Plasma Physics (2014). 50

[75] F. Warmer. "Reactor Extrapolation of Wendelstein 7-X." Tech. Rep. Report No. 13/21, Max-Planck-Institute for Plasma Physics (2013). 51

[76] W. Houlberg, S. Attenberger and L. Hively. "Contour analysis of fusion reactor plasma performance." *Nuclear Fusion*, vol. 22, no. 7, p. 935 (1982). 51

[77] B. B. Kadomtsev. "Tokamaks and dimensional analysis." *Soviet Journal of Plasma Physics*, vol. 1, p. 295 (1975). 52

[78] T. C. Luce, C. C. Petty and J. G. Cordey. "Application of dimensionless parameter scaling techniques to the design and interpretation of magnetic fusion experiments." *Plasma Physics and Controlled Fusion*, vol. 50, no. 4, p. 043001 (2008). 52

[79] J. W. Connor and J. B. Taylor. "Scaling Laws for Plasma Confinement." *Nuclear Fusion*, vol. 17, p. 1047 (1977). 52

[80] K. Lackner. "Dimensionless engineering variables for measuring the iter and reactor relevance

of tokamak experiments." *Fusion Science and Technology*, vol. 54, p. 989 (2008). 52

[81] K. Lackner. "Figures of merit for divertor similarity." *Comments on Plasma Physics and Controlled Fusion*, vol. 15, no. 6, pp. 359 (1994). 53

[82] A. Kallenbach, M. Bernert, R. Dux et al. "Impurity seeding for tokamak power exhaust: from present devices via ITER to DEMO." *Plasma Physics and Controlled Fusion*, vol. 55, no. 12, p. 124041 (2013). 53

[83] T. Eich, B. Sieglin, A. Scarabosio et al. "Empiricial scaling of inter-ELM power widths in ASDEX Upgrade and JET." *Journal of Nuclear Materials*, vol. 438, p. S72 (2013). 53

[84] C. Bustreo, G. Casini, G. Zollino et al. "FRESCO, a simplified code for cost analysis of fusion power plants." *Fusion Engineering and Design*, vol. 88, no. 12, pp. 3141 (2013). 56

LIMITS OF CONFINEMENT ENHANCEMENT FOR STELLARATORS

F. Warmer, C.D. Beidler, A. Dinklage, Y. Turkin, R. Wolf

Max-Planck-Institut für Plasmaphysik, D-17491 Greifswald, Germany

Abstract

In fusion power plant studies a high confinement improvement with respect to empirical scalings is often assumed in order to design compact machines. In this work the limits of such a confinement enhancement is studied for helical-axis advanced stellarators (HELIAS).

As a first exercise, the well-established power balance approach is used to investigate the impact of confinement enhancement (in terms of the ISS04 renormalisation factor) on the required size of HELIAS power plants. It is found that both a lower (0.5) and an upper limit (1.5 − 1.7) exists for which, respectively, ignition is no longer possible or further confinement enhancement irrelevant due to physics limits.

In the second part of the work a predictive neoclassical transport model is introduced and employed in order to determine a self-consistent confinement time based on transport modelling. It is found that the confinement enhancement with respect to the ISS04 scaling decreases in comparison to W7-X as the device is scaled to reactor size dropping from ∼ 2.5 to 1.2 − 1.3. This behaviour is explained with underlying scaling relations and transport effects. The results from both models are consistent and important for future HELIAS systems studies.

Keywords: HELIAS, scaling laws, renormalisation factor, confinement enhancement

I INTRODUCTION

The ultimate goal of fusion research is to demonstrate the feasibility of the economic production of electricity. To achieve this goal, extrapolation to burning plasma devices beyond the scope of current experiments is necessary. Such studies allow one to identify critical technology and research areas to assess necessary future steps, e.g. experiments, simulations and technology development, on the way to fusion power plants. In addition, the dimensions and design parameters of such devices can be estimated.

In the assessment of the required size of stellarator power plants, a critical parameter is the confinement enhancement with respect to empirical scaling laws. As stellarators are subject to high neoclassical transport, such enhancement of the confinement is assumed by postulating further optimisation of magnetic configurations.

From the variety of stellarator magnetic configurations, currently two major, promising concepts are explored in larger experiments. On the one hand, the heliotron-line is investigated with the Large Helical Device (LHD) in Japan where the magnetic field is created by continuous coils. On the other hand the helical-axis advanced stellarator-line (HELIAS) will be studied in the Wendelstein 7-X (W7-X) experiment in Germany employing a modular coil set with a 5-period symmetry.

Based on these concepts several reactor studies have been carried out in the past. For the heliotron-line these center

around the notion of the Force Free Helical Reactor (FFHR) (Ref. 1) while HELIAS power plant studies have considered four and five field period candidates, HSR4/18 and HSR5/22 (Refs. 2, 3) respectievely. The corresponding machine parameters are summarised in Tab. I.

In the references cited different assumptions on confinement enhancement over existing empirical scalings are made but have not been thoroughly checked for consistency. Therefore, in this work the limits of confinement enhancement are investigated (with focus on the helical-axis advanced stellarator line) and their impact on the design process of fusion power plants discussed. Being a complex topic, this work is here seperately discussed from the general HELIAS systems studies[4,5] which apart from confinement properties take many other limitations into account such as neutron wall load, divertor exhaust, as well as engineering considerations. These studies are still ongoing and not subject of this work.

This work is organised as follows: in section II a 0-D global power balance model for a stellarator burning plasma device is derived using the approach of Ref.[6] Before the model is employed, stellarator-specific physics constraints on the magnetic field strength B_t and on the normalised plasma pressure $\langle \beta \rangle = 1/V \int dV\, 2\mu_0 \sum nkT/B^2$ are discussed and the well-known sensitivity on fusion power illustrated. The section is concluded with an analysis of the renormalisation factor, f_{ren}, (representing confinement enhancement / degradation depending on the magnetic field structure) and its impact on the device size required to achieve ignition for a 4- and 5-fieldperiod HELIAS. The section concludes with a direct extrapolation of W7-

	W7-X	HSR4/18	HSR5/22
Major radius R_0 [m]	5.5	18	22
Average minor radius a [m]	0.53	2.1	1.8
Plasma Volume V [m^3]	30	1570	1407
Average magnetic field on axis B_t [T]	2.5	5.0	5.0
Number of coils	50	40	50
Line averaged electron density $\bar{n}_e$ [10^{20} m^{-3}]	< 2.0	2.6	2.12
Central electron temperature T_0 [keV]	< 5.0	15	15
Average plasma $\langle\beta\rangle$ [%]	< 5.0	4.2	4.2

TABLE I: Main physics and engineering parameters for W7-X, HSR4/18 and HSR5/22.

X to power plant conditions under the constraints mentioned above.

Next, in section III, a predictive 1-D neoclassical transport model is introduced. This model allows the simulation of the transport in an up-scaled W7-X high-mirror configuration. The confinement times predicted by the model are compared against the empirical ISS04 scaling[7] and the discrepancies found (in the sense of a confinement enhancement factor) are highlighted and explained. Finally the results from the 0-D and 1-D model are compared yielding consistent conclusions. The various results and implications of the work are discussed and summarised in section IV.

II GLOBAL POWER BALANCE APPROACH

In the following section, a basic power balance model is derived to identify the predominant parameters relevant to arrive at the conditions for plasma ignition. Such approaches are widely used with similar methodologies.

For further discussions in this paper, the energy confinement, being a relevant quantity in the model, was investigated and physical and technical constraints introduced. The energy confinement is quantified through the energy confinement time τ_E and empirical scaling laws give its relation to geometry, heating power, plasma density and magnetic field properties. For the most recent stellarator scaling ISS04 (Refs. 7, 8) this reads:

$$\tau_E^{\text{ISS04}} = f_{ren} \cdot 0.134 \, a^{2.28} R^{0.64} P^{-0.61} \bar{n}_e^{0.54} B_t^{0.84} \iota_{2/3}^{0.41} \quad (1)$$

where a is the plasma minor radius in m, R the major radius in m, P the heating power in MW, $\bar{n}_e$ the line-averaged electron density in 10^{19} m^{-3}, B_t the magnetic field strength on axis in T, and $\iota_{2/3}$ the rotational transform at 2/3 of the minor radius. The renormalisation factor, f_{ren}, can serve the function of a confinement enhancement / degradation factor similar to the H-factor used in tokamaks but, for stellarators, f_{ren} also reflects the complex structure of stellarator magnetic fields and is therefore dependent on the magnetic configuration.

Employing the definition of confinement time τ_E and taking the ISS04 scaling, the power leaving the plasma through transport processes becomes $P_{loss} = W/\tau_E$ where W is the plasma energy. Assuming on the one hand toroidal geometry and on the other hand that density and temperature only depend on the

minor radius r (in analogon to nested flux surfaces) the plasma energy may be described by

$$W = \frac{3}{2} (2\pi a)^2 R_0 \int_0^1 d\rho \, \rho \sum_j n_j(\rho) \, T_j(\rho) \quad (2)$$

where $\rho = r/a$ is the normalised minor radius and n_j, T_j are the local density and temperature of the particle species $j = e$, i (electrons or ions). Neglecting for the moment profile effects, the local plasma pressure $p = \sum_j n_j k T_j$ can be replaced by the volume-averaged plasma beta $\langle\beta\rangle \sim p/B_t^2$. The profile dependencies are collected in a constant c_1 such that the plasma energy becomes the simple expression

$$W = c_1 \frac{\langle\beta\rangle \, B_t^2 \, R_0^3}{A^2} \quad (3)$$

where A is the aspect ratio $A = R_0/a$. The profile parameter c_1 was chosen such that it agrees with the results from the HSR4/18 and HSR5/22 reactor studies.

The fusion power produced by such a device, under the same assumptions, can be expressed as

$$P_{fus} = E \, (2\pi a)^2 R_0 \int_0^1 d\rho \, \rho \, n_D(\rho) \, n_T(\rho) \, \langle\sigma v\rangle(\rho) \quad (4)$$

with $E = 17.6$ MeV being the energy released by one D-T fusion reaction. With $n_D = n_T = n_e/2$ and $T_D = T_T = T_e$ it is possible to approximate the rate coefficient of the D-T reaction by $\langle\sigma v\rangle \sim T^2$ in the relevant reactor temperature regime 10 keV < T < 20 keV. The fusion power then becomes $P_{fus} = E \, (\pi a)^2 R_0 \int_0^1 d\rho \, \rho \, n_e^2(\rho) \, T^2(\rho)$. Combining again density and temperature as the pressure p and replacing this by the volume-averaged $\langle\beta\rangle$ the simple relation

$$P_{fus} = c_2 \frac{\langle\beta\rangle^2 \, B_t^4 \, R_0^3}{A^2} \quad (5)$$

emerges with an additional profile parameter c_2 similarly chosen to agree with HSR4/18 and HSR5/22. The values are summarised in Tab. II.

In addition to the fusion power and the plasma transport losses it is necessary to characterise the power balance of such a fusion reactor. The flow chart of the power balance treated here is illustrated in Fig. 1. As the aim of this work was the investigation of global effects only, the power flow is not broken down to smaller scales. The useable thermal energy in this

2

Configuration	c_1	c_2
HSR4/18	0.1175	0.004276
HSR5/22	0.1169	0.004215

TABLE II: Values of the profile parameters c_1 and c_2 of the global power balance model determined to comply with the results of the HSR4/18 and HSR5/22 reactor studies.

work is defined as the total fusion power modified with a factor M. This additional factor takes into account the additional energy generated by nuclear reactions in the blanket / divertor. Thus, the thermal power P_{th} produced in this model reads

$$P_{th} = M \cdot P_{fus} + P_{Heat} + \eta_{BoP}P_{BoP}. \tag{6}$$

The integrated cooling system, with a thermal conversion efficiency η_{th}, converts the thermal power to the gross electrical power $P_{el} = \eta_{th}P_{th}$. A fraction of this gross electrical power must be recirculated within the power plant itself to operate the various subsystems. In this study this power is referred to as the auxiliary power $P_{AUX} = f_{rec}P_{el}$. The remaining net electrical power can than be provided to the grid.

The auxiliary power in turn consists predominantly of two components. One component is the power required for the balance of plant systems, P_{BoP}, mainly driven by the required pumping power $P_{BoP} \cong P_{pump}$. The other component is the additional heating power, P_{Heat}, needed to compensate the plasma transport and radiation losses in excess of alpha particle heating: $P_{Heat} = P_{loss} + P_{rad} - P_\alpha$. Here, P_{rad} is the power loss by radiation that in a stellarator reactor mainly comes from bremsstrahlung, as synchrotron and line radiation are negligible in comparison, as long as impurities are not introduced on purpose to increase core radiation. With the heating system efficiency η_{heat} the power required to operate the system is $P_{Heat,Gross} = P_{Heat}/\eta_{heat}$.
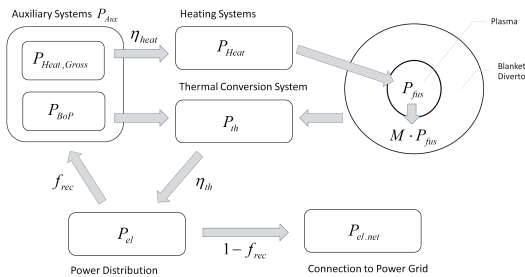
Fig. 1: Flow chart for the basic power balance model of stellarator burning plasma devices.

II.A   Magnetic Field Strength and Plasma Beta

The strength of the magnetic field has a significant influence on the global confinement as can be seen in the empirical confinement time ISS04 ($\tau_E \sim B_t^{0.84}$), introduced at the beginning of this section. Moreover, the substitution of the plasma pressure $p \propto \langle\beta\rangle B_t^2$ reveals a sharp dependence of the plasma energy and of the fusion power on the magnetic field strength B_t and $\langle\beta\rangle$ (equations (3) and (4)). Again, as is well known, an

increase of both parameters is beneficial for the global performance and the constraints for both B_t and $\langle\beta\rangle$ are therefore highlighted.

II.A.1.   Physics and Engineering Constraints

For B_t it was shown in[9] for a 4-periodic HELIAS that 4.4 T magnetic field can be achieved on axis using existing NbTi technology with conventional helium cooling at 4.2 K. The field in this case could be pushed higher up to 5 T if super-critical helium at 1.8 K is applied as indicated in.[2] With the advancement of superconductor material development and the large scale use of Nb_3Sn in ITER, it was concluded in[10] that the Nb_3Sn technology could be safely employed for stellarators allowing a magnetic field strength of up to 5.6 T on axis. However, the application of new materials is limited by availability, costs and the capability of complex 3D shaping. It was also shown in[11] that the forces and stresses arising in 5-period HELIAS with $R_0 = 22$ m and a magnet system achieving 5.6 T on axis are manageable.

While the achievable magnetic field is more an engineering issue the constraints of the achievable $\langle\beta\rangle$ are driven by physics considerations. A HELIAS may operate only within a certain 'window' of $\langle\beta\rangle$. That means both a minimum threshold and a maximum limit on the value of $\langle\beta\rangle$ exists. The lower $\langle\beta\rangle$ limit is related to the confinement of the fast α-particles. In order to confine the collisionless α's in a HELIAS configuration, so-called 'minimum-B' configurations are necessary. To achieve these configurations the diamagnetic effect of the plasma is necessary providing a deeper magnetic well and a faster poloidal ∇B drift beneficial for the fast particle confinement. The minimum-B configurations are not achieved until the local β is sufficiently large. As the before-mentioned effect gets stronger with increasing β, dependent on the profiles a certain minimal value of $\langle\beta\rangle$ must be reached. This value is dependent on the magnetic well in the specific vacuum configuration[12] and for the HELIAS line lies typically around $\langle\beta\rangle = 3 - 4\%$.

The maximum $\langle\beta\rangle$ is anticipated to have a 'soft' limit coming from an increase of MHD instabilities gradually enhancing transport and decreasing confinement, but it is 'soft' in the sense that stellarators are observed to still operate above the ideal MHD ballooning limit and beyond the Mercier limit.[13,14,15,16] Linear MHD stability considerations yield a beta limit of 4.5% in W7-X. But as already pointed out, stellarators are observed to operate above such limits reducing their credibility. In the end, $\langle\beta\rangle$ may be limited by equilibrium-considerations, namely the stochastisation of the magnetic field at increasing beta. At increasing $\langle\beta\rangle$ the magnetic field becomes stochastic at the edge causing a continuous destruction of flux surfaces such that this stochastic region expands thereby decreasing the plasma volume. This effect could ultimately limit beta to the range $5 - 6\%$ as suggested by theoretical studies.[17]

II.A.2.   Sensitivity on Fusion Power

To study the magnetic field strength and $\langle\beta\rangle$ within the constraints outlined above the magnetic field strength was varied continuously between 4 T and 6 T for the global power balance model for two constant $\langle\beta\rangle$ values. The first was $\langle\beta\rangle = 3.6\%$

3

as a lower bound and the other was $\langle\beta\rangle = 4.9\%$ as an upper bound, chosen to be close but still somewhat below the beta-limit pointed out above. All other parameters were chosen as in HSR5/22 and kept constant except that the plasma density was increased along with the magnetic field in order to keep the value of $\langle\beta\rangle$ constant. The fusion power was chosen as the figure of merit for the plant performance. The results are illustrated in Fig. 2.

It can be seen from Fig. 2 that at constant $\langle\beta\rangle$, the fusion power increases substantially with increasing magnetic field strength. The full step from NbTi technology with $B_t = 4.5$ T to Nb_3Sn or Nb_3Al technology with $B_t = 5.6$ T roughly doubles the fusion power. A vertical step from $\langle\beta\rangle = 3.6\%$ (solid line) to $\langle\beta\rangle = 4.9\%$ (dashed line) also nearly doubles the generated fusion power. If both the magnetic field strength and $\langle\beta\rangle$ can be increased simultaneously then a substantial gain in fusion power is achieved.
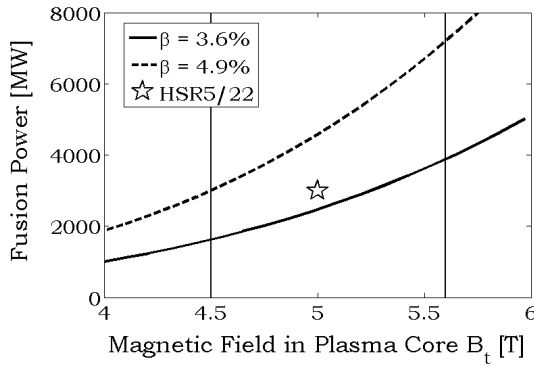
Fig. 2: Fusion power as function of the magnetic field strength for HSR5/22 parameters with constant $\langle\beta\rangle = 3.6\%$ (solid line) and $\langle\beta\rangle = 4.9\%$ (dashed line) where the horizontal line on the left is the maximum field strength of NbTi technology at 4.2 K and the limit on the right is the maximum field strength of Nb_3Sn superconductors at 4.2 K. The star-like symbol is the reference of the HSR5/22 point design.[3]

II.B The Renormalisation Factor (0-D)

The ISS04 data set showed a distinct clustering of sub-sets when plotted in figures of any available stellarator-heliotron scaling.[7] This clustering motivated introduction of a sub-set dependent factor (f_{ren}) which led to much more statistically significant scaling in (a, R, n, P, B, ι). f_{ren} has been determined from reference scalings and is comparable to H-factors in toka-mak scalings. It has been interpreted as reflecting configuration dependent confinement properties, but, although evidence for this interpretation has been found, it has not been conclusively proven.[7] On the other hand, employing f_{ren} to account for confinement enhancement effects appears to be a fairly obvious approach for the model discussed in this paper.

Therefore f_{ren} was varied between $0 - 2$ and the impact on the machine size was investigated. More precisely, the size is the minimum major radius R_{ign} necessary to achieve ignition, which is defined as $Q = \infty$ and $P_{heat} = 0$. The results are illustrated in Fig. 3 for a constant fusion power of 3 GW and for both the 4 and 5-periodic HELIAS (solid and dashed line

respectively). As the increase of f_{ren} reflects improved confinement and in order to keep the fusion power constant, $\langle\beta\rangle$ is increased in line with f_{ren}.

Fig. 3 clearly shows that a confinement enhancement, especially around $f_{ren} = 1$, allows for a reduction in the required device size. But as $\langle\beta\rangle$ is increased with f_{ren} at one point a beta-limit is reached above which further confinement enhancement is pointless. This is shown in Fig. 3 with the circles at $\langle\beta\rangle = 6\%$. That means for the 5-periodic case a confinement enhancement with respect to the ISS04 above 1.7 is not meaningful with a corresponding minimum major radius of $R_{ign} = 17$ m. For the 4-periodic concept already an enhancement factor of about 1.5 reaches the beta-limit at a machine size of $R_{ign} = 13$ m. Another remarkable result of the study is that a minimum $f_{ren} = 0.5$ seems to exist which precludes ignition for smaller values (for reasonable machine sizes $R_0 < 30$ m).
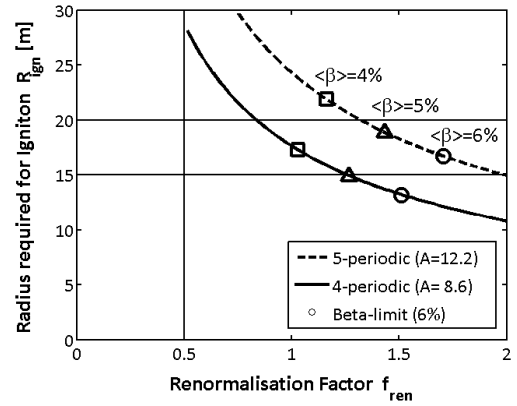

Fig. 3: The minimum major radius for plasma ignition ($Q = \infty$) is shown in dependence of the renormalisation factor f_{ren} for the 4 and 5-periodic HELIAS concepts (solid and dashed line respectively) at constant fusion power of 3 GW. As $\langle\beta\rangle$ is increased with f_{ren}, the circles show the point where $\langle\beta\rangle = 6\%$ is reached. Additionally, $\langle\beta\rangle = 4\%$ (squares) and $\langle\beta\rangle = 5\%$ (triangles) is shown.

From this result it is evident that the improvement and optimisation of the confinement is critical. There exists a minimum value of the confinement that must be achieved to reach ignition conditions at all, while, a very high degree of confinement allows for the reduction of device sizes. Such an improvement allows higher plasma temperatures and densities and is; therefore, interconnected to the plasma $\langle\beta\rangle$, which must be increased (up to the maximum possible value) along with the confinement improvement to truly allow for smaller devices. It is noted that, at the same time, further issues may result from particle confinement and density control.[18] These topics will be treated elsewhere.

II.C Direct Extrapolation of Wendeltein 7-X (0-D)

Employing the introduced power balance model under the physics and engineering constraints listed in subsection II.A and additionally considering possible confinement enhancement with the renormalisation factor as stated above, Wendelstein 7-X can be directly extrapolated to power plant conditions. For this extrapolation two boundary scenarios are used. First a

4

more conservative approach with a magnetic field strength of $B_t = 4.5$ T and line-averaged density $\bar{n}_e = 1.8 \cdot 10^{20}$ m^{-3}, and second a more advanced scenario with $B_t = 5.5$ T and $\bar{n}_e = 2.8 \cdot 10^{20}$ m^{-3}. Stellarators do not exhibit the strong Greenwald density limit observed in tokamaks.[19] Nevertheless, a radiative density limit, known as SUDO-limit,[20] has been observed in some heliotron/stellarator-type devices. However, the Large Helical Device (LHD) demonstrated the ability to operate far beyond this limit, especially if pellet injection is used. Therefore the SUDO-limit has been reinterpreted as a density limit for the plasma edge.[21,22] For the 5-field period case the SUDO-limit yields a value of $1.6 \cdot 10^{20}$ m^{-3} which is very high for an edge-limit. The scenarios investigated in this work are well below these limits and were chosen to be somewhat below the corresponding ECRH cut-off density of the respective field strength assuming O1-mode heating.

For both scenarios W7-X is linearly scaled up at constant aspect ratio $A = 10.3$ with the requirement to yield a fusion power of $P_{fus} = 3000$ MW. Under these constraints a corresponding renormalisation factor is found which is needed to fulfill these conditions. The results for both scenarios are shown in Fig. 4. If W7-X is scaled up by factor 4 to $R_0 = 22$ m major radius, the required renormalisation factor for the 'advanced' case is below 1 meaning that the 3 GW fusion power can be reached without further confinement enhancement. In the 'conservative' case on the other hand, already a confinement enhancement factor of about 1.2 is required to achieve the necessary conditions for the 22 m machine. Looking next at upscaling of W7-X by a factor 3, i.e. 16.5 m major radius, already the 'advanced' scenario needs a renormalisation factor of about 1.2 while the 'conservative' scenario would need a confinement enhancement factor of 1.8 which is here beyond the beta-limit of $\langle \beta \rangle = 6$ % and therefore not realistically accessible. Again, $\langle \beta \rangle$ is increased parallel to f_{ren} and in the case of an upscaled W7-X, the confinement enhancement beyond $f_{ren} = 1.6$ becomes restricted by the beta-limit.

III PREDICTIVE NEOCLASSICAL TRANSPORT MODEL

The 3D magnetic field of stellarators introduces a large class of localised helical trapped particle orbits which leads to so-called 'neoclassical' transport. This is a drawback of the stellarator as the resulting particle and energy fluxes are much higher than in tokamaks. Nonetheless, these effects and the corresponding transport are well understood[23,24] and even allow to predict the stellarator-specific ambipolar electric field. These physics based predictions are especially relevant for larger machines with higher temperatures since the neoclassical transport scales strongly with temperature.

The neoclassical transport model, which will be introduced below, includes profile effects and especially allows to self-consistently calculate the plasma transport and the corresponding confinement time. Two scenarios, one employing conservative and one advanced physics and technology assumptions are simulated by upscaling the W7-X high-mirror configuration. By comparing the calculated confinement time to the
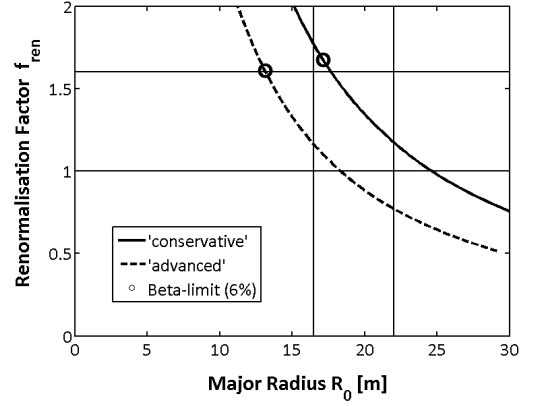

Fig. 4: The required renormalisation factor f_{ren} with respect to the ISS04 confinement time scaling is shown for linear extrapolation of Wendelstein 7-X with major radius at fixed aspect $A = 10.3$ ratio and fusion power $P_{fus} = 3000$ MW. Two scenarios are illustrated, a 'conservative' one with $B_t = 4.5$ T and $\bar{n}_e = 1.8 \cdot 10^{20}$ m^{-3} (solid line) and an 'advanced' one with $B_t = 5.5$ T and $\bar{n}_e = 2.8 \cdot 10^{20}$ m^{-3} (dashed line). As again $\langle \beta \rangle$ is increased with f_{ren} the circles show the point where $\langle \beta \rangle = 6$ % is reached.

ISS04 scaling a predictive f_{ren}^{1D} can be obtained. The last section showed the critical impact of f_{ren}, so the 1-D simulations permit an assessment of the current optimisation of the HELIAS (upscaled W7-X high mirror configuration) with respect to the ISS04. It should be noted that further optimisation of stellarator magnetic configurations is the subject of on-going research.[25,26]

In the predictive neoclassical transport model[27,28,29,30] it is assumed that the plasma may be described by using a local approximation to solve the drift kinetic equation. Additional flux-surface averaging allows reduction of the geometrical description of the plasma to one coordinate, namely the flux surface label ψ that can be related to the average minor plasma radius $r = \sqrt{\psi/\psi_{max}}$. With this radial coordinate the power balance of the plasma is expressed for the electrons $s = e$ and ions $s = i$ by the equations

$$\frac{3}{2} \frac{\partial n_s T_s}{\partial t} + \frac{1}{V'} \frac{\partial}{\partial r} (V' Q_s) = P_s + Z_s \Gamma_s E_r \tag{7}$$

with the power source / loss term P_s consisting of heating power, bremsstrahlung and the collisional coupling between electrons and ions. The neoclassical particle, Γ_s, and energy, Q_s, fluxes are expressed[24] as:

$$\Gamma_s = -n_s L_{11}^s \left[\frac{n_s'}{n_s} - \frac{Z_s e E_r}{T_s} + \left(\frac{L_{12}^s}{L_{11}^s} - \frac{3}{2} \right) \frac{T_s'}{T_s} \right] \tag{8}$$

$$Q_s = -n_s T_s L_{21}^s \left[\frac{n_s'}{n_s} - \frac{Z_s e E_r}{T_s} + \left(\frac{L_{22}^s}{L_{21}^s} - \frac{3}{2} \right) \frac{T_s'}{T_s} \right] \tag{9}$$

where the thermal transport coefficients L_{ij} are obtained by the appropriate energy convolutions with the local Maxwellian distribution function

$$L_{ij} = \frac{2}{\sqrt{\pi}} \int_0^\infty \sqrt{K} e^{-K} D_\perp(K) h_i h_j \, dK \tag{10}$$

5

with $K = mv^2/2T$, $h_1 = 1$, $h_2 = K$ of interpolated results for $D_\perp$ from a full mono-energetic diffusion coefficient database[31,32]

$$D_\perp = D_\perp \left(\rho, \frac{R_0 \, v_s}{v_s \, t}, \frac{E_r}{v_s \, B_0} \right). \tag{11}$$

Here v_s, v_s, Z_s are the collision frequency, velocity and charge number of electrons or ions, B_0 the value of the magnetic field and E_r the radial electric field.

Usually, the ambipolarity constraint $Z_i \Gamma_i = \Gamma_e$ is solved to obtain the radial electric field E_r. However, this approach is often not numerically suitable because of the discontinuity and the bifurcations of the solution. This problem can be circumvented with a diffusion equation for the radial electric field from the poloidal force balance:[33]

$$\frac{\partial E_r}{\partial t} - \frac{1}{V'} \frac{\partial}{\partial r} \left(D_E V' r \frac{\partial}{\partial r} \left(\frac{E_r}{r} \right) \right) = \frac{|e|}{\epsilon} (\Gamma_e - Z_i \Gamma_i) \tag{12}$$

with D_E the 'diffusion coefficient' of the electric field and the dielectric constant ϵ. This is necessary as localised central heating (e.g. with ECRH) can lead to high electron and low ion temperatures amplifying electron transport. The solution of the ambipolarity constraint then becomes the so-called 'electron-root' with a strong, positive electric field in the centre while the edge with similar electron and ion temperatures is governed by the 'ion-root' solution with a negative electric field. Eq. (12) for the electric field allows then for a smooth crossing of E_r from the 'electron' to 'ion-root', especially where several solutions of the ambipolarity constraint coexist.

Due to the strong temperature dependence of the neoclassical transport stellarators are, especially in the plasma centre, dominated by neoclassical transport effects where the temperature is highest. Turbulence is assumed to play only a subdominant role in the centre because of high neoclassical diffusion coefficients. The plasma centre has a higher temperature than the plasma edge and; therefore, the neoclassical transport becomes small at the edge so that the anomalous transport phenomena starts to dominate. This has been observed in many experiments, e.g.[23] This results in the requirement that to the neoclassical description the additional anomalous transport must be accounted for. As models based on first principles for anomalous transport are not yet available, a basic experimentally derived model is employed with:

$$Q_s^{ano} = -\chi_s^{ano} n_s T_s' \tag{13}$$

where the anomalous heat conductivity $\chi \sim P^{3/4} n^{-1}$ is taken from experimental results obtained in W7-AS.[34,35] The discussion of anomalous transport in 3D configurations is the subject of on-going research.[36] To what extent Eq. (13) represents an adequate description is not yet determined.

The neoclassical treatment, on the other hand, as described here has been extensively validated with experiments[23] and the corresponding codes have been benchmarked in detail.[24]

III.A Direct Extrapolation of Wendeltein 7-X (1-D)

In the following the two scenarios from subsection II.C are taken up again and refined in more detail: one assumes conservative and the other advanced physics and technology assumptions, explicitly defined in Tab. I. Both scenarios employ the W7-X high-mirror magnetic configuration linearly upscaled from a major radius of 5.5 to that of 22 m. The impact of these assumptions on fusion power, fusion gain, and the calculated confinement time are investigated. As fueling and exhaust scenarios are beyond the scope of this work, both scenarios were simulated using a flat density profile. Although the 1-D model is capable of self-consistently treat the density profile with respect to fuelling, in this work the profile was held constant and detailed fuelling scenarios will be a topic of future investigations.

The conservative scenario assumes NbTi superconductor technology (at 4.2 K) with 4.5 T magnetic field on axis. The line averaged electron density is chosen to be moderate with $\bar{n}_e \approx 1.8 \cdot 10^{20}$ m^{-3}. On the one hand this leads to a smaller $\langle \beta \rangle$ and as shown in the previous chapter, this implies a lower fusion power. In the advanced scenario, the technologically advanced Nb$_3$Sn superconductor technology is assumed (at 4.2 K) with 5.5 T field strength on axis. The density is also chosen higher with $\bar{n}_e \approx 2.8 \cdot 10^{20}$ m^{-3}.

Both densities were selected to be somewhat below the ECRH cut-off density to allow for controlled heating. The W7-X high-mirror configuration has a mirror term of the magnetic field strength of around 10% in the plasma centre. This provides a highly localised resonance for O1-mode ECRH heating at B_{max} (including mirror term) near the magnetic axis. In the conservative case with $B_0 = 4.5$ T on axis, the W7-X 140 GHz gyrotrons are then applicable which have the resonance at $B = 5$ T and for the advanced scenario with $B_0 = 5.5$ T the 170 GHz ITER gyrotrons would be the choice with the resonance at $B = 6$ T. Therefore the ECRH absorption profile is modelled by a Gaussian shape assuming that the full power can under resonant conditions be deposited in the plasma centre.

The two scenarios introduced above were simulated within the predictive neoclassical transport model by an upscaling of the magnetic configuration for major radii between 5.5 and 22 m. Fusion power and α-heating were calculated self-consistently. The fusion power and the fusion gain $Q = P_{fus}/P_{heat}$ serve as figures of merit where the external ECRH heating was continuously reduced while going to larger device size until ignition is reached ($Q = \infty$). The results are illustrated in Fig. 5. It can be seen that the fusion power increases strongly with machine size (left side of Fig. 5). This increase is due to the growth of the plasma volume with device size. As the field and density are fixed within one scenario, the enhancement of the plasma volume increases the total number of particles and; therefore, the number of fusion reactions, and thus fusion power.

It is also evident that the step from the conservative to the advanced assumptions, with higher density and magnetic field increases the fusion power even more. The enhanced confinement due to the stronger magnetic field results in a higher density of particles leading to a higher plasma pressure and strong increase in fusion power. These findings confirm the results of the global power balance approach.

As the fusion power increases strongly with increasing machine size the need for external heating is correspondingly reduced which was consequently decreased in the simulations.

6

Scenario	Config-uration	SC Tech-nology	B_0 [T]	$\bar{n}_e$ [10^{20}m^{-3}]	Gyrotrons
conservative	W7-X high mirror	NbTi	4.5	1.8	W7-X: 140 GHz
advanced	W7-X high mirror	Nb$_3$Sn	5.5	2.8	ITER: 170 GHz

TABLE III: Summary of the parameters of the conservative and advanced scenario.

Accordingly the fusion gain, which is the ratio of fusion power over external heating, strongly increases with increasing major radius as can be observed on the right side of Fig. 5 until reaching ignition (the lines end as $Q \to \infty$).
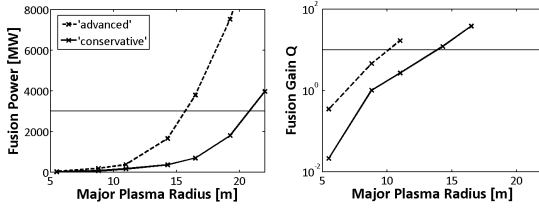
Fig. 5: Self-consistent fusion power (left) and fusion gain (right) for the conservative (solid line) and advanced scenario (dashed line).

At a first glance the advanced scenarios seem capable of drastically reducing the device size. These smaller sizes should be seen as the lowest limit practically achievable under the advanced physics and engineering conditions. But several points are not considered in the simulations which violate the idealised assumptions. These are discussed in the following.

The anomalous (or turbulent) transport has been treated in the predictive simulations only by a simple scaling model based on experimental results. Although theory suggests that some turbulent micro instabilities may be stabilised in stellarators, e.g. trapped electron modes, others like the ion temperature gradient driven modes may contribute more to the overall plasma transport then accounted for by the simple model[37] used in this paper. Transport and thus the confinement time may; therefore, be less favourable than the simulations suggest.

III.B The Renormalisation Factor (1-D)

As stated in section II.B, one important figure of merit to characterise plasma transport is the energy confinement time. The neoclassical transport simulations for the 'conservative' and 'advanced' scenario (cf. previous section) also provided predictive confinement times. With these predictions it is possible to characterise the confinement enhancement found in the simulations by comparison with the empirical ISS04 scaling law. This is done by defining the factor

$$\Theta = \tau_E^{1D}/\tau_E^{ISS04} \qquad (14)$$

which is the ratio of the simulated confinement time over the corresponding ISS04 value, i.e. the confinement enhancement factor obtained from the predictive simulations. In that sense

it could be interpreted as a 1D renormalisation factor f_{ren}^{1D}. The label Θ is chosen to better distinguish the results from the ones obtained for the 0-D power balance model.

The results are illustrated in Fig. 6 where Θ is plotted against the plasma volume for the 'conservative' as well as the 'advanced' scenario. It can be seen that Θ is not a constant factor but decreases when extrapolated to reactor conditions. For both the conservative and the advanced scenario, Θ changes from around 2 (W7-X size) down to $1.1 - 1.3$ (HELIAS reactor size). If Θ is interpreted to be a confinement enhancement factor similar to the renormalisation factor f_{ren}, then this is a large change when compared to the results from the global power balance model (Fig. 3).
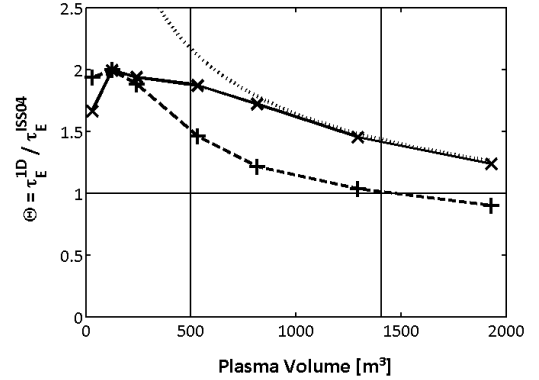

Fig. 6: Confinement time of the predictive neoclassical simulations normalised to the ISS04 scaling for the 'conservative' scenario (solid line) compared to a normalised $\Theta \sim V^{-2/5}$ scaling (dotted line), as well as the 'advanced' scenario (dashed line). The vertical solid lines represent $Q \geq 10$ (left) and HSR5/22 in terms of plasma volume (right).

Before the results are explained, some general remarks regarding confinement scaling laws are necessary in order to avoid unphysical interpretation of the given results. Empirical scalings may accurately describe the available data range but extrapolation outside this range is beyond the validity of the scaling. The used expressions and their combination is not unique and rephrasing with respect to other parameters is possible.

Some insight in the behaviour of the confinement enhancement factor, Θ, may be gained by revisiting the definition of the energy confinement time $\tau_E = W/P$. The energy can be expressed by $W = V\beta B^2$, Eq. (3), and the lost power with $P = P_\alpha - P_{brems} + P_{Ext}$ according to section II. Additionally,

it is assumed that bremsstrahlung P_{brems} only occurs under reactor conditions with usually $P_{brems}/P_\alpha \approx 15\%$ and therefore $P_\alpha \gg P_{brems}$. Neglecting bremsstrahlung, the energy confinement time is

$$\tau_E = \frac{W}{P} \sim \frac{V\beta B^2}{P_\alpha + P_{Ext}} \tag{15}$$

where P_{Ext} is the externally applied heating power. The alpha heating power is 1/5 of the fusion power that may be approximated by $P_\alpha \sim V\beta^2 B^4$ as given by Eq. (5). Inserting in Eq. (15) leads to

$$\tau_E \sim \frac{V\beta B^2}{V\beta^2 B^4 + P_{Ext}}. \tag{16}$$

From this representation it becomes clear that the confinement time consists of two different parts. The first part is the influence of the alpha heating power on the confinement time, while the second part comes from the externally applied heating. The behaviour of τ_E will be different depending on which of these two is dominant and it is therefore useful to consider two distinct asymptotic cases:

i) No fusion power: $P_\alpha = 0$

$$\Rightarrow \tau_E^{Ext} \sim \frac{V\beta B^2}{P_{Ext}} \tag{17}$$

This case corresponds to the situation without fusion power and no significant bremsstrahlung. The externally given heating power P_{Ext} is thus a free parameter. This together with the clear volume dependence is characteristic of the regime in which the empirical confinement time scaling ISS04 was derived.

ii) High fusion power: $P_\alpha \gg P_{Ext}$

$$\Rightarrow \tau_E^{\alpha} \sim \frac{1}{\beta B^2} \tag{18}$$

In this case the external heating is neglected and only alpha particles heat plasma. The heating power is, therefore, no longer a free parameter. Instead, it is interconnected to the plasma volume, beta, and field: $P_\alpha \sim V\beta^2 B^4$. As such, τ_E scales in this representation differently than in case i).

With this analysis, the confinement time of the fusion case τ_E^{α} can be compared with the ISS04 scaling law by inserting the alpha power $P_\alpha \sim V\beta^2 B^4$ in the ISS04 $\tau_E^{ISS04} \sim V n^{3/5} B^{4/5} P_\alpha^{-3/5}$ leading to

$$\tau_E^{ISS04,\alpha} \sim \frac{V^{2/5} n^{3/5}}{\beta^{6/5} B^{8/5}}. \tag{19}$$

Finally, the enhancement factor Θ for the high fusion power case can be approximated with $\Theta^\alpha = \tau_E^\alpha / \tau_E^{ISS04,\alpha}$ resulting in

$$\Theta^\alpha \sim \frac{\beta^{1/5}}{V^{2/5} n^{3/5} B^{2/5}}. \tag{20}$$

As the specific plasma transport and transport regimes play only a role in the achievable β and because n and B were held constant in the predictive transport simulations, it can be concluded that the degradation of the confinement enhancement factor Θ with respect to the ISS04 is directly related to the increase of the volume in the high fusion power scenario

$$\Theta^\alpha \sim V^{-2/5}. \tag{21}$$

This relation is plotted in Fig. 6 and agrees with the simulations at high fusion power giving an indication that the decrease of Θ may be related to the fact that the heating power is determined self-consistently by machine and plasma performance parameters.

III.C Impact of Transport on the Renormalisation Factor

In the last subsection a basic scaling approach was used to conceptually obtain a relation for the decrease of the confinement enhancement factor Θ. In the following a basic analysis of the underlying transport mechanism shall be given which plays an important role for the achievable plasma performance.

III.C.1. Scaling Considerations

Considering first the empirical confinement time scaling ISS04, the majority of data points used for the regression of the scaling have been obtained at moderate to high collisionality, $\nu^* = O(10^{-1})$, corresponding to the neoclassical plateau regime. The analytic limit of the neoclassical plateau regime leads to a confinement time scaling which closely resembles the exponents of the ISS04:[8]

$$\tau_E^{neo,Pl} \propto \frac{nT}{P} \propto n^{3/5} P^{-3/5} B^{4/5} t^{2/5}. \tag{22}$$

Although the neoclassical scaling agrees with the ISS04, in W7-AS, the energy and particle fluxes could not be explained by the neoclassical plateau regime as the fluxes were systematically underestimated. Only a few high-performance discharges of the database at $T \geq 1$ keV matched the predicted neoclassical fluxes. In this context it should be noted, that a gyro-Bohm type turbulence approach for tokamaks, the so-called Lackner-Gottardi scaling,[38] leads to the same exponential relations as exhibited by the ISS04 and neoclassical plateau regime scaling.

These basic scaling considerations already raise doubts about the usage of the ISS04 scaling for extrapolation to stellarator power plant conditions. This is especially true in the regime of a burning plasma with self-sustained alpha heating as shown in the last subsection where the dimensionless parameters ρ^*, ν^*, and β are far outside the experimental results. The similartiy principle requires that the dimensionless quantities describing a geometrical similar system must be the same to allow extrapolation which is violated here.

III.C.2. Neoclassical Transport Considerations

The neoclassical transport coefficients have different scaling properties dependent on the collisionallity regime. In the up-scaling of the 'conservative' as well as in the 'advanced' simulation scenario the core temperature increases with increasing

machine size. This in turn means that the collisionallity is decreasing. Therefore, at increasing machine size both the electron and ion distribution funcion will shift to neoclassical long-mean-free-path regimes ($1/\nu$ for electrons and $\sqrt{\nu}$ for ions). Due to the localised particles, the neoclassical diffusion coefficients in these regimes are an order of magnitude higher for the stellarator than for a corresponding tokamak. The neoclassical theory is also relevant for small stellarators (e.g. W7-AS) where easily $D^{\mathrm{neo}} > 1 \, \mathrm{m}^2/\mathrm{s}$. It should also be noted, that the electrons are well confined in an optimised stellarator, meaning the ion losses would be much larger than those for the electrons. This is prevented by the ambiporaity constraint which causes an inward pointing radial electric field bringing the ion transport down to the electron level while on the other hand somewhat increasing the electron transport.

This complex combination of different transport regimes with distinct scaling relations and additional coupling by the ambipolar radial electric field precludes the derivation of a combined analytic confinement time scaling which can only be given for individual regimes. This means, that although empirical scalings may be derived by regression, the confinement time scales differently dependent on the plasma properties.

III.C.3. Anomalous Transport Considerations

To complicate the situation even more, also the anomalous transport needs to be taken into account. As of today's experiments the anomalous transport has been observed to dominate at the plasma edge. Following this observation the empirical relationship $\chi_{ano} = c \, P^{3/4} \, n^{-1}$ has been employed for the anomalous transport in the 1-D simulations where the prefactor c is a free variable. In the upscaling simulations for both the 'conservative' and 'advanced' scenario the factor was fixed to $c = 1$. But the strong power dependence of this simple model leads to very high anomalous transport for larger machine sizes which seems from today's experiments unlikely. For this reason one simulation has been repeated with reduced c to investigate the general sensitivity. This is illustrated in Fig. 7, where the ratio of the ion neoclassical to anomalous energy flux is given over the normalised minor radius for the 'conservative' scenario at machine size $V = 1300 \, \mathrm{m}^3$ for $c = 1$ and $c = 0.2$ (selected to achieve $\chi_{ano} = 1 \, \mathrm{m}^2/\mathrm{s}$ at the edge observed in many experiments compared to $\chi_{ano} = 2.5 \, \mathrm{m}^2/\mathrm{s}$ for the $c = 1$ case).

It can be seen from the figure that in the case with the reduced prefactor, $c = 0.2$, the anomalous transport is consequently reduced and the neoclassical transport dominates over the greater part of the minor radius except at the very edge with $\chi_{ano} = 1 \, \mathrm{m}^2/\mathrm{s}$. In the case with the 'normal' prefactor, $c = 1$, the neoclassical transport is still larger by a factor 4 in the plasma centre but an increased portion of the edge beyond $\rho \geq 0.7$ is dominated by the anomalous energy flux with $\chi_{ano} = 2.5 \, \mathrm{m}^2/\mathrm{s}$ at the very edge.

Comparing both cases, the prefactor has a strong impact on the plasma transport and performance as the plasma β, volume averaged temperature $\langle T_i \rangle_V$, and the resulting alpha power nearly doubles in the case with the reduced anomalous transport. But the confinement ratio factor Θ, discussed in the previous subsection, changes only modestly from $\Theta = 1.45$ in the
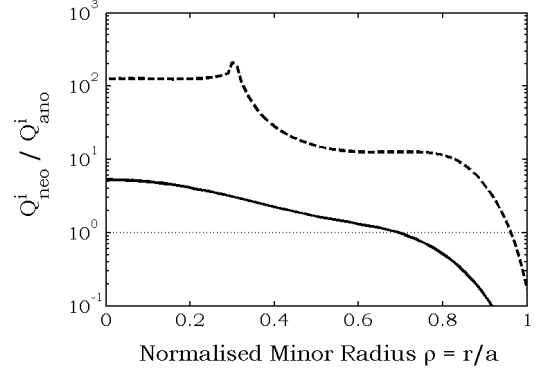

Fig. 7: Comparison of the ratio of ion neoclassical to anomalous heat flux, Q^i_{neo}/Q^i_{ano}, over normalised minor radius, $\rho = r/a$, for the 'conservative' scenario at machine size $V = 1300 \, \mathrm{m}^3$ for two different prefactors in the anomalous transport model: $c = 1$ (solid line) and $c = 0.2$ (dashed line).

case with $c = 1$ to $\Theta = 1.62$ with the reduced anomalous transport $c = 0.2$. Also, due to the impact of the anomalous transport, the lines in Fig. 7 exhibit different shape. The reason is, that the increased anomalous transport reduces the temperature of the plasma leading to reduced fusion power and alpha heating. As the neoclassical transport is very sensitive to temperature in the lmfp-regime ($D \sim T^{7/2}$ for $1/\nu$), neoclassical transport is reduced at increasing anomalous transport. The complex interplay with the electric field then leads to the strongly different ratios of neoclassical to anomalous ion energy flux.

It can be concluded that, apart from neoclassical transport, the anomalous transport plays an important role in reactor-sized HELIAS machines. A detailed understanding and extrapolation of anomalous, i.e. turbulent transport seems necessary to make precise predictions about the plasma performance of a burning plasma HELIAS. Although a simple empirical anomalous transport model was employed and gave first indications, the descriptive significance is limited. Turbulence simulations for 3-D stellarator geometries have been started recently.[36] The aim of this investigation lies especially on the ion-temperature-gradient mode which is anticipated to be a dominant micro-instability contributing to transport. From these studies, more relevant anomalous transport models may be derived compatible with the 1-D code increasing the general predictive capability.

III.D   Comparison of 0-D and 1-D Model

For the conservative scenario the direct extrapolation of W7-X within the 0-D model with $P_{fus} = 3000 \, \mathrm{MW}$ and the ISS04 confinement time scaling at $f_{ren} = 1$ would lead to a machine with a major radius around 25 m. The same conservative scenario achieves within the self-consistent 1-D transport model a fusion power of 3 GW at a major radius of 21 m and reaches a confinement time a factor 1.3 above the ISS04 scaling. If this confinement enhancement factor of 1.3 is applied to the 0-D model a major radius of 21 m is found which is consistent with the transport model.

9

In the advanced scenario the 0-D extrapolation for $f_{ren} = 1$ yields a major radius of around 19 m. In the transport simulations with the high density and field the conditions are already achieved at a upscaling of W7-X times 3, i.e. 16.5 m major radius, where a confinement time is achieved with a factor 1.2 beyond the ISS04 scaling. If this factor is again allowed for the 0-D model then the 16.5 m major radius are likewise found. All values are summarised in Tab. IV.

Model	0-D	0-D	1-D
conservative			
Major Radius [m]	25	21	21*
Conf. Enhancement Factor	1.0*	1.3*	1.3
advanced			
Major Radius [m]	19	16.5	16.5*
Conf. Enhancement Factor	1.0*	1.2*	1.2

TABLE IV: Summary of the major radius from direct extrapolation of Wendelstein 7-X with associated confinement enhancement factors for the comparison between the power balance model and the predictive transport model constraint by achieving 3000 MW fusion power. The values marked with a star are the respective input parameters in the model.

This result is important, as it means, that empirical scalings like ISS04 cannot be straightforwardly taken to extrapolate today's machines to devices of the size of fusion power plants. Rather, extrapolations must be iterated with predictive transport simulations due to the high impact of confinement on plant performance. In this respect it is important to consider the details of the magnetic configuration which plays a major role for the energy confinement. Although this work concentrated on the helical-axis advanced stellarator line, similar effects can be expected from other stellarators as the driving underlying physics are the same.

Therefore, the renormalisation factor cannot be taken as a simple constant in combination with an empirical confinement time scaling, but in total must either be iterated with transport simulations or a new consistent scaling be derived.

Nonetheless, the consistency of the 0-D and the 1-D model is a promising result. It means, that indeed predictive transport simulations can be carried out to narrow down an achievable confinement enhancement factor which then in turn can be used for systematic studies in a more simplified model as e.g. the power balance model of systems codes – as long as the transport simulations are iterated with the corresponding parameters.

IV CONCLUSIONS

From both models it is concluded that the confinement enhancement with respect to the ISS04 scaling has on the one hand a lower limit of about 0.5 under which ignition is not possible anymore. On the other hand, it has an upper limit in the range $1.5 - 1.8$ which is determined by the beta-limit above which the confinement enhancement no longer contributes to higher machine performance. Moreover; from the transport simulations can be learned that a confinement enhancement factor cannot be arbitrarily assumed since the confinement time is self-consistently determined from machine parameters and the complex interplay of transport effects. For the extrapolation of W7-X to reactor conditions using the predictive transport model the confinement enhancement is found to be in the range of 1.2 – 1.3. This means, empirical scalings and constant renormalisation factors cannot be used to directly extrapolate to fusion power plant devices, but, rather extrapolations must be iterated with predictive transport simulations. All these conclusions are in contradiction with the common assumptions of many power plant studies where confinement enhancements factors are arbitrarily assumed up to a factor 2 in order to design compact machines. Results of these studies should be reassessed under the limits of confinement enhancement. It should be noted that similar simulations have also been carried out for a Heliotron configuration which exhibited the same behaviour, but such work was not pursued in detail as the focus of this work is put on HELIAS devices.

In this work the W7-X high-mirror configuration has been upscaled. But optimisation procedures have progressed lately so that new quasi-isodynamic (minimum-B, maximum-J) configurations with poloidally closed contours of B may be an option for the future which exhibit very low neoclassical transport and good confinement of fast particles. Additionally, new insight into occurrence of turbulent micro instabilities allows further optimisation of such advanced configurations for reduced anomalous transport. Such configurations are candidates for HELIAS power plants and achieve even higher confinement enhancement factors (with respect to the ISS04 scaling).

Finally it can be concluded from the consistency of the global power balance approach and the predictive transport model that systems codes (which employ power balance models) can indeed be used to design and study HELIAS power plants as long as the corresponding confinement times are provided iteratively from the detailed predictive transport simulations. This makes the iteration process more complex since f_{ren} introduces new dependencies on all important parameters which must be considered for consistency. Nonetheless, with this approach new systematic studies of HELIAS burning plasma devices are to follow in the future.

V ACKNOWLEDGMENTS

REFERENCES

[1] T. Goto, J. Miyazawa, H. Tamura et al. "Design Window Analysis for the Helical DEMO Reactor FFHR-d1." *Plasma and Fusion Research: Regular Articles*, vol. 7, p. 2405084 (2012).

[2] C. D. Beidler, E. Harmeyer, F. Herrnegger et al. "The Helias reactor HSR4/18." *Nuclear Fusion*, vol. 41, p. 1759 (2001).

[3] J. Kisslinger, ed. *Fusion energy Proc. 17th Int. Conf.*, vol. 4 of *1239-42*. IAEA, Vienna, Yokohama (1998).

10

[4] F. Warmer, C. D. Beidler, A. Dinklage et al. "HELIAS Module Development for Systems Codes." *Fusion Engineering and Design*, vol. 91, p. 60 (2014).

[5] F. Warmer, C. D. Beidler, A. Dinklage et al. "Implementation and Verification of a HELIAS module for the Systems Code PROCESS." *Fusion Engineering and Design*, vol. [in press] (2014).

[6] H. Zohm. "On the minimum size of DEMO." *Fusion Science and Technology*, vol. 58, p. 613 (2010).

[7] H. Yamada, J. H. Harris, A. Dinklage et al. "Characterization of energy confinement in net-current free plasmas using the extended International Stellarator Database." *Nuclear Fusion*, vol. 45, p. 1684 (2005).

[8] A. Dinklage, H. Maaßberg, R. Preuss et al. "Physical model assessment of the energy confinement time scaling in stellarators." *Nuclear Fusion*, vol. 47, p. 1265 (2007).

[9] H. Wobig, T. Andreeva, C. D. Beidler et al. "Concept of Helias ignition experiment." *Nuclear Fusion*, vol. 43, p. 889 (2003).

[10] F. Schauer. "Coil winding pack FE-analysis for a HELIAS reactor." *Fusion Engineering and Design*, vol. 86, p. 636 (2011).

[11] F. Schauer, K. Egorov and V. Bykov. "HELIAS 5-B magnet system structure and maintenance concept." *Fusion Engineering and Design*, vol. 88, p. 1619 (2013).

[12] W. Lotz, P. Merkel, J. Nührenberg et al. "Collisionless alpha -particle confinement in stellarators." *Plasma Physics and Controlled Fusion*, vol. 34, p. 1037 (1992).

[13] H. Yamada, A. Komori, N. Ohyabu et al. "Configuration flexibility and extended regimes in Large Helical Device." *Plasma Physics and Controlled Fusion*, vol. 43, no. 12A, p. A55 (2001).

[14] A. Weller, J. Geiger, A. Werner et al. "Experiments close to the beta-limit in W7-AS." *Plasma Physics and Controlled Fusion*, vol. 45, no. 12A, p. A285 (2003).

[15] W. A. Cooper, L. Brocher, J. P. Graves et al. "Drift Stabilisation of Ballooning Modes in an Inward-Shifted LHD Configuration." *Contributions to Plasma Physics*, vol. 50, p. 713 (2010).

[16] K. Ichiguchi and B. A. Carreras. "Multi-scale MHD analysis incorporating pressure transport equation for beta-increasing LHD plasma." *Nuclear Fusion*, vol. 51, no. 5, p. 053021 (2011).

[17] M. Drevlak, D. Monticello and A. Reiman. "PIES free boundary stellarator equilibria with improved initial conditions." *Nuclear Fusion*, vol. 45, p. 731 (2005).

[18] H. Maaßberg, C. D. Beidler and E. E. Simmet. "Density control problems in large stellarators with neoclassical transport." *Plasma Physics and Controlled Fusion*, vol. 41, p. 1135 (1999).

[19] M. Greenwald. "Density limits in toroidal plasmas." *Plasma Physics and Controlled Fusion*, vol. 44, no. 8, p. R27 (2002).

[20] S. Sudo, Y. Takeiri, H. Zushi et al. "Scalings of energy confinement and density limit in stellarator/heliotron devices." *Nuclear Fusion*, vol. 30, no. 1, p. 11 (1990).

[21] J. Miyazawa, R. Sakamoto, S. Masuzaki et al. "Density limit study focusing on the edge plasma parameters in LHD." *Nuclear Fusion*, vol. 48, no. 1, p. 015003 (2008).

[22] L. Giannone, R. Burhenn, K. McCormick et al. "Radiation power profiles and density limit with a divertor in the W7-AS stellarator." *Plasma Physics and Controlled Fusion*, vol. 44, no. 10, p. 2149 (2002).

[23] A. Dinklage, M. Yokoyama, K. Tanaka et al. "Inter-machine validation study of neoclassical transport modelling in medium- to high-density stellarator-heliotron plasmas." *Nuclear Fusion*, vol. 53, p. 063022 (2013).

[24] C. D. Beidler, K. Allmaier, M. Y. Isaev et al. "Benchmarking of the mono-energetic transport coefficients - results from the International Collaboration on Neoclassical Transport in Stellarators (ICNTS)." *Nuclear Fusion*, vol. 51, p. 076001 (2011).

[25] A. A. Subbotin, M. I. Mikhailov, V. D. Shafranov et al. "Integrated physics optimization of a quasi-isodynamic stellarator with poloidally closed contours of the magnetic field strength." *Nuclear Fusion*, vol. 46, p. 921 (2006).

[26] H. E. Mynick, N. Pomphrey and P. Xanthopoulos. "Optimizing Stellarators for Turbulent Transport." *Physical Review Letters*, vol. 105, p. 095004 (2010).

[27] Y. Turkin, H. Maaßberg, C. D. Beidler et al. "Current Control by ECCD for W7-X." *Fusion Science and Technology*, vol. 50, p. 387 (2006).

[28] Y. Turkin, C. D. Beidler, H. Maaßberg et al. "Neoclassical transport simulations for stellarators." *Physics of Plasmas*, vol. 18, p. 022505 (2011).

[29] A. A. Galeev and R. Z. Sagdeev. "Theory of Neoclassical Diffusion." *Reviews of Plasma Physics*, vol. 7, p. 257 (1979).

[30] D. D.-M. Ho and R. M. Kulsrud. "Neoclassical transport in stellarators." *Physics of Fluids*, vol. 30, p. 442 (1987).

[31] W. I. van Rij and S. P. Hirshman. "Variational bounds for transport coefficients in threedimensional toroidal plasmas." *Phyiscs of Fluids B: Physics of Plasmas*, vol. 1, p. 563 (1989).

[32] S. P. Hirshman, K. C. Shaing, W. I. van Rij et al. "Plasma transport coefficients for nonsymmetric toroidal confinement systems." *Physics of Fluids*, vol. 29, p. 2951 (1986).

[33] K. C. Shaing. "Stability of the radial electric field in a nonaxisymmetric torus." *Physics of Fluids*, vol. 27, p. 1567 (1984).

[34] H. Maaßberg, R. Brakel, R. Burhenn et al. "Transport in stellarators." *Plasma Physics and Controlled Fusion*, vol. 35, p. B319 (1993).

[35] U. Stroth. "A comparative study of transport in stellarators and tokamaks." *Plasma Physics and Controlled Fusion*, vol. 40, p. 9 (1998).

[36] P. Xanthopoulos, F. Merz, T. Grler et al. "Nonlinear Gyrokinetic Simulations of Ion-Temperature-Gradient Turbulence for the Optimized Wendelstein 7-X Stellarator." *Physical Review Letters*, vol. 99, p. 035002 (2007).

[37] J. H. E. Proll, P. Xanthopoulos and P. Helander. "Collisionless microinstabilities in stellarators. II. Numerical simulations." *Physics of Plasmas*, vol. 20, p. 122506 (2013).

[38] K. Lackner and N. A. O. Gottardi. "Tokamak confinement in relation to plateau scaling." *Nuclear Fusion*, vol. 30, p. 767 (1990).

On the Characterisation of the Edge Ion Heat-Flux in Advanced Stellarators

F. Warmer[a,*], P. Xanthopoulos[a], C.D. Beidler[a], H. Maaßberg[a], R. Wolf[a]

[a] *Max Planck Institute for Plasma Physics, D-17491, Greifswald, Germany*

Abstract

Due to the reduction of neoclassical transport in optimised stellarator configurations, it is expected that turbulence will significantly contribute to the heat and particle transport – at least in the edge region of the plasma – and may thus pose a limit to the achievable confinement and performance of such devices. In order to predict the confinement and develop plasma scenarios for W7-X and beyond for Helias reactors in an efficient way, it is important to develop models which can describe the basic characteristics and level of turbulent transport using only a fraction of the computational power which is normally required for gyrokinetic simulations on petaflop scale.

In this work we concentrate on the ion-temperature-gradient (ITG) mode which has so far been well investigated and is considered to strongly contribute to transport. Non-linear full-flux-surface gyrokinetic simulation results are compared for W7-X and its predecessor W7-AS. Although the fluctuations are more localised in W7-X, it is intriguing that the normalised heat-flux scaling is nearly identical.

On this basis experimental results from high performance W7-AS discharges are reviewed which show strong turbulent transport at the plasma edge. As the experimental characteristics of the turbulent ion transport are similar to the theoretical gyrokinetic results, a basic critical gradient model is proposed and tested in 1-D transport simulations against the W7-AS experimental results showing good agreement.

The model is further applied to W7-X showing that, even under consideration of a critical gradient model for the ion heat-flux, the global confinement enhancement with respect to the empirical ISS04 scaling of $\tau_E^{1D}/\tau_E^{ISS04} = 1.7$ is retained. Extrapolation to a Helias reactor scenario shows similar promising results with a confinement improvement factor of 1.3. However, the overall transport is sensitive to the 'stiffness' used in the critical gradient model.

Keywords: Helias, W7-X, W7-AS, Transport modelling, Critical gradient model

1. Introduction

A key property for the success of fusion power plants is the confinement of the plasma energy and particles. The tokamak demonstrates good confinement over a wide range of experimental devices, and this success triggered the ITER project [1], a large tokamak experiment under construction in France, designed to achieve a significant amount of fusion power. Despite this encouraging feature, tokamaks suffer from disruptions and plasma instabilities driven by the internal current, thus limiting their performance. In addition, tokamaks are difficult to operate in steady-state considering the required high amount of current drive, leading to very high demands on the control system.

The stellarator concept, on the other hand, is free of all of the above mentioned drawbacks. However, at increasing temperatures stellarator experiments demonstrated a degradation of confinement attributed to the effective transport of particles 'trapped' in certain unfavorable locations of the complicated magnetic field, i.e. the neoclassical transport. In modern optimised stellarators of the Helias-type this issue is overcome thanks to a sophisticated three-dimensional shaping of the magnetic field. This optimisation principle will be validated by the Wendelstein 7-X (W7-X) experiment [2], which started operation in 2015. Further, enhanced optimisation for so-called 'quasi-isodynamic' configurations is subject of ongoing research [3, 4].

With the drastic improvement of trapped-particle confinement in advanced stellarators, however, transport losses induced by turbulence will inevitably play a significant role. Due to its strong temperature dependence, neoclassical transport is expected to still be predominant in the high temperature plasma core, but as the temperature decreases strongly towards the plasma edge, neoclassical transport is reduced and turbulent transport becomes important. Already in Wendelstein 7-AS (W7-AS), the predecessor of W7-X, it was shown that turbulent losses overcome the neoclassical transport in the outer third of the minor radius even in plasmas with 'optimum confinement' [5].

In this context, renewed attention is focused on the prospects of optimised stellarators as fusion power plants. However, in order to assess the size and performance of such devices, an accurate prediction of the plasma transport is required, which crucially affects confinement. So far such predictions were achieved by employing empirical confinement time scalings. These estimations, despite their merit of being obtained by regression from a large database of various stellarators worldwide [6], are hardly adequate for studies on optimised configurations [7]. In these devices plasma turbulence is expected to play an important role perhaps even overcoming the neoclassical transport which dominates in existing stellarator experiments.

While many well-validated codes and tools have been developed in the course of stellarator research for the prediction and analysis of the neoclassical transport effects [8], the treatment of turbulence in 3D magnetic fields has only recently been started [9]. So far, complex gyrokinetic codes are used to investigate turbulent behaviour in stellarators which require peta-flop scale supercomputers to run. But in order to prepare operation of high-performance discharges of W7-X efficiently, predictive capability of turbulent transport is required on a more efficient computational scale. Such a development is the topic of this paper with concentration on the ion energy-flux induced by the ion-temperature-gradient instability (ITG).

---
*Corresponding author, Tel.: +49 (0)3834 88-2583
Email address: `Felix.Warmer@ipp.mpg.de` (F. Warmer)

In section 2 indications and features of ITG transport from gyrokinetic simulations of W7-X and W7-AS are presented and the similarity of the ITG behaviour between those two devices is highlighted. Further, experimental results of W7-AS high performance discharges are reviewed in view of the edge turbulent transport. On the basis of the qualitative agreement between theory and experiment, in section 3 a basic critical gradient model (CG) is proposed to describe the turbulent ion heat-flux which is compatible with a neoclassical 1-D transport code. Application to a W7-AS test case shows, that the model can capture the basic transport features. Consequently the model is also applied for W7-X in section 4. As still several uncertainties remain in this approach the section is concluded by sensitivity analysis of W7-X confinement with respect to parameter variations in the basic CG-model. Beyond that, the model is also applied for a reactor scenario of the Helias line in section 5. The various results and implications of the work are discussed and summarised in section 6.

2. Turbulence in Advanced Stellarators

In tokamak and stellarator plasmas, two important microinstabilities which are thought to be responsible for turbulent transport are the ion-temperature-gradient (ITG) mode and the trapped-electron-mode (TEM), and as such both should be considered as relevant for predictive transport modeling. Recent advances in stellarator gyrokinetics [10, 11] have demonstrated, however, that the role of the electrons in W7-X is not as great as in tokamaks. For instance, TEMs appear to be much less unstable and the kinetic electrons do not exert a high impact on ITG. These findings justify to a certain degree the simplifying premise that the electrons follow a Boltzmann distribution, which also renders turbulence simulations on the stellarator surface feasible, in terms of computational resources. Notwithstanding this favorable behavior, future work should encompass the full electron dynamics in order to contain additional turbulence channels, like TEMs, electron temperature gradient driven turbulence and, of course, electromagnetic effects.

The focus of this paper is therefore the turbulent ion heat-flux and the ITG instability. In the following the properties of ITG-induced transport in W7-X from full flux-surface gyrokinetic simulations are reviewed and new results for W7-AS are presented for the first time. The ITG features of both devices are compared and experimental results from W7-AS are reviewed.

2.1 Indications for ITG-induced Transport from Gyrokinetic Simulations

It is well known from tokamaks (in particular in L-mode) how temperature gradient driven instabilities have strong impact on the plasma transport leading to so-called profile 'stiffness'. When the temperature gradient exceeds a critical threshold, the transport in tokamaks is observed to increase severely thus holding the temperature gradient at its critical value. The temperature profile is therefore independent of any heating scheme and the temperature which can be reached is largely determined by the boundary condition. An exception may be tokamak plasmas with an internal transport barrier which exhibit improved core confinement with steeper pressure gradients. In tokamak H-mode, the edge develops a so-called pedestal which

shifts the stiff temperature profile as a whole towards higher temperatures by a sharp increase of the edge temperature [12].

But so far, neither profile stiffness nor pedestals have been observed in stellarator experiments. In the absence of a plausible assumption for the temperature profile, it is advisable to conduct a theoretical investigation of ITG-induced turbulence in stellarators using a numerical gyrokinetic formulation. In tokamaks, it is usually sufficient to simulate a single flux tube to determine the transport on a flux-surface, as thanks to axisymmetry, all flux tubes are identical. In stellarators, in contrast, different flux tubes are not geometrically equivalent, thus requiring the simulation of the entire flux-surface to determine quantitatively the transport level. For this purpose, the gyrokinetic code GENE [13, 14] was employed, which is capable of treating an entire flux-surface of any toroidal configuration [15], while maintaining the local approximation in the radial direction.

The results of a full flux-surface GENE simulation for W7-X is illustrated in Fig. 1 [16]. The turbulence is driven by the ion-temperature-gradient for gyrokinetic ions and Boltzmann distributed (adiabatic) electrons.

All simulations were done at the radial location where the normalised toroidal flux takes the value $s = 0.5$, ignoring the gradients of density and electron temperature. In addition, due to the computational limitations, both the shear and the radial electric field could not be taken into account.

Beyond that, only little is known about turbulent particle transport in advanced stellarators. In particular, are gyrokinetic simulations of stellarators not yet able to calculate the turblence induced particle flux. However, this is beyond the scope of this work.

In future works, it is foreseen to include both the effect of the density gradient as well as the electric field which are anticipated to reduce ITG turbulence.
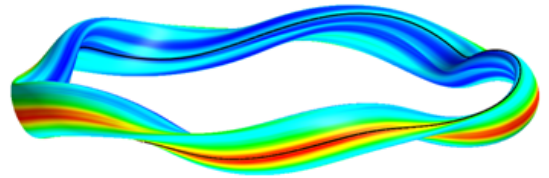

Figure 1: ITG-induced root-mean-squared electrostatic potential fluctuations of a full-flux-surface GENE simulation of Wendelstein 7-X [16].

As can be seen from Fig. 1, a remarkable stellarator-specific outcome is that the strongest turbulent fluctuations are located on a thin band on the outboard side of the flux-surface while the remainder of the surface is relatively quiescent. This is in strong contrast to tokamaks where typically the full outboard side is dominated by strong fluctuations. Thus, it has been identified that the variation of the curvature on a flux-surface in a stellarator such as W7-X causes the localisation of the turbulent fluctuations. This localisation affects the scaling of the energy transport with respect to the ion gyroradius normalised to the minor radius, $\rho^* = \rho_i/a$. It turns out that, already when a single flux-surface is considered, i.e. the radial direction is treated locally, the ion heat-flux varies with ρ^* such that as ρ^* takes larger values, the transport stiffness (i.e. the rate
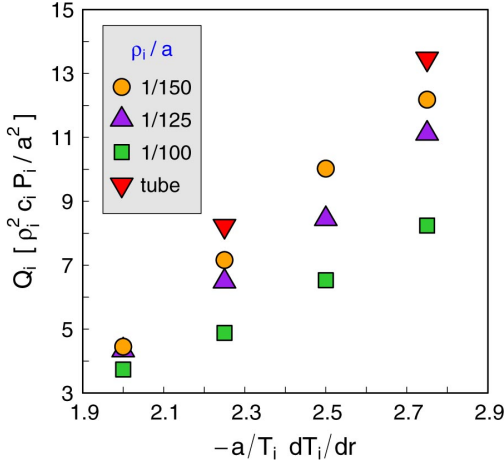
2

Figure 2: Normalised heat-flux density over the ion-temperature-gradient length for non-linear full-flux-surface GENE simulations of W7-X for three different values of the normalised ion gyroradius $\rho^* = \rho_i/a$. Results from simulations of the most unstable flux tube at two values of the temperature gradient length are shown for comparison [16].

at which the heat-flux increases with the temperature gradient length) is decreased as seen in Fig. 2. In tokamaks, on the other hand, it was shown that a similar ρ^*-dependence of the turbulent transport is established, once radially non-local effects were introduced in gyrokinetic simulations [17, 18]. Although numerical evidence is still lacking, a plausible assumption is that stellarator transport would behave in a similar way, and therefore the individual dependencies (surface plus radius) could in principle combine, so that the trend shown in Fig. 2 could be even more pronounced.

In the limit $\rho^* \to 0$, the stiffness converges to a maximum value which can be regarded as the worst case in view of the ITG-mode and thus the stiffness becomes independent of ρ^*, which will be important for the comparability of W7-AS and W7-X in the next subsection.

2.2 Comparison of W7-AS and W7-X

In order to clarify if conclusions about W7-X can be extrapolated from its predecessor W7-AS, similar non-linear full-flux-surface gyrokinetic simulations for W7-AS had to be carried out as well. The resulting time-averaged root-mean-squared electrostatic potential fluctuations are for both devices compared in Fig. 3.

It turns out that there is some qualitative difference in the poloidal distribution of the fluctuations. While the fluctuations for W7-X are quite localised in a small band on the outboard side, for W7-AS the fluctuations are somewhat more broadly distributed. Still, the fluctuations in W7-AS are stellarator-specific compared to tokamaks where the full outboard side has equally high fluctuations. Also, the fluctuations distribution in W7-AS is similar to other investigated quasi-omnigenous stellarator configurations such as MPX which showed a similar pattern [16].

Despite this difference, the question arises if the unique fluctuation pattern has some impact on the heat-flux. To answer this, the normalised heat-flux density $\widehat{Q} = Q_i/Q_{gB}$ is compared for W7-X and W7-AS in Fig. 4. The radial flux-surface

averaged heat-flux density Q_i is thereby normalised to the gyro-Bohm value

$$Q_{gB} = \frac{\rho_i^2 v_{Ti} p_i}{a^2} \tag{1}$$

where ρ_i is the ion gyroradius, v_{Ti} the thermal speed, p_i the ion pressure and a the minor radius of the machine.

The normalised temperature gradient a/L_{Ti}, being the driving factor of the ITG mode, has been varied between 2 and 2.75 in order to compare the stiffness of both configurations.

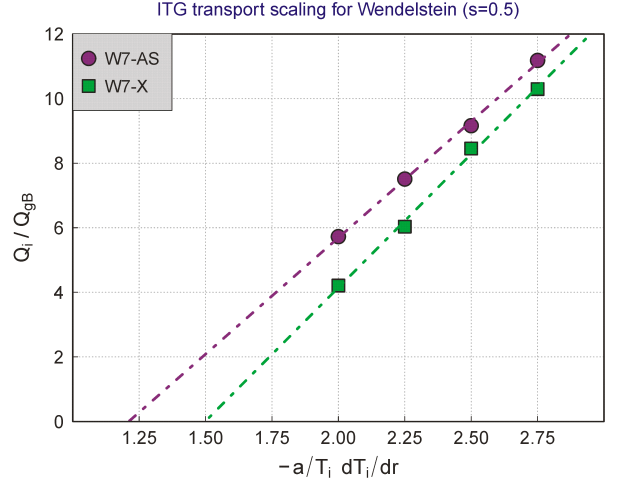

Figure 4: Normalised heat-flux density as a function of the ion-temperature-gradient for non-linear full flux-surface GENE simulations of W7-X ($\rho^* = 1/400$) and W7-AS ($\rho^* = 1/150$).

As has been pointed out in the last subsection, the stiffness depends on the normalised gyroradius if its value is larger than $\rho^* > 1/150$. Therefore, both for W7-X and W7-AS a very small ρ^* was chosen, such that one can assume the results of the stiffness presented in Fig. 4 to be independent of ρ^*. This is important in order to be able to compare the stiffness in these simulations for both devices as this limit represents the absolute worst case for either configuration, thus ensuring comparability.

Interestingly, the scaling of the normalised heat-flux density is very similar for both W7-X and W7-AS in the local limit. The critical gradient length is for W7-X slightly shifted upwards with $(a/L_{Ti})_{\text{crit}}^{\text{ITG}} = 1.5$ compared to 1.25 for W7-AS. The stiffness, i.e. the linear increase of the heat-flux density with increasing ion-temperature-gradient length, is nearly identical. This favorable similarity allows to employ existing experimental results from W7-AS, in order to predict salient transport properties for W7-X, as presented in the following.

One has to keep in mind, that with a plasma volume of 30 m^2 W7-X is much larger than W7-AS with 1 m^2 and will employ much higher heating powers. In order to be able to relate the heat-flux densities of both devices some global scaling aspects must be considered. Starting with the power balance, the total power crossing the flux-surface is

$$P = \int \frac{Q \cdot \nabla r}{|\nabla r|} dS = A \langle Q \cdot \nabla r \rangle \tag{2}$$

where $\langle \ldots \rangle$ represents the flux-surface average and $A = V' \simeq 4\pi^2 R \cdot r$ is the radial derivative of the volume enclosed by the surface with the major radius R at the radial location r. The
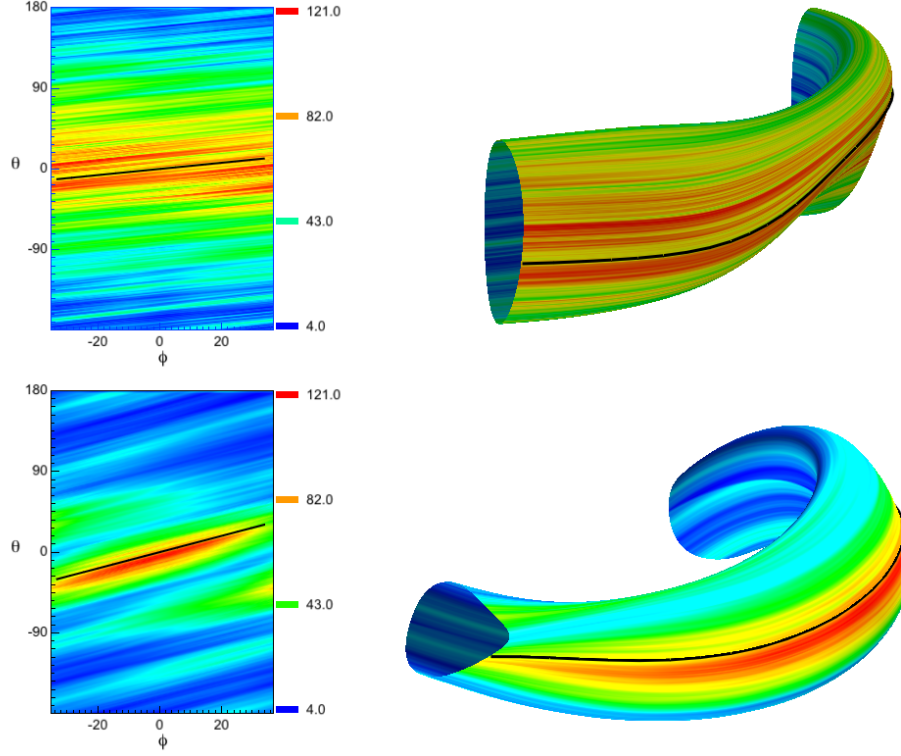
3

Figure 3: ITG induced root-mean-squared electrostatic potential fluctuations of a full flux-surface GENE simulation of W7-AS (top) and W7-X (bottom).

radial flux-surface averaged heat-flux density is as above denoted by $\langle Q \cdot \nabla r \rangle = Q_i$.

In steady-state the total heating power injected into the plasma must also be exhausted. The total power crossing the last closed flux-surface (assuming low radiation) thus becomes

$$P \simeq 4\pi^2 R \cdot a \cdot Q \qquad (3)$$

where a is the minor radius of the device. This equation can now be used to compare the heat-flux density in two differently sized machines with different heating power as for W7-AS and W7-X and one arrives at

$$Q_{\text{W7X}} = \frac{P_{\text{W7X}}}{P_{\text{W7AS}}} \cdot \frac{(R \cdot a)_{\text{W7AS}}}{(R \cdot a)_{\text{W7X}}} \cdot Q_{\text{W7AS}}. \qquad (4)$$

However, equation (4) is only valid for the last closed flux-surface of the considered volume. In order to extend this total balance to a local description, one can make use of the results presented in Fig. 4 taking $\widehat{Q}_{\text{W7X}} = \widehat{Q}_{\text{W7AS}} = \widehat{Q}$. Replacing Q_{W7AS} by $Q_{gB}^{\text{W7AS}} \cdot \widehat{Q}$, a local model for W7-X based on W7-AS results can be formulated to

$$Q_{\text{W7X}}\left(\frac{a}{L_T}\right) = \frac{P_{\text{W7X}}}{P_{\text{W7AS}}} \cdot \frac{(R \cdot a)_{\text{W7AS}}}{(R \cdot a)_{\text{W7X}}} \cdot Q_{gB}^{\text{W7AS}} \cdot \widehat{Q}\left(\frac{a}{L_T}\right). \qquad (5)$$

In order to use this ansatz to describe the ITG heat-flux density in W7-X, it remains to define $\widehat{Q}(a/L_T)$. One could use the theoretical findings as shown in Fig. 4. However, here we refrain from doing so, as several important effects were not accounted for in the GENE simulations.

In order to check if the theoretical findings are consistent with experimental results and further to build a broader basis to define $\widehat{Q}(a/L_T)$, the experimental results of W7-AS are reviewed in these respects in the next section.

As in the following the main parameters of W7-AS, W7-X and a Helias reactor scenario [19, 20] (described in more detailed in section 5) are frequently used, the main parameters of these machines are summarised in Tab. 1.

	W7-AS	W7-X	Reactor
R [m]	2	5.5	22
a [m]	0.17	0.53	1.6
B_0 [T]	2.5	2.5	5.5
P [MW]	1	9	600
T_{edge} [keV]	0.1	0.1	2.5

Table 1: Main design parameters of W7-AS, W7-X and a Helias reactor scenario.

2.3 W7-AS Experimental Results

The results of the gyrokinetic simulations suggests that transport induced from ITG turbulence could play a significant role in quasi-isodynamic advanced stellarators. In the following, the experimental data from W7-AS is reviewed with respect to indications for edge turbulent transport. For such a study two well documented high performance discharges of W7-AS, #34609 and #34313, are selected, which have been analysed in terms of neoclassical transport [21]. The profiles for the discharge #34609 are shown in Fig. 5. The corresponding profiles for the discharge #34313 are similar with about half the density in the centre compared to #34609.

It can be seen from Fig. 5, that a clear discrepancy arises between the experimental, Q_i^{exp}, and the neoclassical ion energy-flux, Q_i^{neo}, in the outer region of the minor radius $r/a > 2/3a$
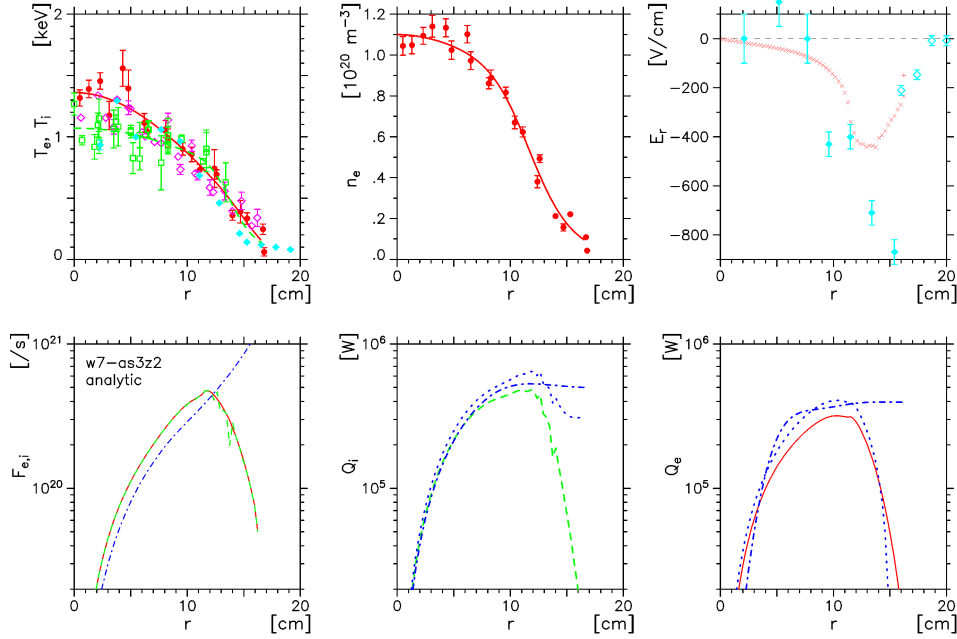
4

Figure 5: Experimental ion (green) and electron (red) temperature (top-left), experimental plasma density (red, top-middle) as well as experimental (blue points) and neoclassical (red) radial electric field (top-right) for the W7-AS discharge #34609. Also shown are experimental (dashed-blue) and neoclasscial (red and green lines) particle fluxes (bottom-left), ion energy-flux (bottom-middle) and electron energy-flux (bottom-right). The experimental curves have been obtained by integration of the particle and power sources excluding for the energy-fluxes the term $q\Gamma E_r$ (see discussion below). The neoclassical fluxes have been obtained using equation (11) and thermal transport coefficients from the DKES code.

of the presented discharges. This indicates that, apart from neoclassical transport, other transport mechanisms must determine the energy-flux at the edge.

In order to assess the contribution of turbulence to the ion transport, the driving factor, namely the normalised ion temperature gradient length

$$\frac{a}{L_{Ti}} = a \cdot \frac{|\nabla T_i|}{T_i} \qquad (6)$$

is plotted as function of the minor radius in Fig. 6.
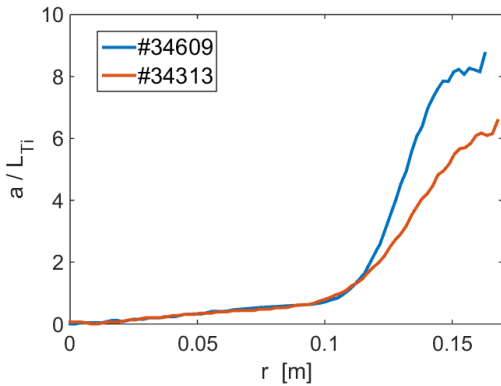
Figure 6: Normalised ion-temperature-gradient over the minor radius of the experimental results from W7-AS for #34609 and #34313.

The normalised ion temperature gradient length increases

for both #34609 and #34313 sharply in the outer third of the minor radius which coincides with the region where the neoclassical and experimental ion energy-flux deviate. It seems therefore likely that the edge energy-fluxes of the presented cases of W7-AS are related to turbulent transport driven by micro-instabilities. These observations are in contrast to the behaviour seen in tokamaks where – especially in L-mode plasmas – the normalised temperature gradient length is constant over nearly the entire minor radius [12]. It cannot yet be conclusively answered why the temperature gradient length is low in the core region of W7-AS. However, the focus here is on the ion heat-flux at the edge which is analysed in the following in more detail.

From a time-scale separation argument [22] one can argue that neoclassical and turbulent energy-fluxes are additive, thus one can define the 'residual' energy-flux Q_i^{res} derived from the experimental profiles as

$$Q_i^{\mathrm{res}} = Q_i^{\mathrm{exp}} - Q_i^{\mathrm{neo}}. \qquad (7)$$

As this residual energy-flux is here speculated to be driven by turbulence, in the following the residual energy-flux is related implicitly over the minor radius to the normalised temperature gradient, see Fig. 7.

Looking again at Fig. 5 one realises that there is a very high particle flux Γ at the plasma edge which cannot be explained by the neoclassical analysis. This particle flux Γ has been obtained by integration of the particle sources from gas puff, NBI deposition and recycling using the EIRENE code [23].

If one distinguishes the power balance between electrons and ions, as is done here, one has to consider the power loss/gain

5

of the individual particle species due to the raidal electric field, i.e. the term $q \cdot \Gamma \cdot E_r$ needs to be considered in the power balance of each species. For the ions, the integral form of the power balance thus becomes

$$Q_i^{\exp}(r) = \frac{1}{V'} \int_0^r \left[P_h + P_{ei} - P_{cx} - \Gamma T_i + q\Gamma E_r \right] V' \mathrm{d}r \quad (8)$$

where P_h is the absorbed heating power, P_{ei} the collisional power exchange between electrons and ions and P_{cx} the power loss through charge exchange.

In the original analysis carried out in [21] the term $q \cdot \Gamma \cdot E_r$ was not included due to the uncertainty of the radial electric field. However, for the sake of relevance to the present work, an analysis was carried out including the power loss due the radial electric field. Due to the uncertainty of the radial electric field measurements, we consider on the one hand a case using the neoclassical ambipolar radial electric field and and on the other hand a case using a fit of the experimental data points of E_r. The results are shown in Fig. 7,
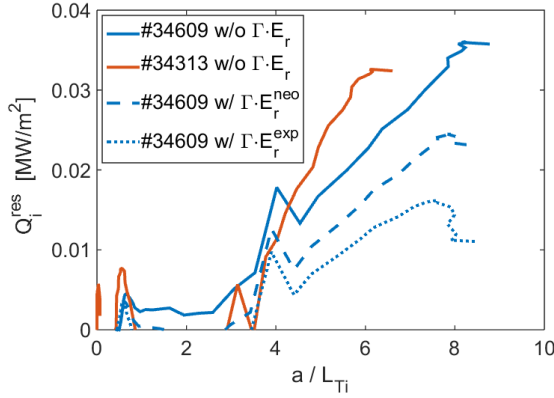
Figure 7: Residual edge ion energy-flux density as function of the normalised temperature gradient length of the experimental results from W7-AS for discharges #34609 (blue) and #34313 (orange) excluding $q \cdot \Gamma \cdot E_r$ for the experimental heat-flux. Further are shown cases for #34609 including the term for the neoclassical (dashed line) and a fitted experimental radial electric field (pointed line).

In Fig. 7 a clear correlation between the residual edge ion energy-flux and the normalised temperature gradient is observed. It is intriguing that such an experimental mapping resembles very much the typical critical gradient behaviour found in the ITG gyrokinetic simulations – even when $q \cdot \Gamma \cdot E_r$ is considered. Following this argumentation, the critical gradient from the W7-AS experiments is in the range of $(a/L_{Ti})_{\mathrm{crit}} \approx 2 \dots 3$, which is higher than the value obtained from the GENE simulation for W7-AS with 1.25.

The total residual ion energy-flux is comparable in both discharges. The normalised density gradient length at the edge is also comparable in both discharges, reaching large values towards the edge.

3. The Transport Model

Following a widely used practice in the tokamak community [24, 25, 26, 27, 28], in the following we introduce a basic critical gradient heat-flux model (CG). The basic features of the turbulent transport found in Helias-type configurations can be used for transport estimations based on simulations and existing experimental results alike. We should mention that a similar approach has also recently been proposed for the LHD experiment combining fits from linear ITG growth rates and the zonal flow (ZF) residual levels [29]. This approach, although quite successful for LHD, would not be applicable to W7-X. For instance, it has been shown that the dynamic as well as the long term ZF behavior is entirely different in the two devices, due to the distribution of trapped particles [10].

The contribution of anomalous transport in W7-AS has historically been expressed via a rule following the inverse plasma density, also involving a fudge factor, obtained from a regression of experimental data [30, 31]. In this work, we concentrate instead on a basic critical gradient model, in which the energy-flux density is directly related to the driving gradient. Below criticality, no heat-flux is assumed, while beyond that threshold the heat-flux is expected to quickly grow. As demonstrated by the non-linear gyrokinetic simulations, see Fig. 2, such a relation can very well be described by a linear relation [26]. In its most basic form we can describe these features with the expression

$$Q_i^{\mathrm{CG}} = w \cdot y \cdot H(y), \quad (9)$$

where w is the linear increase, from here on called 'stiffness', y the normalised temperature gradient minus the critical value:

$$y = \frac{a}{L_{Ti}} - \left(\frac{a}{L_{Ti}} \right)_{\mathrm{crit}} \quad (10)$$

and H is the Heaviside function to ensure that the energy-flux is zero below marginality, i.e. $y < 0$. The model in this form has thus two free parameters, the stiffness w and the critical gradient $(a/L_{Ti})_{\mathrm{crit}}$, which need to be determined.

For the analysis of the neoclassical transport, it is assumed that the plasma may be described in the local approximation to solve the drift kinetic equation. Consequently all quantities are assumed to be constant on flux-surfaces such that the plasma is described only in one dimension by the flux-surface label ψ. The transport code [32, 33] solves the power balance for the electrons and ions and the neoclassical ion energy-flux density is as usual expressed as

$$Q_i^{\mathrm{neo}} = -n_i T_i \left[D_{21}^i \left(\frac{\nabla n_i}{n_i} - \frac{Z_i E_r}{T_i} \right) + D_{22}^i \frac{\nabla T_i}{T_i} \right] \quad (11)$$

where the thermal transport coefficients D_{ij} are obtained by the appropriate energy convolutions with the local Maxwellian distribution function and the mono-energetic diffusion coefficient describing the radial transport. A database of the mono-energetic diffusion coefficients is prepared in advance for each magnetic configuration using the DKES code [34, 35]. The radial electric field E_r is obtained by solving the ambipolarity constraint $Z_i \Gamma_i = \Gamma_e$ where Z_i is the charge number and $\Gamma_{i,e}$ the particle fluxes of ions and electrons, respectively.

In our approach here, the total ion energy-flux considered in the power balance is according to the scale separation argument the sum of the neoclassical part and the turbulent energy-flux (here described by the CG-model):

$$Q_i = Q_i^{\mathrm{neo}} + Q_i^{\mathrm{CG}} \quad (12)$$

6

The neoclassical transport of the electrons is modeled in the same way as for the ions, while the turbulent transport of the electrons is modeled as

$$Q_e^{\mathrm{ano}} = -\chi_e^{\mathrm{ano}} n_e \nabla T_e \tag{13}$$

where the turbulent heat conductivity $\chi_e^{\mathrm{ano}} \sim n^{-1}$ has been derived empirically from a regression over a wide range of experimental data from W7-AS [30, 31].

There is no specific reason to assume that the electron-driven edge transport cannot be described via micro-turbulence, similarly to what the present work suggests for the ion-driven transport. However, in the absence of simulations involving electrons as gyrokinetic species, we are forced to fall back on the empirical description expressed by Eq. (13). A more physics motivated model, as has been proposed for the ion transport, will be the subject of a future study. In the next step, the transport model shall be applied to the W7-AS experimental data with focus on the ion energy-flux in order to test the applicability of the proposed critical gradient model.

3.1 Test of CG-Model against W7-AS Data

It is self-evident that the model cannot be validated at this point, not even within W7-AS, as no other well documented high performance discharges are available. However, by simulating W7-AS including the critical gradient model, it can be tested that the model, at least, does not contradict the experimental observations and is capable of reproducing the profiles.

For the preparation of the W7-AS simulations in the first step a database of mono-energetic transport coefficients must be created. This has been done with DKES employing the W7-AS magnetic configuration with a finite beta-profile reaching a volume-averaged value of $\langle \beta \rangle = 0.4$ %. In the experimental discharges of relevance here, the full field was used with $B_t = 2.5$ T.

For the simulations the density profile is used as input and kept constant since we are not interested in transient behaviour and, in particular, a model for the turbulent particle flux is missing. The plasma heating is also taken constant, and modelled according to the calculated absorption profiles from which the radiation from impurities is directly subtracted.

The turbulent electron heat conductivity is adjusted such as to reach the same value at the edge as in the experimental data with $\chi_e^{\mathrm{edge}} = 1.6$ m^2/s.

As the transport model solves a set of coupled diffusion equations, the required boundary conditions play an important role. Both the edge ion and electron temperatures are set at $T_{i,e} = 0.1$ keV in agreement with the experimental values.

Finally the two free parameters of the critical gradient model are adjusted according to the experimental observations with the W7-AS stiffness parameter being $w_{\mathrm{W7AS}} \approx 0.006$ MW/m^2 per unit length of a/L_{Ti} and $(a/L_{Ti})_{\mathrm{crit}} = 2.3$.

With these inputs the integrated 1-D simulations are conducted, and the temperature profiles, the energy-fluxes as well as the radial electric field are calculated self-consistently. The simulation results for discharge #34609 are compared to the experimental results of W7-AS in Figs. 8, 9 and 10.

As can be seen from the figures, the integrated transport modeling is capable of reproducing the experimental profiles. Only the ion temperature profile deviates in the 'transition-region' around $r = 0.1$ m where the plasma transport changes
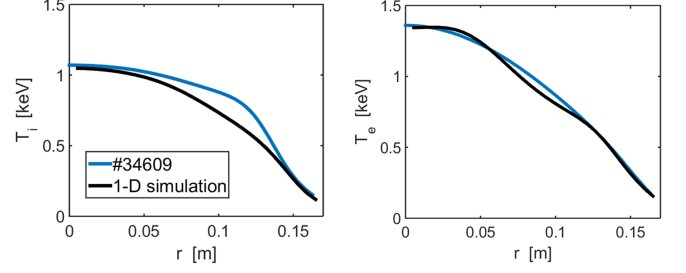

Figure 8: Results for the ion and electron temperature from the 1-D simulations with the critical gradient model (black) in comparison with the experimental results from W7-AS for #34609 (blue).
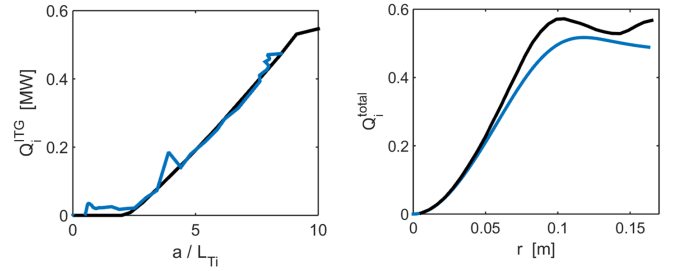

Figure 9: Results for the turbulent ion energy-flux over the ion-temperature-gradient length (left) and total ion energy-flux over minor radius (right) from the 1-D simulations with the critical gradient model (black) in comparison with the experimental results from W7-AS for #34609 (blue).
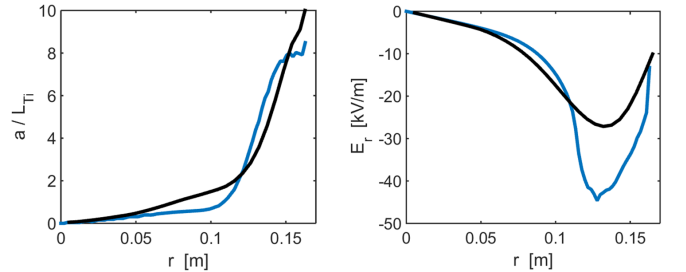

Figure 10: Results for the ion-temperature-gradient length (left) and the radial electric field (right) from the 1-D simulations with the critical gradient model (black) in comparison with the experimental results from W7-AS for #34609 (blue).

from neoclassically driven towards being dominated by turbulent transport. Interestingly, the near-axis as well as the edge regions are in good agreement. It is unlikely that the CG-model is responsible for this deviation as the turbulent transport starts to a play role only for $r > 0.1$ m. Fig. 9 shows that the critical gradient behaviour is captured well by the CG-model and the total ion energy-flux is in agreement with experiment. Only at the very edge, the model seems to slightly overestimate the energy-flux. This can be understood from the right side of Fig. 10 which shows that the ion-temperature-gradient deviates from the experimental values, being somewhat larger at the edge thus leading to increased energy-flux. This is most likely caused by the boundary condition since only small changes of the edge temperature directly influence the edge temperature gradient.

Recalling the experimental data, Fig. 5, one recognises that there is rather strong scattering of data points in the region around $r = 0.1$ m. Nonetheless, the agreement between simulation and experiment is well within experimental accuracy.

It can be concluded that the critical gradient model is indeed suited to capture the basic features of the ion turbulent transport observed in the W7-AS experiment and moreover allows a quantitative assessment of the ion energy-flux. In the next step this modeling approach shall be applied to a W7-X scenario, where reference parameters for the stiffness and the critical gradient are derived from a combination of the W7-AS experimental values and the gyrokinetic results.

4. Transport Prediction for W7-X

Similar to the W7-AS simulations, several general inputs need to be defined in order to carry out the simulations for W7-X. First, for the preparation of the DKES database, the so-called 'standard case' (all coils carry equal current) magnetic configuration of W7-X has been selected with a volume-averaged plasma beta of $\langle \beta \rangle = 2$ %. Although W7-X has been optimised for a small Shafranov shift, the magnetic field is still modified by a finite beta, which has impact on the neoclassical transport coefficients.

For the density, a 'standard' profile has been selected and kept constant to avoid a fuelling scenario which requires detailed knowledge of particle sources and sinks. In fact, density control in large stellarators is generally problematic and requires central sources such as pellet injection to avoid hollow density profiles [36].

Regarding the turbulent electron transport, as so far no better quantitative assessment exists, the turbulent electron heat conductivity has been set to $\chi_e^{\mathrm{edge}} = 1.6$ m^2/s at the very edge and falling off towards the centre at a rate $\chi_e^{ano} \sim 1/n$, in line with the W7-AS experimental data.

4.1 Reference Scenario

In the reference scenario, the heating scheme is chosen to be neutral beam injection (NBI), which in combination with the power transfer from electrons to ions by collisions is necessary to effectively heat the ions and thus bring the ion temperature to a maximum value which in turn leads to a significant ion-temperature-gradient. Consequently the heating power of the NBI has been chosen very high at 9 MW absorbed power. Such a heating scenario is not only most relevant for the investigated

ion heat-flux, but also most relevant for future reactor scenarios where $T_i \approx T_e$.

For the CG-model the same value for the critical gradient has been used as found in the experimental discharge #34609. The stiffness, however, had to be modified according to the used normalisation. Starting from equation (5) and replacing therein the W7-AS heat-flux density by the critical gradient model, an expression for the modeling of the ion heat-flux in W7-X is obtained with

$$Q_{\mathrm{W7X}}\left(r, \frac{a}{L_T}\right) = \frac{P_{\mathrm{W7X}}}{P_{\mathrm{W7AS}}} \cdot \frac{(R \cdot a)_{\mathrm{W7AS}}}{(R \cdot a)_{\mathrm{W7X}}} \cdot w_{\mathrm{W7AS}} \cdot y \cdot H(y). \quad (14)$$

where

$$y = \frac{a}{L_{Ti}} - \left(\frac{a}{L_{Ti}}\right)_{\mathrm{crit}}^{\mathrm{W7AS}}. \quad (15)$$

The stiffness parameter to be employed for the W7-X simulations is consequently

$$w_{\mathrm{W7X}} = \frac{P_{\mathrm{W7X}}}{P_{\mathrm{W7AS}}} \cdot \frac{(R \cdot a)_{\mathrm{W7AS}}}{(R \cdot a)_{\mathrm{W7X}}} \cdot w_{\mathrm{W7AS}} \approx 1.0 \cdot w_{\mathrm{W7AS}} \quad (16)$$

for a W7-X heating power of 9 MW. Implicitly it is assumed that the critical temperature gradient length is similar in both devices (as indicated in section 2).

This is of course only true under certain assumptions. First, we assume that the effect of the finite gyroradius, density gradient and radial electric field have a similar impact on both configurations. Secondly, the local plasma parameters at the edge must be similar according to equation (3). Consequently, the Dirichlet boundary condition for the temperature has been set to $T_{i,e} = 0.1$ keV which corresponds to the experimental values from W7-AS.

In this context, equation (3) also explains why we do not expect a much higher edge temperature (something like a pedestal) in W7-X. Reformulating equation (3) in terms of temperature one obtains

$$P \sim n_i T_i^{5/2} \widehat{Q}. \quad (17)$$

Although the heating power is a factor 10 higher in W7-X than in W7-AS, the strong temperature scaling indicates that the edge temperature may not increase much more than a factor two from 0.1 to 0.2 keV at the edge. However, this depends also on the coupling of the confinement region to the scrape-off layer.

Results for the 1-D predictive transport simulation including the CG-model using W7-AS parameters are presented in Fig. 11.

The turbulent transport, as represented by the CG-model, starts to overcome the neoclassical transport at a radius of 0.4 m. This means, that more than 2/3 of the core plasma are still dominated by neoclassical transport and 'only' the outer third of the plasma is governed by the turbulent energy-flux.

The most striking result of this predictive simulation is the fact, that the improvement of the global confinement with respect to the empirical ISS04 scaling [6] is retained. In this reference case using the W7-AS parameters for the stiffness of the CG-model, the confinement improvement is $f_{\mathrm{ren}} = \tau_E/\tau_E^{\mathrm{ISS04}} = 1.7$ reaching a volume averaged beta of $\langle \beta \rangle = 2.4\%$ and central temperatures of about $T_{e,0} \approx T_{i,0} = 4$ keV. In the present methodological context, these results are promising suggesting a good global confinement for W7-X.
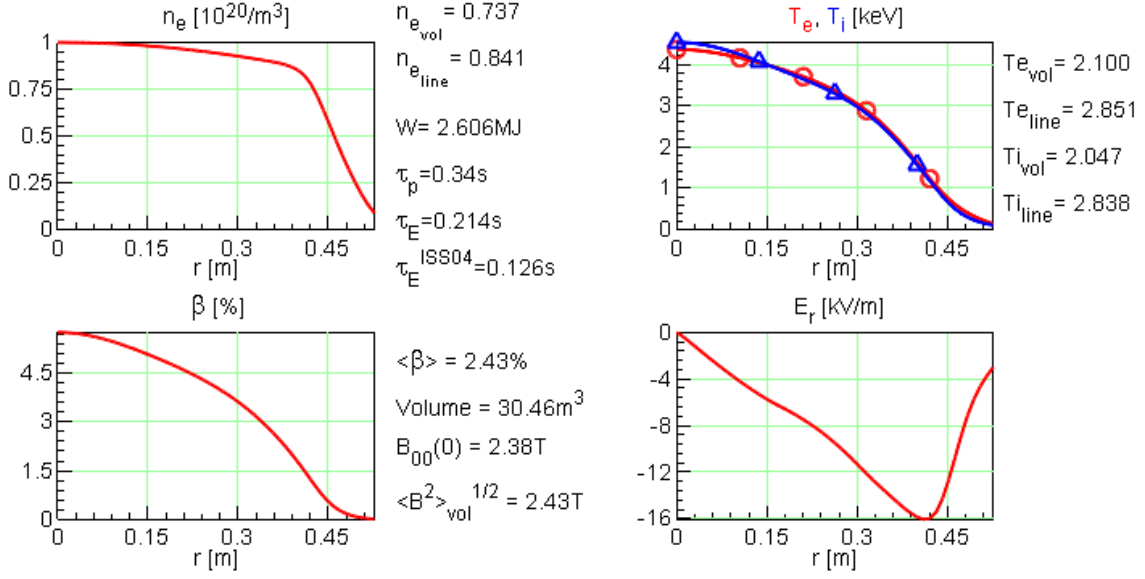
8

Figure 11: Profiles for the density (top left), temperature (top right), plasma beta (bottom left) and radial electric field (bottom right) for the 1-D predictive transport simulation of the W7-X 'reference' scenario with 9 MW absorbed NBI heating power, 0.1 keV edge temperature and experimental W7-AS parameters for the CG-model.

It should be noted that the empirical ISS04 scaling has been derived at moderate to high collisionality and the exponential relations resemble very much those of the gyro-Bohmtype Lackner-Gottardi scaling [37] representing the ion plateau regime. Nonetheless, the scaling serves as reference to assess the improvement (or degradation) of confinement with respect to experimental experience.

As several assumptions (mostly conservative) have been made throughout this work, the sensitivity of the global confinement is studied in the next subsection with respect to variations in the parameters introduced for the critical gradient model. Such a sensitivity study is important in order to assess to what degree a critical gradient model can be trusted regarding deviations in the underlying assumptions.

4.2 Sensitivity Analysis

Due to the introduced assumptions and uncertainties, in the following the sensitivity of the global confinement of W7-X with respect to variations in the stiffness of the CG-model shall be investigated. For this purpose the predictive transport simulations for W7-X described above have been repeated both with smaller and higher stiffness w compared to the reference scenario while keeping the critical gradient $(a/L_{Ti})_{\text{crit}}$ at the same value. The corresponding results are shown in Fig. 12.

A considerable increase of the stiffness by a factor two leads to degradation of the confinement from $f_{\text{ren}} = 1.7$ down to 1.4. Still, the global confinement stays well above the ISS04 empirical scaling retaining the generally good confinement properties of W7-X. A reduction of the stiffness by a factor two increases the global confinement to $f_{\text{ren}} = 1.9$. The confinement further increases to $f_{\text{ren}} = 2.2$ for a marginal level of stiffness.

The variation of the critical gradient length $(a/L_{Ti})_{\text{crit}}$, on the other hand, does not impact the confinement at all in the
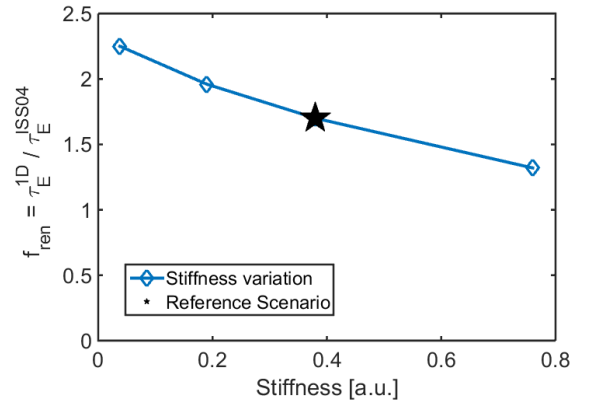

Figure 12: Sensitivity of the confinement time normalised to the emiprical ISS04 scaling with respect to the variation of the stiffness of the CG-model in the 1-D simulations at fixed NBI heating power with 9 MW. The reference scenario is displayed in the middle.

9

predictive simulations as the edge normalised temperature gradients are much higher than the critical gradient. Generally the stiffness in advanced stellarators is not so pronounced – quite in contrast to tokamaks. Consequently, also the critical gradient in the predictive simulations does not play a significant role. Due to the rather low stiffness, the ion temperature profile becomes very steep towards the edge, as has been shown in subsection 2.3 from the W7-AS experimental data. Those gradients are much larger than the critical gradient. If the critical gradient is reduced, the turbulent transport shifts a few centimeter closer towards the centre, however, the neoclassical transport still dominates over 2/3 of the minor radius.

The boundary condition for the edge temperature has not been varied to a great degree since an increase of the edge temperature strongly increases the ion heat-flux which in turn should lead again to a temperature reduction. This is in line with existing experimental data from stellarators worldwide which so far did not observe pedestal structures as known from tokamaks.

A final variation has been carried out for the heating scheme. For this, the reference scenario was modified to use 9 MW absorbed ECRH power instead of NBI. The density was kept fixed and the ECRH absorption is very localised at the resonance in the centre of the plasma compared to rather broad power deposition with NBI. This leads to so-called electron-root confinement [38], i.e. the electron temperature in the centre is much higher than the ion temperature. Additionally a positive electric field arises holding back the electrons. In this case the confinement improvement with respect to the NBI case is clear and the confinement improvement reaches $f_{\mathrm{ren}} = 2.8$ compared to $f_{\mathrm{ren}} = 1.7$ for the reference case. However, this result is obtained for a fixed value of the turbulent electron heat conductivity. In reality it could be possible that the turbulent electron heat-flux increases with increasing electron temperature gradient although this has not been observed in W7-AS.

This sensitivity study shows, that even if the stiffness in the presented approach is underestimated, the prediction for the improvement of the W7-X plasma confinement with respect to the ISS04 scaling holds. Unless the turbulent electron transport is also substantially underestimated or other transport channels become apparent, the predictive transport simulations for W7-X are promising.

Based on these results it is intriguing to extend the modeling approach beyond W7-X and to apply the model for a Helias reactor scenario, which is consequently followed in the next section.

5. Extrapolation to Helias Reactor

The reactor version of the 1-D code includes some additional reactor-specific features. The plasma is therein assumed to consist equally of deuterium and tritium and the fusion power output is self-consistently calculated according to the density, temperature and geometry. The resulting alpha-particle power mostly heats the electrons which at the high densities considered transfer their power by collisional coupling to the ions. Based on these input power profiles for the electrons and ions, the power balance equations are solved including neoclassical and turbulent transport (here CG-model). From this, the temperature profiles are self-consistently calculated until an equilibrium is reached.

The 'Helias 5-B' engineering design [19] serves as reference case for the reactor scenario. This is a recent study where the usage of Nb_3Sn as superconductor is discussed and a support structure is proposed based on bolted plates. In addition, the design point has been checked with Helias systems studies using a systems code approach and parametric variations therein [20]. The parameters of this reactor case are summarised in Tab. 1.

In order to carry out predictive transport simulations of a Helias reactor, a suitable magnetic configuration has to be defined. As dedicated reactor configurations are still a topic of ongoing research, the existing W7-X 'high-mirror' configuration was selected due to its reactor-relevance. Although the coil setup and currents are different, this configuration is very similar to the initial Helias 5-B configuration. The DKES database has been prepared for a $\langle \beta \rangle = 4\%$ equilibrium to account for finite beta effects. The dimensionless nature of the DKES approach allows a linear upscaling of the magnetic configuration [32]. The configuration has been scaled by a factor 3.6 to match a plasma volume of 1400 m^3, which corresponds to the described reactor design point with a fusion output of 3 GW. The magnetic field on-axis has been set to 5.5 T accordingly.

Again, a 'standard' flat density profile has been used and kept constant. Also the turbulent electron heat conductivity has again been described by $\chi_e^{ano} \sim 1/n$ and falling off towards the centre with $\chi_e^{\mathrm{edge}} = 10.0$ m^2/s at the very edge. Such a high value has been chosen to avoid an unphysical decoupling of the electron and ion temperature at the edge.

In Fig. 4 it was shown that the normalised heat-flux density $\widehat{Q}$ obtained from the non-linear GENE simulations has the same behaviour and values both for W7-AS and W7-X. Since gyrokinetic simulations for a reactor are not yet available, a consistent study is not yet at hand. Nevertheless, in order to provide a first estimate, we might work under the unverified assumption that

$$\widehat{Q}_{\mathrm{R}} = \widehat{Q}_{\mathrm{W7X}} = \widehat{Q}_{\mathrm{W7AS}}. \tag{18}$$

It is then possible to obtain the stiffness for the Helias reactor similar as has been done above for W7-X with

$$w_{\mathrm{R}} = \frac{P_{\mathrm{R}}}{P_{\mathrm{W7AS}}} \cdot \frac{(R \cdot a)_{\mathrm{W7AS}}}{(R \cdot a)_{\mathrm{R}}} \cdot w_{\mathrm{W7AS}} \approx 5.0 \cdot w_{\mathrm{W7AS}}. \tag{19}$$

Due to the higher power to surface area ratio the stiffness parameter for the reactor would in this ansatz be a factor five higher than in W7-AS and in the reference scenario of W7-X. Since we assumed $\widehat{Q}_{\mathrm{R}} = \widehat{Q}_{\mathrm{W7AS}}$ for the normalised heat-flux density, it follows from the difference of the power to surface area ratio that also the edge temperature must be different in the reactor case.

As the coupling of the bulk plasma transport to the scrape-off layer in a stellarator reactor is not yet fully clear, we use a scaling approach to define the temperature at the plasma edge. Recalling the definition of the heat-flux density

$$Q_i = \widehat{Q} \cdot Q_{gB} = \frac{P}{A} \tag{20}$$

and setting this equation into relation for the reactor case and W7-AS, it follows that

$$\left(\frac{T_{\mathrm{R}}}{T_{\mathrm{W7AS}}}\right)^{5/2} = \frac{P_{\mathrm{R}}}{P_{\mathrm{W7AS}}} \cdot \left(\frac{B_{\mathrm{R}}}{B_{\mathrm{W7AS}}}\right)^2 \frac{n_{\mathrm{W7AS}}}{n_{\mathrm{R}}} \tag{21}$$

where the definition of Q_{gB} has been explicitly used. Inserting the appropriate parameters, results in a edge temperature ratio
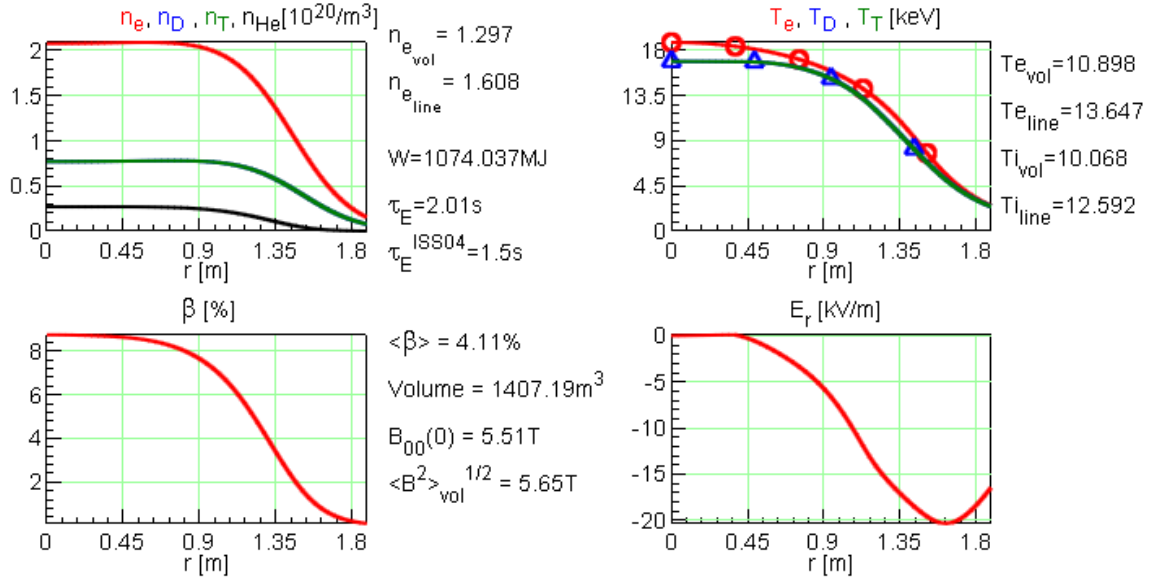
Figure 13: Profiles for the density (left) and temperature (right) for the 1-D predictive transport simulation of the reactor scenario using a 5 times higher stiffness as in W7-AS and W7-X as well as an 5 times increased turbulent electron heat conductivity.

between the reactor case and W7-AS by a factor 25, i.e. $T_{\mathrm{R}} = 2.5$ keV compared to $T_{\mathrm{W7AS}} = 0.1$ keV at the edge.

Using the stiffness parameter $w_{\mathrm{R}} = 5.0 \cdot w_{\mathrm{W7AS}}$, the same critical gradient length as in W7-AS, and as boundary condition for the edge temperature $T = 2.5$ keV, predictive transport simulations for the reactor scenario were carried out. The resulting density and temperature profile of the reactor scenario are shown in Fig. 13.

It can be seen, that in this scenario the turbulent transport dominates over the outer third of the plasma minor radius and the temperature in this region is considerably reduced. The global confinement in this case is $\tau_E^{\mathrm{1D}}/\tau_E^{\mathrm{ISS04}} = 1.3$ in terms of the empirical ISS04 scaling. The stiffness cannot be increased much beyond $w_{\mathrm{R}} = 5.0 \cdot w_{\mathrm{W7AS}}$ as otherwise the temperature would shrink further and the fusion output reduced such that the scenario would not be reactor capable anymore if the density is not further increased. It may seem surprising that the reactor scenario reaches a confinement improvement factor of only $f_{\mathrm{ren}}^{\mathrm{R}} = 1.3$ compared to W7-X with $f_{\mathrm{ren}}^{\mathrm{W7X}} = 1.7$. However, this is due to the paradigm change of the underlying scaling relations. Under fusion conditions, on the one hand the tranpsort regimes change which exhibit different scalings [32] and on the other hand the heating power is no longer a free parameter, rather it is interconnected to the plasma volume, plasma beta, and the magnetic field, also influencing the scaling of the confinement time [7].

An interesting result for these scenarios is, that if the stiffness for the reactor scenario could be reduced by a factor two, the confinement would improve from $\tau_E^{\mathrm{1D}}/\tau_E^{\mathrm{ISS04}} = 1.3$ to 1.5. Thus, the device size could be reduced while achieving the same fusion power output.

It remains unclear to what degree the presented scenario for the reactor is an adequate description of the plasma transport under fusion conditions. However, the finding that $w_{\mathrm{R}} = 5.0 \cdot w_{\mathrm{W7AS}}$ is close to an upper limit for the Helias reactor is an

important result. Experimental results of W7-X will allow us to draw the connection between W7-AS and W7-X such that the presented model can be validated and further improved. This in turn will allow a further refinement of reactor scenarios.

It should be noted again, that the predictive simulations are very much dependent on the boundary condition. If the edge temperature in the reactor case is decreased to 0.1 keV instead of 2.5 keV, the stiffness parameter must be decreased by a factor five, i.e. down to $w_{\mathrm{R}} = 1.0 \cdot w_{\mathrm{W7AS}}$, in order to stay at the same fusion power output.

6. Conclusions and Outlook

In an effort to achieve predictive capability of neoclassical and turbulent transport behaviour in the W7-X experiment at an efficient computational level, current understanding of the properties of turbulence in the W7-X magnetic configuration has been reviewed. While the TEM is considered to be strongly stabilized due to the separation of bad curvature and the localisation of the trapped particles, the ITG mode is expected to be a major driver of transport even though it is much more localised on the outboard side of a flux-surface than compared to tokamaks.

In order to assess the relevance of these theoretical findings in terms of their applicability to real experiments, the properties of the turbulence induced transport in W7-X have been compared to its predecessor W7-AS. For this purpose non-linear gyrokinetic ITG-mode simulations on a full flux-surface have, for the first time, been carried out for the W7-AS configuration. While there is qualitative agreement between both devices, the electrostatic potential variations in W7-X are more localised on a thin band on the outboard side of a flux-surface than in W7-AS. However, the scaling of the heat-flux density normalised by gyro-Bohm values with respect to increase of

11

the ion-temperature-gradient length (excluding density gradient and radial electric field) is nearly identical in both devices.

In order to draw a connection to experimental data, high performance W7-AS discharges have been reviewed. It is intriguing that the observed turbulent transport shows the typical critical gradient behaviour found in the simulations and scales accordingly with the ion-temperature-gradient length.

Following this, a basic critical gradient model has been proposed which describes the observed behaviour and characteristics. The model has been implemented in a 1-D transport code framework. For testing, the code and the model have been applied to W7-AS discharge #34609 where additionally the turbulent electron heat-flux was fixed according to an empirical description. It was found that the CG-model is able to reproduce the experimental profiles.

Based on the similarity of the ITG heat-flux scaling of W7-AS and W7-X in GENE, the integrated 1-D transport model has been applied for the prediction of the confinement in W7-X. A high-performance scenario with 9 MW NBI power and a density of $1 \cdot 10^{20}$ m^{-3} was simulated and found, that even with the CG-model the global confinement improvement with respect to the empirical ISS04 scaling is retained with a confinement improvement factor of $\tau_E^{1D}/\tau_E^{ISS04} = 1.7$. A sensitivity analysis showed that a factor two increase of the stiffness decreases the confinement improvement to a factor 1.4 while a reduction of the stiffness by a factor two increases the confinement to 1.9.

Finally, the same methodology was applied to a Helias reactor scenario using again the same critical gradient length as in W7-AS and W7-X, but a five times higher stiffness and an accordingly scaled edge temperature of 2.5 keV to remain consistent. The turbulent electron heat-conductivity was increased in order to prevent a decoupling of the electron and ion temperature at the edge. But even with the turbulence induced transport and the increased electron transport a suitable reactor solution is found with a global confinement improvement of 1.3 with respect to the ISS04 scaling. However, the stiffness in this reactor scenario cannot be increased very much as otherwise the reduction of the ion temperature would reduce the fusion power output which can only to some degree be compensated by an increase of the density. Further, if the edge temperature is set to 0.1 keV, the stiffness must be reduced to the W7-AS / W7-X level to achieve the same fusion power output.

It should be noted that, although the introduced CG-model is rather basic, this work represents a first attempt to include first-principle physics motivated models for the prediction of turbulent transport in integrated plasma scenarios. In the next steps, it is foreseen to include both the effect of the density gradient as well as the electric field which are anticipated to reduce ITG turbulence. It will also be investigated to what degree modes can be considered which drive electron transport.

7. Acknowledgments

References

[1] B. J. Green. "ITER: burning plasma physics experiment." *Plasma Physics and Controlled Fusion*, vol. 45, p. 687 (2003).

[2] G. Grieger and I. Milch. "Das Fusionsexperiment WENDELSTEIN 7-X." *Physikalische Blätter*, vol. 49, p. 1001 (1993).

[3] A. A. Subbotin, M. I. Mikhailov, V. D. Shafranov et al. "Integrated physics optimization of a quasi-isodynamic stellarator with poloidally closed contours of the magnetic field strength." *Nuclear Fusion*, vol. 46, p. 921 (2006).

[4] J. Nührenberg. "Development of quasi-isodynamic stellarators." *Plasma Physics and Controlled Fusion*, vol. 52, no. 12, p. 124003 (2010).

[5] M. Hirsch, J. Baldzuhn, C. D. Beidler et al. "Major results from the stellarator Wendelstein 7-AS." *Plasma Physics and Controlled Fusion*, vol. 50, p. 053001 (2008).

[6] H. Yamada, J. H. Harris, A. Dinklage et al. "Characterization of energy confinement in net-current free plasmas using the extended International Stellarator Database." *Nuclear Fusion*, vol. 45, p. 1684 (2005).

[7] F. Warmer, C. Beidler, A. Dinklage et al. "Limits of Confinement Enhancement for Stellarators." *Fusion Science and Technology*, vol. 68, p. 727 (2015).

[8] C. D. Beidler, K. Allmaier, M. Y. Isaev et al. "Benchmarking of the mono-energetic transport coefficients - results from the International Collaboration on Neoclassical Transport in Stellarators (ICNTS)." *Nuclear Fusion*, vol. 51, p. 076001 (2011).

[9] P. Xanthopoulos, F. Merz, T. Görler et al. "Nonlinear Gyrokinetic Simulations of Ion-Temperature-Gradient Turbulence for the Optimized Wendelstein 7-X Stellarator." *Physical Review Letters*, vol. 99, p. 035002 (2007).

[10] P. Helander, T. Bird, F. Jenko et al. "Advances in stellarator gyrokinetics." *Nuclear Fusion*, vol. 55, no. 5, p. 053030 (2015).

[11] J. H. E. Proll, P. Xanthopoulos and P. Helander. "Collisionless microinstabilities in stellarators. II. Numerical simulations." *Physics of Plasmas*, vol. 20, p. 122506 (2013).

[12] R. C. Wolf. "Characterization of ion heat conduction in JET and ASDEX Upgrade plasmas with and without internal transport barriers." *Plasma Physics and Controlled Fusion*, vol. 45, p. 1757 (2003).

[13] F. Jenko, W. Dorland, M. Kotschenreuther et al. "Electron temperature gradient driven turbulence." *Physics of Plasmas*, vol. 7, p. 1904 (2000).

[14] P. Xanthopoulos, W. A. Cooper, F. Jenko et al. "A geometry interface for gyrokinetic microturbulence investigations in toroidal configurations." *Physics of Plasmas*, vol. 16, p. 082303 (2009).

[15] T. Görler, X. Lapillonne, S. Brunner et al. "The global version of the gyrokinetic turbulence code {GENE}." *Journal of Computational Physics*, vol. 230, no. 18, p. 7053 (2011).

[16] P. Xanthopoulos, H. Mynick, P. Helander et al. "Controlling Turbulence in Present and Future Stellarators." *Physical Review Letters*, vol. 113, p. 155001 (2014).

[17] B. F. McMillan, X. Lapillonne, S. Brunner et al. "System Size Effects on Gyrokinetic Turbulence." *Phys. Rev. Lett.*, vol. 105, p. 155001 (2010).

[18] Y. Idomura and M. Nakata. "Plasma size and power scaling of ion temperature gradient driven turbulence." *Physics of Plasmas*, vol. 21, p. 020706 (2014).

[19] F. Schauer, K. Egorov and V. Bykov. "HELIAS 5-B magnet system structure and maintenance concept." *Fusion Engineering and Design*, vol. 88, p. 1619 (2013).

[20] F. Warmer, S. Torrisi, C. D. Beidler et al. "Systems Code Analysis of Helias Fusion Reactor and Economic Comparison to Tokamaks." *IEEE Transactions on Plasma Science*, vol. [under review] (2016).

[21] J. Baldzuhn, M. Kick, H. Maassberg et al. "Measurement and calculation of the radial electric field in the stellarator W7-AS." *Plasma Physics and Controlled Fusion*, vol. 40, no. 6, p. 967 (1998).

[22] P. Helander. "Theory of plasma confinement in non-axisymmetric magnetic fields." *Reports on Progress in Physics*, vol. 77, no. 8, p. 087001 (2014).

[23] D. Reiter, M. Baelmans and P. Börner. "The EIRENE and B2-EIRENE Codes." *Fusion Science and Technology*, vol. 47, p. 172 (2005).

[24] P. Rebut, P. Lallia and M. Watkins. "Plasma Physics and Control Nuclear Fusion Research 1988: Proc. 12th Int. Conf. (Nice, 1988)." vol. 2 (Vienna: IAEA), p. 191 (1989).

[25] M. Kotschenreuther, W. Dorland, M. A. Beer et al. "Quantitative predictions of tokamak energy confinement from first-principles simulations with kinetic effects." *Physics of Plasmas*, vol. 2, no. 6, pp. 2381 (1995).

[26] F. Imbeaux, F. Ryter and X. Garbet. "Modelling of ECH modulation experiments in ASDEX Upgrade with an empirical critical temperature gradient length transport model." *Plasma Physics and Controlled Fusion*, vol. 43, no. 11, p. 1503 (2001).

92

[27] P. Mantica, D. Strintzi, T. Tala et al. "Experimental Study of the Ion Critical-Gradient Length and Stiffness Level and the Impact of Rotation in the JET Tokamak." *Phys. Rev. Lett.*, vol. 102, p. 175002 (2009).

[28] F. Merz and F. Jenko. "Nonlinear interplay of TEM and ITG turbulence and its effect on transport." *Nuclear Fusion*, vol. 50, no. 5, p. 054005 (2010).

[29] S. Toda, M. Nunami, A. Ishizawa et al. "How to apply a turbulent transport model based on a gyrokinetic simulation for the ion temperature gradient mode in helical plasmas." *Journal of Physics: Conference Series*, vol. 561, no. 1, p. 012020 (2014).

[30] H. Maaßberg, R. Brakel, R. Burhenn et al. "Transport in stellarators." *Plasma Physics and Controlled Fusion*, vol. 35, p. B319 (1993).

[31] U. Stroth. "A comparative study of transport in stellarators and tokamaks." *Plasma Physics and Controlled Fusion*, vol. 40, p. 9 (1998).

[32] Y. Turkin, H. Maaßberg, C. D. Beidler et al. "Current Control by ECCD for W7-X." *Fusion Science and Technology*, vol. 50, p. 387 (2006).

[33] Y. Turkin, C. D. Beidler, H. Maaßberg et al. "Neoclassical transport simulations for stellarators." *Physics of Plasmas*, vol. 18, p. 022505 (2011).

[34] W. I. van Rij and S. P. Hirshman. "Variational bounds for transport coefficients in threedimensional toroidal plasmas." *Phyiscs of Fluids B: Physics of Plasmas*, vol. 1, p. 563 (1989).

[35] S. P. Hirshman, K. C. Shaing, W. I. van Rij et al. "Plasma transport coefficients for nonsymmetric toroidal confinement systems." *Physics of Fluids*, vol. 29, p. 2951 (1986).

[36] H. Maaßberg, C. D. Beidler and E. E. Simmet. "Density control problems in large stellarators with neoclassical transport." *Plasma Physics and Controlled Fusion*, vol. 41, p. 1135 (1999).

[37] K. Lackner and N. A. O. Gottardi. "Tokamak confinement in relation to plateau scaling." *Nuclear Fusion*, vol. 30, p. 767 (1990).

[38] M. Yokoyama, H. Maaßberg, C. Beidler et al. "Core electron-root confinement (CERC) in helical plasmas." *Nuclear Fusion*, vol. 47, no. 9, p. 1213 (2007).

13

HELIAS Module Development for Systems Codes

F. Warmer[a,*], C.D. Beidler[a], A. Dinklage[a], K. Egorov[a], Y. Feng[a], J. Geiger[a], F. Schauer[a], Y. Turkin[a], R. Wolf[a],
P. Xanthopoulos[a]

[a]Max Planck Institute for Plasma Physics, D-17491, Greifswald, Germany

Abstract

In order to study and design next-step fusion devices such as DEMO, comprehensive systems codes are commonly employed. In this work HELIAS-specific models are proposed which are designed to be compatible with systems codes. The subsequently developed models include: a geometry model based on Fourier coefficients which can represent the complex 3-D plasma shape, a basic island divertor model which assumes diffusive cross-field transport and high radiation at the X-point, and a coil model which combines scaling aspects based on the Helias 5-B reactor design in combination with analytic inductance and field calculations. In addition, stellarator-specific plasma transport is discussed. A strategy is proposed which employs a predictive confinement time scaling derived from 1-D neoclassical and 3-D turbulence simulations.

This paper reports on the progress of the development of the stellarator-specific models while an implementation and verification study within an existing systems code will be presented in a separate work.

This approach is investigated to ultimately allow one to conduct stellarator system studies, develop design points of HELIAS burning plasma devices, and to facilitate a direct comparison between tokamak and stellarator DEMO and power plant designs.

Keywords: HELIAS, stellarator-specific models, Systems Code

1. Introduction

With ITER [1] under construction, design studies now concentrate on a fusion facility which is to follow ITER. This follow-up step is often referred to as 'DEMO', short for demonstration fusion power plant with the aim of demonstrating the technical maturity of the magnetic confinement fusion concept. But even the conceptual design of such a power plant like fusion device is a complex and demanding task. Therefore, to facilitate such studies, so-called 'systems codes' are often employed as valuable tools for the design process.

Systems codes, also known as design codes, are comprehensive yet simplified models of a complete fusion facility. Since they bring together physics, engineering and economic aspects as outlined above, self-consistent design points can be developed and their sensitivity against variation of critical parameters tested. With this approach especially critical development directions for physics scenarios or technology advancements can be identified. Following this, dedicated experiments and simulations may be performed and as a result of that, systems codes models updated, as is conceptually shown in Fig. 1 below.

For the tokamak concept, design activities have progressed lately employing different systems codes worldwide. For example, in the ARIES systems studies [2] a broad range of devices and corresponding possibilities have been studied, but also in the European PPCS studies [3], employing the systems code PROCESS [4], different tokamak scenarios have been investigated. Also basic power balance models can be employed to assess the required size of DEMO, taking also into account pulsed devices [5]. Many additional tokamak systems codes and studies exist, but it is beyond the scope of this work to cover all of them.
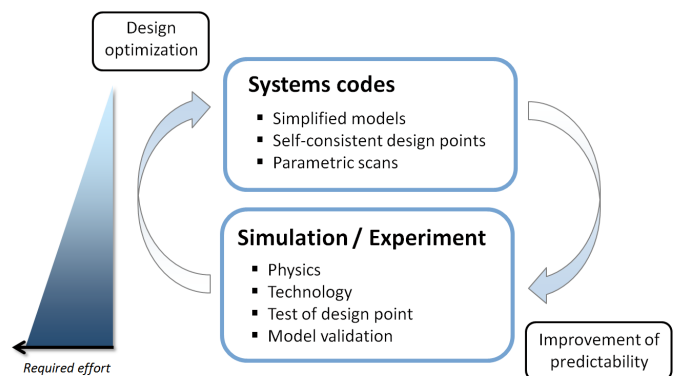

Figure 1: Concept of systems codes and their interaction with detailed simulations and experiments. The left scala illustrates the required effort (in terms of complexity and time) to carry out the individual tasks.

Systems codes have also been employed outside the tokamak community for the conceptual design of a heliotron

---

DEMO. In contrast to the tokamak, the heliotron magnetic field is created by continuous helical coils. This means the 3D effects of the helical coils and plasma shape must be considered, introducing additional complexity compared to axissymmetric tokamaks. This is done in the design approach within the heliotron systems code HELIOSCOPE [6] which led to the concept of a Force Free Helical Reactor DEMO (FFHR-d1) [7, 8].

Another magnetic confinement concept is the helical advanced stellarator (HELIAS). The HELIAS is a modular stellarator concept with periodic symmetry including integrated optimisation of the magnetic field with respect to several criteria at the same time, e.g. Shafranov shift, neoclassical transport, etc., where the magnetic field is established by extneral non-planar coils. But so far no systems code exists capable of modelling a HELIAS. Therefore this work concentrates on the development of a HELIAS systems code module with the aim of implementation in the systems code PROCESS. PROCESS is a well-established, partly modular, tokamak systems code which gained maturity through many applications. A solver based on Lagrangian multipliers is employed within PROCESS to allow for design optimisation with respect to the descriptive models and constraints. Such an approach is followed to allow for stellarator systems studies and design point development of HELIAS burning plasma devices as well as comparative studies to tokamaks.

The purpose of this work is to report on the progress of the development of HELIAS models for systems codes and is organised as follows: In section 2 the essential differences between tokamak and stellarator are identified which require preparation of new systems code modules. The corresponding models are described in section 3 which include a geometry model based on Fourier coefficients, a basic island divertor model which assumes cross-field transport and high radiation, and a model for the non-planar, modular coils based on scaling aspects with respect to the Helias 5-B reactor design [9] in combination with analytic calculations. Furthermore, stellarator-specific plasma transport is discussed and a strategy proposed for the development of a predictive confinement time scaling. The work is summarised and the results are discussed in section 4. A detailed verification study of the HELIAS module will be presented in a seperate work [10] where the models have been implemented in the systems code PROCESS.

2. Identification of Required Models

The tokamak and the stellarator differ in the point of how the rotational transform is created. In the tokamak this is done by driving a toroidal current in the plasma. The helical advanced stellarator concept, considered here, in contrast twists the magnetic field by poloidally rotating the elongated flux surfaces around a non-planar magnetic axis achieved exclusively by a set of non-planar modular coils. This fundamental difference has several implications:

A tokamak may only be operated as long as a current is driven in the plasma, which is either limited in time by the available magnetic flux, if driven inductively, or requires a large amount of power if driven non-inductively, e.g. by neutral beam injection (NBI). The HELIAS, in contrast, operates intrinsically steady-state, 'current-free' and without disruptions. 'Current-free' means that HELIAS configurations are optimised with respect to minimal bootstrap and Pfirsch-Schlüter currents and the net toroidal current is, therefore, several orders of magnitude below tokamak levels.

As the poloidal field component in the tokamak is created by the plasma current, the toroidal field component is achieved by planar, identical, typically 'D-shaped' coils. This makes the tokamak plasma shape (flux-surfaces) axisymmetric. The plasma geometry of the stellarator, in contrast, is fully three-dimensional with a periodic symmetry. Also the stellarator coils for the HELIAS line are 3D, non-planar, modular, and comparably numerous.

The complex 3D shaping of the stellarator magnetic field structure generally introduces localised helically trapped particle orbits which have an overall impact on the plasma transport. The resulting, so-called, 'neoclassical' transport can be very high in stellarators and is an essential optimisation criterion of helical advanced stellarators. Usually also an ambipolar electric field arises connected to the neoclassical transport. Additional 3D anomalous transport must be considered making the description of stellarator transport a complex task, especially since 3D turbulence simulations for stellarators have just been started. In tokamaks, in contrast, the turbulent transport is observed to be dominant drawing on a solid base of experiments and experience. In addition, tokamaks are geometrically similar which more confidently allows to describe the transport by empirical confinement time scalings based on the similarity principle.

Last, but not least, the axisymmetry of the tokamak allows to employ a toroidally closed divertor, either only on the bottom (so-called 'single-null') or up-down symmetric (so-called 'double-null'). In the HELIAS concept a chain of naturally occuring magnetic islands at the plasma edge is employed. Independent divertor plates are placed symmetrically at the top and bottom of each module intersecting the magnetic islands at the edge in order to efficiently control the particle and energy exhaust. From a tokamak viewpoint this could be seen as a discontinuous multi-null divertor.

In order to identify specific and independent models which need to be developed for a HELIAS systems code approach, the general considerations from above need to be checked with an existing systems code. For this purpose the well-developed and commonly employed systems code PROCESS has been selected. The source code of PROCESS and its corresponding tokamak models have been thoroughly reviewed with respect to stellarator-specific considerations. From this investigation it is concluded that in a systems code such as PROCESS, the plasma geome-

2

try, the modular coils, the island-divertor and the plasma transport models require independent treatment compared to the tokamak models while treatment of current-related aspects can be neglected. The correspondingly developed[195] models are described in the next section.

3. The Stellarator Module

In the following stellarator-specific models are proposed which are designed to be applicable to systems codes and which together build up a consistent HELIAS module. One requirement of this development is to retain small calculation times without compromising the necessary ac-[205] curacy and complexity of the 3D stellarator-specific properties.

3.1. Plasma Geometry

At finite normalised plasma pressure $\langle \beta \rangle = 2\mu_0 \left\langle p/B^2 \right\rangle$[210] the shape of the confined plasma is determined by the shape of the nested closed flux surfaces (in stellarators even at $\langle \beta \rangle = 0$). In position-space those surfaces may be represented by cylindrical coordinates (R, φ, z), but in[215] practice it is more convenient to decompose these coordinates in a Fourier series with respect to poloidal and toroidal angle coordinates, respectively u and v as wells as the flux surface label s:

$$
\begin{aligned}
R\left(s, u, v\right) &= \sum_{m=0}^{m_{\max}} \sum_{n=-n_{\max}}^{n_{\max}} R_{m,n}(s) \cos(mu - Nnv) \\
z\left(s, u, v\right) &= \sum_{m=0}^{m_{\max}} \sum_{n=-n_{\max}}^{n_{\max}} z_{m,n}(s) \sin(mu - Nnv)
\end{aligned}
$$

where N is the number of field periods and $\varphi\left(s, u, v\right)$ is defined in the same way as R and z.

Using this representation allows one to accurately cal-[225] culate the important geometrical parameters relevant for the systems analysis by summation over the corresponding combination of Fourier coefficients. The important geometrical parameters are the effective average plasma cross-sectional area $\langle F \rangle$ in m^2, the plasma volume V in[230] m^3 as well as the total surface area of the confined plasma S in m^2. These parameters are important due to their direct impact on relevant physics and engineering quantities, e.g. the volume for the confinement time and fusion power or the surface area for neutron wall load.

In order to employ and use this model, the Fourier coefficients $R_{m,n}$ and $z_{m,n}$ of the last closed flux surface (LCFS) must be provided. These can be obtained from equilibrium calculations employing e.g. the equilibrium code VMEC.

The advantage of this model is its generality as every arbitrary toroidal shape can be treated, including tokamak[240] and heliotron geometry. Moreover, it is possible to scale both the minor and major plasma radius by scaling of the corresponding Fourier coefficients making it very flexible while sustaining the general shape.

3.2. Island Divertor

For tokamaks, often so-called 2-point models are used to describe the particle and energy transport from an upstream position parallel along the magnetic field to the divertor target. For stellarators, in contrast, such 2-point models are more complex and additional terms and parameters must be considered [11, 12]. However, the correlations of some of these parameters are to-date unclear. For this reason the 2-point model approach is avoided here. Instead, a more basic and fundamental model is proposed based on geometrical considerations. The model combines relations of physics as well as engineering and is therefore well suited for scaling. Another advantage of such a basic model is that parts of it can be easily replaced once a more detailed understanding, e.g. of the power decay width, is available.

The heat load on the divertor plates, q_{div}, is defined as the ratio of the power transported to the divertor, P_{div}, over an effective wetted area, A_{eff}. The total power arriving at the divertor is the power crossing the separatrix, P_{SOL}, provided from the plasma transport model, less the SOL and X-point radiation: $P_{\mathrm{div}} = P_{\mathrm{SOL}}(1 - f_{\mathrm{rad}})$, where the radition fraction is contained in the factor f_{rad}.

The wetted area can be seen as the product of the total length of all divertor plates, L_{T}, and the power decay width, λ_q, at the divertor plate. Accounting additionally for some asymmetry with a factor f_a the heat load becomes

$$
q_{\mathrm{div}} = \frac{P_{\mathrm{div}}}{A_{\mathrm{eff}}} = \frac{P_{\mathrm{SOL}}(1 - f_{\mathrm{rad}})}{L_{\mathrm{T}} \cdot \lambda_q} \cdot f_a. \tag{1}
$$

The total length L_{T} of the discontinuous island divertor is the sum over all identical divertor plates of which there are two in every field period, therefore $L_{\mathrm{T}} = 2nL_{\mathrm{D}}$ with the toroidal and poloidal mode number n and m respectively.

Here, the length of a single divertor plate L_{D} may be estimated from a geometric approach. Starting from the X-point and following a flux tube, the field lines experience a radial pitch of angle Θ in the island region while going helically around the torus until striking the divertor plate as illustrated in Fig. 2. A field line which just passes the divertor plate on the inner side will strike the divertor plate at the far outer point after m field periods. The radial distance from the inner to the outer side of the plate is then the helical length $2\pi Rm/n$ times the pitch angle Θ. The radial extent is enhanced by diffusive broadening of the flux channel F_x and the length of the divertor plate is then determined from the inclination of the divertor plate relative to the field lines α_{lim}. Combining this, the wetted length of one divertor plate is

$$
L_{\mathrm{D}} = 2\pi R \cdot \frac{m}{n} \frac{\Theta}{\alpha_{\mathrm{lim}}} F_x. \tag{2}
$$

Both F_x and λ_q are attributed to cross-field transport. Two main assumptions are made in the island divertor model:

3

- diffusive cross-field transport is considered (due to much longer connection lengths in stellarators compared to tokamks)

- high radiation fraction is assumed in the SOL and at the X-point (which is necessary to protect the divertor from severe heat loads)

From general diffusive transport behavior the power decay width is described by $\lambda_q = \sqrt{\chi_\perp \cdot \tau_\parallel}$ with the perpendicular diffusion coefficient $\chi_\perp$ and the characteristic diffusion time $\tau_\parallel$ which is determined by parallel transport. The second assumption made above implies a cold island in which the temperatures are so low that the remnant heat is mainly transported by convective processes onto the targets.

From the geometric view introduced above it is clear that the characteristic time for a flux channel to undergo diffusion is determined by the connection length from the X-point to the target plate $L_{X \to T}$ and the ion sound speed $c_s = \sqrt{2T/m}$ of the particles $\tau_\parallel = L_{X \to T}/c_s$. The connection length in turn may be estimated from the distance between X-point and divertor plate Δ, as illustrated in Fig. 2. This is related to the connection length and field pitch Θ by $L_{X \to T} = \Delta/\Theta$. The typical dimension of Δ is related to the radial width of the magnetic islands w_r such that

$$\Delta = f_w \cdot w_r = f_w \cdot 4\sqrt{\frac{R \cdot b_{m,n}}{n \cdot \iota'}} \tag{3}$$

where f_w is a fractional factor of order 1/2, $b_{m,n} \sim \Theta$ the radial field perturbation, and ι' the magnetic shear in the SOL. The flux channel broadening which determines the divertor plate length can be derived with the same general diffusive transport behavior with the connection length now being one helical circumference and therefore

$$F_x = 1 + \frac{1}{\Theta}\sqrt{\frac{\chi_\perp}{c_s 2\pi R \frac{m}{n}}}. \tag{4}$$
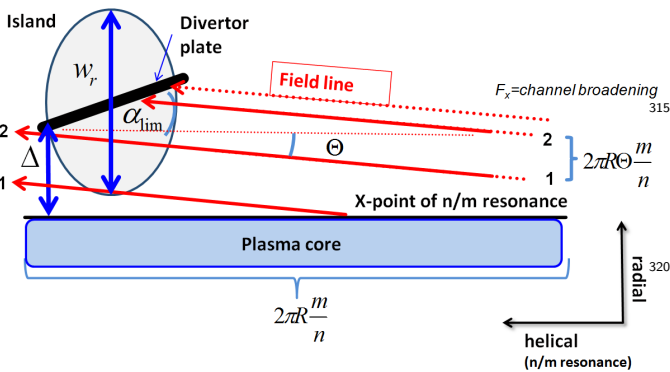
Figure 2: Geometrical illustration of a flux tube in the scrape-off layer intersected by a divertor plate.

Due to the analytic nature of the model, the single aspects can be consolidated in a single formula for the head load with respect to the required input parameters as:

$$q_{\mathrm{div}} = \frac{P_{\mathrm{SOL}}(1 - f_{\mathrm{rad}})}{4\pi R \, m \, F_X} \frac{\alpha_{lim}}{\Theta \cdot \chi_\perp} \frac{1}{2}\sqrt{\frac{c_s}{f_w}} \sqrt[4]{\frac{n \cdot \iota'}{R \cdot b_{m,n}}} \cdot f_a. \tag{5}$$

The input parameters are obtained from the envisaged reactor design, e.g. R, P_{SOL}, the considered magnetic configuration, e.g. Θ, m, n, as well as from experience from existing devices for engineering, e.g. α_{lim}, and physics, e.g. $\chi_\perp$, c_s.

It should be noted, that due to the basic nature of the model, the quantitative accuracy is limited and sensitive to the input parameters. The model should rather be interpreted to predict the dimension of the heat load. More importantly, as the heat load is usually limited by material constraints the model is useful to estimate the required radiation fraction f_{rad} in order to ensure safe divertor operation for a specific design.

3.3. Modular Coils

Since the design of coils for an optimised stellarator configuration is a demanding process requiring complex codes, computational power and, experience, several major approximations must be considered to represent modular coils in a systems code approach:

- the sophisticated Helias 5-B reactor design study and its coil design are used as reference basis [9]

- the coil shapes of this design are assumed to be 'fixed' but the overall size shall be scalable

- based on physics principles, scaling factors and relations are introduced to flexibly scale the design according to a set of desired parameters

With the Helias 5-B coil design as basis and under the assumption of fixed coil shapes several scaling factors can be introduced with relation to Helias 5-B parameters. Namely a scaling factor for the major radius f_R and one for the coil radius f_s. As HELIAS devices have closely positioned coils, the total coil current can be consequently scaled with $f_I = f_B \cdot f_R$ where f_B is the scaling factor for the magnetic field strength on axis.

A semi-analytic method is employed, in order to calculate the maximal magnetic field on the surface of the coil, B_{max}, the total stored magnetic energy, W_{mag}, as well as the cross-sectional dimension of the winding pack (WP). Each coil consists of N turns placed in the winding pack as in Helias 5-B where the size of the WP is considered an input in the analytic description for the moment (but is later calculated self-consistently with an additional constraint). The turns are approximated by circular filaments. The mutual inductance, M, between two arbitrarily spaced and oriented circular filaments can then be calculated analytically [13].

4

The total inductance L_{tot} is obtained by summation over all mutual inductances of circular filaments and the self-inductances of the coils. The latter are simply approximated by the inducance of a circular loop with circular cross section of radius $(A_{\text{sect}}/\pi)^{1/2}$, where A_{sect} is the recangular winding pack section area. From this follows the total stored magnetic energy simply by $W_{mag} = \frac{1}{2}L_{\text{tot}}I^2$ with the total coil current I.

The magnetic field at any point in space can be straightforwardly calculated as sum of solenoid fields, using standard loop formulas and elliptic integrals as, e.g., found in [14]. This way the average magnetic field on the plasma axis as well as the maximal field, B_{max}, at the coils can be found.

Until this point the dimensions of the winding pack were a free parameter, but the aim of this model is to self-consistently calculate important parameters. For this purpose the critical current density behavior of the respective superconducting material may be employed as a natural constraint. Treating the coil winding packs as single current carrying conductors, the Nb_3Sn ITER scaling [15] - assuming constant operation temperature - can be simplified to

$$f_q = 10.9 \cdot \sqrt{f_I} \; \frac{B_{\text{max}}^{1/4}}{33 - B_{\text{max}}} \qquad (6)$$

where f_q is the scaling factor for the winding pack cross section area. The constant factor contains the critical field of the superconductor and the maximal field of Helias 5-B. With this constraint the magnetic energy and field calculations given above can be iterated with respect to f_q and determined self-consistently. The cross-sectional area of the winding pack is subsequently scaled by f_q^2 from which the radial and toroidal width of the WP can be obtained. But it should be noted that the WP aspect ratio of radial to toroidal extension is kept fixed according to Helias 5-B. Similar formulas can be derived for other superconductors such as e.g. NbTi.

Based on the magnetic field and the corresponding stored magnetic energy, the total required mass of support structure can be estimated. Since the Virial theorem links the magnetic energy and the minimal mass of support structure, this principle can be used to derive an empirical scaling between these parameters on the basis of existing superconducting devices, as e.g. demonstrated in [16]. By considering in addition the most recent superconducting devices such as W7-X, LHD, and ITER the empirical scaling of [16] is updated to

$$M_{\text{struc}} = 1.3483 \cdot W_{\text{mag}}^{0.7821} \qquad (7)$$

with the stored magnetic energy W_{mag} in MJ and the mass of support structure M_{struc} in t, illustrated in Fig. 3. It can be seen from the figure that several experiments, both tokamaks and stellarators, are well aligned with the empirical fit (blue line) reaching over several orders of magnitude. It should still be noted that the figure represents a double logarithmic plot and a single device may deviate up to a factor two as e.g. W7-X where it was not considered to minimise the support structure mass. Another uncertainty is introduced by the fact that it is not everywhere clear whether the conductors and other structural elements within the winding packs (e.g. conductor jackets) are counted as structural material or not. It is clear from the figure, that with increasing stored magnetic energy the used support structure is getting closer to Viriral limit which represents the minimal required support structure from an energy point of view. This means that the support structure is optimised and used more efficiently with increasing stored energy. This can be understood as the support structure becomes a costing factor with increasing mass.
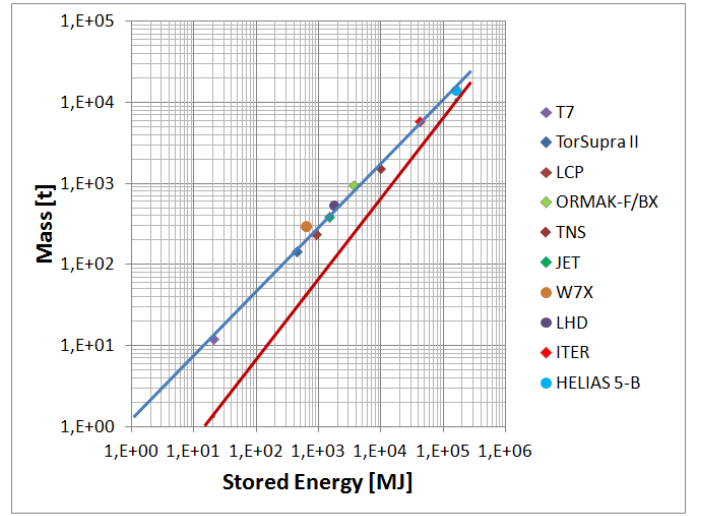

Figure 3: Virial limit of the required support structure with respect to magnetic energy (red line) and an empirical scaling (blue line) based on engineering designs of shown devices (colored rectangles).

Since the casing of the Helias 5-B coils is part of the support structure, and as the circumferential length of the coils is known from the calculations above, the cross-sectional area of the coil casing can similarly be related to the magnetic energy. Is should be noted here, that based on the advanced and optimised support structure design of Helias 5-B it is intrinsically assumed in the coil model, that the high magnetic forces and stresses on the order of 650 MPa are within allowable limits as investigated in [9, 17] in detail and not treated further here.

3.4. Plasma Transport

The current description of plasma transport in PROCESS is based on confinement time scalings. It is thereby possible to choose between different existing emprirical scalings which have been derived from experiments. Also for stellarators, several empirical confinement time scalings exist. The most recent is the so-called 'ISS04' scaling which has been obtained from combined experimentel

5

data of the international stellarator heliotron confinement database [18]. Such scalings can be easily integrated into the systems code PROCESS.

Alternatively to relying for the plasma transport description on empirical confinement time scalings derived in parameter regimes which are outside the range of a reactor, the idea here is to follow a predictive ansatz based on available theoretical and numerical knowledge.

In this approach an uncertain, yet likely influential, part is the so-called anomalous transport which is dominant in stellarator experiments at the plasma edge [19]. Since it is believed that the underlying mechanism to anomalous transport is turbulence caused by micro-instabilities inside the plasma, complex 3D turbulence, gyrokinetic GENE simulations have been started for helical advanced stellarator geometries [20]. The goal thereby is the assessment of turbulent behaviour of e.g. ion-temperature-gradient instabilities (ITG) in 3D geometry. From such an analysis simplified 1D models may be developed compatible with well-established neoclassical transport simulations [21, 22]. With such a combination of neoclassical and turbulent transport, predictive physics scenarios can be simulated allowing one to derive the corresponding confinement times which may be compactly employed to describe the plasma transport in a systems code.
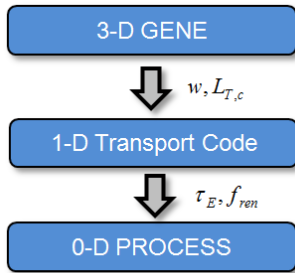
Figure 4: Startegy for predictive confinement time scaling development. The 3D GENE simulations for the ITG transport may allow one to derive a critical temperature gradient length $L_{T,c}$ and linear increase w with respect to the gradient. These results can be combined with a 1D transport code to derive predictive confinement times τ_E and a renormalisation factor f_{ren} with respect to empirical scalings.

This strategy is conceptually illustrated in Fig. 4. It was shown in [23] that the trapped electron modes (TEM) are stabilised in helical advanced stellarator configurations in a large region of the parameter space. Instead, ITG modes may still contribute significantly to the plasma transport. For this reason the strategy for the predictive confinement time exploration concentrates on the ITG induced transport.

In tokamaks ITG transport is usually well described by a critical-gradient model. This means that the ITG modes are destabilised above a certain threshold of the temperature gradient length, $L_{T_i}^{-1} = -1/T_i \, dT_i/dr$ (where r denotes the radial coordinate), or in dimensionless form

$\omega_{T_i} = a/L_{T_i}$ (here, a denotes the averaged minor radius of the stellarator). Then, the ion heat diffusivity defined as $\langle Q_i \rangle / \omega_{T_i}$ is found from the GENE simulations to increase almost linearly (at least well above marginality) with respect to the gradient ω_{T_i} (the brackets $\langle \cdots \rangle$ denote averaging with respect to the simulation box and time). The critical gradient $L_{T_i,c}$ and the slope of the linear fit are readily derived as illustrated by the example in Fig. 5.
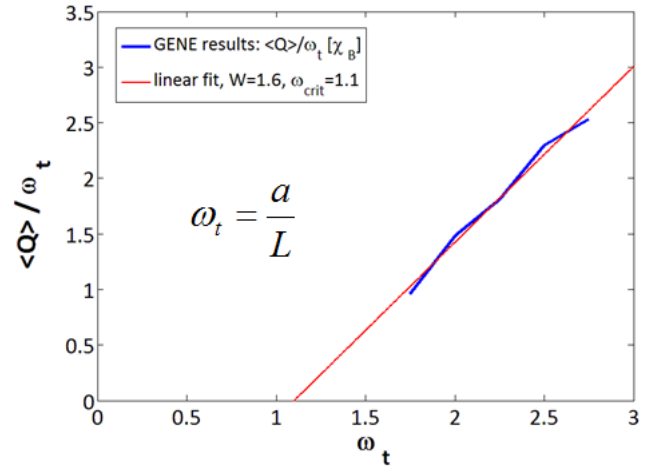

Figure 5: Scaling of the ion heat diffusivity as a function of the ion temperature gradient from GENE simulations (blue) and a linear fit (red).

It should be noted that the inclusion of a density gradient and the equilibrium radial electric field is lacking in the present results. Preliminary studies for W7-AS data, however, show a significant reduction of the ITG instability with increasing density gradient. The same is true for the radial electric field, as long as the sign of the electric field is favourable (in the opposite case, a further amplification of the ITG dynamics might occur; detailed calculations are ongoing).

Nonetheless, an exemplary application of the neoclassical 1D transport code with an ITG critical gradient model shall be demonstrated here. For this purpose two simulations are carried out. To put the results of the simulation with the ITG model in relation, the first simulation employs for comparison an empirical anomalous transport model which has been obtained from W7-AS where the diffusion coefficient scales with the absorbed power and inversely with the density, $\chi_a \sim P^{3/4} n^{-1}$ [24, 25]. For this first simulation the diffusion coefficient has been adjusted to be on the order of 1 m^2/s at the plasma edge. The second simulation employs the ITG critical gradient model where the diffusion coefficient scales with the ion temperature gradient using the corresponding values obtained from the GENE calculations. For both simulations presented here, as additional boundary condition, the temperature at the edge was chosen to be below 100 eV since the strong temperature pedestals found in tokamak H-mode discharges have yet to be observed in stellarators.
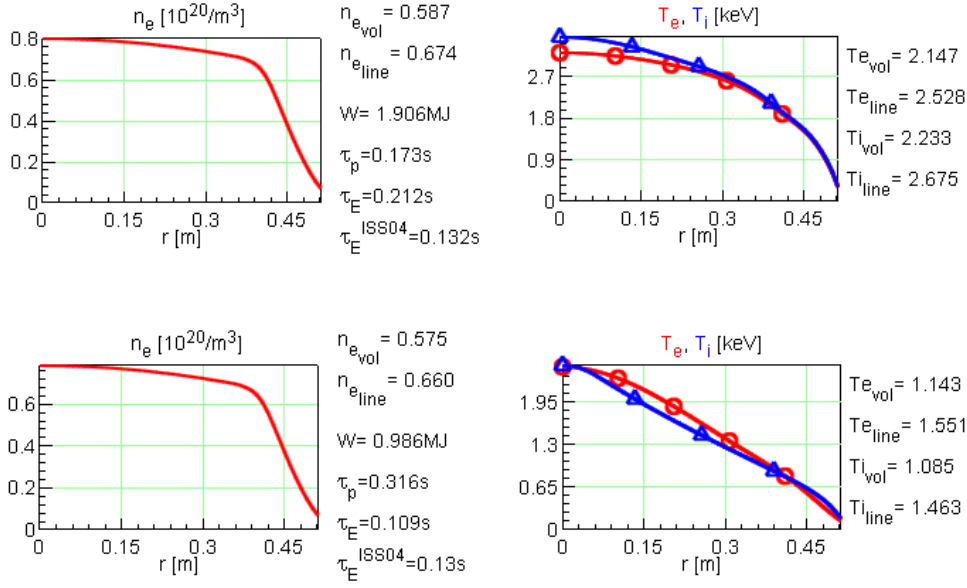
Figure 6: Transport model study: Comparison of a neoclassical 1D transport simulation employing an empirical anomalous transport model obtained from W7-AS (up) and an ITG critical gradient model (bottom). Both simulations are done for $P_{NBI} = 10$ MW heating power and similarly flat density profiles (left). Next to the figures, also the corresponding line- and volume-averaged densities and temperatures can be found as well as particle and energy confinement times.

For both simulations, the most reactor-relevant, W7-X high-mirror configuration has been chosen and both simulations were carried out with the same fixed density profile (neglecting fuelling and particle exhaust issues) with a central electron density of $0.8\ 10^{20}$ m^{-3}. For compatibility also the heating scheme for both simulations was chosen to be 10 MW neutral beam injection. This heating scheme was selected in order to heat the ions and reach significant ion temperature gradients. The resulting temperature profiles are shown in Fig. 6 and the corresponding neoclassical and anomalous diffusion coefficients are illustrated in Fig. 7.
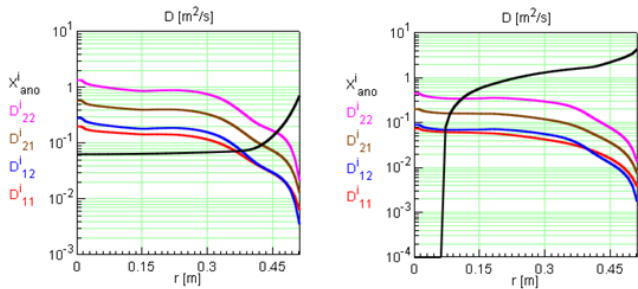
Figure 7: Comparison of neoclassical (coloured) and anomalous diffusion coefficients (black) for an empirical anomalous transport model obtained from W7-AS (left) and an ITG critical gradient model (right).

As the neoclassical effects were an optimisation criterion for the W7-X magnetic configuration, the neoclassical transport has been minimised to a level were it becomes comparable to turbulent transport. It can be seen from Fig. 7 that ITG turbulence may thus be the dominating transport channel over the whole plasma. This would lead to 'stiff' temperature profiles well-known from tokamaks as can be inferred from Fig. 6 (bottom-right). The ITG simulation here showed that the performance of the plasma in terms of confinement time and central temperature is a factor 2 below the neoclassical simulation which employs an empirical anomalous transport model.

It should be noted, that in tokamaks 'stiff' temperature profiles are usually observed in combination with a strong edge pedestal structure. Such large structures are not seen in stellaratros and are therefore excluded in the simulation here. But depending on the assumptions on a pedestal the anomalous diffusion profile would shift which in turn would have impact on plasma transport and performance.

Interestingly, to date 'stiff' temperature profiles have not been observed in stellarator experiments. This discrepancy with the presented results might admit several explanations, the most probable of which is the use of a local (flux-tube) model for the simulations, which is not able to capture the overall geometrical effects on the magnetic surface. Indeed, incorporating such an information (which is outside the scope of the present investigation) provides a milder heat-flux scaling to the one obtained here, in view of the dependence on the normalized ion gyroradius ρ_i/a, which is peculiar to stellarators only.

As already noted, also the inclusion of a density gradient and the equilibrium radial electric field is lacking in the present results. A significant reduction of the ITG in-

100

stability is expected with increasing density gradient and the radial electric field, as long as the sign of the electric field is favourable. Further improvements in terms of the density gradient and the equilibrium electric field might also alleviate these differences and will be addressed in a future work.

4. Summary

HELIAS-specific models were developed for a systems code approach, especially with respect to modular systems codes as e.g. PROCESS. The main differences between the tokamak and the helical advanced stellarator concept have been reviewed. Since the stellarator is a steady-state device working without plasma current, the poloidal magnetic field must be created by the external coils. This implies a complex three-dimensional plasma shape as defined by flux surfaces as well as non-planar coils of several different geometries. The 3D shape of the plasma introduces additional localised particle orbits which cause significant neoclassical transport. The naturally occurring magnetic islands at the edge lead to a discontinuous island divertor concept.

By thorough comparison and review of these considerations with the models found in the well-established systems code PROCESS, four independent, specific models were identified for which stellarator-specific developments are required. By taking into account that systems codes models should require low calculation times while preserving the stellarator complexity, up to now the following three models have been successfully developed. A geometry model based on Fourier coefficients which can represent the complex 3D plasma shape, a basic island divertor model which assumes diffusive cross-field transport and high radiation at the X-point and a coil model based on the Helias 5-B design in combination with inductance and field calculations.

The implementation of the proposed stellarator module to the systems code PROCESS and its verification is described in detail in a separate work [10]. In the mentioned work the HELIAS models are tested with respect to W7-X and, exploiting the generality of the models, with respect to a tokamak DEMO reference case. Both benchmarks exhibit very good agreement, justifying the use of the HELIAS module for future systems studies.

Beyond that, a transport description strategy has been developed which is anticipated to employ a confinement time scaling derived from sophisticated 1D neoclassical and 3D turbulence simulations. Using gyrokinetic GENE simulations, critical parameters for the important ion-temperature-gradient mode can be obtained. With these simulations it is possible to develop a critical gradient model compatible with the 1D transport code. Although a systematic study of the ITG transport in W7-X with respect to the density gradient length and the electric field is still under investigation, the basic principle of the strategy could be demonstrated by comparison of an empirical anomalous transport model with a 'worst-case' ITG transport model. The developed module will now be employed for detailed parameter studies for upscaled HELIAS configurations.

5. Acknowledgments

References

[1] B. J. Green. "ITER: burning plasma physics experiment." *Plasma Physics and Controlled Fusion*, vol. 45, p. 687 (2003).

[2] F. Najmabadi and The ARIES Team. "The ARIES-AT advanced tokamak, Advanced technology fusion power plant." *Fusion Engineering and Design*, vol. 80, p. 3 (2006).

[3] D. Maisonnier, D. Campbell, I. Cook et al. "Power plant conceptual studies in Europe." *Nuclear Fusion*, vol. 47, p. 1524 (2007).

[4] D. J. Ward. "Newly Developing Conceptions of DEMOs: Pulsing and Hydrogen." *Fusion Science and Technology*, vol. 56, p. 581 (2009).

[5] H. Zohm. "On the minimum size of DEMO." *Fusion Science and Technology*, vol. 58, p. 613 (2010).

[6] T. Goto, Y. Suzuki, N. Yanagi et al. "Importance of helical pitch parameter in LHD-type heliotron reactor designs." *Nuclear Fusion*, vol. 51, p. 083045 (2011).

[7] A. Sagara, T. Goto, J. Miyazawa et al. "Design activities on helical DEMO reactor FFHR-d1." *Fusion Engineering and Design*, vol. 87, p. 594 (2012).

[8] A. Sagara, H. Tamura, T. Tanaka et al. "Helical reactor design FFHR-d1 and c1 for steady-state DEMO." *Fusion Engineering and Design*, vol. 89, p. 2114 (2014).

[9] F. Schauer, K. Egorov and V. Bykov. "HELIAS 5-B magnet system structure and maintenance concept." *Fusion Engineering and Design*, vol. 88, p. 1619 (2013).

[10] F. Warmer, C. D. Beidler, A. Dinklage et al. "Implementation and Verification of a HELIAS module for the Systems Code PROCESS." *Fusion Engineering and Design*, vol. XX, p. YY (2014).

[11] Y. Feng. "Up-scaling the island divertor along the W7-stellarator line." *Journal of Nuclear Materials*, vol. 438, p. S497 (2013).

[12] Y. Feng, M. Kobayashi, T. Lunt et al. "Comparison between stellarator and tokamak divertor transport." *Plasma Physics and Controlled Fusion*, vol. 53, p. 024009 (2011).

[13] S. Babic, F. Sirois, C. Akyel et al. "Mutual Inductance Calculation Between Circular Filaments Arbitrarily Positioned in Space: Alternative to Grovers Formula." *Transaction on Magnetics*, vol. 46, p. 3591 (2010).

[14] B. Montgomery. *Solenoid Magnet Design.* Wiley-Interscience, New York (1969).

[15] Y. Ilyin, A. Nijhuis and E. Krooshoop. "Scaling law for the strain dependence of the critical current in an advanced

ITER Nb$_3$Sn strand." *Superconductor Science and Technology*, vol. 20, p. 186 (2007).

[16] F. C. Moon. "The virial theorem and scaling laws for superconducting magnet systems." *Journal of Applied Physics*, vol. 53, p. 9112 (1982).

[17] F. Schauer. "Coil winding pack FE-analysis for a HELIAS reactor." *Fusion Engineering and Design*, vol. 86, p. 636 (2011).

[18] H. Yamada, J. H. Harris, A. Dinklage et al. "Characterization of energy confinement in net-current free plasmas using the extended International Stellarator Database." *Nuclear Fusion*, vol. 45, p. 1684 (2005).

[19] A. Dinklage, M. Yokoyama, K. Tanaka et al. "Inter-machine validation study of neoclassical transport modelling in medium- to high-density stellarator-heliotron plasmas." *Nuclear Fusion*, vol. 53, p. 063022 (2013).

[20] P. Xanthopoulos, F. Merz, T. Grler et al. "Nonlinear Gyrokinetic Simulations of Ion-Temperature-Gradient Turbulence for the Optimized Wendelstein 7-X Stellarator." *Physical Review Letters*, vol. 99, p. 035002 (2007).

[21] C. D. Beidler, K. Allmaier, M. Y. Isaev et al. "Benchmarking of the mono-energetic transport coefficients - results from the International Collaboration on Neoclassical Transport in Stellarators (ICNTS)." *Nuclear Fusion*, vol. 51, p. 076001 (2011).

[22] Y. Turkin, C. D. Beidler, H. Maaßberg et al. "Neoclassical transport simulations for stellarators." *Physics of Plasmas*, vol. 18, p. 022505 (2011).

[23] J. H. E. Proll, P. Helander, J. W. Connor et al. "Resilience of Quasi-Isodynamic Stellarators against Trapped-Particle Instabilities." *Physical Review Letters*, vol. 108, p. 245002 (2012).

[24] H. Maaßberg, R. Brakel, R. Burhenn et al. "Transport in stellarators." *Plasma Physics and Controlled Fusion*, vol. 35, p. B319 (1993).

[25] U. Stroth. "A comparative study of transport in stellarators and tokamaks." *Plasma Physics and Controlled Fusion*, vol. 40, p. 9 (1998).

9

Implementation and Verification of a HELIAS module for the Systems Code PROCESS

F. Warmer[a,*], C.D. Beidler[a], A. Dinklage[a], K. Egorov[a], Y. Feng[a], J. Geiger[a], R. Kemp[b], P. Knight[b], F. Schauer[a],
Y. Turkin[a], D. Ward[b], R. Wolf[a], P. Xanthopoulos[a]

[a]*Max Planck Institute for Plasma Physics, D-17491, Greifswald, Germany*
[b]*Culham Centre for Fusion Energy, Abingdon, Oxfordshire, OX14 3DB, United Kingdom*

Abstract

In order to study design points of next-step fusion devices such as DEMO, comprehensive systems codes are commonly employed. The code package PROCESS is such a tool, widely used for tokamak systems studies. In this work, the implementation and verification of a HELIAS module into PROCESS is addressed. These HELIAS models include: a plasma geometry model based on Fourier coefficients, a basic island divertor model, as well as a coil model which combines scaling aspects based on the Helias 5-B reactor design in combination with analytic inductance and field calculations. The models are verified firstly with respect to W7-X. Secondly, the generality of the models is used to represent the tokamak which is compared against the original tokamak PROCESS models using a DEMO design as reference case. Both approaches show very good agreement.

Keywords: HELIAS, PROCESS, Systems Code, verification

1. Introduction

Systems codes are simplified, yet comprehensive models of an entire fusion power plant used to carry out respective systems studies. These studies focus on the analysis of the complex interplay between physics, engineering, and economic considerations allowing assessment of parametric dependencies on the design of the plant. The goal of systems studies and systems codes is the development and optimisation of design points for next-step fusion devices. With this approach critical research areas can be identified. This ansatz is commonly applied in the tokamak community, especially with respect to a tokamak demonstration fusion power plant, also known as 'DEMO', for which many studies are ongoing.

The systems code PROCESS has been assessed to identify changes necessary to accommodate helical advanced stellarators (HELIAS). Based on this assessment, HELIAS-specific models have been developed in [1] designed for a systems code approach consisting of three major models. First, a geometry model to describe the plasma shape (flux surfaces) based on Fourier coefficients. Second, a basic island divertor model for the energy exhaust is derived from geometrical considerations, in addition assuming cross-field transport and radiation at the X-point. And third, a coil model which calculates the maximal field at the coils, the total stored magnetic energy, and the dimensions of the winding pack based on the sophisticated Helias 5-B [2] reactor design. For this purpose scaling relations and analytic inductance and field calculations are employed in combination with a critical current density scaling of the superconducting material used.

Moreover, a strategy for a predictive confinement time scaling has been discussed in [1] where it is shown that 3D turbulence, gyrokinetic GENE simulations have been started for

HELIAS geometries [3] with the aim of assessing the behaviour of e.g. ion-temperature-gradient instabilitites. The guiding results can be combined with well-established neoclassical considerations [4] allowing to carry out predictive transport simulations to derive corresponding confinement times which may be compactly employed in systems codes. This development is underway. Meanwhile, stellarator-specific empirical confinement time scalings like ISS04 [5] are available and can be used within PROCESS.

In this work progress is reported on the implementation of the HELIAS models into PROCESS [6] and also the verification of the models with respect to two test cases. In section 2 the architecture of PROCESS and the implementation of the HELIAS models are briefly reviewed. The verification of the HELIAS module is then discussed in section 3 in two parts. First, the models are compared against the stellarator Wendelstein 7-X design and predictions for its performance and second, the generality of the models is used to represent the tokamak and in turn assessed with respect to the original PROCESS tokamak models using a DEMO design as reference case. The work is summarised and the results discussed in section 4.

2. PROCESS Architecture

PROCESS is a well-established, partly modular, European tokamak systems code which gained maturity through years of applications. A solver based on Lagrangian multipliers is employed within PROCESS to allow for design optimisation with respect to the descriptive models and constraints. This is done by minimising (or maximising) a user-defined Figure of Merit consistent with the relevant inputs (iteration variables, constraint equations, and limits). The framework of PROCESS consists of detailed, well-developed plasma physics, engineering and economic models allowing for a broad scope of application.

The modularity of PROCESS also allows implementation options for different confinement concepts. This means, the

---

*Corresponding author, Tel.: +49 (0)3834 88-2583
Email address: Felix.Warmer@ipp.mpg.de (F. Warmer)

HELIAS models for the plasma geometry, island divertor, and modular coils could be straightforwardly implemented with only minor adaptations. This allows also to retain the use of the non-device-specific systems in PROCESS, such as the balance of plant and economic models, and the numerical solver which allows constrained optimisation of the design.

3. Verification of the HELIAS Models

In order to verify the stellarator module a twofold comparison is carried out. First, the stellarator module is applied to represent Wendelstein 7-X and the results are compared to the W7-X design and predictions for its performance. Second, the generality of the models allows modification of the stellarator module so that it can represent the tokamak. This tokamak representation of the stellarator module is then compared against a tokamak DEMO reference design point created by the orginal tokamak PROCESS models.

3.1. Comparison to Wendelstein 7-X

3.1.1. Plasma Geometry

The plasma geometry model [1] is based on Fourier coefficients which allows one to describe arbitrarily complex flux-surfaces. For the validation study the W7-X high-mirror configuration is chosen and the specific Fourier coefficients are obtained from the corresponding VMEC [7] equilibrium. The geometrical parameters of the plasma major radius, plasma minor radius, plasma volume and surface area calculated by the plasma geometry model are in very good agreement with the VMEC results, yielding for both $R = 5.5$ m, $a = 0.53$ m, $S = 120$ m^2 and $V = 30.1$ m^3.

3.1.2. Island Divertor

The model of the island divertor concept [1, 8] consists of a geometrical description including cross-field diffusion and radiation around the X-point. For the verification with W7-X, experimental data are not yet available. Therefore, the island divertor model is compared against a 3D EMC3-Eirene [9] simulation of a W7-X high-power discharge scenario. For the EMC3 simulation a heating power of $P = 10$ MW and perpendicular heat diffusion coefficient of $\chi_\perp = 1.5$ m^2/s have been chosen. In accordance with W7-X and the simulation results the following values were selected as additional input for the island divertor model: the inclination of the divertor plate relative to the field lines $\alpha_{\lim} = 2°$, the temperature in front of the divertor plates $T_t = 15$ eV, the radiation fraction in the SOL $f_{rad} = 0.05$, and the field line pitch angle $\Theta = O(10^{-3})$. The EMC3 simulation is illustrated in Fig. 1 and the results are compared in Tab. 1.

	EMC3	ID Model
Island Size [cm]	14	14*
X-point - target distance [cm]	12.5	12.5*
Divertor plate Length [m]	$1 \sim 1.5$	1.6
Power Decay Width [cm]	7.4	9.3
Effective wetted area [m^2]	$1 \sim 2$	1.5
Heat load [MW/m^2]	6.5	6.9

Table 1: Comparison of the important parameters of an EMC3-Eirene simulation of Wendelstein 7-X with the corresponding output from the island divertor model. The values marked with a star have here been used as inputs to the island divertor model.

It can be seen from the EMC3 simulation results in Fig. 1, that the energy deposition has a 3D pattern, e.g. long tail in the front of the plate. This means that the parameters defined in the island divertor model cannot be straightforwardly represented by a single value. Especially for the effective length of the wetted area of the divertor, only a range of values can be given (Tab. 1). The value for the effective wetted area calculated by the island divertor model lies within this range and the value for the divertor plate length at the boundary of the EMC3 range. The power decay width and the heat load agree to the right order of magnitude but show a discrepancy of about 20 %.
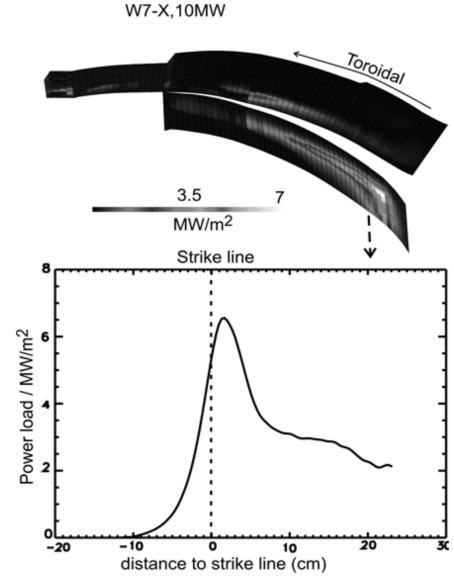

Figure 1: Heat load distribution on a W7-X divertor plate for an EMC3-Eirene simulation and perpendicular cut of the divertor plate front for $P = 10$ MW and $\chi_\perp = 1.5$ m^2/s.

Contributing to this discrepancy is the fact that the basic island divertor model assumes two stellarator-symmetric targets in each field period, while in reality there are four in W7-X. Although the island divertor model does not take such details into account the first comparison results are encouraging. This preliminary result suggests that the island divertor model provides an acceptable estimation of the heat load within the frame of a systems code but nedds to be justified in a future work.

3.1.3. Modular Coils

The model for the modular coils [1] is a combination of analytical calculations and scaling relations which are based on the detailed Helias 5-B coil design employing Nb$_3$Sn as superconductor. To be able to compare the coil model with the existing W7-X coils a scaling for the critical current density of NbTi was implemented. This was done in the same fashion as for Nb$_3$Sn. Apart from that, the size has been scaled to represent the geometrical parameters of W7-X. The results are compared in Tab. 2.

Agreement is found between the self-consistent model and the values for W7-X except for the estimated masses. The mass of the support structure is calculated from an empirical scaling which goes over several orders of magnitude. This scaling gets closer to the virial limit at high magnetic energy representing

2

	W7-X	Coil Model
Field on Axis [T]	3.0	3.0*
Field on Coil [T]	6.7	6.6
Magnetic Energy [MJ]	620	640
Mass of Sup. Struc. [t]	$\sim$300	212
Winding pack [mm$\times$mm]	166×226	167×177
Ampere Turns [MA]	1.74	1.74
Total weight of WP [t]	$\sim$100	62
Average Coil Length [m]	8.5	8.5

Table 2: Comparison of the important parameters of the coil design of Wendelstein 7-X with the corresponding output of the coil model. The value marked with a star has been used as input.
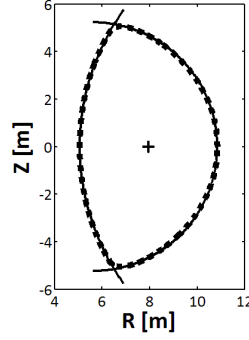

Figure 2: Comparison of the PROCESS DEMO cross-section consisting of two circular arcs (solid lines) with the corresponding VMEC equilibrium (squares).

the necessary for mass optimisation. In W7-X minimisation of the mass of the support structure was not attempted and it therefore deviates from the model

Also the winding pack aspect ratio is more radially elongated for the W7-X coils which introduces a discrepancy for the winding pack dimensions between W7-X and the coil model as well as for the winding pack mass. In addition, the electrical insulation and winding pack embedding require relatively more cross section in W7-X than in a reactor coil.

Next-step HELIAS devices will have very high stored magnetic energy requiring much more support structure, meaning that optimisation with respect to minimal mass will play a role. Therefore, it is expected that the mass calculations will have better validity for extrapolation of larger devices closer to Helias 5-B while the other parameters are expected to retain their very good agreement.

3.2. Application to Tokamak-DEMO: a test-case

In order to further verify the stellarator module, the corresponding models are applied to an axisymmetric tokamak case and the results are compared to the original tokamak PROCESS module. For this study an advanced tokamak DEMO design point was selected as reference case with a major radius $R_0 = 7.95$ m, minor radius $a = 2.9$ m, plasma elongation $\kappa = 1.78$ and plasma triangulartiy $\delta = 0.5$.

3.2.1. Plasma Geometry

The axisymmetric plasma shape in the tokamak PROCESS geometry model is described by two intersecting circles, from which the plasma volume, surface and cross-sectional area can be obtained with simple analytic formulas.

As the stellarator geometry model is based on Fourier coefficients, a magnetic equilibrium has been created with VMEC closely representing the tokamak DEMO design point. The toroidal cut for the PROCESS tokamak DEMO shape and the VMEC magnetic equilibrium are both shown in Fig. 2. It can be seen that the created VMEC equilibrium properly resembles the tokamak PROCESS shape.

A comparison of the important geometrical parameters, namely the plasma volume, the surface area and the cross-sectional area for the PROCESS tokamak shape yields very good agreement within 1 % (Tab. 3). Subsequently, the VMEC tokamak DEMO equilibrium has been read in and processed by the stellarator geometry model yielding very good agreement for the plasma volume and the cross-sectional area.

3.2.2. Coil Model

While the generality of the geometry model allowed a straightforward application and comparison with the tokamak DEMO reference case, the stellarator coil model is more specific. Although the analytic part of the coil model is general, the scaling relations are based on the Helias 5-B reactor design which hardly makes a direct application to tokamaks meaningful. Since the coil model is a combination of analytical calculations and scalings based on the Helias 5-B design, it is possible to replace the scaling part with an available tokamak design. For this basis, ITER has been chosen while the analytic part of the coil model is kept unchanged.

With ITER as basis, an 'adapted' coil model can be employed to recreate the tokamak DEMO reference case, comparing it with the original PROCESS results. In order to model the DEMO reference case, the machine geometrical parameters (e.g. major radius, minor radius, shield and blanket width) were adjusted accordingly as well as the dimensions of the individual turns. The corresponding results for the coil dimensions and associated field parameters are shown in Tab. 4.

	DEMO	Coil Model
Field on Axis [T]	5.2	5.2*
Field at Coil [T]	12.9	13.2
Magnetic Energy [GJ]	111	113
Winding Pack [m$\times$m]	0.88×0.91	0.82×0.98
Ampere Turns [MA]	12.8	12.8
Conductor mass per coil [t]	132.5	127.8
Case mass per coil [t]	520.7	509.5
Average Coil Length [m]	46.6	47.3

Table 4: Comparison of the important parameters of the PROCESS DEMO reference case with the corresponding output from the adapted coil model (the PROCESS trapezoidal toroidal winding pack form has been averaged for simplicity). The value marked with a star has been used as input.

It is found that the adapted coil model yields results very similar to those of the original PROCESS model with a maximal relative difference of less than 10 % which is well within the accuracy of such a systems code approach. The main difference arises for the winding pack dimensions which have a different radial to toroidal aspect ratio which is fixed in the adapted coil model based on ITER and more flexible for the original PROCESS model. Overall the adapted coil model shows very good agreement with the PROCESS tokamak DEMO reference case establishing confidence for the use of the model.

3

	PROCESS representation	VMEC equilibrium	Stellarator Geometry Model
Plasma Volume [m^3]	2131	2117	2117
Plasma Surface Area [m^2]	1231	1217	1235
Cross-Sectional Area [m^2]	43.7	43.5	43.5

Table 3: Comparison of the Plasma Volume, Surface Area and Cross-Sectional Area of the DEMO PROCESS representation with the correspondingly created VMEC equilibrium and the HELIAS Geometry model.

3.2.3. Divertor Plausibility Check

The island divertor is conceptually different from the tokamak axisymmetric divertor. Nevertheless, the island divertor model makes use of a basic geometrical approach which, with minor modifications, can be adopted to represent the tokamak. The major physical differences between the two concepts are the scales of the connection lengths and the magnetic field pitch angle. In the stellarator the connection lengths are an order of magnitude longer, $L_c \sim O(10^3)$ m, than in comparable tokamaks, $L_c \sim O(10^2)$ m, while the field pitch on the other hand is much smaller in stellarators, $\Theta \sim O(10^{-3})$, compared to tokamaks with $\Theta \sim O(10^{-1})$. This means that in tokamaks the parallel SOL transport is dominant while in stellarators also the perpendicular transport plays an important role competing with parallel transport. Taking additionally into account that the tokamak divertor is toroidally closed, the island divertor model can be modified accordingly. The heat load is given as [1]:

$$ q_{\mathrm{div}} = \frac{P_{\mathrm{div}}}{A_{\mathrm{eff}}} = \frac{P_{\mathrm{SOL}}(1 - f_{\mathrm{rad}})}{L_{\mathrm{T}} \cdot \lambda_q}. \tag{1} $$

The total length of the available divertor is for the tokamak modified to $L_T \approx 2 \cdot 2\pi R$ and the geometric flux expansion, $f_x \approx 1/\alpha_{pol}$ [10], is now considered within the power width on the divertor plates: $\lambda_q = f_x \cdot \sqrt{\chi_\perp \cdot \tau_\parallel}$.

Considering the DEMO reference case, the distance from X-point to divertor plate is fixed to $\Delta = 0.4$ m and a perpendicular heat diffusion coefficient of $\chi_\perp = 1$ m^2/s is assumed. In addition, the values for $\alpha_{pol} = 20°$, $T_t = 10$ eV and $\Theta = 0.1$ have been estimated for this case. Applying the modified model, the power width on the divertor for the tokamak DEMO reference case becomes then $\lambda_q = 4$ cm yielding an effective wetted area of $A_{\mathrm{eff}} = 4$ m^2. The DEMO case is designed for 2 GW fusion power resulting in about 400 MW transport power which cross the separatrix. In order to keep the heat load below $q_{\mathrm{div}} \leq 5$ MW/m^2, it is found in the model that only 5 % (20 MW) of this power is allowed to reach the divertor.

These results agree on the order of magnitude with values found in e.g. [10] where the divertor broadening for a DEMO case is anticipated to be on the order of $1 - 3$ cm at temperatures below 10 eV.

4. Conclusions

HELIAS models have been successfully implemented in the systems code PROCESS. A verification study of the HELIAS module has been carried out. First, W7-X was modeled within the HELIAS-representation of PROCESS and compared to the real machine parameters. The comparison showed very good agreement for the plasma geometry and the coil model, except for the coil masses which could be traced back to the fact that the W7-X support structure is not optimised with respect to mass. Also the island divertor model showed agreement on the dimensions with an EMC3-Eirene simulation with deviations on the order of 20 %.

Secondly, the generality of the HELIAS-module has been used to represent the tokamak where the coil module has been adopted using ITER paramters as basis. Moreover, the divertor model was modified taking into account the tokamak symmetry. The subsequent modelling of a DEMO reference case showed very good agreement for the plasma geometry model and the coil model within this representation compared to the original PROCESS tokamak models. Also the modified divertor model gives plausible results agreeing with values found in [10].

With this tool available, stellarator systems studies can be conducted. Moreover, a direct comparison between tokamak and stellarator DEMO and power plant designs can be carried out within the common framework of PROCESS which is subject to ongoing investigations.

5. Acknowledgments

References

[1] F. Warmer, C. D. Beidler, A. Dinklage et al. "HELIAS Module Development for Systems Codes." *Fusion Engineering and Design*, vol. [submited] (2014).

[2] F. Schauer, K. Egorov and V. Bykov. "HELIAS 5-B magnet system structure and maintenance concept." *Fusion Engineering and Design*, vol. 88, p. 1619 (2013).

[3] P. Xanthopoulos, F. Merz, T. Grler et al. "Nonlinear Gyrokinetic Simulations of Ion-Temperature-Gradient Turbulence for the Optimized Wendelstein 7-X Stellarator." *Physical Review Letters*, vol. 99, p. 035002 (2007).

[4] Y. Turkin, C. D. Beidler, H. Maaßberg et al. "Neoclassical transport simulations for stellarators." *Physics of Plasmas*, vol. 18, p. 022505 (2011).

[5] H. Yamada, J. H. Harris, A. Dinklage et al. "Characterization of energy confinement in net-current free plasmas using the extended International Stellarator Database." *Nuclear Fusion*, vol. 45, p. 1684 (2005).

[6] M. Kovari, R. Kemp, H. Lux et al. "PROCESS: A systems code for fusion power plants - Part 1: Physics." *Fusion Engineering and Design*, vol. [in Press] (2014).

[7] S. P. Hirshman, W. I. van Rij and P. Merkel. "Three-dimensional free boundary calculations using a spectral Green's function method." *Computer Physics Communications*, vol. 43, p. 143 (1986).

[8] Y. Feng. "Up-scaling the island divertor along the W7-stellarator line." *Journal of Nuclear Materials*, vol. 438, p. S497 (2013).

[9] D. Reiter, M. Baelmans and P. Börner. "The EIRENE and B2-EIRENE Codes." *Fusion Science and Technology*, vol. 47, p. 172 (2005).

[10] B. Sieglin. *Experimental Investigation of Heat Transport and Divertor Loads of Fusion Plasma in All Metal ASDEX Upgrade and JET.* Ph.D. thesis, Technische Universität München (2014).

4

Systems Code Analysis of HELIAS-type Fusion Reactor and Economic Comparison to Tokamaks

F. Warmer, S.B. Torrisi, C.D. Beidler, A. Dinklage, Y. Feng, J. Geiger, F. Schauer, Y. Turkin, R. Wolf, P. Xanthopoulos

Max Planck Institute for Plasma Physics
D-17491, Greifswald, Germany

R. Kemp, P. Knight, H. Lux, D. Ward
Culham Centre for Fusion Energy
Oxfordshire, OX14 3DB, United Kingdom

Contact: Felix.Warmer@ipp.mpg.de

Abstract— **Systems codes are commonly employed for the analysis and conceptual design of fusion reactors. For the helical-axis advanced stellarator (HELIAS) line a new set of systems code models have been developed to account for the stellarator-specific 3D aspects. The models have been recently been implemented in the systems code PROCESS and verified with respect to different test cases.**

After having established confidence in the stellarator models, systems studies were carried out for the 5-field period HELIAS case to define the accessible reactor design window. In the multi-dimensional physics and engineering parameter space sensitivity studies are carried out for the reactor regime to ascertain trade-offs between different parameters and costs. Exemplary design points are analysed in more detail using the plasma operation contour approach which, for example, can be used to determine the optimum start-up path to ignition.

Finally, with a common set of non-device-specific models, the PROCESS framework allows a direct comparison of tokamaks and stellarators. Although the 5-period HELIAS is a larger machine in terms of major radius, the required mass for both concepts is comparable leading to similar construction costs.

Keywords—Helical-Axis Advanced Stellarator (HELIAS), PROCESS, Systems Code, tokamak-stellarator comparison

I. INTRODUCTION

For an assessment of next-step fusion devices, it is not only important to find realistic design points consistent in physics and engineering but also to optimize these design points with respect to the high-level goals and costs. Furthermore, in such a conceptual design phase it is essential to show the robustness of design points with respect to variations in the underlying assumptions. Such a design process is commonly referred to as 'systems studies' where engineering and physics parameters are varied to define the accessible reactor design window and to study the sensitivity of the reactor regime considering trade-offs between important parameters and costs.

Such an approach has the advantage of revealing ambiguities in the underlying assumptions. These can then be clarified in dedicated experiments and simulations, thus defining a critical research path. Consequently, risks and uncertainties are mitigated before the actual engineering design process is started, thereby saving resources which would otherwise be needed for design iterations.

In order to carry out systems studies for next-step fusion devices associated 'systems codes' are used which are simplified, yet comprehensive models of an entire fusion power plant. Such an ansatz is commonly applied in the tokamak community, especially with respect to the assessment of a tokamak demonstration fusion power plant, also known as 'DEMO' [1]. Considering helical confinement concepts, similar studies have been done for the heliotron concept [2] and compact stellarators [3]. For the helical-axis advanced stellarator line (HELIAS), results of such a study are presented in this work for the first time.

For this purpose HELIAS-specific models have been developed [4]. These models include:

- First, a geometry model to describe the plasma shape (flux surfaces) based on Fourier coefficients. In position-space the geometry is described by cylindrical coordinates, which have been decomposed in a Fourier series allowing modeling of any arbitrary 3D toroidal surface. Such a formulation allows one to accurately calculate the important geometrical parameters such as plasma volume, surface area and cross-section which have direct impact on e.g. fusion power or neutron wall load. Moreover, it is possible to scale both the minor and major plasma radius by scaling of the corresponding Fourier coefficients making the model very flexible and suitable for a systems code approach.

- Second, a basic island divertor model for the energy exhaust was derived from geometrical considerations, in addition assuming cross-field transport and radiation at the X-point. The model is of analytic nature and combines physics and engineering relations. From the engineering side, the length of the divertor plate is estimated by considering how a helical field line in the scrape-off layer just passes the divertor plate on the inner side and the field line which hits the divertor on the outer side where the radial distance is given by the

size of the magnetic island. The broadening of the heat along such a field line is estimated by assuming diffusive cross field transport where the time it takes to reach the divertor is determined by the connection length.

- And third, a coil model which calculates the maximum field at the coils, the total stored magnetic energy, and the dimensions of the winding pack based on the sophisticated HELIAS 5-B [5] engineering design. For this purpose scaling relations and analytic inductance and field calculations are employed in combination with a critical current density scaling of the superconducting material used, i.e. scalings for both NbTi and Nb_3Sn have been implemented.

For the plasma transport, an empirical confinement time scaling is used. For stellarators, the most recent scaling is the so-called ISS04 scaling which was derived from the international stellarator-heliotron confinement database [6]. In such an ansatz, it is common to include a 'confinement enhancement factor' which describes the envisaged improvement of the confinement with respect to the empirical scaling. To improve the predictive capability of the confinement properties, transport simulations (including neoclassical and turbulent contributions) have been done [7]. The results of the transport simulations have been used to define the confinement enhancement factor for the studies presented here.

These models were implemented in the systems code PROCESS [8] which is a well-established, partly modular, European tokamak systems code which has gained maturity through years of applications. After the successful implementation, a verification study was carried out, in detail described in [9]. W7-X was modeled within the stellarator representation of PROCESS and compared to the real machine parameters. This comparison showed good agreement of the important parameters with maximum 10% deviation providing confidence for the use of the models for HELIAS systems studies. Their implementation in the original tokamak-centric code PROCESS has the additional advantage that the tokamak and stellarator concept can be compared within a common framework.

This work is divided into two parts. The first part, section II, is dedicated to HELIAS systems studies with emphasis on the general design window analysis and plasma operation contour analysis as well as specific examples such as the effect of tungsten impurities on start-up and plasma operation. The second part, presented in section III, makes use of the aforementioned common PROCESS framework (version 389) to compare exemplary tokamak and stellarator design points. Finally, the work is summarized and the results discussed in section IV.

II. HELIAS SYSTEMS STUDIES

A. Design Constraints and Goals

Before a design window of a HELIAS power plant type device can be outlined several general assumptions must be made about the constraints and goals of such a device. As the

stellarator is intrinsically designed for steady-state operation, a HELIAS power plant aims for an economic base-load power output which must be at least comparable to the level of existing large power plants. Here, this is formulated as a constraint to achieve ~1GW net electric power. The production of net electric power is closely interconnected to two other systems of a fusion power plant, namely the power conversion system as well as the blanket structure. Both systems must be conceptually specified for a HELIAS systems analysis.

The power conversion system of thermal to electric energy is mainly dependent on the chosen coolant which determines the thermal conversion efficiency η_{th}. Common technologies employ either pressurized water or gaseous helium cooling. Water cooling is a well established technology requiring a moderate amount of pumping power but has a lower efficiency compared to helium. In turn, helium cooling requires a much higher pumping power. A detailed discussion of the advantages and disadvantages of both systems is still ongoing in the fusion community. In this work, the Brayton power cycle with helium cooling technology has been chosen for the cooling system due to the possibility of working at higher temperatures and avoiding the unresolved safety issues regarding water cooling [10]. Additionally, the higher thermal conversion efficiency, η_{th} = 0.4, compensates for the higher pumping power, P_{pump} = 200MW, assumed throughout this work [11, 12].

Several different technologies also exist for the blanket composition and its structure. It is beyond the scope of this work to compare the different blanket possibilities and benefits and drawbacks. For this work the dual-coolant (helium and lithium-lead) ferritic steel modular blanket concept was chosen described in [11] compatible with the outlined power conversion system above. This choice has been made here in order to facilitate the comparison to a tokamak. The in- and outboard thicknesses are summarized in Tab. 1, where the full blanket thickness is assumed everywhere to ensure a high tritium breeding ratio (TBR) for self-sustained tritium supply.

It should be noted that the application of these technologies do not represent a final decision but are chosen for a realistic representation of a HELIAS power plant. A decision about the heat conversion and blanket system can only be made after the experimental testing of blanket technologies and detailed assessment of the cooling systems. In fact, the European helium cooled pebble bed (HCPB) blanket design [12] seems more favorable for a stellarator due to the low space requirements. A detailed neutronics analysis of a HELIAS power reactor is ongoing [13].

TABLE I.   MAIN DESIGN PARAMETERS ASSUMED FOR THE HELIAS SYSTEMS STUDIES UNLESS OTHERWISE STATED.

Main design parameters	
Thermal efficiency for He-cooling η_{th}	0.4
Pumping Power for He-cooling [MW]	200
Inboard blanket thickness [m]	0.7
Inboard shield thickness [m]	0.4
Outboard blanket thickness [m]	0.8
Outboard shield thickness [m]	0.7
Superconducting Material	Nb_3Sn
HELIAS Field Periods	5
Number of Coils	50

In order to have enough space between the plasma and the coils to accommodate the specified blanket a higher aspect ratio of $A = 12.2$ has been chosen compared to the aspect ratio of $A = 10.5$ in W7-X [15]. The modular coil design and its cross-section are based on [16] where Nb_3Sn is used as superconducting material reflecting the experience gained from ITER.

This work concentrates on a HELIAS magnetic configuration with 5 field periods due to the more favorable physics properties, including better confinement of fast particles and reduced bootstrap current. A more compact 4-field-period device with lower aspect ratio may be of interest in future studies.

Empirical confinement time scalings have been widely used in the fusion community to assess and predict the confinement time τ_E in terms of global physics and engineering parameters. However, it was shown in [7] that an empirical scaling is not sufficient to predict the confinement properties of 5-field period HELIAS since results from detailed transport simulations deviate from the scaling at reactor-relevant parameters.

Although modern stellarators, like W7-X, are optimized for reduced neoclassical transport, the improvement of the global confinement by such measures remains to be proven. First indications, however, could be obtained by analyzing the dataset of the ISS04 scaling. Different devices, and even different magnetic configurations of the same device, are displaced with regard to the overall regression. Indeed, different clusters have been identified within the dataset used for the ISS04 scaling [6]. Consequently, a configuration-dependent factor, f_{ren}, has been introduced to account for a general improvement or degradation with respect to the reference scaling which is defined as $\tau_E = f_{ren} \cdot \tau_E^{ISS04}$. The renormalization factor f_{ren} can thus serve as a measure for the optimization of the magnetic configuration. The function of the renormalization factor is similar to the H-factor used in tokamaks. However, as described above, the underlying concept is quite different.

Transport codes can be employed to calculate the neoclassical and anomalous transport for a specific magnetic configuration to obtain a predictive confinement time [17]. Comparing the confinement time obtained from such simulations to the value given by the direct extrapolation of the ISS04-scaling allows one to obtain a predictive renormalization factor. For this reason, the renormalization factor is taken here to be synonymous with a confinement enhancement factor.

The transport simulations have been applied to a HELIAS reactor scenario and iterated back and forth with the systems codes studies. For conservative reactor parameters a maximum confinement enhancement factor of $f_{ren} = \tau_E / \tau_E^{ISS04} \leq 1.5$ was found [7] and serves as the upper limit for the present studies. According to the 1-D transport simulations with dominating neoclassical transport in the plasma centre and anomalous transport at the plasma edge the volume averaged temperature has been fixed for the HELIAS reactor studies to $\langle T \rangle_V = 7keV$. The density on the other hand is iterated in the design window analysis to achieve the desired goals such as 1GW net electric power.

Stellarators are not subject to a density limit of the Greenwald type [18] and the radiative density limit, i.e. SUDO-limit [19], observed in some heliotron/stellarator-type devices is not considered in this work since the Large Helical Device (LHD) has demonstrated the ability to operate far beyond this limit, especially if pellet injection is used. Therefore the SUDO-limit has been reinterpreted as a density limit for the plasma edge [20, 21]. For the 5-field period HELIAS the SUDO-limit yields a value of $1.6 \cdot 10^{20} m^{-3}$ which is very high for an edge-limit and thus not relevant for the design window analysis considered here.

Another important aspect of a fusion power plant is the controlled exhaust of energy and particles through the divertor. The model of the island divertor concept consists of a geometrical description including cross-field diffusion and radiation in the SOL and around the X-point [4, 9, 22]. In order to model the island divertor, a set of assumptions is needed: For the SOL a perpendicular heat diffusion coefficient of $\chi = 1.5 m^2/s$ has been chosen from experimental experience. The inclination between field lines and the divertor target plates was selected to be $\alpha_{lim} = 2°$ with a field line pitch angle $\Theta = O(10^{-3})$. The temperature in front of divertor is estimated to be $T_t = 3eV$ with an effective charge of $Z_{eff} = 3$ due to the radiating impurities. A heat load limit of $q < 5MW/m^2$ is expected for steady-state reactor conditions [23]. In the following the radiation fraction in the SOL, $f_{rad}*$, is varied to stay within the heat load limit and serves as a figure of merit for the exhaust challenge.

As the scenarios investigated in this work concern a burning plasma with production of alpha-particles, helium dilution of the plasma must be taken into account. In order to estimate the helium 'ash' in the plasma, first a source profile has been defined by taking the alpha particle birth profile and assuming slowing down on the flux surface (i.e. neglecting losses of alpha particles). Secondly, using the neoclassical transport approach as discussed before, the particle flux of the helium ash is calculated and in combination with the source profile a helium density profile is obtained. This leads to a concentration of 10% helium 'ash' in the plasma. This cannot be ignored as helium dilution reduces the fusion power output. Apart from helium no further impurities have been taken into account for the plasma core. Only in the dedicated sensitivity study in section II.D have intrinsic tungsten impurities been considered. In future studies other seeded impurities may be taken into account to increase the radiation in the plasma core reducing the power crossing the separatrix and therefore easing the exhaust scenario.

B. Design Window Analysis

Design window analysis has originally been carried out for heliotron reactors as described in [24]. The aim of such an analysis is to define the accessible engineering and physics parameter range for a fusion power plant device respecting specified constraints and goals as described above. For this purpose the main engineering parameters of a HELIAS power plant (the major radius and the magnetic field strength on axis) were systematically varied within a reasonable range (18m < R < 24m; 4.5T < B_t < 5.6T). In this study the high-level goals were kept constant. That means, in every design point a net

electric power of 1GW should be reached. To achieve this while varying the machine size and magnetic field, the plasma density and the confinement enhancement factor were iterated (subject to the limit obtained from the transport simulations).

Two cases are presented in the following, called (A) and (B). In the first case (A) the design window analysis is presented according to the assumptions and goals outlined above. In case (B) the helium ash concentration in the plasma is assumed to be 5% compared to the 10% in case (A) in order to assess the impact of helium dilution on the design window.

It should be noted that a single run of a stellarator scenario in PROCESS takes a few minutes on a modern computer. The total calculation time of a 2D-scan as presented in the following is therefore dependent on the chosen resolution. For the design window analysis a 16 x 16 resolution was chosen which corresponds to ~1 day of calculation time per figure [25].

1)   *Case (A)*

The results of case (A) are shown in Fig. 1 where isocountours of the volume-averaged plasma beta and the averaged neutron wall load are used as limitations to the design window.
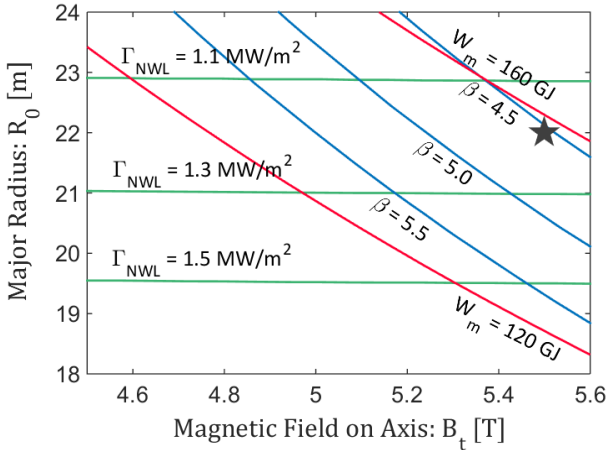
Fig. 1. Case (A): Design window for a HELIAS power plant device with 10% helium ash concentration constrained to achieve $P_{net,el}$ = 1 GW showing isocountours of the volume-averaged thermal plasma β (blue), the average neutron wall-load (green), and the stored magnetic energy (red).

An upper bound on the stored magnetic energy of W_{mag} = 160GJ was selected in accordance with [5] in order to keep the stress to components moderate, i.e. to stay below the typical stress limit for steel of 750MPa [16]. The average neutron wall load in this analysis is not a limiting factor. At a machine size of R = 23m the average neutron wall load is rather moderate with 1.1MW/m^2. A reduction of the machine size from 23m to 21m would increase the average neutron wall load by 20% which is still about a factor two lower than in a tokamak reactor [26]. However, the plasma beta (blue lines) is a limiting

factor in the design window analysis. A conservative beta-limit of 4.5% as predicted by linear stability would lead to a narrow accessible reactor design range. But stellarator experiments have demonstrated the capability to operate above this limit [27, 28, 29, 30] such that beta may be ultimately limited by stochastisation of the plasma edge and corresponding destruction of flux surfaces resulting in a shrinking of the plasma volume. Such a beta-limit has been predicted to be in the range of 5 - 6% [29]. As shown in the figure an increase of beta from 4.5 to 5.5% would expand the available design window. A broader design window allows more freedom to choose a robust design point and further optimize the device with respect to costs, e.g. going to smaller field or machine size for cost reduction.

As already stated, the confinement enhancement factor has been iterated to be in line with [7]. For clarity, the associated isocontours of f_{ren} are illustrated separately in Fig. 2. In addition, the radiation fraction, f_{rad}*, which is needed to achieve a peak heat load limit of 5MW/m^2 on the divertor plates, is given in percent of the power crossing the separatrix.
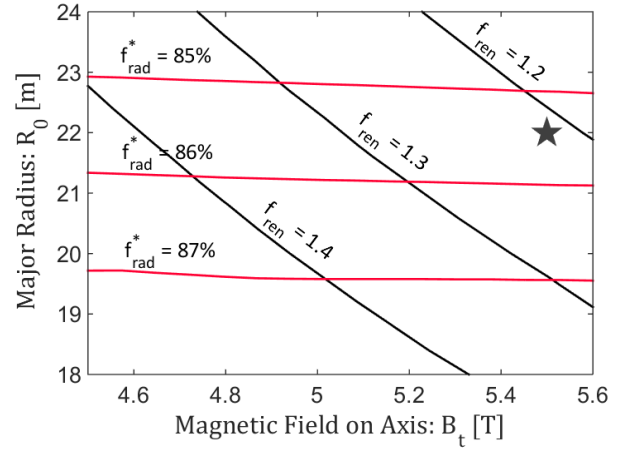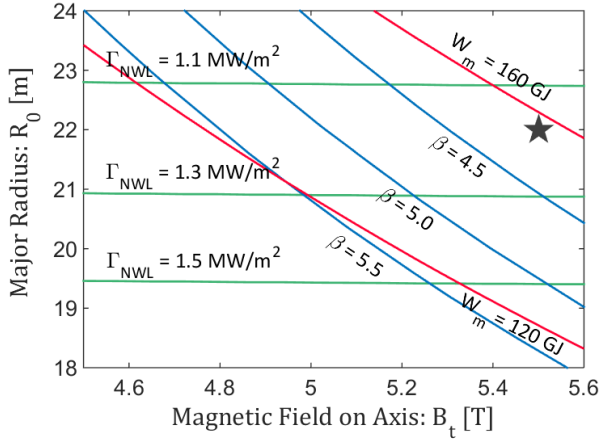

Fig. 2. Case (A): Complement to the design window for a HELIAS power plant device with 10% helium ash concentration constrained to achieve $P_{net,el}$ = 1 GW showing isocontours of the confinement enhancement factor f_{ren} (black) and the radiation fraction of the power crossing the separatrix to keep the peak heat load on the divertor plates at 5 MW/m^2 (red).

As can be seen in the complementary Fig. 2 the confinement enhancement factor is conservatively chosen for large machine sizes on the order of $f_{ren} \sim 1.2$ and increasing for smaller device sizes up to 1.4. The required radiation fraction varies only slightly between 85% - 87%. This is clear as in this design window the net electric power was fixed and thus the alpha heating power and consequently the power crossing the separatrix is nearly constant. Moreover the effective wetted area scales linearly with the major radius and thus changes only from A_{eff} = 12m^2 for the smallest device up to 15m^2 for the maximum size. It should be noted that a change of the radiation fraction of 1% is in this case equivalent to an additional power of 5MW going directly to the divertor.

2)   Case (B)

The design window analysis for Case (B) is shown in Fig. 3. The contours of the neutron average wall load do not change in comparison to case (A) as the same fusion power is required to achieve 1GW net electric power and consequently, the neutron production stays the same. The β-contours on the other hand shift by about 1m to smaller device sizes and show the impact of the helium ash dilution on the plasma performance. A higher helium concentration in the plasma 'costs' beta and electron density without increasing the performance of the device.

A complementary figure with contours of the required radiation fraction and the confinement enhancement factor for case (B) is not shown as these parameters are similar to the results presented for case (A), Fig. 2.

Fig. 3. Case (B): Design window for a HELIAS power plant device with 5% helium ash concentration constrained to achieve $P_{net,el}$ = 1 GW showing isocontours of the volume-averaged thermal plasma β (blue), the average neutron wall-load (green), and the stored magnetic energy (red).

If an operation scenario can be found which effectively flushs out the helium ash while keeping the confinement for the background plasma high, the size of the machine could be reduced to achieve the same power output or the power output can be increased for the same device size. E.g. if the density profile could be sufficiently controlled one could create a centrally hollow density profile. As the core transport in a stellarator is assumed to be dominated by neoclassical transport, the ambipolarity constraint would give rise to a positive electric field in the plasma centre [32] potentially increasing helium and impurity transport. The development and test of advanced scenarios is an ongoing research topic.

Another option are advanced quasi-isodynamic configurations with poloidally closed contours of B which are stable up to β = 7 – 8%. However, the design of a suitable coil set for such configurations remains a challenge.

C. Plasma Operation Contour Analysis

In the previous section a design window analysis of the HELIAS was carried out in which every point corresponded to a full reactor concept. Once a suitable design point is found through such a study, it is of interest to further investigate its properties and performance. This can be done by applying the methodology of Plasma Operation Contour Analysis [33] where density and temperature are varied and the external heating power is iterated to reach power balance.

As an example, such a study is presented in the following for the design point with R = 22m, B_t = 5.5T, and a confinement enhancement factor of f_{ren} = 1.2 lying well within the conservative accessible design window outlined by Fig. 1. The volume averaged temperature $<T>_V$ and density $<n>_V$ has been varied between 3 - 10keV and 0.3 - $3 \cdot 10^{20}$m^{-3}, respectively. The associated core radiation is assumed to be mainly bremsstrahlung and synchrotron radiation. Only for the tungsten case in section II.D is additional charge-state-averaged line radiation included. The results are illustrated in Fig. 4 where isocontours of the external heating power are shown. The heating power is required to balance the power loss through transport and radiation.
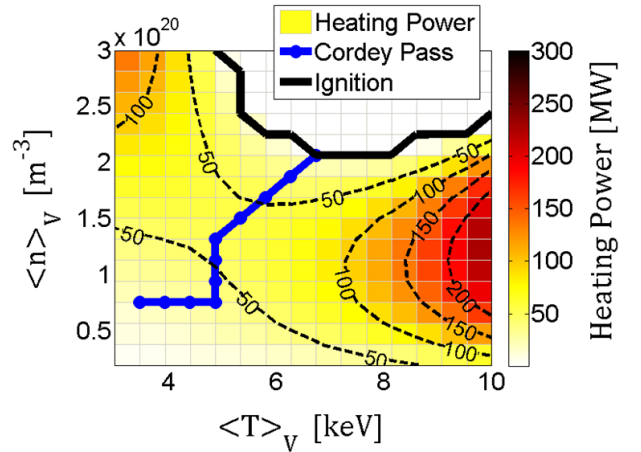

Fig. 4. Plasma Operation Contour Analysis (POPCON) for a HELIAS power plant design point with R = 22 m, BT = 5.5 T, 10% helium ash concentration, and f_{ren} = 1.2. Shown in colour-code and isocontours are the external heating power and in blue the Cordey-Pass to the ignition regime (white area).

As is well known and can be seen in Fig. 4, a 'valley' of minimum external heating power exists. This valley represents the optimum start-up path considering the minimisation for external heating power reserves. This optimum path is illustrated by a blue line and commonly referred to as the 'Cordey-Pass'. This path ends when the ignition region is reached where the plasma is self-sustained by the alpha heating power, shown as the white region with the black line serving as boundary.

A closer look at this Cordey-Pass can be taken by projection of the associated powers along the steps of this path, illustrated in Fig. 5. Shown are the increasing alpha heating and the increasing radiation while going in the

direction of start-up as well as the required external heating power which in this case has a maximum at 55MW. That means, that the minimum required heating power (MRHP) of 55MW must be available to achieve plasma start-up.
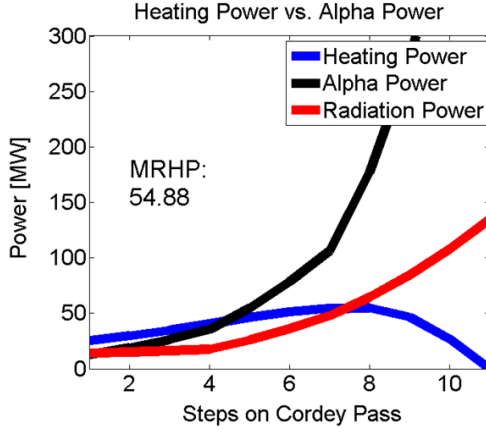

Fig. 5. Projection of the Cordey-Pass from Fig. 4 along its 'steps'. Shown are the external heating power (blue), alpha heating power (black), and the radiation loss power (red) along this path to ignition with a maximum required heating power of about 55 MW.

POPCON plots give insight into the performance of a single design point and the projection of the associated Cordey-Pass allows assessment of the required heating power for start-up. Even for the conservative HELIAS design point investigated here a self-sustained ignition window emerges which can be reached by applying 55MW external heating power during start-up.

D. Plasma Operation Sensitivity

Beyond the standard approach to POPCON plots, this methodology can be used for sensitivity studies of a design point against variations in different physics parameters. In the following the influence of two parameters on the plasma performance is studied.

The first parameter is the confinement enhancement factor. An improvement of the confinement leads to a reduction of power loss through transport if the plasma energy is to be kept constant. Consequently, this leads to a reduction of the required heating power as a smaller power loss must be compensated. Secondly, the impact of tungsten impurities on the plasma performance is investigated. This is important as a divertor must consist of a resilient material to sustain the strong heat loads. Currently, tungsten is discussed as a promising candidate which will be employed in ITER. But the bombardment of a tungsten metal divertor with energetic particles leads to sputtering and thus tungsten could be an intrinsic impurity in a reactor scenario.

The exemplary design point with $R = 22m$ and $B_t = 5.5T$ is considered for two different confinement enhancement factors, namely $f_{ren} = 1.2$ (top row) as well as $f_{ren} = 1.4$ (bottom row) as

illustrated in Fig. 6. Also the tungsten concentration is changed from $c_W = 0$ (left column) to $c_W = 10^{-5}$ (right column).

As can be seen from Fig. 7 a moderate increase of confinement not only reduces the required external heating power to reach ignition but also generally increases the whole ignition parameter regime. A self-sustained ignition state is therefore reached at lower temperatures and densities. For the left side without tungsten impurities the required external heating power is reduced from 55MW to 20MW for an increase of the confinement enhancement from 1.2 to 1.4.

If now a moderate tungsten contamination is considered, the required external heating power strongly increases compared with the case without tungsten such that in the low-confinement scenario the ignition regime nearly vanishes in the considered parameter region. In this case the required heating power rises to a value of 120MW while in the high-confinement case the increase to 50MW is more tolerable. A closer comparison of the case with and without tungsten impurities also reveals that the impact of the tungsten contamination is greatest in the low temperature regime while the high temperature regime is nearly unchanged. This becomes clear when the radiative loss function of tungsten is examined which has a strong maximum at 2keV, see Fig. 6.
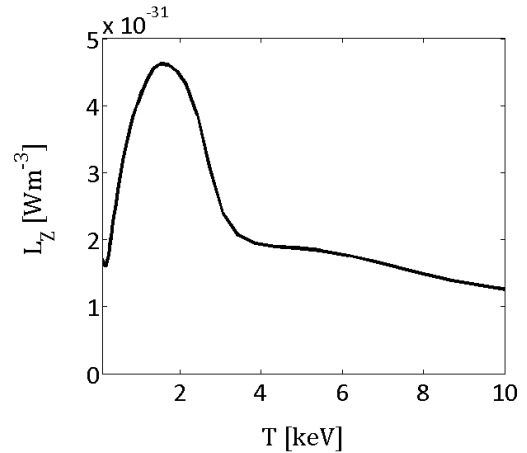

Fig. 6. Charge state averaged radiative loss function of tungsten in the relevant core-plasma temperature range.

From these results it can be concluded that the plasma must be kept free of highly radiating impurities during start-up in order to minimise the required external heating power. In the ignition phase, in contrast, a moderate concentration of impurities such as tungsten is tolerable or even favorable. As long as the confinement is not degraded, an increase of the core radiation through impurities reduces the power flow to the SOL. Thus, less radiation is required in the SOL easing the exhaust scenario.
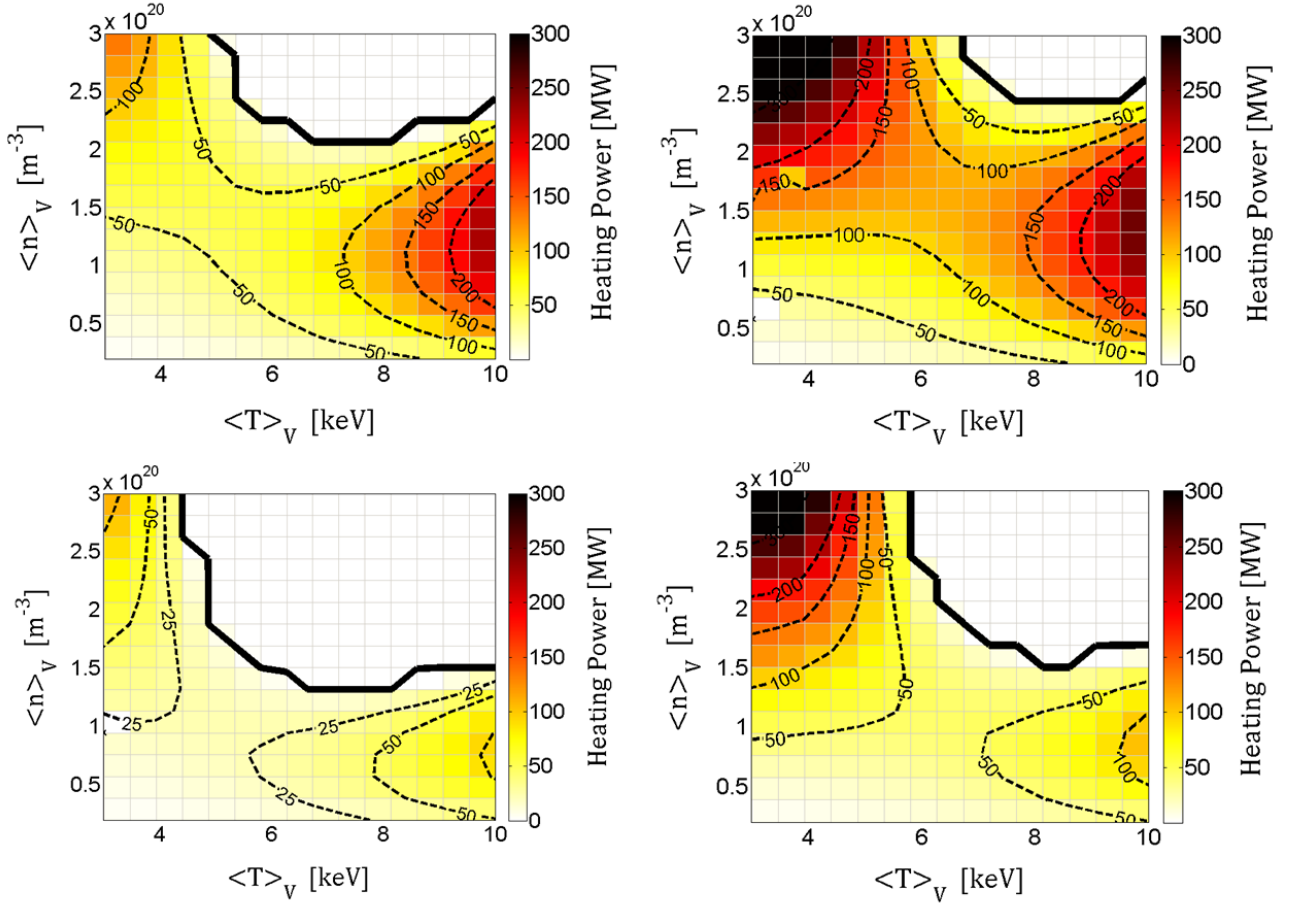
Fig. 7. Plasma operation contour plots are shown with isocontours for external heating power for a HELIAS scenario with R = 22 m, B_T = 5.5 T, 10% helium ash concentration, and a confinement renormalisation factor of 1.2 (top row) as well as 1.4 (bottom row). The left corresponds to cases without tungsten impurities in the plasma and the right to $c_W = 10^{-5}$.

III. COMPARISON TO TOKAMAKS

A. Cost Assessment and Direct Comparison

In order to allow a comparison between tokamak and stellarator the same design goals and constraints, as outlined in section II.A, are applied to both concepts in the systems studies. In particular, the same blanket thickness has been taken for the tokamak case. Further, the tokamak H-factor has been used as iteration variable for the confinement enhancement similar to the renormalization factor used in stellarators. Current drive is employed to achieve steady-state operation of the tokamak in order to be comparable to the stellarator. The exhaust scenario, however, cannot be compared in this study as PROCESS currently does not feature a universally accepted tokamak divertor model.

Since every design point in the design window analysis represents a whole reactor design with hundreds of parameters, each point can be associated with corresponding construction costs. In a design point of PROCESS the size of each component is calculated. Each component is associated with a material or even a fractional composition of several materials. Based on the size of the components and the material densities the total weight for each material can be estimated. With a unit cost-per-weight the costs of each component are calculated. These are the direct costs of the device that are complemented by indirect costs which are in the current model simply a flat rate of the direct costs. The PROCESS cost model has been benchmarked with the dedicated cost analysis code FRESCO which showed a reasonable agreement for the total construction costs with deviations on the order of 20% [34].

In the following, exemplary design points are selected for both concepts and compared in a cost-breakdown. For the stellarator, the design point from section II.C is used with R = 22m, and B_t = 5.5T. For the tokamak a design point has been chosen which is similar to the 'Model B' of the European PPCS study [26]. This point lies in the middle of the PPCS parameter range and is therefore neither a too optimistic nor a too pessimistic design point with R = 8.5m, and B_t = 6T. The total construction cost of both these design points have been broken down to their major contributions, which are the magnets, the blanket, the buildings, the equipment and indirect costs, compared in Fig. 8.

A major contribution of the magnet costs is due to the coil conductors which are dominated by the high material costs for the superconductors (Nb_3Sn). A further cost driver of the magnets is the cost for assembly of such large coils. In total, the magnets contribute significantly to the total costs of a fusion power plant. It should be noted, that the 3D complexity of the stellarator will most likely increase the magnet costs, but this has not been taken into account here. However, while the modular coils of the HELIAS have about the size of the ITER TF-coils [5], the poloidal and toroidal field coils of the tokamak case are much larger. That means, while the HELIAS coils can still be produced by industry and shipped to the construction site, the tokamak coils must be built on-site. This requires a dedicated facility increasing the magnet costs for the tokamak, but which so far is also not taken into account. Thus arguments for cost increases can be found for both concepts and should be considered in future studies.

The blanket costs in this model are governed by the material costs for the breeder components. In addition, the large amount of steel required for the structural support and shield is a major contribution. The building costs reflect the high costs for both the reactor and turbine building. Additional building costs sum up all the smaller buildings which are required for the equipment, maintenance, etc. In this analysis the equipment costs themselves are also a major part of the total construction costs. This is clear as the equipment costs comprise several important reactor systems. Major contributions of the equipment costs come from the heating and fueling systems as well as from the cooling, cryogenic, and pumping systems and, last but not least, from the maintenance equipment and instrumentation and control. The last part in the construction costs are the so-called indirect costs. These are all costs which are not directly associated with a specific cost account, e.g. administration, safety, etc. These are assumed here to be a flat percentage of the direct costs.
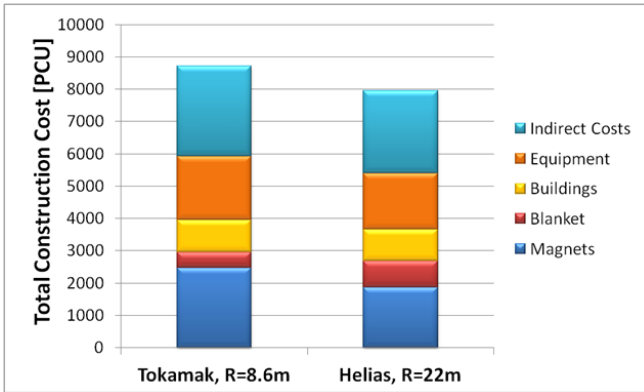

Fig. 8. Cost breakdown of total construction costs to major costing accounts for the selected tokamak and stellarator design point.

As can be seen from Fig. 8 and Tab. II the total magnet costs are higher for the tokamak than for the HELIAS as the massive PF coils and transformer add considerable mass of superconducting material (Nb_3Sn) and additional costs for assembly. The blanket costs on the other hand are higher for the HELIAS as the total surface area covered by the blanket is

higher due to the higher aspect ratio. This in turn means also that the average neutron wall load is lower in the stellarator ensuring longer lifetime of the exposed inner components. The costs for the buildings are comparable in both the tokamak and stellarator case. The reactor building for the HELIAS must be broader but the tokamak reactor building on the other hand higher while the requirement for other buildings are similar. The equipment costs, in contrast, are higher for the tokamak as consequence of the requirement for external current drive.

TABLE II. COMPARISON OF RELEVANT PARAMETERS IN THE COST ASSESSMENT BETWEEN THE SELECTED TOKAMAK CASE AND THE HELIAS 5-B DESIGN POINT.

	Tokamak, R=8.6m	Helias 5-B
Fusion Power [GW]	3300	3000
Stored Magn. Energy [GJ]	170 (TF) + 20 (PF)	160
Vol. Averaged Plasma Beta [%]	4.3	4.4
Magnetic Field on Axis [T]	6.0	5.5
Av. Neutron Wall Load [MW/m²]	1.7	1.1
Cold Mass [kt]	43	40
Superconductor Mass (Nb_3Sn) [kt]	1.3	1.3

B. Cost Sensitivity of Helias Reactor

In order to further elucidate the construction costs of stellarator reactors, their sensitivity with respect to major engineering parameters shall be investigated in the following. Again, the design window analysis serves as basis for this study since each reactor design point can be associated with a detailed cost assessment. For this purpose, a range of isocontours for the total construction costs are illustrated in Fig. 9.
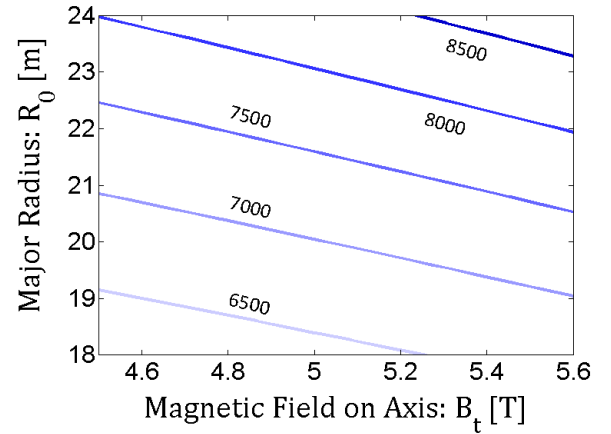

Fig. 9. Different isocontours of the total construction costs for the 5 field-period HELIAS design window analysis for a constant net electricity production of $P_{net,el} = 1$ GW at constant aspect ratio, A = 12.2.

As can be derived from Fig. 9, the isocontours of the total construction costs are rather flat with respect to the investigated range of the magnetic field strength. Indeed, a reduction of the field from 5.5 to 4.5T on axis would reduce the total construction costs only by about 6-7% (for the same

superconductor material and for constant major radius and aspect ratio). The reduction of the field has mainly impact on the coil cross-section and thus on the total required superconductor mass and with the reduced field also on the required mass of support structure. While the magnet system becomes cheaper the costs for the blanket, buildings, and equipment remain the same, and consequently the reduction of the total construction costs is moderate. Decreasing the magnetic field seems therefore problematic as the reduction of the field would lead to a higher plasma beta if the fusion power is to be kept constant. This is in contradiction to the beta-limit discussed in Sec. II.B. On the other hand, a minimum plasma beta is required as the diamagnetic effect contributes to the confinement of the fast particles. Thus, operation at high beta is desirable from a physics point of view and economically meaningful. The confinement of the plasma is decreased, however, if the magnetic field strength is reduced. This means a higher confinement improvement of the configuration with respect to the ISS04 reference scaling is required in order to achieve the same power output.

Considering the major radius as an engineering parameter, the same cost saving of 6-7% can be achieved by reducing the major radius by about 1.5m (for constant magnetic field strength and aspect ratio). Therefore, reduction of the major radius provides more opportunity for cost savings. This is clear as the major radius has impact on all major components. The coils become smaller saving superconductor material. Further, the required support structure is reduced. In addition the surface area is reduced and with this the blanket and the associated breeder materials and steel. This in turn saves costs for cryogenic and pumping systems. Only the building costs remain constant as the reactor building is only slightly affected while the turbine building remains the same. The monetary gain by reduction of the major radius comes at the price of a higher neutron wall load and the requirement to go to a higher plasma beta (at constant fusion power). Thus, one may reverse the argument. Instead of focusing on cost reduction one can argue that by increasing the major radius by about 2m from 22 to 24m it is possible to strongly increase the fusion power output due to the increasing plasma volume while only moderately increasing the total construction costs by about 8-9%. As will be discussed below, an assessment of the cost-of-electricity is beyond the scope of this work, but the results presented in Fig. 9 suggest that a HELIAS reactor becomes more cost efficient at larger device sizes, which is also true for other toroidal reactor concepts.

Summarizing, the costs for a tokamak and a HELIAS reactor are comparable for the same set of goals in the common PROCESS framework with a simple cost model. Depending on which exact design points are compared construction costs can differ in the range of 10 – 20% for 'equivalent' assumptions. The cost-of-electricity (COE) is not investigated in this work. It was already shown in [33] that a variation and statistical sensitivity analysis of different cost factors leads to a non-uniform probability distribution of the COE where the COE with the maximum probability can significantly deviate from the reference value with fixed cost parameters. This is especially important as ambiguities regarding availability and maintenance time and costs exist which have a high impact on the COE. A detailed COE analysis is left for future studies once a better understanding of maintenance schemes is acquired.

IV. CONCLUSIONS

For the first time, a systems code approach has been applied to the helical-axis advanced stellarator line with the aim of defining the accessible design window for a power plant-sized-device. For this purpose, the major radius and the magnetic field on axis were varied over a wide range with the set goal to achieve 1GW net electric power. The results from the design window analysis have shown that the accessible design window depends strongly on the envisaged beta-limit. As the beta-limit for HELIAS devices has not yet been experimentally investigated one must await results from W7-X. The average neutron wall load on the other hand does not limit the design of a HELIAS as it does not exceed $1.5MW/m^2$ even at smaller machine sizes due to the larger aspect ratio and surface area than typical for tokamak designs. The required confinement enhancement factor with respect to the ISS04 scaling lies between 1.2 - 1.3 for machines of every size at high field which is in line with results from detailed 1D transport simulations. In order to control the power exhaust of such a HELIAS device 85 - 87% of the total power must be radiated to ensure a peak heat load limit on the divertor targets of $5MW/m^2$. In the plasma core, so far only bremsstrahlung and synchrotron radiation were considered, but additional power could potentially be radiated from the core if impurities were to be injected. Even under the most conservative assumptions with $\beta = 4.5\%$ and 10% helium concentration a feasible design window emerges around R = 22m, B_t = 5.5T. But if a scenario with effective helium ash exhaust can be found and/or the beta-limit can be verified to be higher, the design window notably increases opening many more options for potential devices and robust design points.

Beyond the design-window analysis, single design points were studied in more detail using plasma operation contour analysis. The start-up path to ignition was illustrated and it was shown that for a standard scenario about 55MW of external heating power are required. Furthermore, sensitivity studies were carried out varying the confinement enhancement and the tungsten impurity concentration. It became clear that a higher confinement strongly reduces the required external heating power while increasing the available ignition window. In contrast, an intrinsic impurity concentration of tungsten would make the start-up very difficult as tungsten has a strong radiation maximum at around 2keV while plasma operation at higher temperatures is not nearly so strongly affected.

Finally, the stellarator has been compared to the tokamak concept within the common PROCESS framework. A tokamak design point was studied for the same set of constraints and assumptions and the total construction costs compared. It is an important finding that the costs for a stellarator are on the same level as the costs for an equivalent tokamak. Although the stellarator is a larger machine in terms of its dimensions, the masses for the different components are comparable to those of a tokamak leading in this analysis to similar costs. A detailed cost break-down and comparison of a tokamak and stellarator

design point have shown that the costs of the tokamak magnet system are higher due to the high costs for the large PF and TF coils as well as the transformer. Also the equipment costs are higher in the tokamak case since the tokamak requires current drive to operate in steady-state which is more cost intensive and also decreases the net efficiency of the concept.

For the next steps, a detailed 3D neutronic analysis of the HELIAS concept has been started with the aim of defining and optimising a stellarator-specific breeder blanket. Moreover, systems and transport studies are being continued, which include in particular the concept development for a HELIAS burning plasma experiment.

REFERENCES

[1] D. Maisonnier, D. Campbell, I. Cook et al. "Power plant conceptual studies in Europe" Nuclear Fusion, vol. 47, p. 1524 (2007).

[2] T. Goto, J. Miyazawa, H. Tamura et al. "Design Window Analysis for the Helical DEMO Reactor FFHR-d1" Plasma and Fusion Research: Regular Articles, vol. 7, p. 2405084 (2012).

[3] F. Najmabadi, A. R. Raffray, ARIES-CS Team "The ARIES-CS Compact Stellarator Fusion Power Plant" Fusion Science and Technology, vol. 54, p. 655 (2008).

[4] F. Warmer, C. D. Beidler, A. Dinklage et al. "HELIAS Module Development for Systems Codes." Fusion Engineering and Design, vol. 91, p. 60 (2014).

[5] F. Schauer, K. Egorov and V. Bykov. "HELIAS 5-B magnet system structure and maintenance concept." Fusion Engineering and Design, vol. 88, p. 1619 (2013).

[6] H. Yamada, J. H. Harris, A. Dinklage et al. "Characterization of energy confinement in net-current free plasmas using the extended International Stellarator Database." Nuclear Fusion, vol. 45, p. 1684 (2005).

[7] F. Warmer, C. D. Beidler, A. Dinklage et al. "Limits of Confinement Enhancement in Stellarators." Fusion Science and Technology, vol. 68, p. 727 (2015).

[8] M. Kovari, R. Kemp, H. Lux et al. "PROCESS: A systems code for fusion power plants - Part 1: Physics." Fusion Engineering and Design, vol. 89, p. 3054 (2014).

[9] F. Warmer, C. D. Beidler, A. Dinklage et al. "Implementation and Verification of a HELIAS module for the Systems Code PROCESS." Fusion Engineering and Design, vol. 98-99, p.2227 (2015).

[10] M. Tillack, P. Humrickhouse, S. Malang et al. "The use of water in a fusion power core." Fusion Engineering and Design, vol. 91, p. 52 (2015).

[11] A. R. Raffray, L. El-Guebaly, S. Malang et al. "Engineering Design and Analysis of the ARIES-CS Power Plant." Fusion Science and Technology, vol. 54, p. 725 (2008).

[12] U. Fischer, P. Pereslavtsev and S. Hermsmeyer. "Neutronic design optimisation of modular HCPB blankets for fusion power reactors" Fusion Engineering and Design, vol. 75-79, p. 751 (2005).

[13] A. Häussler, U. Fischer, F. Warmer. "Neutronics source modeling for stellarator power reactors of the HELIAS-type" submitted to the Proceedings of the Annual Meeting on Nuclear Technology (2016)

[14] H. Zohm. "On the minimum size of DEMO." Fusion Science and Technology, vol. 58, p. 613 (2010).

[15] G. Grieger and I. Milch. "Das Fusionsexperiment WENDELSTEIN 7-X." Physikalische Blätter, vol. 49, p. 1001 (1993).

[16] F. Schauer. "Coil winding pack FE-analysis for a HELIAS reactor." Fusion Engineering and Design, vol. 86, p. 636 (2011).

[17] Y. Turkin, C.D. Beidler, H. Maaßberg, et al. „Neoclassical transport simulations for stellarators" Physics of Plasmas, vol. 18, p. 022505 (2011).

[18] M. Greenwald, "Density limits in toroidal plasmas" Plasma Physics and Controlled Fusion, vol. 44 (2002)

[19] S. Sudo, Y. Takeiri, H. Zushi et al. "Scalings of energy confinement and density limit in stellarator/heliotron devices." Nuclear Fusion, vol. 30, p. 11 (1990).

[20] J. Miyazawa, R. Sakamoto, S. Masuzaki et al. "Density limit study focusing on the edge plasma parameters in LHD." Nuclear Fusion, vol. 48, p. 015003 (2008).

[21] L. Giannone, R. Burhenn, K. McCormick et al. "Radiation power profiles and density limit with a divertor in the W7-AS stellarator." Plasma Physics and Controlled Fusion, vol. 44, no. 10, p. 2149 (2002).

[22] Y. Feng. "Up-scaling the island divertor along the W7-stellarator line." Journal of Nuclear Materials, vol. 438, p. S497 (2013).

[23] H. Zohm, C. Angioni, E. Fable, et al. "On the physics guidelines for a tokamak DEMO" Nuclear Fusion, vol. 53, p. 073019 (3013).

[24] T. Goto, J. Miyazawa, H. Tamura et al. "Design Window Analysis for the Helical DEMO Reactor FFHR-d1." Plasma and Fusion Research: Regular Articles, vol. 7, p. 2405084 (2012).

[25] S. Torrisi and F. Warmer. "Design of an N-Dimensional Parameter Scanner for the Systems Code PROCESS." Report No. 13/23, Max-Planck-Institute for Plasma Physics (2014).

[26] D. Maisonnier, D. Campbell, I. Cook et al. "Power plant conceptual studies in Europe." Nuclear Fusion, vol. 47, p. 1524 (2007).

[27] H. Yamada, A. Komori, N. Ohyabu et al. "Configuration flexibility and extended regimes in Large Helical Device." Plasma Physics and Controlled Fusion, vol. 43, no. 12A, p. A55 (2001).

[28] A. Weller, J. Geiger, A. Werner et al. "Experiments close to the beta-limit in W7-AS." Plasma Physics and Controlled Fusion, vol. 45, no. 12A, p. A285 (2003).

[29] W. A. Cooper, L. Brocher, J. P. Graves et al. "Drift Stabilisation of Ballooning Modes in an Inward-Shifted LHD Configuration." Contributions to Plasma Physics, vol. 50, p. 713 (2010).

[30] K. Ichiguchi and B. A. Carreras. "Multi-scale MHD analysis incorporating pressure transport equation for beta-increasing LHD plasma." Nuclear Fusion, vol. 51, no. 5, p. 053021 (2011).

[31] M. Drevlak, D. Monticello and A. Reiman. "PIES free boundary stellarator equilibria with improved initial conditions." Nuclear Fusion, vol. 45, p. 731 (2005).

[32] F. Warmer. "Reactor Extrapolation of Wendelstein 7-X." Report No. 13/21, Max-Planck-Institute for Plasma Physics (2013).

[33] W. Houlberg, S. Attenberger and L. Hively. "Contour analysis of fusion reactor plasma performance." Nuclear Fusion, vol. 22, no. 7, p. 935 (1982).

[34] C. Bustreo, G. Casini, G. Zollino et al. "FRESCO, a simplified code for cost analysis of fusion power plants." Fusion Engineering and Design, vol. 88, no. 12, pp. 3141 (2013).

[35] C. Bustreo, T. Bolzonella and G. Zollino. "The Monte Carlo approach to the economics of a DEMO-like power plant." Fusion Engineering and Design, [in press], (2015).

From W7-X to a HELIAS Fusion Power Plant:
Motivation and Options for an Intermediate-Step Burning-Plasma Stellarator

F. Warmer*, C.D. Beidler, A. Dinklage, R. Wolf, and the W7-X Team[1]

Max Planck Institute for Plasma Physics, D-17491, Greifswald, Germany

Abstract

As a starting point for a more in-depth discussion of a research strategy leading from Wendelstein 7-X to a HELIAS power plant, the respective steps in physics and engineering are considered from different vantage points. The first approach discusses the direct extrapolation of selected physics and engineering parameters. This is followed by an examination of advancing the understanding of stellarator optimisation. Finally, combining a dimensionless parameter approach with an empirical energy confinement time scaling, the necessary development steps are highlighted. From this analysis it is concluded that an intermediate-step burning-plasma stellarator is the most prudent approach to bridge the gap between W7-X and a HELIAS power plant. Using a systems code approach in combination with transport simulations, a range of possible conceptual designs is analysed. This range is exemplified by two bounding cases, a fast-track, cost-efficient device with low magnetic field and without a blanket and a device similar to a demonstration power plant with blanket and net electricity power production.

Keywords: HELIAS, research strategy, intermediate-step burning-plasma stellarator, systems studies

1. Introduction

One of the high-level missions of the European Roadmap [2] to the realisation of fusion energy is to bring the HELIAS stellarator line to maturity. The near-term focus is the scientific exploitation of the Wendelstein 7-X experiment in order to assess stellarator optimisation in view of economic operation of a stellarator fusion power plant [3]. The high-level scientific goals of W7-X are consequently the demonstration of improved neoclassical confinement as well as improved confinement of fast ions, further, plasma stability up to a volume-averaged β of 5%, and a stiff magnetic equilibrium to facilitate the island divertor concept while achieving steady-state operation. W7-X will play a decisive role for these studies but will be too small to investigate stellarator burning-plasma issues. Therefore, an intermediate burning plasma stellarator appears prudent to mitigate the risks which would otherwise arise from the incomplete physics basis [4]. The focus of such an intermediate device would be the investigation of effects associated with a 3D burning plasma and the corresponding confinement and control of fast alpha particles. A decision on the necessity of a burning plasma experiment, however, should wait for the results of the high-performance steady-state operation of W7-X and the burning plasma phase of ITER.

To be more specific, the optimisation of fast-particle confinement needs to be proven, especially involving collective effects in burning plasmas within a sufficiently large plasma volume [5]. 3D-specific, Alfvénic instabilities may give rise to physics which cannot be explored in tokamaks (like ITER) [6]. In particular, Alfvénic instabilities driven by fast alpha particles may result in increased losses of the latter. The threshold in terms of the fast alpha particle pressure, above which such effects occur, cannot yet be precisely predicted, but is likely above what

can be achieved in W7-X. In addition, looking at the extrapolation of relevant physics and engineering parameters, the step from W7-X directly to a power plant is significant for some of the relevant quantities (e.g. energy of the magnet system, stored energy in the plasma, heating power, ratio of heating power to major radius P/R, fusion power gain, triple product, normalised gyroradius).

These arguments lead to the concern that a direct step from W7-X to a HELIAS reactor bears large scientific and technological risks. Plasma conditions anticipated in a burning plasma experiment of smaller size than a reactor are therefore investigated to assess the potential for risk mitigation with an intermediate-step, burning-plasma HELIAS device. Such a device will require far fewer resources than a reactor due to its smaller size, much relaxed requirements for structure materials (dpa limits) and space. At the same time, this intermediate-step device offers accessibility for scientific exploration and could also serve as a facility for fusion engineering tests. Such an approach would offer synergy effects in line with the parallel development of technology for tokamaks.

This work discusses the latest developments towards a stellarator power plant using three methods: the extrapolation of selected physics and engineering parameters, the consideration of progress in stellarator optimisation, and the application of dimensional analysis techniques. The gaps revealed in physics and engineering understanding are presented in section 2 from today's point of view. A risk-reducing strategy foresees an intermediate-step stellarator to bridge those gaps and the resulting high-level requirements for such a device are outlined in section 3. On this basis, systems studies have been carried out for two possible devices with different technological sophistication and the results are presented in section 4. The economic aspects of these different concepts are compared in section 5 and the implications and conclusions of this work are summarised in section 6.

---

*Corresponding author, Tel.: +49 (0)3834 88-2583
Email address: Felix.Warmer@ipp.mpg.de (F. Warmer)
[1]See author-list in [1].

2. Development steps towards a stellarator power plant

The understanding of the physics and technology of stellarators has made significant progress in recent years. Essential contributions came from the design process of W7-X (stellarator optimisation [7]), from the construction experience itself [8], and from the ongoing theoretical work during the construction phase [9, 10]. Nevertheless, stellarators are still less mature than tokamaks. The underlying reason is the three-dimensionality of the magnetic configuration which produces a rotational transform by magnetic field coils without needing a toroidal plasma current, but also introduces an additional level of complexity. As a consequence, stellarators need an elaborate optimisation procedure [11] to fulfil basic confinement properties. Before the advent of high-performance computers, this problem could not be solved. In addition, the 3-dimensional configuration offers more degrees of freedom to find the optimum magnetic field configuration. This, however, also means that finding and empirically testing the optimum configuration can be a very costly procedure. The optimisation, which forms the basis of the W7-X design, already includes an extensive set of criteria. However, it is not immediately obvious how to extrapolate to a HELIAS power plant, even assuming that the optimisation can be verified in the coming years of W7-X operation.

2.1 Extrapolation of Physics and Engineering Parameters

To improve the understanding of the necessary steps between W7-X and a power plant one can look at several aspects. First, one can compare important physics and engineering parameters. An overview, comparing such parameters for W7-X, ITER and a HELIAS power plant, is given in Table 1. The ITER values are taken from [14]. ITER is included in this discussion because it represents a confinement experiment aiming at a burning fusion plasma which can be characterised by an alpha-power exceeding the auxiliary heating power, i.e. $P_\alpha > P_{\mathrm{aux}}$ or $Q > 5$. Extrapolating from the W7-X design, the HELIAS 5-B has the typical parameters of a stellarator fusion power plant [13]. The increase of the size of the devices, e.g. reflected by the plasma volume, and the increase of the magnetic field strength is required to achieve the necessary energy confinement times which for a burning fusion plasma or even an ignited plasma have to be in the range of a few seconds. The magnetic field strength, however, is limited by the mechanical forces, which have to be accommodated by the support structure, and by the available superconductor technology. Interestingly, the magnetic field strength of ITER is similar to the HELIAS 5-B values. In fact, the case has been made that a HELIAS 5-B could use the ITER toroidal magnetic field technology [15].

As a consequence, the triple product rises by about two orders of magnitude in the step from W7-X to HELIAS 5-B. While also plasma densities and temperatures increase, the dominating part of the increase of $nT\tau$, when going from W7-X to ITER or a HELIAS reactor, is the increase of the energy confinement time by about a factor of ten. In contrast, the expected MHD stability limit for W7-X already has the value of a power plant. This is in contrast to tokamaks which require a further increase to achieve the desired pulse lengths when extrapolating from ITER to a demonstration power plant [16]. The steady-state heating power of W7-X, given in the table is the initial value (the numbers in paranthesis represent a possible power upgrade).

W7-X will not be operated with tritium. Therefore, the heating power comes entirely from external sources. Nevertheless, the heating technology using electron-cyclotron resonance heating (ECRH) is, at least for a stellarator power plant, a promising candidate [17] as stellarators do not need any significant amount of current drive. In ITER the heating power is composed of alpha-heating and auxiliary heating. The HELIAS 5-B is assumed to operate ignited. Thus, the auxiliary heating during steady-state operation is zero. This does not mean that auxiliary heating systems are not required. Depending on the actual confinement time and impurity content during plasma build-up heating power on the order of 100 MW may become necessary [18]. The heating power divided by the plasma surface area gives an approximate value for the average heat flux reaching the in-vessel components assuming a completely homogenous heat deposition. Plasma radiation supports such a homogenous distribution, but full homogeneity will never be achieved.

With respect to these values the different devices do not lie so far apart. In contrast, the P/R-scaling considers the heat-flux arriving in the divertor assuming that the power decay length does not change with size [19]. This means, the wetted area on the divertor scales only with R, but as the power must be exhausted by the divertor, a consequent figure-of-merit for the power exhaust results in P/R [20], which has in particular been used in ASDEX Upgrade to mimic conditions to be expected in ITER and beyond [21].

Here, the step from W7-X to a HELIAS results in a factor for P/R of about ten. ITER lies in-between. The much larger aspect ratio of the stellarator devices leads to generally lower values of P/R which helps to reduce the peak heat-fluxes. However, one should also keep in mind that the magnetic island divertor as tested in W7-AS and realised in W7-X [22] is different in many other aspects to the poloidal divertor used in ITER. The long connection lengths of the open magnetic field lines in the scrape-off layer of an island divertor configuration (about 300 m in W7-X, 110 m in ITER and about 1200 m in a HELIAS [23]) support the broadening of the power deposition zones. On the other hand, while the strike zones are toroidally continuous in a poloidal divertor, they are discontinuous along the helical coordinate of the island divertor leading to a focusing of the power. The peak heat-fluxes which form the basis of the W7-X and ITER divertor designs are the same. The lower value for the HELIAS 5-B takes into account that, in order to achieve a reasonable full power life time in the presence of the neutron fluxes expected in a power plant, the heat flux reaching the divertor has to be reduced [16].

Finally, Tab. 1 also shows the average neutron fluxes expected for the ITER $Q = 10$ operation and for the HELIAS power plant. Although the fusion power is much larger in the HELIAS 5-B device the average neutron flux increases only by a factor of two since its aspect ratio is larger. However, the main difference between ITER and any power-plant-like device are the integrated neutron fluxes which over time determine the life-time of the in-vessel components and the blanket. While ITER is designed for neutron load range corresponding to values below 10 dpa [24], the highly loaded components of a power plant will have to achieve 100 to 150 dpa to accomplish sufficiently long intervals between the replacement of divertor and blanket [25]. Here, the larger aspect ratio of the HELIAS

2

	W7-X	ITER	HELIAS 5-B
Major Radius / (average) minor radius [m]	5.5 / 0.55	6.2 / 1.8	22 / 1.8
Plasma volume [m^2]	30	830	1400
Magnetic field on axis	2.5 T	5.3 T	$5-6$ T
$nT\tau$ [10^{20}m^{-3}keVs]	~ 1	~ 30	~ 50
Volume-averaged thermal β	5%	2.5%	5%
Steady-state heating power [MW]	10 (18)	120	600
Average heat-flux to invessel components [MW/m^2]	0.08 (0.15)	0.2	0.4
P/R [MW/m]	1.8 (3.6)	19.4	27
Divertor heat-flux limit [MW/m^2]	10	10	5
Fusion power [MW]	–	400	3000
Burning-plasma Fusion Gain Q	–	10	∞
Average neutron wall load [MW/m^2]	–	0.5	1.2

Table 1: Selected physics and engineering parameters of W7-X [3], ITER [12] and HELIAS-5B [13].

compared to a tokamak DEMO helps as the neutron fluxes normalised to the fusion power decrease by about a factor of two thereby increasing the lifetime of the exposed components. Comparing the spatial neutron flux distribution in the plasma vessel and normalising the values to the fusion power the values range between 0.32–0.86·10^{-3}m^{-2} for a 1.57 GW tokamak DEMO [26] and 0.07–0.50·10^{-3}m^{-2} for a 3 GW HELIAS [18].

2.2 Advances in Stellarator Optimisation

Another viewpoint concerning how to extrapolate from W7-X to a power plant is obtained by looking at the original physics optimisation of W7-X and comparing it to the scientific progress during the construction period of W7-X. The original optimisation forming the basis of the W7-X design comprised several criteria: Improved neoclassical confinement, a drift optimisation for improved fast ion confinement, plasma stability up to a volume averaged β of 5%, and low Shafranov-shift and low bootstrap currents for a stiff equilibrium facilitating a magnetic island divertor in combination with low magnetic shear and a rotational transform of $\iota = 1$ at the plasma edge [11, 27]. Aspects which have not been part of the optimisation are density and impurity control. To avoid hollow density profiles caused by neoclassically driven thermo-diffusion central particle sources are required [28]. Thus, pellet injection is now a part of the future W7-X programme. Concerning the prevention of impurity accumulation a suitable confinement regime has to be established. A promising candidate is the so-called high-density H-mode found in W7-AS [29], although it is not clear how this regime will extrapolate to W7-X with its lower collisionality.

Concerning the drift-optimisation based on an quasi-isodynamic configuration, it has been realised that the region of improved fast ion confinement is rather narrow making it difficult to verify this effect by neutral beam injection [5]. Studies about the possibility to use ion cyclotron resonance heating for this purpose are ongoing [30, 31]. However, at this stage it already can be said that achieving a large fast ion population will be difficult as the slowing down times at the high plasma densities, at which the improvement of the neoclassical confinement is most effective, are rather short. While minimising the fast ion population is desirable in a burning fusion plasma, the short slowing-down times constrain fast ion studies considerably. As the isodynamic drift-optimisation requires a minimum β (of about 4%) to become effective, reducing the density and at the

same time increasing the temperature might be an option for increasing the fast-particle population in W7-X. However, the strong temperature dependence of the neoclassical heat diffusivity $\left(D_{1/\nu} \sim T^{7/2}\right)$ in combination with the limited heating power restricts this option. All in all, to provide a configuration in which alpha-particle production and the region of improved fast-ion confinement are consistent, further optimisation of the magnetic field configuration is required [32]. Finally, turbulent transport was not considered at all during the W7-X optimisation. It turns out that the magnetic field configuration of W7-X has a profound effect on turbulent modes, e.g. stabilising trapped-electron-modes [33] or leading to poloidal localisation of the ion-temperature-gradient modes [34]. With the growing understanding of the behaviour of turbulence in 3D magnetic field configurations, tailoring of turbulent transport may become a future criterion of stellarator optimisation [35].

2.3 Step-Ladder Approach

Another approach, in order to link the physical behaviour of existing experiments to power plant devices, is to consider dimensionless parameter scaling techniques [36]. For this purpose, dimensional analysis [37] or transformation invariance of basic plasma physics equations [38] can be employed. Following this approach, a set of dimensionless quantities can be obtained where the exponents are restricted in a way that makes the quantities dimensionless. Consequently, any linear combination of the selected set of dimensionless parameters is valid. For the concept of magnetic confinement the three commonly employed dimensionless plasma physics parameters are the normalised plasma pressure β, the normalised gyroradius ρ^* and the collisionality ν^*, defined as:

$$\beta = 2\mu_0 \frac{p}{B_t^2}, \qquad \rho^* = \frac{v_i\, m_i}{e\, B\, a}, \qquad \nu^* = \frac{R\, \nu_{th}}{v_{th}\, \iota}, \qquad (1)$$

where a is the minor radius, R_0 the major radius, p the plasma pressure, v_{th} the thermal velocity, ν_{th} the thermal collision frequency and ι the rotational transform. Despite the great insight which can be obtained from dimensionless scaling techniques, the method has some limitations which should be kept in mind for the following analysis. In particular, the dimensionless quantities give no information about the dependence of phenomena which do not scale according to the dimensionless principle, e.g. atomic physics are not reflected in such an ansatz.
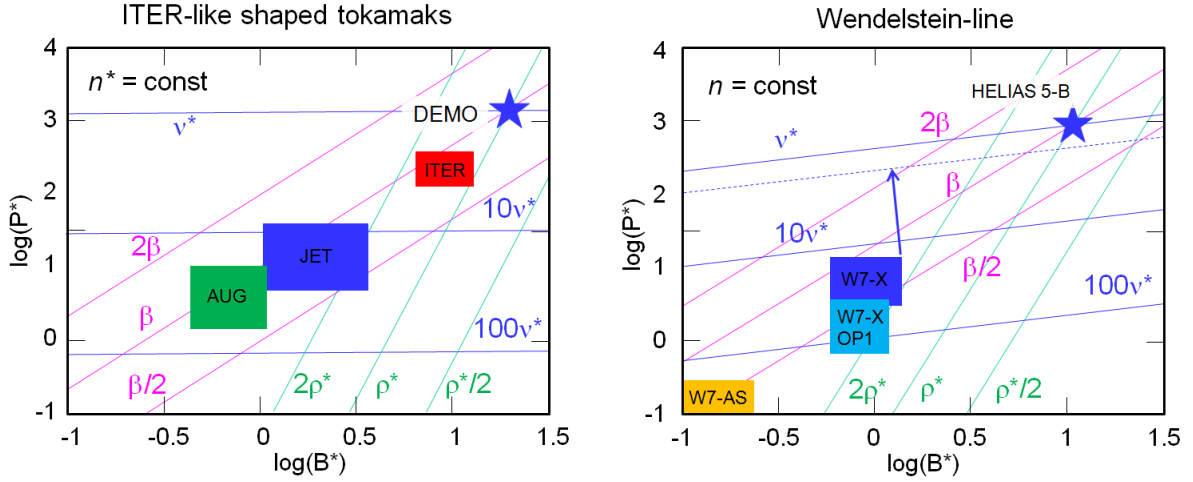
3

Figure 1: Step-ladder plots for ITER-like tokamaks (left) and the HELIAS line (right). The left side shows operation windows of ASDEX Upgrade (AUG), JET and ITER in dimensionless engineering parameters with isocontours of dimensionless physics parameters at constant n^*. The right side shows the same for the HELIAS line. The W7-X operation windows refer to operation phase 1 (OP1) and 2 (OP2) for X2 and O2 heating, respectively, where n^* has been adapted to ECH cut-off densities and 'HELIAS 5-B' is an engineering-based reactor study [13]. The dotted line on the right side is the projection of the collisionallity of W7-X into the plane of HELIAS 5-B.

Although it is possible to simply compare the specific values of the dimensionless parameters between today's experiments and future fusion devices, such an approach is not very conclusive. In order to measure the reactor relevance of existing and planned magnetic confinement devices, it is convenient to additionally rephrase the leading operation parameters of a device in so-called 'dimensionless' engineering parameters $B^* \sim Ba^{5/4}$, $P^* \sim Pa^{3/4}$ and $n^* \sim na^{3/4}/B$ [39]. Considering the Kadomtsev similarity constraints [37], B^*, P^* and n^* must remain constant in differently sized devices, in order to obtain the same dimensionless plasma physics parameters (omitting dimensional constants). In this approach the principle of similarity requires that the magnetic geometry of the compared devices is identical, i.e. the aspect ratio A, elongation κ, as well as the rotational transform ι (the inverse of the safety factor, q) must be identical.

The formulation of such dimensionless engineering parameters allows one to link both the governing dimensionless physics quantities and the device parameters. To this extent scaling laws (empirical or theoretical) can be employed to transform the engineering to the physics parameters. This approach has the advantage that anticipated physic regimes can simultaneously be displayed within expected operation windows. Such a representation is referred to as a 'step-ladder' plot due to its characteristic appearance.

The combined engineering-physics parameter view can be seen in Fig. 1, where the left side shows the step-ladder plot for ASDEX Upgrade, JET and ITER assuming the normalized plasma density $n^* = $ const. which has been adapted from [39].

The right side of Fig. 1 reflects the same approach for the HELIAS line employing the scaling law ISS04 for the energy confinement time τ_E [40] with the same configuration factor $f_{\mathrm{ren}} = \tau_E/\tau_E^{\mathrm{ISS04}}$ for all devices. The renormalization factor f_{ren} can serve as a confinement enhancement or degradation factor similar to the H-factor used in tokamaks but, for stellarators, f_{ren} also reflects the complex structure of stellarator magnetic fields and is therefore, dependent on the magnetic

configuration [40, 41].

For the HELIAS-line, the transformation of the dimensionless parameters are determined by the relations

$$\rho^* \sim B^{*-0.8104} P^{*0.1934} n^{*-0.2302}, \qquad (2)$$

$$\nu^* \sim B^{*0.2418} P^{*-0.7737} n^{*1.9207}, \qquad (3)$$

$$\beta^* \sim B^{*-0.6209} P^{*0.3868} n^{*0.5397}. \qquad (4)$$

Since the density is assumed to be determined by the ECH cut-off, changes in n^* need to be considered in the sequence from W7-X to HELIAS 5-B, which is in particular important for the collisionality which scales as $\nu^* \sim n^{*1.9207}$. In the tokamak picture, n^* is similar to the Greenwald density limit [42] and if all devices operate at a fixed ratio of the Greenwald density limit, n^* is constant for all devices meaning that all tokamak devices lie in the same plane of n^*. In the stellarator picture, however, n is constant instead of n^* such that the right side of Fig. 1 becomes actually a 3D-plot with n^* as the 'Z-axis'. Therefore, one has to consider the projection of the n^* plane from todays devices to the n^* plane of the power plant device. This is, however, only important for ν^* since ρ^* and β^* depend only weakly on n^*. The visualisation of differences of the dimensionless parameter ν^* is given by the dotted line on the right side of Fig. 1, which is a projection of the W7-X plane to the HELIAS 5-B plane. The difference in collisionality between W7-X and the power plant scenario is therefore not a factor ten, but rather a factor two to three.

Comparing the step-ladder plot of ITER-like tokamaks with the HELIAS-like devices, indicates that the physics basis of advanced stellarators is less well covered than that of tokamaks. In physics dimensionless parameters, the gap from existent devices to burning plasmas appears evident. Comparing the gap between W7-X and HELIAS 5-B with the gap between JET and ITER or the gap between ITER and DEMO, the change both in B^*, P^* and n^* as well as in ρ^* and ν^* is more substantial for the discussed stellarators. In fact, the gap between

4

120

W7-X and HELIAS 5-B is similar to the gap between JET and DEMO.

The analysis of required control parameters in the form of dimensionless variables shows that the step from W7-X to a HELIAS reactor would be very large in the dimensionless engineering and physics quantities. Especially reactor relevant ν^* and ρ^* are hardly accessible. In particular, simultaneous attainment of ν^*, ρ^* and β of an envisaged reactor working point cannot be achieved in W7-X.

Although the step-ladder approach is a powerful tool to measure the reactor-relevance of today's experiments in terms of a number of representative dimensionless (plasma-core) physics and engineering parameters, a number of additional constraints exist which cannot be incorporated into such a representation. In particular the physics and technology of the divertor and plasma exhaust is governed by very different similarity conditions. Nonetheless, it is possible to define global parameters which are not necessarily dimensionless but which can be employed to characterise the required step-size to reactor conditions. For example, a commonly employed figure of merit which measures the challenge for the exhaust system is the parameter P/R.

An additional important challenge for stellarators, which is not directly covered by Fig. 1, is the confinement of fast particles and their interaction with Alfénic instabilities. Therefore we introduce an additional dimensionless quantity $f_{p,\alpha}$ which serves as figure of merit to describe the importance of fast particles in comparison with the background plasma. The normalised alpha particle pressure $f_{p,\alpha}$ is therefore defined as the ratio of the fast particle pressure in relation to the pressure of the background plasma

$$f_{p,\alpha} = \frac{p_\alpha}{p_{\text{back}}} \quad (5)$$

where $p_{\text{back}} \sim n\,T$ is the plasma pressure in its usual definition and the alpha particle pressure $p_\alpha \sim n_\alpha\,T_\alpha$. In this ansatz T_α is constant and corresponds to the average energy of the alphas over the slowing-down time. In order to define n_α, the equation for the fusion power can be used which is equivalent to the number of generated alpha particles per time interval. Taking the derivative with respect to the volume and further the slowing down time $\tau_s \sim T^{3/2}/n$ as characteristic time interval in which the alpha particles remain 'energetic', the density of the alpha particles becomes

$$n_\alpha \sim \frac{dP_{\text{fus}}}{dV} \cdot \tau_s. \quad (6)$$

Approximating dP_{fus}/dV in the relevant temperature regime of $10-20$ keV by $\sim n^2 T^2$ and substituting in equation (5), a scaling for the normalised alpha particle pressure can be obtained with

$$f_{p,\alpha} \sim T^{5/2} \quad (7)$$

which allows us to represent $f_{p,\alpha}$ in the dimensionless step-ladder approach. However, as intrinsically assumed, this scaling is only correct as long as the heating power is dominated by the fusion alphas.

Last, but not least, we consider the fusion triple product $nT\tau_E$ which is a measure for the burn or ignition of a fusion device. It is generally accepted that $nT\tau_E$ must reach a certain value above which the plasma can be considered to be ignited. According to the above introduced step-ladder methodology,

isocontours for P/R, $f_{p,\alpha}$ and $nT\tau_E$ are given within the dimensionless engineering parameter space in Fig. 2.
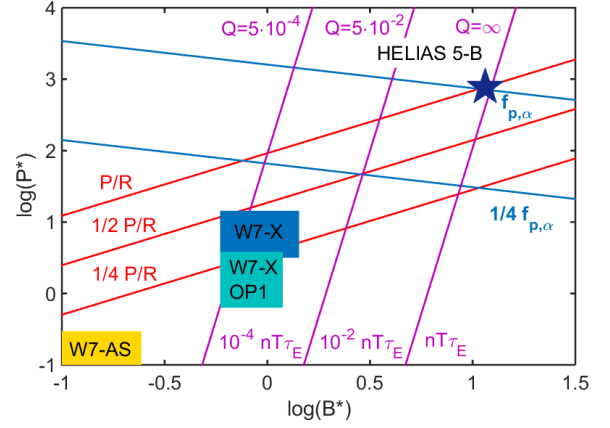

Figure 2: The figure shows the operation windows of HELIAS devices in dimensionless engineering parameters with isocontours of the parameters P/R, $f_{p,\alpha}$ and $nT\tau_E$ which serve as figure of merits for the challenges regarding exhaust, fast particle confinement and fusion burn, respectively. The W7-X operation windows refer to operation phase 1 (OP1) and 2 (OP2) for X2 and O2 heating, respectively, where n^* has been adapted to ECH cut-off densities and 'HELIAS 5-B' is an engineering-based reactor study [13]. Also shown are values for the fusion gain Q whose contours coincide with the contours from the triple product.

It can be seen in Fig. 2, that for either of the presented 'challenges' regarding exhaust, fast particles and fusion burn, substantial gaps exist in the chosen representative figures of merit.

Comparing Fig. 2 with the values presented in Tab. 1 one realises some deviations. For example, the difference of P/R is less in the dimensionless plot, while the difference in $nT\tau$ is greater than in the table. The renormalisation factor has been fixed in the dimensional analysis, however detailed 1D transport simulations have shown [43] that the renormalisation factor is quite different for W7-X and a HELIAS. Furthermore, the dimensionless extrapolation uses the empirical confinement time scaling ISS04 and is thus dependent on the scaling relations therein. It has also been shown in [43], that the transport regimes change from W7-X to a power plant and that for an ignited plasma the heating power is no longer an external variable, but rather determined by plasma volume, beta, and magnetic field. Taken together, this causes the underlying scaling relations of the confinement time scaling to change. While this can be reflected in Tab. 1 for single design points, it is much more complicated to accurately account for such effects in the dimensionless scaling which covers several orders of magnitude in different parameters. However, the conclusions which can be drawn from Fig. 2 remain intact, but absolute values should be taken with care.

The existence of the gaps for the HELIAS-line leads to the conclusion that the experimental program of W7-X needs to demonstrate the physics of high-beta discharges at lowest ρ^* and ν^* (high-performance discharges). Since substantial gaps in ρ^* and ν^* exist with regard to HELIAS reactor plasmas, it is mandatory to develop predictive capabilities about any issues related to collisionality and gyro-radius effects. Examples

5

are the interplay of neoclassical and turbulent transport and the confinement of fast particles and their excitation of Alfénic instabilities.

Overall, the step from W7-X to a power plant contains significant extrapolations of a number of physics and engineering parameters. While a further increase of β is not foreseen and an envisaged increase of the magnetic field by a factor of about two appears to be sufficient, quantities such as plasma volume, stored magnetic energy, energy stored in the plasma and power levels increase substantially. Associated with the high power levels of a power plant is the fact that the plasma heating is governed by alpha-particles which entails not only additional physics effects, but also adds requirements to the design of the device. Finally, the handling of high neutron fluxes and fluences generated by a D-T fusion plasma introduces an entirely new level of complexity.

For the advancement of the tokamak-line the ITER device is seen to play a key role in Fig. 1 bridging the gap between JET and DEMO. Similary for the advancement of the stellarator line, an intermediate-scale HELIAS may be envisaged to bridge the gap between W7-X and a HELIAS power plant. Therefore, the conclusion of this analysis is to introduce a burning-plasma HELIAS as a reasonable next step after W7-X. The main purpose of such a device would be to investigate the burning plasma physics and to a limited extent also the associated technologies while the risk related to the extrapolation from W7-X results is kept at an appropriate level. As outlined in [16], this intermediate-step burning-plasma HELIAS would rely on the parallel development of the tokamak line. In particular, it is assumed that after such an intermediate device, the following development step might already be on the commercial power plant level. This scenario, however, requires that validated technology solutions are available for a HELIAS power plant without the need for another major experimental verification. From the physics and engineering point of view, as presented in Figures 1 and 2, this argument is substantiated by the fact that the operating point of HELIAS-5B already represents an ignited plasma.

On this basis a set of high-level requirements can be derived which a potential intermediate-step HELIAS device must fulfill in order to bridge the gap from today's experiments to commercial fusion for the HELIAS line. A tentative list of these high-levels goals is summarised in the next section.

Some specifications, however, are still ambiguous. For example, it remains to be shown by detailed theoretical studies which value of $f_{p,\alpha}$ must be achieved by an intermediate HELIAS device to allow a meaningful experimental study of the important fast particle effects. Generally speaking, more in-depth studies are necessary to substantiate the list of high-level requirements presented below.

3. High-Level Requirements for a next-step Stellarator

An intermediate device is assumed to bridge the gap between W7-X and a HELIAS power plant. The high-level objective of such a device is to demonstrate and investigate the physics of a burning plasma and the corresponding confinement and control of fast alpha particles.

In this sense an intermediate step stellarator is very much comparable with the general requirements for ITER [12]. New aspects would be the stellarator-specific physics and 3D engineering issues. Especially the divertor concept must be able to handle the heat and particle exhaust of a burning 3D plasma. Nonetheless, an intermediate step HELIAS is expected to have far fewer requirements and constraints than a HELIAS reactor on the power plant scale. Also with regard to accessibility, an intermediate step HELIAS can be regarded to be more a scientific experiment than an electricity generating plant. Consequently, an intermediate-step HELIAS is a device which uniquely allows for an optimisation of 3D reactor scenarios by fully investigating the plasma physics properties of 3D burning plasmas. Based on the step-ladder analysis of the last section, a tentative list of high-level specifications can be defined which is summarised in the list below:

- sufficient fast-particle pressure (to assess, e.g. the effect of Alfvénic instabilities)
- high plasma β ($\sim 4\%$ to enable fast-particle confinement and to demonstrate high-performance operation)
- ρ^* and ν^* must be sufficiently close to reactor conditions
- steady-state operation to allow for reactor scenario development (e.g. exhaust)
- optimised magnetic configuration with respect to neoclassical and turbulent transport of the main plasma, impurities as well as for fast particle confinement
- availability and feasibility of modular magnet system
- reliable divertor concept and operation (e.g. impurity control and [partial] detachment with high SOL radiation to reduce the divertor heat load to acceptable levels)

The definition of such high-level goals is important, since these form the guidelines and constraints for the development of design concepts. In particular, the specifications listed here, serve as input for the systems studies of next-step HELIAS devices as will be discussed in the sections below.

4. Systems Studies of possible next-step Scenarios

A well-established method to investigate the impact of engineering and physics parameter variations on a conceptual design are so-called 'systems studies'. In the design phase of a next-step HELIAS device such studies allow the investigation of a wide parameter range and its impact on the design of the device. Ultimately, such an investigation allows one to show the robustness of a design point and optimise it with respect to the high-level goals taking into account trade-offs between different parameters and limitations. To conduct such systems studies usually 'systems codes' are employed, which are in this context simplified, yet comprehensive models of an entire fusion power plant.

While this approach has a long tradition for tokamaks, heliotrons and compact stellarators, only recently have systems code models been developed for the HELIAS concept [44] including descriptions for the 3D topology, the modular coil set, and the island divertor. These models were implemented in the European systems code PROCESS [45] and tested succesfully [46].

First design window analyses of helical devices were originally carried out for the heliotron concept [47]. Following the developments described above, systems studies have also recently been carried out for HELIAS reactor concepts [18]. In

6

the following the same methodology is applied for different design concepts of an intermediate-step stellarator of the HELIAS line. Having the purpose to bridge the gap between W7-X and a HELIAS power plant, such a device must fulfill the high-level requirements outlined in the previous section.

However, the systems code PROCESS employs empirical confinement time scalings to extrapolate the confinement time, i.e. the plasma transport, to power-plant-sized devices. But as already outlined in the strategy presented in [44] and discussed in [43] empirical confinement times are not sufficient to confidently predict the confinement properties of a HELIAS power plant. Therefore, in addition to the systems code approach, a dedicated 1-D transport code [48] is employed to calculate and estimate the neoclassical and turbulent transport and thus provide a more sophistacted estimation of the confinement in a HELIAS power plant and intermediate-step burning-plasma stellarators.

Since the step from W7-X to a HELIAS power plant is rather large both in engineering and physics quantities, a number of different devices could be envisaged to fit the stated goals. In the following studies the focus is put on two cases. The first case represents the smallest possible device, which could be realised on a near-term time scale using mostly today's technology, in the following called 'Option A'. The second case, which can be seen as an upper boundary, is meant to be a DEMO-like design which employs reactor-ready technology and should consequently produce a net amount of electricity. Since there are still possibilities for a design compromise between those two cases, the DEMO-like concept is referred to here as 'Option C' (i.e. 'Option B' would be a compromise between these two options but is not investigated in this work).

4.1 Workflow

Before the individual options are presented in detail, the general workflow which is followed in this work is introduced; see Fig. 3 for the flowchart.
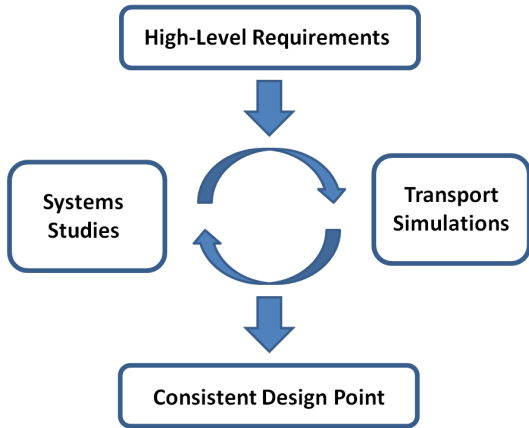

Figure 3: Flowchart for the integrated concept development of design point options for an intermediate-step stellarator.

Generally, the first step is to define a number of high-level requirements which directly influence certain parameters and in addition serve as limits and constraints in the subsequent calculations. With the general inputs defined, the next step is to carry out simulations. One could either start with systems studies and make assumptions on the transport or start with transport simulations and make assumptions on the size of the device. In any case, both tools need to be coupled by iterations. E.g. starting from systems studies, engineering parameters such as the size and the magnetic field can be narrowed down which serves as input for the transport simulations which in turn provide plasma parameters such as the temperature and the confinement time. This in turn, is fed back to the systems studies improving the modeling. After a few iterations back and forth between the systems studies and the transport simulations, a consistent design is obtained. The 'final' set of major input parameters for the systems studies is summarised in Tab. 2.

In the next section, this approach is used for Option A. First the systems studies are discussed and afterwards the transport simulations. However, one has to keep in mind, that these are not separated but are actually interconnected and the results presented are an outcome of several iterations back and forth between both tools.

4.2 Option A

As the rationale for Option A is to be a small device which should be realisable on a fast track, i.e. shortly after W7-X has demonstrated the achievements of optimisation and steady-state operation, the device should mostly employ today's technology or technology expected to be ready in the near future. This option can thus be regarded more as a scientific experiment to clarify the gaps in physics mentioned earlier. In this approach it is expected that reactor-relevant technology is developed for a tokamak DEMO which should then be transferable to the HELIAS line.

Under this guideline, a subset of goals can be defined in addition to the high-level goals of the last section. Being more a scientific experiment on a near time-scale, it is not a requirement for this option to produce electrical power. Rather, a fair amount of fusion power is required to achieve plasma parameters relevant for reactor conditions. To be more precise, not the amount of fusion power is the real design constraint for Option A, but the required alpha pressure in terms of $f_{p,\alpha}$ and the fusion gain Q. However, as a detailed specification for these parameters is still lacking and subject of ongoing research, the fusion power as been taken as proxy for the design constraint. Using transport simulations (see section 4.2.2) and varying density and heating power, it was found, that the achievment of $P_{\mathrm{fus}} = 500$ MW for Option A provides sufficiently high values of $f_{p,\alpha}$ and Q. If the plasma is driven with 50 MW of external heating power, $Q = 10$ is achieved which is also the goal for ITER. At the same time the normalised alpha pressure in the centre of the plasma reaches values of $f_{p,\alpha,0} = 7\%$ compared to 11% in Option C and 18% in HELIAS 5-B. However, it remains to be shown by theoretical studies whether these values are sufficient to study the properties of a 3D burning plasma. Once more precise predictions are available, $f_{p,\alpha}$ and Q will be used as constraints in future design studies.

Consequently, a blanket is not assumed and only a shield is considered to protect the coils. Without the blanket, space should be available to have an aspect ratio similar to that of W7-X with $A = 10.5$. To further save costs, NbTi superconductor technology is assumed for Option A. The device will be designed for steady-state operation as this is one of the great advantages of the stellarator concept. Based on helium cooling technology, about 100 MW of pumping power are assumed

[49]. High-pressure gaseous helium cooling has advantages in terms of safety considerations [50] and in view of power plant requirements. On the physics side, 5% Helium is assumed in the plasma as 'ash' and the volume-averaged temperature is fixed to $\langle T \rangle = 7$ keV. Correspondingly, the renormalisation factor representing the confinement enhancement with respect to the empirical confinement time scaling law ISS04 was limited to $f_{\mathrm{ren}} = \tau_E / \tau_E^{\mathrm{ISS04}} \leq 1.8$ (i.e. the systems studies have been iterated in combination with detailed transport simulations, discussed in subsection 4.2.2). For comparison, the confinement enhancement in W7-X is expected to be on the order of $f_{\mathrm{ren}}^{\mathrm{W7X}} \approx 2$ [48].

For the controlled particle and energy exhaust, the island divertor concept is assumed which was succesful during operation of W7-AS and will be further qualified in the later operation phases of W7-X. The island divertor model assumes cross-field diffusion and radiation around the X-point in combination with a geometrical represenation [44]. The heat-load limit on the divertor is specified to be $q_{\mathrm{div}}^{\mathrm{max}} = 5$ MW/m^2 which has been proposed as the limit for power plants considering the material constraints under high neutron fluences [51]. Due to the low neutron fluence in Option A one could also discuss a higher limit. As input for the divertor model the perpendicular heat diffusion coefficient was set to $\chi_{\perp} = 1.5$ m^2/s. Further, the inclination of the divertor plate relative to the field lines is assumed to be $\alpha_{\mathrm{lim}} = 2°$, the temperature in front of the divertor plates $T_t = 3$ eV and the field line pitch angle $\Theta = O(10^{-3})$ [46, 23]. Tab. 2 summarises the parameters of Option A and compares them to Option C (described later).

Option A	Option C
• 500 MW fusion power	• 200 MW net el. power
• no blanket, only shield	• blanket, maintenance
• Aspect ratio as in W7-X ($A = 10.5$)	• high aspect ratio as in HELIAS-5B ($A = 12$)
• NbTi superconductor	• Nb$_3$Sn superconductor
• 100 MW pumping power, He	• 150 MW pumping power, He
• $q_{\mathrm{div}}^{\mathrm{max}} = 5$ MW/m^2	• $q_{\mathrm{div}}^{\mathrm{max}} = 5$ MW/m^2
• 5% Helium, $\langle T \rangle = 7$ keV	• 5% Helium, $\langle T \rangle = 9$ keV
• $f_{\mathrm{ren}} \leq 1.8$	• $f_{\mathrm{ren}} \leq 1.5$

Table 2: Summary and comparison of additional, concept-specific sub-goals (inputs for the systems studies) for Option A (left) and Option C (right). The volume-averaged temperature $\langle T \rangle$ as well as the renormalisation factor f_{ren} have been obtained from 1-D transport simulations, see subsection 4.2.2 and 4.3.2.

4.2.1. Design Window Analysis – Option A

For the design window analysis of Option A, the main engineering parameters (i.e. the major radius and the magnetic field strength on axis) were systematically varied within a predefined range of $R = 12 - 15$ m and $B_t = 4.0 - 5.6$ T. Both the high-level and the above-mentioned subsequent goals have been taken as constraints / limits and held constant in the systems

studies. Thus, every design point is set to reach 500 MW fusion power. To achieve this while varying device size and magnetic field, the density, the external heating power and the confinement enhancement factor were used as iteration variables. The corresponding result for Option A is shown in Fig. 4 where isocontours of the volume-averaged thermal plasma $\langle \beta \rangle$, the average neutron wall-load Γ_{NWL}, and external heating power are highlighted as important parameters.

It should be noted that due to the 3D topology and the resulting higher complexity of the systems code models, the calculation time for a single run of a HELIAS design point is on the order of a few minutes on a modern CPU. For the design window analysis presented here a resolution of 16×16 for the varied engineering parameters was chosen corresponding to ~ 1 day calculation time per figure [52].
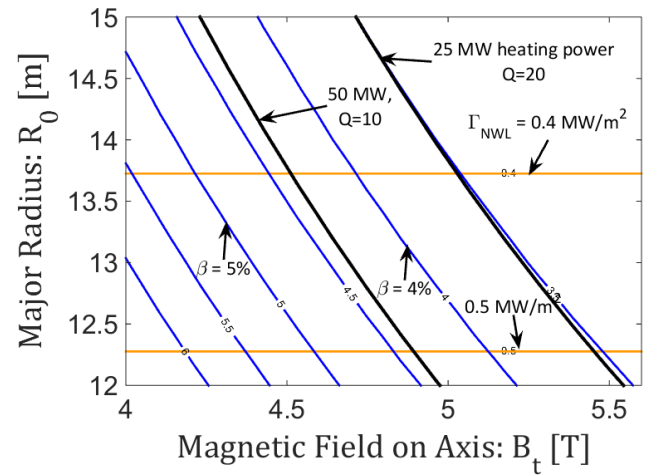

Figure 4: Design window analysis for the intermediate-step HELIAS – Option A, constrained to achieve 500 MW fusion power with a confinement enhancement factor of $f_{\mathrm{ren}} \leq 1.8$. Shown are isocontours of the volume-averaged thermal plasma $\langle \beta \rangle$ (blue), the average neutron wall-load Γ_{NWL} (orange), and external heating power (black). Since the fusion power was kept constant, the heating power contours are equivalent to the fusion gain contours (black). The normalised alpha-pressure is constant reaching a value of $f_{p,\alpha,0} = 7\%$ in the plasma centre.

As can be seen from Fig. 4, reasonable beta-values in the range of $3 - 5\%$ can be obtained in the engineering parameter range considered (blue lines). While the beta-limit is a strongly limiting factor for the HELIAS reactor studies, it's importance for the intermediate-step stellarator, Option A, is rather low. Linear stability predicts the beta-limit to be in the range of $\beta = 4.5\%$, but stellarator experiments have demonstrated the capability to operate above this limit [53] such that beta may be ultimately limited by stochastisation of the plasma edge and corresponding destruction of flux surfaces and shrinking of the plasma volume. However, these effects are much reduced in a HELIAS due to the optimisation of the magnetic configuration. Such a beta-limit has been predicted to be in the range of 5 – 6% [54]. In the design window analysis of Option A, the isocontours of the external heating power and beta are nearly parallel. Already at $\beta = 4.5\%$, an external heating power of 50 MW is required. It would not seem desirable to select a design requiring more heating power which reduces the fusion gain Q, and the beta-limit therefore does not play a role.

8

However, since the plasma is maintained by external heating using ECRH, the cut-off density of O1-mode heating must be taken into account. The magnetic field provides a highly localized resonance for O1-mode ECRH heating at $B_{t,\max}$ near the magnetic axis. As the considered magnetic configurations have a mirror term for the magnetic field strength of around 10% in the plasma center, the (cold) resonance is $B_{t,\max} = 1.1 \cdot B_t$. For example at $B_t = 4.5$ T the resonance is at 5 T which would be exactly the O1-resonance for the 140 GHz W7-X gyrotrons. The cut-off for O1-mode heating is then $2.4 \cdot 10^{20} \mathrm{m}^{-3}$ which leaves about 10% of margin with respect to central densities on the order of $2.2 \cdot 10^{20} \mathrm{m}^{-3}$. Access to lower fields than $B_t = 4.5$ T is therefore problematic as the cut-off density decreases with B^2, i.e. at $B_t = 4.0$ T it drops to $1.85 \cdot 10^{20} \mathrm{m}^{-3}$.

As outlined above, the systems studies have been iterated in alternation with 1D transport simulations and the confinement enhancement factor was set accordingly to $f_{\mathrm{ren}} \leq 1.8$. Since considerable external heating power is used to maintain the plasma, the confinement has a relatively small effect on the beta contours. However, the required external heating power is very sensitive to f_{ren} as an overall degradation of the confinement from $f_{\mathrm{ren}} = 1.8$ to 1.6 would double the required heating power, e.g. from 50 to 100 MW. This illustrates how critical it is to accurately predict confinement. While advanced optimisation procedures should ensure that the magnetic configuration for an intermediate-step stellarator has good confinement properties, recent advances in gyrokinetic simulations of stellarator geometry [55] and the comparison with upcoming experimental results of W7-X are anticipated to increase the predictive capability of transport codes.

The average neutron wall load Γ_{NWL} (orange) varies only moderately over the engineering range considered. This is clear as the fusion power is constant and only the first wall area is changing with size, i.e. decreasing the device size by 1.5 m from 13.75 to 12.25 m increases the neutron wall load from 0.4 to 0.5 $\mathrm{MW/m}^2$. Consequently, the neutron wall load is a factor three lower than in a HELIAS power plant, but still high enough for e.g. material testing, especially as the device could be designed for steady-state. However, without further material qualifying, the lifetime of componentes and the device is limited by the neutron damage in terms of displacements-per-atom (dpa).

Isocontours of other parameters are not shown in Fig. 4 to retain clarity. E.g. the radiation fraction, which is required in the scrape-off-layer (SOL) to reduce the heat load of the divertor to 5 $\mathrm{MW/m}^2$ must be for the maximum considered size on the order of 40% and increases to 50% for the smallest device sizes. Impurities in the plasma core for additional radiation have not been considered here but will be included in future studies.

Another engineering parameter which is often of interest is the stored magnetic energy in the coil system which is a proxy for the required support structure. For the smallest device size at low field this value is on the order of $W_{mag} = 30$ GJ and increases up to 50 GJ for the highest field and largest size.

The systems studies suggest that NbTi can be used to achieve the desired fields, however the maximum field on the surface of the coils is for e.g. $R = 14$ m and $B_t = 4.5$ T on the order of $B_{max} \approx 10$ T. To push NbTi to such a high field, super-critical helium cooling at 1.8 K is needed requiring a higher effort for the cooling systems. It should be noted, that the NbTi critical current density scaling was obtained from W7-X and the calculations for the maximum field on the coil subsequently verified against W7-X. The device considered here, however, is nearly a factor three larger than W7-X (in terms of the major radius) which may result in some deviations and an error of about 10% is easily imaginable, but is sufficient to distinguish between the requirements for normal (4.2 K) and critical helium cooling (1.8 K). For comparison, in the more detailed 'HSR 4/18i' HELIAS study [4] NbTi could be employed with normal helium cooling with 4.5 T on axis by trapezoidally shaping the winding pack and thereby reducing the maximum magnetic field on the coils. A more detailed engineering study is required to clarify this aspect for Option A.

The results of the design window analysis for Option A may suggest higher fields to reduce the device size. But with higher field on-axis also the maximum field at the coils increases. According to the argument above it is unlikely that NbTi can be employed for fields up to 5.5 T. Nb_3Sn could be used to achieve this, but this would considerably increase the costs of the magnets and negate the savings due to reduced device size.

4.2.2. 1-D Transport Scenario – Option A

In order to make predictions about the expected confinement in next-step devices such as an intermediate-step stellarator, a 1-D transport code [48, 56] is employed which solves the power balance for the electrons and ions and calculates the neoclassical energy fluxes given DKES [57, 58] data sets. Additional anomalous energy fluxes are considered at the plasma edge based on experimental data from W7-AS [59, 60, 61].

In order to carry out predictive transport simulations for an exemplary design for Option A, a suitable magnetic configuration has to be defined. As dedicated configurations for such a next-step device are still a topic of ongoing research, the existing W7-X 'high-mirror' configuration was selected due to its reactor-relevance. The DKES database has been prepared for a $\beta = 4$ % equilibrium to account for finite beta effects. The dimensionless nature of the DKES approach allows a linear upscaling of the magnetic configuration. The configuration has been scaled by a factor 2.5 which corresponds to the design point found in systems studies with a major radius of $R = 14$ m. The magnetic field on-axis has been set to 4.5 T accordingly. Additionally, 50 MW of ECRH steady-state external heating power are assumed with central deposition modeled by a Gaussian profile to reach the desired fusion power of 500 MW. The associated 100 MW of internal alpha-heating are self-consistently taken into account in the code.

For the density a 'standard' profile has been selected and kept constant to avoid a fuelling scenario which requires detailed knowledge of particle sources and sinks. In fact, density control in large stellarators is generally problematic and requires central sources such as pellet injection to avoid hollow density profiles [28]. This is beyond the scope of this work, but will be investigated in future studies.

Regarding the anomalous transport, as so far no better quantitative assessment exists, the anomalous heat conductivity has been described by $\chi^{ano} \sim 1/n$ and falling off towards the centre with $\chi^{\mathrm{edge}} = 3.0$ m^2/s at the very edge. A new physics motivated critical gradient model is subject of ongoing research [61].

The resulting density and temperature profile of an exemplary scenario of Option A are shown in Fig. 5. The global confinement according to the simulations is in this scenario $\tau_E^{\mathrm{1D}}/\tau_E^{\mathrm{ISS04}} = 1.8$ in terms of the empirical ISS04 scaling. As
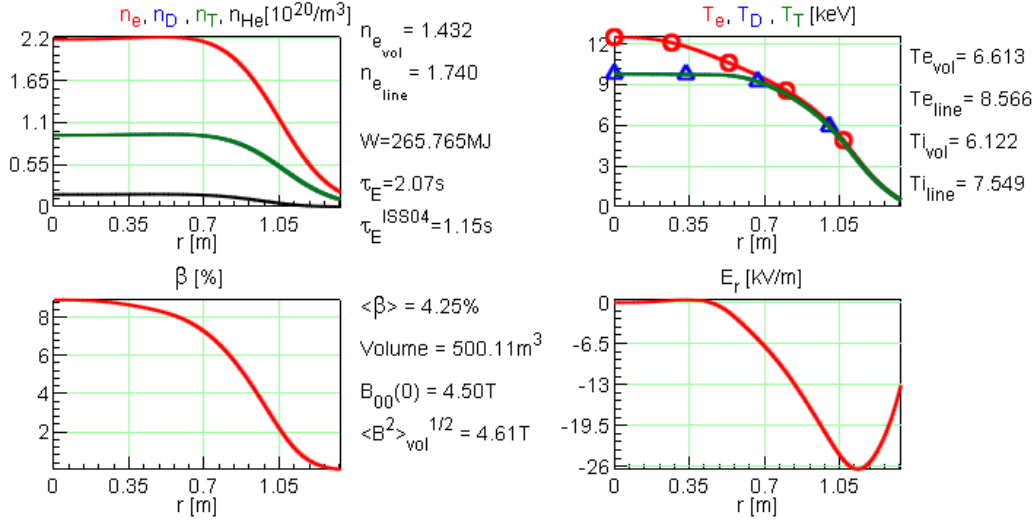
9

Figure 5: Profiles for the density, $n_D = n_T$, $n_{He} \approx 0.05 \cdot n_e$, (top left), temperature (top right), plasma beta (bottom left) and radial electric field (bottom right) for the 1-D predictive transport simulation for the intermediate-step stellarator, Option A, with $R = 14$ m and $B_t = 4.5$ T and 50 MW external heating power.

already stated, this result, including the density and temperature profiles and values, have been taken as input for systems studies of Option A.

4.3 Option C

While 'Option A' represents a bounding scenario for a small, fast-track intermediate-step stellarator, 'Option C' in contrast is meant to be an upper boundary scenario for a large, DEMO-like device employing reactor-ready technology. Consequently, a pre-requisite of Option C is the research and development of reactor-relevant technology similar to a tokamak DEMO [16] which is usually defined as a device demonstrating an integral workable solution (i.e. concerning all components) for a fusion power plant. DEMO must not be economically competitive but allow extrapolation to commercially attractive applications. The essential difference between Option C and a tokamak DEMO would be the fact, that the tokamak line can rely on the burning plasma experiment ITER. Option C, in contrast, would be a direct step from W7-X and as explained ealier, the step in physics and engineering parameters larger than that from ITER to DEMO.

As for Option A, a set of concept-specific sub-goals can be defined for Option C which need to be realised in addition to the high-level requirements outlined in section 3. Under the premise of a DEMO-like device, Option C should produce a reasonable net amount of electricity, set here at 200 MW, to demonstrate the power plant capability of the concept. Consequently, a full blanket and shield are required and enough space must be foreseen to accommodate these components. As a result, the aspect ratio is increased to $A = 12$ compared to $A = 10.5$ for Option A. This value is based on the HELIAS 5-B engineering study [13] where the aspect ratio was raised to $A = 12$ to accomodate enough space for blanket and shield.

The power conversion system of thermal to electric energy is mainly dependent on the chosen coolant which determines the thermal conversion efficiency η_{th}. Common technologies employ either pressurized water or gaseous helium cooling. Water cooling is a well established technology requiring a moderate amount of pumping power but has a lower efficiency compared to helium. In turn, helium cooling requires a much higher pumping power. A detailed discussion of the advantages and disadvantages of both systems is still ongoing in the fusion community. In this work, the Brayton power cycle with helium cooling technology has been chosen for the cooling system due to the possibility of working at higher temperatures and avoiding the unresolved safety issues regarding water cooling [50]. This is also consistent with the European 'Helium-cooled Pebble Bed' (HCPB) blanket concept [62]. Additionally, the higher thermal conversion efficiency, $\eta_{th} = 0.4$, compensates for the higher pumping power, $P_{pump} = 150$ MW, assumed here [49, 63].

Further, Nb$_3$Sn is foreseen as superconductor, which could also be a possible conductor for a HELIAS power plant. Similar to Option A, the device will be designed for steady-state operation. According to the detailed predictive physics transport simulations, see subsection 4.3.2, which have been iterated with the systems studies, the helium 'ash' is set to 5% and the volume-averaged temperature to $\langle T \rangle = 9$ keV. Correspondingly, the renormalisation factor representing the confinement enhancement with respect to the ISS04 confinement time scaling law was limited to $f_{ren} = \tau_E / \tau_E^{ISS04} \leq 1.5$.

It may seem surprising that the confinement enhancement factor from Option C is different to that from Option A. However, this is due to the paradigm change of the underlying scaling relations. In the regression of the empirical confinement time scaling it is assumed that the heating power P is an independent parameter. Under fusion conditions, however, alpha particles heat the plasma and the heating power is, therefore, no longer a free parameter. Instead, it is interconnected to the plasma volume, plasma beta, and the magnetic field. As such, τ_E scales differently for a reactor than for an experimental sce-

10

nario where the heating power can be externally adjusted as an independent parameter. This has been explained in detail in [43]. The sub-goals of Option C are summarised in Tab. 2.

4.3.1. Design Window Analysis – Option C

Again, the high-level requirements and the above-mentioned sub-goals have been taken as constraints for the design window analysis of Option C. This time the major radius was varied in the range $R = 15-20$ m and the magnetic field on-axis between $B_t = 4.5 - 5.6$ T while the density, the confinement enhancement factor as well as the external heating power were taken as iteration variables. The corresponding result for Option C is shown in Fig. 6 where isocontours of the volume-averaged thermal plasma $\langle\beta\rangle$, the average neutron wall-load Γ_{NWL}, and external heating power are highlighted.
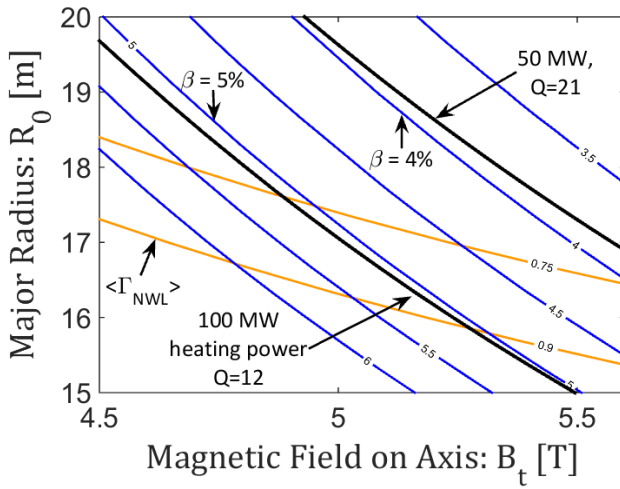
Figure 6: Design window analysis for the intermediate-step HE-LIAS – Option C, constrained to achieve 200 MW net electric power. Shown are isocontours of the volume-averaged thermal plasma $\langle\beta\rangle$ (blue), the average neutron wall-load Γ_{NWL} (orange), and external heating power (black). Since the fusion power varies only moderately, the contours of the fusion gain follow very closely the contours of the heating power (black). The normalised alpha-pressure is roughly constant reaching a value of $f_{p,\alpha,0} = 11\%$ in the plasma centre.

A first result which can be inferred from Fig. 6 is the fact that, under the given confinement and size constraints, the design points within the systems study are not ignited. The black curves show the required external heating power which is needed to fulfill the power balance. Again, the beta-contours (blue) run approximately parallel to the heating power contours. The plasma beta takes reasonable values of $4\ldots5\%$ in the range between 50 and 100 MW external heating power.

Consequently for Option C, the beta-limit also does not play a large role unless one would be restricted in the achievement of higher field strengths. But as outlined above, Nb$_3$Sn superconductor is envisaged from the beginning for this option allowing a higher maximum field on the coil and therefore magnetic field strengths of up to 5.5 T on-axis should be unproblematic. In particular for $R = 18$ m and $B_t = 5.5$ T, the maximum magnetic field on the surface of the coils is about $B_{\max} \approx 12$ T which is consistent with Nb$_3$Sn technology and normal Helium cooling (4.2K). As already shown in the systems studies for HELIAS power plant devices, the contours of construction cost

are rather flat with respect to the magnetic field, i.e. it is very desirable to employ a high field for Option C.

At a field of about 5.5 T on-axis (6 T including the mirror term), the ECRH cut-off is at $3.5 \cdot 10^{20}$ m^{-3}, and therefore not a concern for the systems studies and the achievable density. Even in the centre of the plasma, a density not higher than $n_e \sim 2.0 \cdot 10^{20}$ m^{-3} is required, cf. subsection 4.3.2.

Since the considered range of device sizes is greater for Option C than for A it follows that the average neutron wall load Γ_{NWL} (orange) also has a broader variation over the whole design window analysis between $0.5-1.0$ MW/m^2. This is mostly due to the change of first wall area with changing major radius. However, as seen from Fig. 6, the isocontours of the neutron average wall load are not horizontal lines as for Option A, but rather decreasing with increasing magnetic field. This is simply due to the fact, that for lower magnetic field the confinement time is lower and the required heating power must increase. As the net electric power is held constant, the density and fusion power must increase to provide additional gross electric power to sustain the additional heating. Thus, the higher fusion power for lower magnetic field leads directly to an increase of neutrons. At 4.5 T the required fusion power is about 1400 MW and can be reduced to 1100 MW for 5.5 T on-axis at a constant net electric power of 200 MW.

For the same reasons also the required radiation fraction in the SOL varies over a wider range from 60% for the largest device and field up to 80% for the smallest. And the stored magnetic energy in the coil system varies vice versa from 60 GJ to 130 GJ.

Similar to Option A, the required external heating power is rather sensitive to changes in the confinement enhancement factor f_{ren}, which was set here according to the 1D transport simulations to $\tau_E^{\mathrm{1D}}/\tau_E^{\mathrm{ISS04}} \leq 1.5$. However, for Option C not only the external heating power would change but also the beta-contours would shift to lower fields as for Option C considerable heating power is coming from the fusion alphas. The transport simulation for Option C are discussed in the next section.

4.3.2. 1-D Transport Scenario – Option C

The same methodology for the predictive transport simulations is applied here which was already used for Option A. Again, the W7-X 'high-mirror' configuration was selected for its reactor relevance. However, the aspect ratio of this magnetic configuration is with $A = 10.5$ not the same as the one used in the systems studies of Option C with $A = 12$. Therefore the configuration has been scaled such, that the plasma volume corresponds to the design point with $R = 18$ m. It is clear that this is not completely consistent, but is nevertheless a reasonable approximation. Dedicated magnetic configurations for an intermediate-step HELIAS will be further optimised and are therefore expected to have better confinement than the results derived based on the W7-X 'high-mirror' configuration.

For the simulation a high field has been chosen with $B_t = 5.5$ T and the external heating power by ECRH adjusted to 50 MW with a Gaussian profile and central deposition. The alpha heating power is self-consistently taken into account in the simulations. Again as for Option A, a standard flat density profile has been used and kept constant and the anomalous heat conductivity – described by $\chi_e^{ano} \sim 1/n$ and falling off towards the centre – has been set to $\chi^{\mathrm{edge}} = 3.0$ m^2/s at the very edge.

The resulting profiles of this simulation are shown in Fig. 7. The simulation results were taken as input for the systems
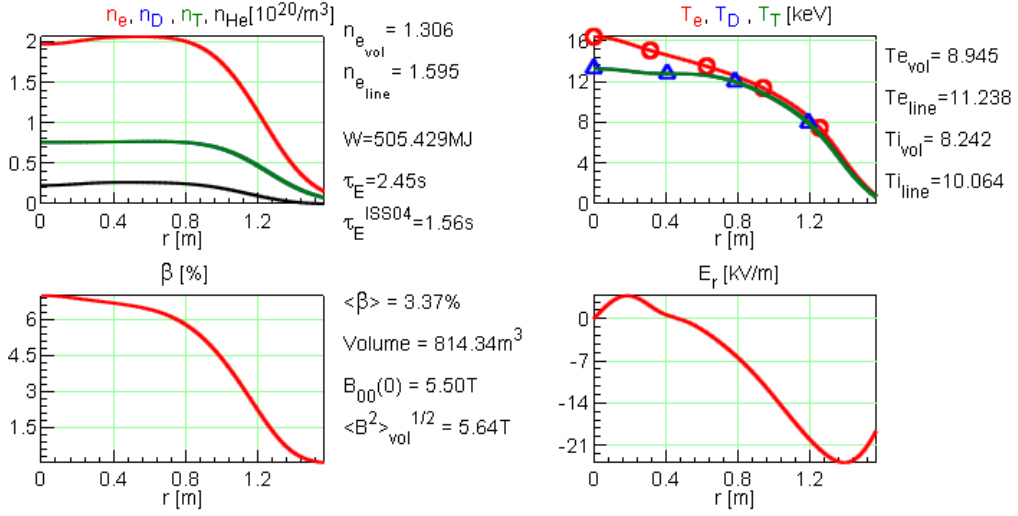
11

Figure 7: Profiles for the density (top left), temperature (top right), plasma beta (bottom left) and radial electric field (bottom right) for the 1-D predictive transport simulation for the intermediate-step stellarator, Option C, with $R = 18$ m and $B_t = 5.5$ T and 50 MW external heating power.

studies of Option C and have been iterated until both the design window analysis and the 1D simulations were in agreement.

4.4 Step-Ladder including Options A and C

With the presented design window analysis of Options A and C and the corresponding parameters, it is now possible to include these cases in the step-ladder approach of the Wendelstein line, see Fig. 8.
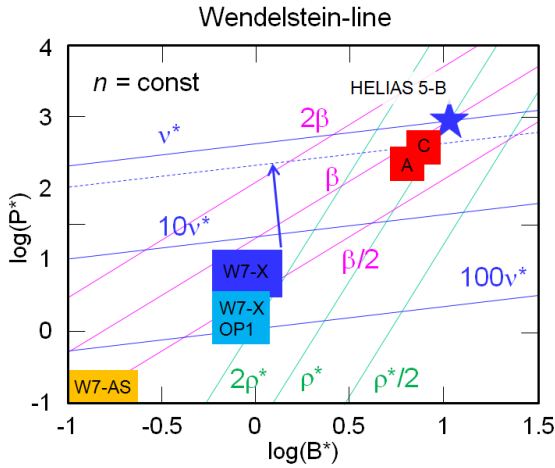
Figure 8: Step-ladder plot for the HELIAS line. The figure shows operation windows of W7-AS and W7-X in dimensionless engineering parameters with isocontours of dimensionless physics parameters at constant n^*. The W7-X operation windows refer to operation phase 1 (OP1) and 2 (OP2) for X2 and O2 heating, respectively, where n^* has been adapted to ECH cut-off densities. 'HELIAS 5-B' is an engineering-based reactor study [13]. The dotted line is the projection of the collisionallity of W7-X into the plane of HELIAS 5-B. In addition, the design window of the intermediate-step stellarator Options A and C are shown in red.

One can see, that an intermediate-step stellarator helps to strongly reduce the gap between W7-X and a HELIAS power plant (one should keep in mind that the figure is logarithmic). Thus, the step between W7-X and Option A is similar to the step between W7-AS and W7-X or to compare it with the tokamak line, similar to the step between JET and ITER.

5. Economic Comparison

As the options presented here for an intermediate-step stellarator represent boundary cases with quite a conceptual difference between Option A and C, it is meaningful to carry out an economic comparison in order to rate the effect of the respective sub-goals on the construction costs.

The current version of PROCESS accommodates a basic cost-model with which it is possible to estimate the construction costs of a design point based on the total sum of material costs. In fact, the systems code PROCESS can calculate for each component of a fusion device the size. Each component is described by a material or even several materials. Based on the size of the components and the material densities the total weight for each material can be estimated. Every material in turn is associated with a specific cost-per-weight which allows estimation of the costs of each component and in total the direct costs of the device as a sum of all individual components. The direct costs are complemented by indirect costs which are a flat rate of the direct costs and represent together the total construction costs. A cost penalty for the complexity of components is not yet included in the model (costs of certain components may thus be underestimated). The PROCESS cost model has been benchmarked with the dedicated cost analysis code FRESCO which showed a reasonable agreement for the total costs of a tokamak test case with about 20% difference [64]. The cost estimates are obtained from the PROCESS cost model and will be given here as 'PROCESS currency units' (PCU) since the cost analysis is carried out for all devices in
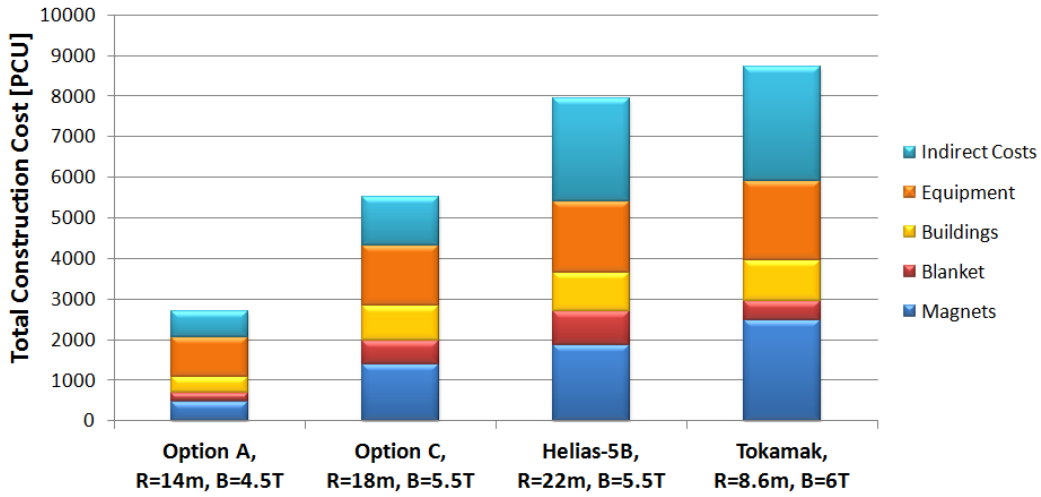
12

Figure 9: Total construction costs obtained from the PROCESS cost model in 'PROCESS currency units' (PCU) broken down to major costing accounts for exemplary design points of Option A, Option C as well as for a HELIAS power plant and an exemplary tokamak reactor (similar to Model B of the European PPCS study [25]).

the same framework allowing a relative comparison between the individual devices while absolute values should be taken with care.

For this comparison, favourable design points are selected from each design window analysis and compared in a cost-breakdown. For Option A, a medium-sized low-field device was selected with $R = 14$ m and $B_t = 4.5$ T while for Option C, a high-field, larger device seems to be a favourable design point with $R = 18$ m and $B_t = 5.5$ T; important parameters are summarised in Tab. 3. The total construction cost of both these design points have been broken down into their major contributions, which are the magnets, the blanket (including the shield), the buildings, the equipment and indirect costs. The results are shown in Fig. 9. Additional to these design points, the total construction costs of a HELIAS power plant and an 'equivalent' tokamak (Model B of the European PPCS study [25]) are presented as reference which have been discussed in [18].

It should be noted that the 3D complexity of the stellarator will most likely increase the magnet costs, but this has not been taken into account here. However, while the modular coils of a HELIAS are rather small (even for power-plant size they are comparable to the ITER TF-coils [15]), the poloidal and toroidal field coils of the tokamak case are much larger. That means, while the HELIAS coils can still be produced by industry and shipped to the construction site, the tokamak coils, on the other hand, must be built on-site or transported by 'unconventional' means. This requires a dedicated facility increasing the magnet costs for the tokamak, but which so far is also not taken into account. Thus arguments for cost increases can be found for both concepts and should be considered in future studies.

A very striking result from this comparison as seen in Fig. 9 is the fact that the cost difference between the boundary cases Option A and C is about a factor two. In particular the magnet costs contribute to this difference which are much higher for the DEMO-like device than for the near-term step. This is

attributed to two reasons. First, Option C is a larger device with higher field and requires therefore a higher amount of superconducting material and second, the costs for Nb$_3$Sn are considerably higher than for NbTi. This confirms the strategy to employ NbTi for the near-term device.

The costs for the blanket are of course higher for Option C which foresees a full blanket concept in contrast to Option A with solely a shield. However, in this analysis the total blanket costs are a rather small fraction of the total construction costs. It is unclear if this is an underestimation compared to the other costs since the blanket is also a complex component for a HELIAS device. In additional, little practical experience exists. As already stated above, the complexity of components is not yet considered for the costs, but is relevant for future studies. The upgrade of the cost model is an ongoing and continous process.

Also the building and equipment costs are higher for Option C which is understandable as Option C requires more buildings and equipment for the power conversion systems in order to produce a net amount of electricity.

In comparison to a HELIAS power plant design point, Option A would require only a third of the construction costs, while Option C reaches two-thirds of the costs of a power plant. If one were to model an idealised version of ITER [65] in PROCESS, the construction costs would lie nearly in the middle between the exemplary design points of HELIAS Option A and C.

Although PROCESS has been developed for modelling of power plant devices, it is possible to also model W7-X. However, the uncertainties associated with this analysis are rather high. With respect to the cost analysis presented in Fig. 9, Option A would be about three times more expensive than W7-X.

Using the actual costs of the W7-X construction (until 2014) as a reference for real costs and applying this scaling to the costs of ITER given by PROCESS, one realises that the PROCESS ITER costs scaled as real costs are about a factor three

13

lower than the current estimate of the actual ITER costs [66]. How much this discrepancy can be attributed to the limitations of the PROCESS cost model and how much of this is due to the project structure and first-of-a-kind nature of the ITER enterprise is unclear.

Device Option	A	C
Major Radius [m]	14	18
Fusion Power [GW]	500	1100
Stored Magn. Energy [GJ]	35	110
Vol. Averaged Plasma Beta [%]	4.3	3.4
Magnetic Field on Axis [T]	4.5	5.5
Maximum Field on Coil [T]	10	12
Av. Neutron Wall Load [MW/m^2]	0.4	0.65
Cold Mass [kt]	15	30
SC Mass [kt]	0.3	1.0
Fusion Gain	10	20
Norm. Alpha Pressure (centre) [%]	7	11

Table 3: Summary and comparison of relevant parameters for the exemplary design points of Option A and C.

A Remark on Tritium

As Option C should be designed with a tritium breeding ratio larger than one, the tritium supply should be self-sufficient apart from the start-up inventory. Tritium supply for Option A, in contrast, needs to be supplied from external sources due to the lack of a blanket. Comparing with the ITER fusion burn phase, tritium consumption could be on the order of one kilogram per year [67] for ~ 5 years.

Nonetheless, in either of the presented options for an intermediate-step stellarator, a tritium start-up inventory is required to initiate operation of the devices. One of the main commercial tritium sources are the Canada Deuterium Uranium (CANDU) type pressurised heavy-water reactors which have a total supply capacity of several kilogram tritium per year. The shutdown of the CANDU type reactors would thus have a great impact on the tritium supply. However, recently discussions started regarding a 30 year life-time extensions of these reactors [68] potentially improving the situation for tritium supply in the upcoming decades. Once a 'fleet' of fusion power plants is running, the surplus of produced tritium can be used for the start-up of new fusion power plants. Apart from that, other possibilities exist to breed tritium commercially [67].

Costs for tritium have not yet been taken into account in the cost assessments since the estimation of the tritium start-up inventory of a stellarator power plant are still too vague. The resulting contribution of the tritium start-up inventory to the total construction costs and, for Option A, also the operation costs cannot be calculated.

6. Summary and Conclusions

This work is thought of as a starting point for a more in-depth discussion of a research strategy leading from Wendelstein 7-X to a HELIAS power plant. The experimental results of Wendelstein 7-X, which has just started operation, will of course play an essential role in the continuing refinement of this analysis. In particular, the better understanding and modelling of turbulence as well as the verification of stellarator optimisation will allow a more refined prediction of the confinement in next-step devices. Further aspects are the investigation of suitable plasma scenarios with impurity and density control (pellet injection) and the plasma stability at high $\langle \beta \rangle$ (5%).

Looking at the extrapolation from W7-X to a power plant, three approaches or viewing perspectives have been presented. They shed light on the level of extrapolation required or in other words they indicate the gaps in physics and engineering parameters which have to be bridged. Selected physics and engineering parameters (e.g. energy of the magnet system, stored energy in the plasma, heating power, P/R, fusion power gain, triple product), already show increases by orders of magnitude when going from W7-X to a power plant. Other quantities (plasma β, average magnetic field) need no or only moderate extrapolation which is a particular property of the HELIAS concept. Considering the scientific progress which has been made since the optimised design of W7-X was frozen, a further refinement of the optimisation seems possible and also meaningful. This concerns, in particular, the fast-ion confinement and the inclusion of the turbulent transport in the optimization procedure. Finally, combining dimensionless physics quantities with dimensionless engineering parameters and employing empirical confinement scaling laws show the necessary steps between different experiments or fusion devices in a more rigorous way. Comparing the HELIAS development to the tokamak line, from ASDEX Upgrade and JET to ITER and a tokamak DEMO, it becomes clear that between W7-X and HELIAS 5-B the step or gap is much larger than between JET and ITER or ITER and DEMO.

Taking these arguments together, two possible options for filling this gap are investigated. Based on a tentative list of high-level requirements, guidelines for the conceptual study of an intermediate-step HELIAS are developed. The two options represent different levels of sophistication and basically can be considered as bounding cases for such a device. Option A is defined as a reasonably small fast-track device, while Option C is a DEMO-like device with net electrical power output. For Option A, the fusion power is fixed to a value comparable to ITER (500 MW). Selecting an example within the design window analysis, this suggests a device with a major radius of 14 m, an average magnetic field on axis of 4.5 T and a fusion power gain of $Q = 10$. The moderate magnetic field allows the use of conventional NbTi superconductor. This may require supercritical helium cooling but needs a more detailed engineering assessment. For Option C, a fixed net electrical power of 200 MW is assumed. This results in a larger device ($R = 18$ m) with a larger aspect ratio ($A = 12$ instead of 10 for Option A), a larger magnetic field (5.5 T) and a significantly higher fusion power of 1100 MW. The higher magnetic field requires a different type of superconductor. Nb_3Sn, as used for the ITER toroidal field coils, would fulfil this requirement. With a fusion power gain of $Q = 20$, this device would still not be ignited.

A first cost assessment indicates that Option C is more expensive by approximately a factor of two, ignoring the costs for tritium. Option C requires a start-up inventory, while Option A depends on a continuous tritium supply as it does not have a breeding blanket.

As the Options A and C represent bounding cases, of course any compromise between them is conceivable. The further

14

development and refinement of the conceptual design of an intermediate-step HELIAS will depend on the validation of the optimisation principles by W7-X, on the advancement of the theoretical understanding of confinement and stability of optimised stellarators and on the capability to extrapolate to a fusion power plant. Moreover, the exact design will also depend on the general development of fusion technologies and how easily these can be transferred to such a device.

7. Acknowledgments

References

[1] H.-S. Bosch, R. Wolf, T. Andreeva et al. "Technical challenges in the construction of the steady-state stellarator Wendelstein 7-X." *Nuclear Fusion*, vol. 53, no. 12, p. 126001 (2013).

[2] F. Romanelli, L. H. Federici, R. Neu et al. "A roadmap to the realization of fusion energy." *Proc. IEEE 25th Symp. Fusion Eng*, pp. 1–4 (2013).

[3] G. Grieger and I. Milch. "Das Fusionsexperiment WENDELSTEIN 7-X." *Physikalische Blätter*, vol. 49, p. 1001 (1993).

[4] H. Wobig, T. Andreeva, C. D. Beidler et al. "Concept of Helias ignition experiment." *Nuclear Fusion*, vol. 43, p. 889 (2003).

[5] M. Drevlak, J. Geiger, P. Helander et al. "Fast particle confinement with optimized coil currents in the W7-X stellarator." *Nuclear Fusion*, vol. 54, no. 7, p. 073002 (2014).

[6] A. Mishchenko, A. Könies, T. Fehér et al. "Global hybrid gyrokinetic simulations of fast-particle effects on Alfvn Eigenmodes in stellarators." *Nuclear Fusion*, vol. 54, no. 10, p. 104003 (2014).

[7] J. Nuehrenberg, W. Lotz, P. Merkel et al. "Overview on Wendelstein 7-X theory." *Fusion Technology*, vol. 27 (1995).

[8] T. Brauer, T. Klinger and H.-S. Bosch. "Progress, Challenges, and Lessons Learned in the Construction of Wendelstein 7-X." *Plasma Science, IEEE Transactions on*, vol. 40, no. 3, pp. 577 (2012).

[9] P. Helander. "Theory of plasma confinement in non-axisymmetric magnetic fields." *Reports on Progress in Physics*, vol. 77, no. 8, p. 087001 (2014).

[10] P. Helander, C. D. Beidler, T. M. Bird et al. "Stellarator and tokamak plasmas: a comparison." *Plasma Physics and Controlled Fusion*, vol. 54, p. 124009 (2012).

[11] G. Grieger, W. Lotz, P. Merkel et al. "Physics optimization of stellarators." *Physics of Plasmas B*, vol. 4 (1992).

[12] "Summary of the ITER final Design Report." International Atomic Energy Agency, Vienna (2001).

[13] F. Schauer, K. Egorov and V. Bykov. "HELIAS 5-B magnet system structure and maintenance concept." *Fusion Engineering and Design*, vol. 88, p. 1619 (2013).

[14] D. Campbell. "The physics of the international thermonuclear experimental reactor FEAT." *Physics of Plasmas*, vol. 8, no. 5, pp. 2041 (2001).

[15] F. Schauer. "Coil winding pack FE-analysis for a HELIAS reactor." *Fusion Engineering and Design*, vol. 86, p. 636 (2011).

[16] H. Zohm. "Assessment of {DEMO} challenges in technology and physics." *Fusion Engineering and Design*, vol. 88, no. 68, pp. 428 (2013). Proceedings of the 27th Symposium On Fusion Technology (SOFT-27); Lige, Belgium, September 24-28, 2012.

[17] V. Erckmann, W. Kasparek, B. Plaum et al. "Large Scale CW ECRH Systems: Meeting a Challenge." *AIP Conference Proceedings*, vol. 1406, no. 1, pp. 165 (2011).

[18] F. Warmer, S. Torrisi, C. D. Beidler et al. "Systems Code Analysis of HELIAS-type Fusion Reactor and Economic Comparison to Tokamaks." *accepted by IEEE Transactions on Plasma Science* (2016).

[19] T. Eich, B. Sieglin, A. Scarabosio et al. "Empiricial scaling of inter-ELM power widths in ASDEX Upgrade and JET." *Journal of Nuclear Materials*, vol. 438, p. S72 (2013).

[20] K. Lackner. "Figures of merit for divertor similarity." *Comments on Plasma Physics and Controlled Fusion*, vol. 15, no. 6, pp. 359 (1994).

[21] A. Kallenbach, M. Bernert, R. Dux et al. "Impurity seeding for tokamak power exhaust: from present devices via ITER to DEMO." *Plasma Physics and Controlled Fusion*, vol. 55, no. 12, p. 124041 (2013).

[22] H. Renner, J. Boscary, H. Greuner et al. "Divertor concept for the W7-X stellarator and mode of operation." *Plasma Physics and Controlled Fusion*, vol. 44, no. 6, p. 1005 (2002).

[23] Y. Feng. "Up-scaling the island divertor along the W7-stellarator line." *Journal of Nuclear Materials*, vol. 438, p. S497 (2013).

[24] G. Kalinin, V. Barabash, A. Cardella et al. "Assessment and selection of materials for {ITER} in-vessel components." *Journal of Nuclear Materials*, vol. 283-287, Part 1, pp. 10 (2000). 9th Int. Conf. on Fusion Reactor Materials.

[25] D. Maisonnier, D. Campbell, I. Cook et al. "Power plant conceptual studies in Europe." *Nuclear Fusion*, vol. 47, p. 1524 (2007).

[26] P. Pereslavtsev, L. Lu, U. Fischer et al. "Neutronic analyses of the {HCPB} {DEMO} reactor using a consistent integral approach." *Fusion Engineering and Design*, vol. 89, no. 910, pp. 1979 (2014). Proceedings of the 11th International Symposium on Fusion Nuclear Technology-11 (ISFNT-11) Barcelona, Spain, 15-20 September, 2013.

[27] R. Wolf. "A stellarator reactor based on the optimization criteria of Wendelstein 7-X." *Fusion Engineering and Design*, vol. 83, no. 79, pp. 990 (2008). Proceedings of the Eight International Symposium of Fusion Nuclear TechnologyISFNT-8 {SI}.

[28] H. Maaßberg, C. D. Beidler and E. E. Simmet. "Density control problems in large stellarators with neoclassical transport." *Plasma Physics and Controlled Fusion*, vol. 41, p. 1135 (1999).

[29] K. McCormick, P. Grigull, R. Burhenn et al. "New Advanced Operational Regime on the W7-AS Stellarator." *Phys. Rev. Lett.*, vol. 89, p. 015001 (2002).

[30] J. Ongena, A. Messiaen, D. Van Eester et al. "Study and design of the ion cyclotron resonance heating system for the stellarator Wendelstein 7-X." *Physics of Plasmas*, vol. 21, no. 6, 061514 (2014).

[31] J. M. Faustin and et al. "ICRH induced particle losses in Wendelstein 7-X." *Plasma Physics and Controlled Fusion* (2016).

[32] M. Drevlak and et al. "Stellarator Optimisation with ROSE." *20th International Stellarator-Heliotron Workshop*, pp. P2S5–54 (2016).

[33] J. H. E. Proll, P. Helander, J. W. Connor et al. "Resilience of Quasi-Isodynamic Stellarators against Trapped-Particle Instabilities." *Physical Review Letters*, vol. 108, p. 245002 (2012).

[34] P. Xanthopoulos, F. Merz, T. Görler et al. "Nonlinear Gyrokinetic Simulations of Ion-Temperature-Gradient Turbulence for the Optimized Wendelstein 7-X Stellarator." *Physical Review Letters*, vol. 99, p. 035002 (2007).

[35] P. Xanthopoulos, H. Mynick, P. Helander et al. "Controlling Turbulence in Present and Future Stellarators." *Physical Review Letters*, vol. 113, p. 155001 (2014).

[36] T. C. Luce, C. C. Petty and J. G. Cordey. "Application of dimensionless parameter scaling techniques to the design and interpretation of magnetic fusion experiments." *Plasma Physics and Controlled Fusion*, vol. 50, no. 4, p. 043001 (2008).

[37] B. B. Kadomtsev. "Tokamaks and dimensional analysis." *Soviet Journal of Plasma Physics*, vol. 1, p. 295 (1975).

[38] J. W. Connor and J. B. Taylor. "Scaling Laws for Plasma Confinement." *Nuclear Fusion*, vol. 17, p. 1047 (1977).

[39] K. Lackner. "Dimensionless engineering variables for measuring the iter and reactor relevance of tokamak experiments." *Fusion Science and Technology*, vol. 54, p. 989 (2008).

[40] H. Yamada, J. H. Harris, A. Dinklage et al. "Characterization of energy confinement in net-current free plasmas using the extended International Stellarator Database." *Nuclear Fusion*, vol. 45, p. 1684 (2005).

[41] H. Yamada, A. Komori, N. Ohyabu et al. "Configuration flexibility and extended regimes in Large Helical Device." *Plasma Physics and Controlled Fusion*, vol. 43, no. 12A, p. A55 (2001).

[42] M. Greenwald. "Density limits in toroidal plasmas." *Plasma Physics and Controlled Fusion*, vol. 44, no. 8, p. R27 (2002).

[43] F. Warmer, C. Beidler, A. Dinklage et al. "Limits of Confinement Enhancement for Stellarators." *Fusion Science and Technology*, vol. 68, p. 727 (2015).

[44] F. Warmer, C. D. Beidler, A. Dinklage et al. "HELIAS Module Development for Systems Codes." *Fusion Engineering and Design*, vol. 91, p. 60 (2014).

[45] M. Kovari, R. Kemp, H. Lux et al. "PROCESS: A systems code for fusion power plants - Part 1: Physics." *Fusion Engineering and Design*, vol. 89, p. 3054 (2014).

[46] F. Warmer, C. D. Beidler, A. Dinklage et al. "Implementation and Verification of a HELIAS module for the Systems Code PROCESS." *Fusion Engineering and Design*, vol. 98-99, p. 2227 (2014).

[47] T. Goto, J. Miyazawa, H. Tamura et al. "Design Window Analysis

1380 for the Helical DEMO Reactor FFHR-d1." *Plasma and Fusion Research: Regular Articles*, vol. 7, p. 2405084 (2012).

[48] Y. Turkin, C. D. Beidler, H. Maaßberg et al. "Neoclassical transport simulations for stellarators." *Physics of Plasmas*, vol. 18, p. 022505 (2011).

[49] A. R. Raffray, L. El-Guebaly, S. Malang et al. "Engineering Design and Analysis of the ARIES-CS Power Plant." *Fusion Science and Technology*, vol. 54, p. 725 (2008).

[50] M. Tillack, P. Humrickhouse, S. Malang et al. "The use of water in a fusion power core." *Fusion Engineering and Design*, vol. 91, no. 0, pp. 52 (2015).

[51] H. Zohm, C. Angioni, E. Fable et al. "On the physics guidelines for a tokamak DEMO." *Nuclear Fusion*, vol. 53, p. 073019 (2013).

[52] S. Torrisi and F. Warmer. "Design of an N-Dimensional Parameter Scanner for the Systems Code PROCESS." Tech. Rep. Report No. 13/23, Max-Planck-Institute for Plasma Physics (2014).

[53] A. Weller, J. Geiger, A. Werner et al. "Experiments close to the beta-limit in W7-AS." *Plasma Physics and Controlled Fusion*, vol. 45, no. 12A, p. A285 (2003).

[54] M. Drevlak, D. Monticello and A. Reiman. "PIES free boundary stellarator equilibria with improved initial conditions." *Nuclear Fusion*, vol. 45, p. 731 (2005).

[55] P. Helander, T. Bird, F. Jenko et al. "Advances in stellarator gyrokinetics." *Nuclear Fusion*, vol. 55, no. 5, p. 053030 (2015).

[56] Y. Turkin, H. Maaßberg, C. D. Beidler et al. "Current Control by ECCD for W7-X." *Fusion Science and Technology*, vol. 50, p. 387 (2006).

[57] W. I. van Rij and S. P. Hirshman. "Variational bounds for transport coefficients in threedimensional toroidal plasmas." *Phyiscs of Fluids B: Physics of Plasmas*, vol. 1, p. 563 (1989).

[58] S. P. Hirshman, K. C. Shaing, W. I. van Rij et al. "Plasma transport coefficients for nonsymmetric toroidal confinement systems." *Physics of Fluids*, vol. 29, p. 2951 (1986).

[59] H. Maaßberg, R. Brakel, R. Burhenn et al. "Transport in stellarators." *Plasma Physics and Controlled Fusion*, vol. 35, p. B319 (1993).

[60] U. Stroth. "A comparative study of transport in stellarators and tokamaks." *Plasma Physics and Controlled Fusion*, vol. 40, p. 9 (1998).

[61] F. Warmer, P. Xanthopoulos, C. Beidler et al. "On the Characterisation of the Edge Ion Heat-Flux in Advanced Stellarators." *submitted to Nuclear Fusion* (2016).

[62] S. Hermsmeyer, B. Dolensky, J. Fiek et al. "Revision of the EU helium cooled pebble bed blanket for DEMO." In "20th IEEE/NPSS Symposium on Fusion Engineering," (2003).

[63] U. Fischer, P. Pereslavtsev and S. Hermsmeyer. "Neutronic design optimisation of modular {HCPB} blankets for fusion power reactors." *Fusion Engineering and Design*, vol. 75-79, pp. 751 (2005). Proceedings of the 23rd Symposium of Fusion TechnologySOFT 23.

[64] C. Bustreo, G. Casini, G. Zollino et al. "FRESCO, a simplified code for cost analysis of fusion power plants." *Fusion Engineering and Design*, vol. 88, no. 12, pp. 3141 (2013).

[65] B. J. Green. "ITER: burning plasma physics experiment." *Plasma Physics and Controlled Fusion*, vol. 45, p. 687 (2003).

[66] I. Organisation. "Frequently Asked Questions." (2016).

[67] M. Ni, Y. Wang, B. Yuan et al. "Tritium supply assessment for {ITER} and {DEMOnstration} power plant." *Fusion Engineering and Design*, vol. 88, no. 910, pp. 2422 (2013). Proceedings of the 27th Symposium On Fusion Technology (SOFT-27); Lige, Belgium, September 24-28, 2012.

[68] http://www.brucepower.com/amended-agreement-secures-bruce-power-role-in-long-term-energy-plan/ (19.01.2016).

16

132

Neutronics source modeling for stellarator power reactors of the HELIAS-type

André Häußler[1], Ulrich Fischer[1], Felix Warmer[2]

[1]Karlsruhe Institute of Technology (KIT), Institute for Neutron Physics and Reactor Technology (INR)

[2]Max Planck Institute for Plasma Physics (IPP), Greifswald

1. Introduction

Different magnetic confinement concepts are currently considered for a future fusion power reactor. Two major concepts are the tokamak and the stellarator, which both use magnetic fields to confine hot plasma inside a torus in which the fusion reactions take place.

In a tokamak reactor, like ITER [1], the main magnetic field is provided by identical shaped planar toroidal field coils. This results in an elliptic-axisymmetric plasma shape and azimuthally symmetric reactor geometry. In order to confine the plasma, a helical magnetic field is required to overcome basic drifts. This is achieved by inducing a current in the plasma which generates a poloidal magnetic field. The tokamak reactor thus needs to be operated in pulsed mode, unless a large amount of external power is spent to drive a current continuously.

The plasma in a stellarator is confined by a steady state magnetic field, which is generated by several specifically designed, non-planar field coils. Thus no current needs to be induced in the plasma. Due to the usage of non-planar coils, the reactor has a discrete rotational symmetry that is given by the number of field periods.

The Helical-Axis Advanced Stellarator (HELIAS) is a design study for a five-periodic stellarator reactor at the Max Planck Institute for Plasma Physics (IPP) in Greifswald [2]. Helias-5B is a specific design of the HELIAS concept which will be operated with a Deuterium-Tritium fusion reaction and is designed for a fusion power of 3000 MW [2].
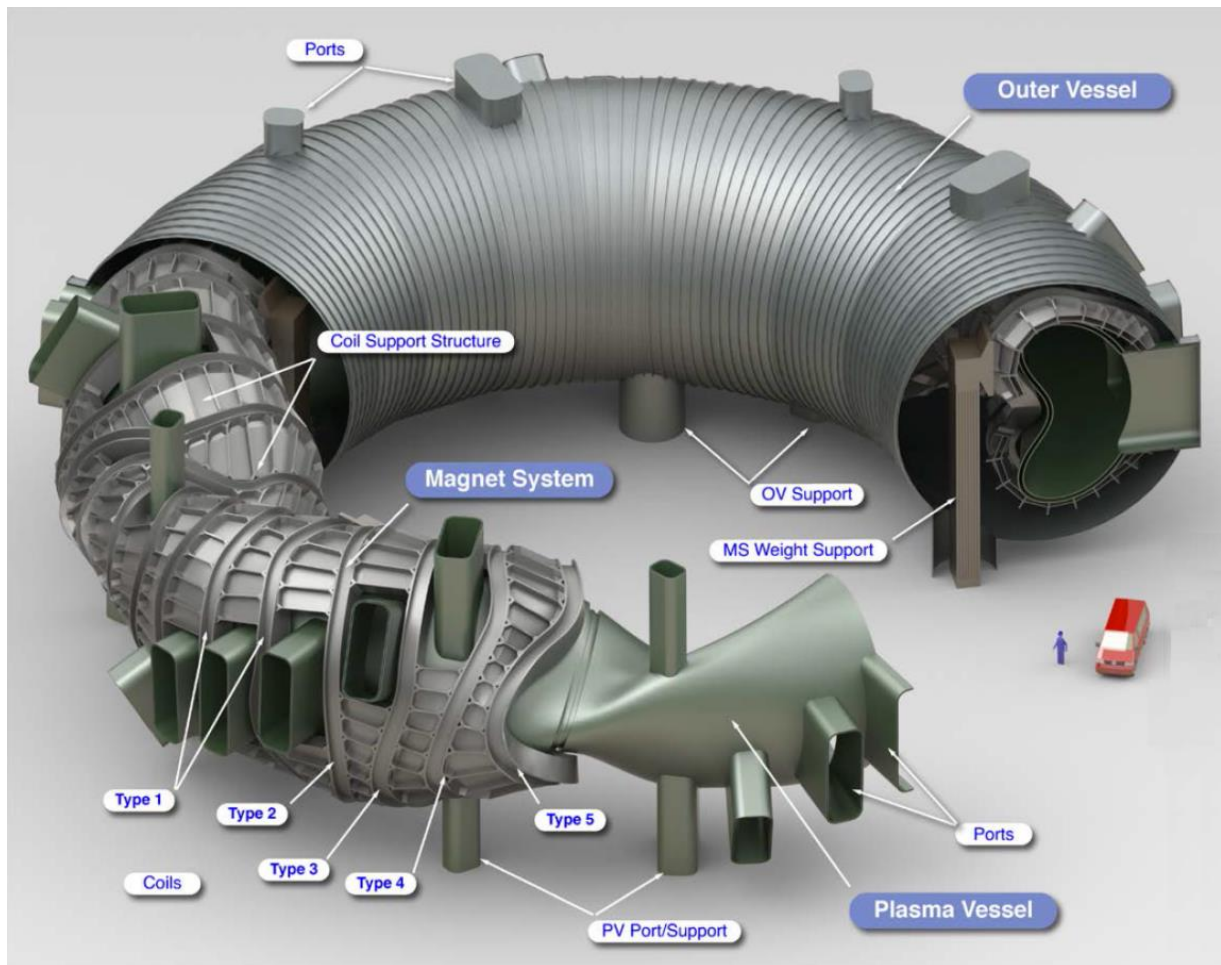
Figure 1: 3-D view of the Helias-5B power reactor [2]

Figure 1 show a 3-D view of Helias-5B with the plasma vessel surrounded by the magnet system and the outer vessel. The non-planar field coils and the resulting 3-D shape of the plasma vessel can be seen as well. The reactor has a major radius of 22 m and a plasma volume of 1400 m^3. Compared to ITER tokamak, it has six times larger fusion power, 3.5 times larger major radius and roughly two times larger plasma volume [2].

2. Neutron Source development

The predominant fusion reaction in Helias-5B is the Deuterium-Tritium (DT) reaction, which produces a Helium nucleus and a neutron with energy of approximately 14.1 MeV:

$$^2_1H + \,^3_1H \rightarrow \,^4_2He + \,^1_0n$$
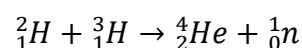
Neutrons produced in the fusion reaction are not trapped by the magnetic field, they escape from the plasma chamber and interact with the atomic nuclei of the surrounding components. Due to the non-planar shaped field coils, these components are of high complexity and present a challenging task for neutronics calculations.

The objective of neutronics calculations is to provide the distribution of the neutrons in space and energy and, based on this distribution, calculate the nuclear responses

of interest in the reactor components. To this end, the geometry and the neutron source need to be represented in the neutronic calculation as accurately as possible. The Monte Carlo method tracks particles on a microscopic level and is well suited to solve the problem for a complex geometry. In this work the Monte Carlo n-particle (MCNP) code is used [3].

The primary distribution of the DT source neutrons is provided with a plasma physics simulation using a transport code [4] to obtain the density and temperature profiles. As these quantities are assumed to be constant on flux surfaces, the neutron emission rate can be calculated using a field representation from the VMEC code [5]. The result of the calculation is a volumetric 3-D distribution of the neutron emission rate density, which is constant on each individual flux-surface. To obtain the neutron emission rate, the density is integrated over the flux-surface coordinates, which are the poloidal angle, the toroidal angle and the flux-surface label [5]. This yields a spatial 3-D distribution of the emission rate with a constant value in each element. The corresponding neutron emission probability within an element is related to a source data point representing this element. The resulting data is stored in tabular form in a file which contains more than 2×10^6 3-D source points, but can be adjusted to required accuracy.
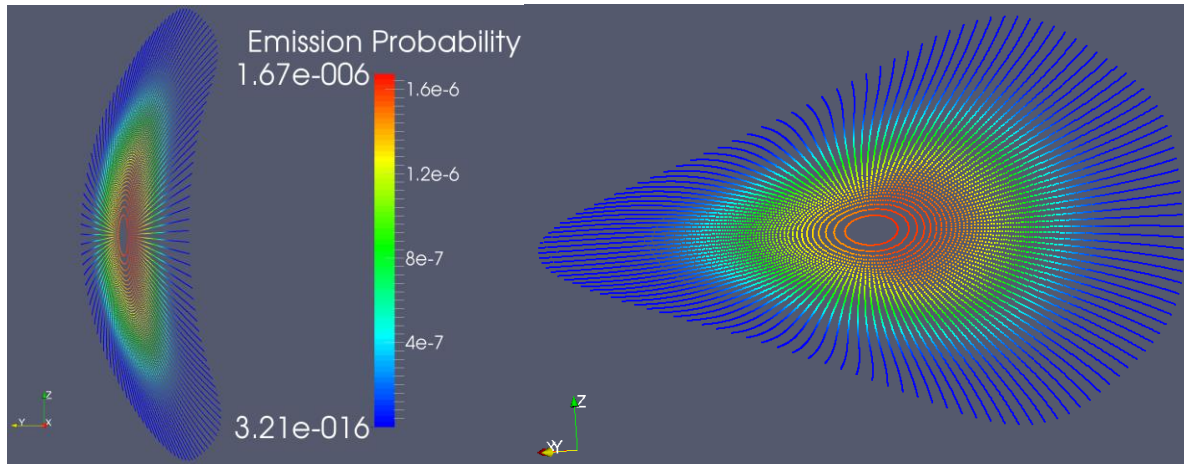

Figure 2: Emission Probability of the source perpendicular to the main axis

Figure 2 shows the source points and emission probabilities in two different vertical cuts through the plasma. On the left is the "bean" shaped and on the right is the "triangular" shaped plasma cut, both represent the extrema of the plasma variation. The neutron emission probabilities, which vary over ten orders of magnitude from 10^{-6} to 10^{-16}, are normalized to the accumulated probability of 1.

MCNP requires a source description to perform a calculation, which can be provided to the code in different ways. A straightforward way is to utilize the standard source definition in the MCNP input file for the problem calculation. Another way is to write a user specific source subroutine in Fortran90 and compile it with the MCNP source code. In both cases it is required to give source specifications like particle type, starting point, energy and weighting of the particle. Additionally information like angular distributions or emission probabilities can also be specified in the source description.

In this paper the second approach was adopted, because the plasma distribution in the stellarator reactor is too complex to be defined as a standard source definition in MCNP. The user specific source subroutine reads and processed the external stored data from plasma physics calculation. For the source point sampling procedure, the cumulative probability (CP) of the emission probability is calculated and every value

of the CP is associated to its corresponding source point. This approach allows sampling the source position through the CP. Every CP can be seen as a specific bin for one source point. A larger CP conducts to a larger bin width for one specific point and to a higher sampling frequency of regions with a higher emission probability.
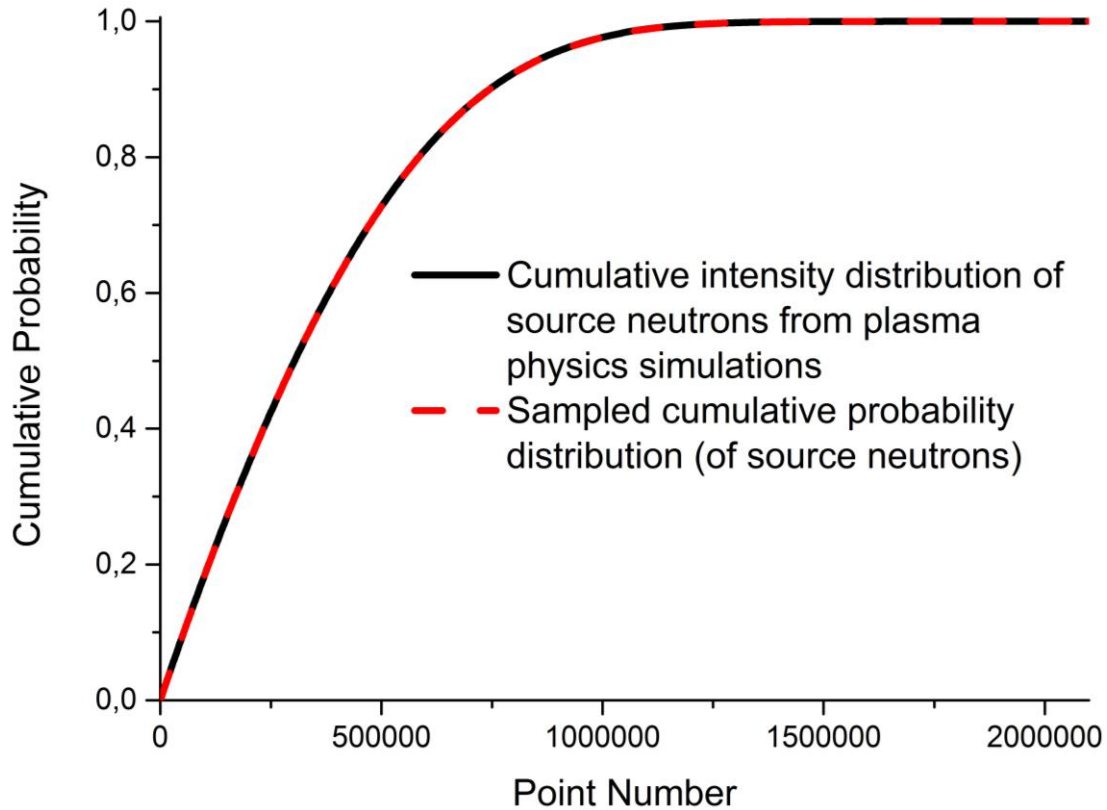
Figure 3: Cumulative probability for the neutron emission in Helias-5B: plasma physics simulation vs. source sampling algorithm.

Figure 3 compares the CP for the emission of source neutrons in Helias-5B as obtained from the emission rates provided with the plasma physics calculation and represented with the developed sampling algorithm in a Fortran90 program for the source subroutine. It is shown that both graphs fit perfectly to each other. The CP distribution as represented with the sampling algorithm is thus verified and can be used with confidence in the source subroutine and neutronics calculations for Helias-5B.
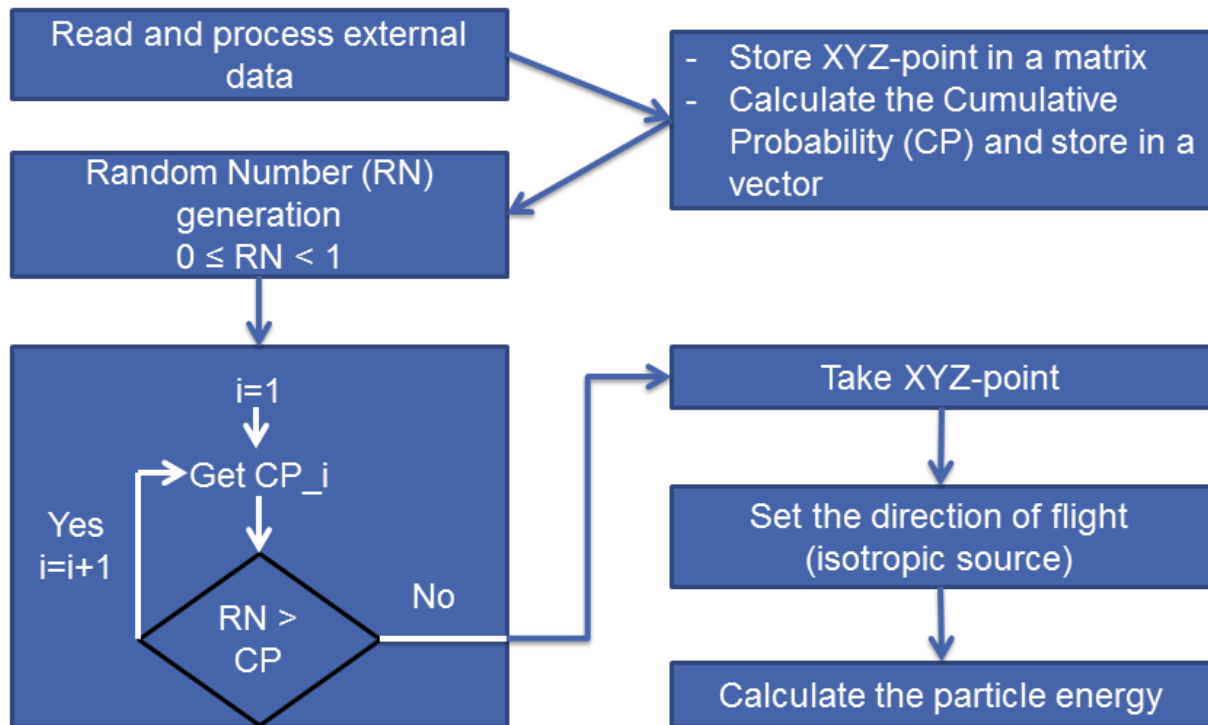
Figure 4: Schematic representation of the neutron source sampling implemented in the user specific MCNP source subroutine for 3-D stellarator specific geometry

In Figure 4 a schematic representation of the source sampling algorithm is shown implemented in the user specific source subroutine for Helias-5B. The external data is the result of the plasma physics calculation, which are read and processed. During the processing step, the source points are stored in the computer memory and the emission rates of the original data is processed into a CP and is stored in the memory as well. This procedure is carried out only once and the data is stored in the memory for the whole execution of the neutronics calculation. All following steps are repeated for every emitted neutron.

At the beginning, a random number (RN) is generated in MCNP. This generated RN can be used to find the CP and the corresponding source point. As shown in Figure 4, a sequential search is represented in the flow chart. The control variable "i" is set equal to 1 at the beginning and the search algorithm starts. If the RN at position i of the CP is greater, i will be increased by 1 and the search loop repeats again. This loop runs until a CP is found which is smaller than the RN, then i is used to fetch the corresponding source point in the computer memory. The sequential search algorithm illustrated in Figure 4 was not implemented in the source subroutine due to its slow searching speed. Instead, the binary search algorithm was implemented. A comparison between sequential search and binary search was carried out in order to verify the applicability of the binary search. Based on the same RN generator and the same input data, identical results were produced and the analysis shows that the binary search is approximately 22 times faster than the sequential search.

A source point obtained by this procedure is used as a starting point for a neutron. The direction of flight is set automatically by MCNP assuming an isotropic distribution of the neutron emission at every source point. Finally, the initial neutron energy is calculated and the transport calculation for the sampled neutron is performed.

3. Verification of MCNP source subroutine

The developed MCNP source subroutine needs to be tested and verified before it can be used for neutronics calculations. The test has to show agreement of the normalized frequency of source point sampling in MCNP and the emission probabilities as given by the plasma physics calculation.

For the test, a simple void geometry was used to cover the whole plasma area. To obtain the sampling frequency on each source point, the capability of MCNP in recording the emission point of a particle was utilized. 10^9 particles were sampled and their emission points were detected, which were preserved in a MCNP output file with a data size of ~115 Gigabyte. To carry out the comparison, the sampling frequency of each emission point is processed from the file and divided by the total number of sampled particles. This value will be named as emission frequency.
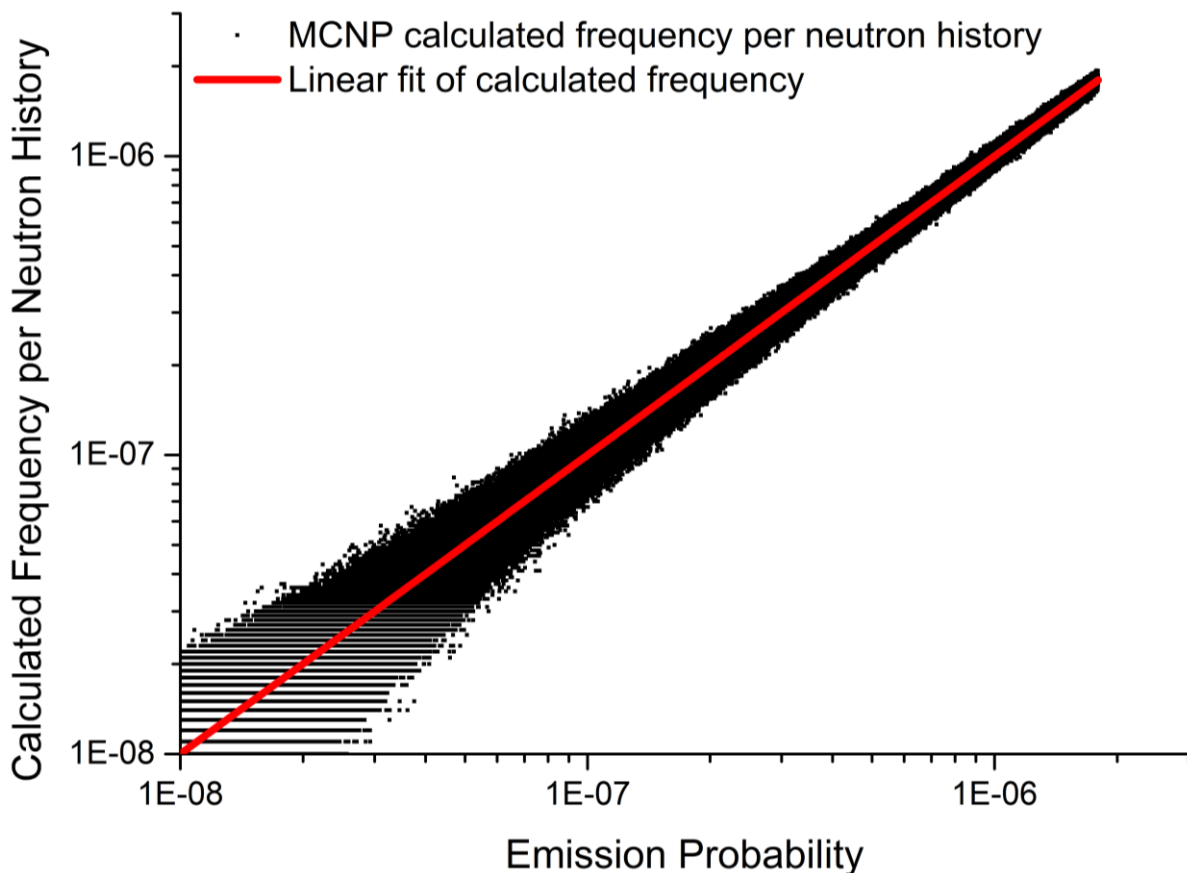
Figure 5: Calculated frequency of the source positions compared with the original emission probability

In Figure 5, the MCNP calculated frequency per neutron history (emission frequency) is plotted against the emission probability of the original data. The emission frequency is an integer value of $n/Number\ of\ sampled\ Particles$, where n is the number of hits (frequency) of one source point. This results in discrete steps that are visible in the low frequency region.

Additional, a linear fit of the emission frequency is also shown in the diagram. The gradient of the linear fit is $0.99997 \pm 2.4 \times 10^{-5}$. The linear fit confirms the expectations of equality between the emission frequency and the original emission probabilities.

138

This test was performed for two MCNP versions (MCNP5 1.60 and MCNP6 1.0 [6]). Both versions should later be used in neutronics calculations to benefit from the broad spectrum of tools developed for MCNP5 and from new geometry modelling features of MCNP6.

For the test, the same random number generator with the same random number seed was used in both runs, and the produced output files are identical. This means that the user specific source subroutine can be used both in MCNP5 and MCNP6 for upcoming neutron transport calculations.

4. Conclusion

The complex 3-D fusion plasma of the Helias-5B power reactor, as provided with a plasma physics calculation, can be represented in a dedicated source subroutine for MCNP and thus used in neutronics Monte Carlo calculations.

Several tests were performed to verify that this user specific source subroutine can accurately represent the neutron source. First, the cumulative probability as generated from the plasma physics data and from the source sampling algorithm was compared and shown to fit perfectly. Second, the source sampling subroutine was verified by comparing sampled frequencies of source points to the plasma physics calculation results.

In summary, the method developed for the neutron source simulation of Helias-5B in MCNP has successfully been tested and verified against plasma physics calculation results. The neutron source can be thus used with confidence for the design analysis of Helias-5B.

Acknowledgement

Reference

[1]	B.J. Green, ITER: burning plasma physics experiment, Plasma Phys. Control. Fusion 45 (2003), 687-706
[2]	F. Schauer, et al., HELIAS 5-B magnet system structure and maintenance concept, Fus. Eng. Des. 88 (2013), 1619-1622
[3]	X-5 Monte Carlo Team, MCNP - Version 5, Vol. I: Overview and Theory, LA-UR-03-1987 (2003)
[4]	Y. Turkin, et. al., Neoclassical transport simulations for stellarators, Physics of Plasma 18, 022505 (2011)
[5]	F. Warmer and U. Fischer, internal EUROfusion Report (unpublished) (2014)
[6]	T. Goorley, et al., Initial MCNP6 Release Overview, Nuclear Technology, 180, pp 298-315 (Dec 2012)

Wendelstein 7-X Programme – Demonstration of a Stellarator Option for Fusion Energy –

R. C. Wolf, C. D. Beidler, A. Dinklage, P. Helander, H. P. Laqua, F. Schauer, T. Sunn Pedersen, F. Warmer
and the Wendelstein 7-X Team[1]
Max-Planck-Institut für Plasmaphysik
17491 Greifswald, Germany
robert.wolf@ipp.mpg.de

Abstract—**The superconducting stellarator Wendelstein 7-X is currently being commissioned. First plasmas are expected for the second half of 2015. W7-X is designed to overcome the main drawbacks of the stellarator concept and simultaneously demonstrate its intrinsic advantages relative to the tokamak – i.e. steady-state operation without the requirement of current drive or stability control. An elaborate optimization procedure was used to avoid excessive neoclassical transport losses at high plasma temperature, simultaneous to achieving satisfactory equilibrium and stability properties at high β, and a viable divertor concept. In addition, fast-ion confinement must be consistent with the requirements of alpha-heating in a power plant. Plasma operation of Wendelstein 7-X follows a staged approach following the successive completion of the in-vessel components. The main objective of Wendelstein 7-X is the demonstration of steady-state plasma at fusion relevant plasma parameters. Wendelstein 7-X will address major questions for the extrapolation of the concept to a power plant. These include divertor operation at high densities, plasma fuelling at high central temperatures, avoiding impurity accumulation, an assessment of the effect of neoclassical optimization on turbulent transport and fast-ion confinement. A power plant concept based on an extrapolation from Wendelstein 7-X, the Helical Advanced Stellarator (HELIAS), has been developed.**

Keywords—stellarator, steady-state magnetic confinement, fusion power plant

I. INTRODUCTION

Magnetic confinement in stellarators can be provided without a toroidal plasma current. A rotational transform is generated by magnetic field coils only. This has several advantages [1]: (1) Steady-state confinement is provided without any current drive. Compared to a tokamak, this should significantly reduce the re-circulating power in a stellarator power plant. (2) Current driven instabilities and disruptions do not occur. Even if a significant bootstrap current is generated the negative magnetic shear prevents the destabilization of neoclassical tearing modes [2]. As result, elaborate stability control is not required. (3) Without strong toroidal plasma currents the Greenwald density limit is not observed and – at a given fusion power – the alpha-particle pressure and the drive for fast-ion driven instabilities is reduced. As a consequence densities far beyond an equivalent Greenwald limit have been observed [3, 4]. However, stellarator confinement also has

several disadvantages. Generally, the coil configuration is more complicated. Generating the rotational transform by external coils breaks the toroidal symmetry. As a result, sufficient confinement of the thermal plasma and fast ions for a fusion reactor is not automatically reached. The neoclassical transport in the 1/ν -regime at low collisionality [5],

$$\chi_{1/\nu} \propto \varepsilon_{eff}^{3/2} T^{7/2}/(nR_0^2 B_0^2), \qquad (1)$$

shows a very strong dependence on the plasma temperature, T (R_0 is the major radius of the device, B_0 the magnetic field on axis and n the plasma density). To avoid an unacceptable increase of the plasma transport at reactor relevant temperatures, a minimization of the effective ripple, ε_{eff}, in the design of a stellarator is mandatory. From equation (1) it also becomes clear that confinement benefits from high density and low temperature. Other optimization criteria for stellarators are the fast-ion confinement, plasma stability at high normalized pressure, β, a plasma equilibrium which does not deteriorate with increasing β, and – as a prerequisite for steady-state operation – a feasible exhaust concept. With regard to fast-ion confinement, the ability to operate at high density is a positive feature of the stellarator, as it keeps the fast ion population low.

From the technological point of view it is important to find a coil configuration that is capable of producing a magnetic field simultaneously fulfilling these criteria. A technical solution to generate such magnetic field configurations are modular coils [6]. Finally, a reactor or power plant requires sufficient space for a breeding-blanket between coils and plasma. This is a major constraint for a fusion power plant design.

II. WENDELSTEIN 7-X DESIGN

Wendelstein 7-X (W7-X) is a drift-optimized stellarator with improved neoclassical confinement [7]. An effective ripple, ε_{eff}, of about 1% at all plasma radii ensures that the neoclassical plasma transport, even at higher temperatures, remains sufficiently low. Improved fast-ion confinement is provided by a quasi-isodynamic configuration, requiring high β to achieve improved confinement.

The basic philosophy of the W7-X equilibrium is to decouple the plasma equilibrium and plasma β as far as possible. This is achieved by minimizing bootstrap and Pfirsch-Schlüter currents. As a result the Shafranov-shift and the

changes of the rotational transform profile, *ɨ(r)*, remain small when β is increased. The latter is closely linked to the exhaust concept. Establishing low magnetic shear with *ɨ* = 1 at the plasma edge, large magnetic islands intersected by target plates serve as a divertor (so-called magnetic island divertor). The first magnetic island divertor was successfully tested in Wendelstein 7-AS [8]. One important characteristic is the very large target-to-target connection length of the open magnetic field lines in the scrape-off layer. Compared for instance to the poloidal divertor in ASDEX Upgrade, which has a connection length of about 50 m, the connection lengths in W7-X amount to about 300 m [9]. This should have a profound effect on the heat flux distribution on the divertor target plates [10].
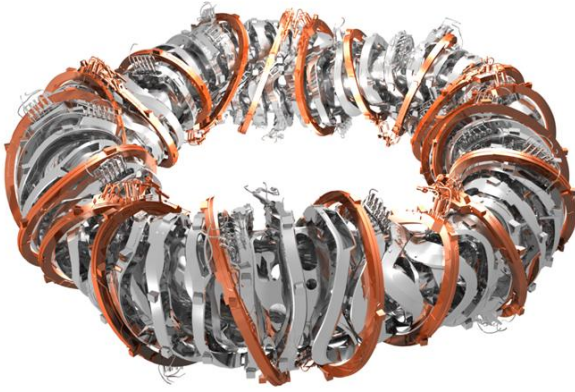

Fig. 1: Technical drawing of the W7-X magnetic field coils surrounding the plasma vessel. 50 non-planar coils (grey) and 20 planar coils (copper-coloured) produce the confining magnetic field and can be used to change the rotational transform and the radial position of the plasma.

W7-X has been designed for steady-state plasma operation. For this purpose superconducting coils are employed. The actively cooled plasma-facing components are designed for heat fluxes between 100 kW/m^2 (water cooled stainless steel panels), 1 MW/m^2 (water cooled CuCrZr heat sinks covered with graphite tiles), and 10 MW/m^2 divertor targets (water cooled CuCrZr heat sinks covered with carbon fibre composite, CFC). A newly developed electron-cyclotron-resonance heating (ECRH) system provides up to 9 MW steady-state heating power at 140 GHz corresponding to second harmonic heating at 2.5 T. Limited by the overall cooling capability of the water cooling plant, 10 MW plasmas will be restricted to about 30 minutes pulse duration. Compared to present day devices this is a significant step forward in steady-state plasma operation. All plasma time scales lie far below 30 minutes – confinement time and fast-ion slowing down time are below one second; and the L/R time is at most about 100 seconds.

The magnetic field configuration of W7-X is generated by 70 super-conducting coils [11] (figure 1). Five essentially identical magnetic field modules form the toroidal coil arrangement. 50 non-planar coils (10 in each module) generate both toroidal and poloidal components of the magnetic field. 20 planar coils (4 in each module) are arranged in such a way that they produce vertical and toroidal magnetic field components. The vertical magnetic field can be used to change the radial position of the plasma, while the toroidal component

modifies the rotational transform. Inside the plasma vessel 10 normally conducting saddle coils have been installed to provide divertor strike-point sweeping. Outside the cryostat vessel, providing the cryogenic vacuum for the super-conducting coils, 5 normally conducting trim coils can be used to correct low-order error fields or otherwise modify the control magnetic field components [12].

Year Name of operational period (Duration)	Plasma configuration Plasma species Plasma characteristics	Available heating power and heating systems Predicted plasma temperatures, densities and β-values
2015 OP 1.1 (13 weeks)	Limiter configuration He and H plasmas Pulse limit ∫ P dt ≤ 2 MJ τ_{pulse} ~ 1 s at 1 MW	P ≤ 5 MW (ECRH) T_e (T_i) < 3 (1) keV n < 0.2 x 10^{20} m^{-3} β < 1.6 %
2016 / 17 OP 1.2 (60 weeks)	Uncooled divertor configuration (test divertor unit, TDU) H plasmas Pulse limit ∫ P dt ≤ 80 MJ τ_{pulse} ~ 10 s at 8 MW, (up to 60 s at reduced power)	P ≤ 10 MW (ECRH, NBI, ICRH) T_e, T_i < 3 keV n < 1.2 x 10^{20} m^{-3} β < 3 %
> 2019 OP 2 ...	Steady-state operation Actively cooled HHF divertor H and D plasmas Divertor cryo-pump Heat flux limit P/A ≤ 10 MW/m^2 Technical limit τ_{pulse} ≤ 30 minutes at 10 MW	P_{cw} ~9 MW (ECRH) P_{pulse} ~10 MW (NBI, ICRH, pulse length ~ 10 s) T_e, T_i < 5 keV n < 2.4 x 10^{20} m^{-3} β < 5 %

Tab.1. Scientific programme of W7-X and corresponding technical capabilities and plasma characteristics towards steady-state operation. Temperatures, densities and β-values are estimates provided by transport calculations, assuming neoclassical transport in the core of the plasma and turbulent transport at the plasma edge. In this sense, the β-values are upper limits.

W7-X has a major radius of R_0 = 5.5m and an effective minor radius of $<a>$ = 0.55 m. The resulting plasma volume is 30 m^3. The maximum magnetic field strength on axis is 3 T, corresponding to a magnetic field energy of approximately 600 MJ. The nominal field, which is the reference for second harmonic ECRH, is 2.5 T. The total mass of the device amounts to 725 t. Including magnetic field coils and the support structure the cold mass is 423 t. The super-conductor is made of NbTi operating at 4 K to produce the field values mentioned above.

III. APPROACH TO STEADY-STATE OPERATION

The experimental capabilities of W7-X and the corresponding scientific programme of W7-X are defined by the progress of the completion of the in-vessel components. Table 1 summarizes these capabilities and gives approximate values for the predicted plasma parameters. Accordingly, the programme of W7-X until 2019, when the full steady-state capability is reached, is subdivided into distinct operational campaigns (OP).

A. First plasma (OP 1.1)

At present W7-X is being commissioned [13]. The first plasma is expected in the second half of 2015[2]. During the operational phase OP 1.1 up to 5 MW of ECRH power (at 140 GHz corresponding to 2.5 T) from six gyrotron tubes will be available. The plasma boundary will be defined by five in-board limiters, one in each module (figure 2a). Integrated heating power and pulse duration are limited by the passive cooling capacity of these limiters.

The primary goal of OP 1.1 is the integral plasma commissioning of W7-X including ECRH and diagnostics. The draft physics plan foresees flux surface measurements, ECRH wall conditioning and start-up optimization with helium, ECRH heated helium plasmas, first experience with hydrogen plasmas, and finally piggy-back experiments aiming at an even heat flux distribution between the five limiters, feed-forward density control and scrape-off layer physics. More detailed plans for OP 1.1 physics operation can be found in [14].

For OP 1.1 already six 140 GHz gyrotrons have been taken into operation delivering about 5 MW of heating power. The power transmission from the gyrotrons to the plasma relies on a quasi-optical system (through air) [15]. It is characterized by an easy accessibility for alignment and maintenance. The overall power loss is about 3-5%. Four front-steering launchers (with altogether 12 launch positions) in the outboard mid-plane of W7-X deliver the power to the plasma. Poloidal steering angles of ±25° and toroidal steering angles from −15° to +35° or from +15° to −35° can be used for changing the (vertical) deposition position or for current drive (toroidal launch). The frequency of 140 GHz corresponds to a central deposition at 2.5 T. The temperature and β-values given in table 1 are derived from 1-D transport calculations prescribing the density profile, calculating the ECRH power deposition profile, and assuming neoclassical transport in the core of the plasma and turbulent transport at the plasma edge [16, 17]. Since a possible
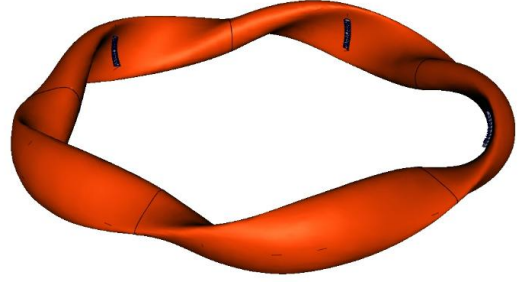
Fig. 2: Plasma contour (orange) with (a) 5 inboard limiters made of graphite (black stripes) defining the last closed flux surface. Fig. 2(b) shows the ten divertor units with the target plates following the topology of the resonant magnetic island divertor.

turbulent transport contribution in the plasma core is neglected these values can be regarded as upper limits.

B. First divertor operation (OP 1.2)

Between OP 1.1 and OP 1.2 the limiters will be removed and a test divertor unit (TDU) made of graphite will be installed. In addition, the installation of the graphite tiles inside the plasma vessel will be completed. The TDU already has the shape of the actively cooled high heat flux divertor (see figure 2(b)), which will be installed by 2019. Since the TDU relies only on passive cooling, the pulse duration will be limited to about 10 s at 8 MW of heating power. However, the design without any water-cooling is robust against heat-flux overloading. Carbon sublimation and a radiation collapse of the plasma would occur if excessive heat fluxes were to be present, but the divertor itself would remain functional. This serves the main goal of OP 1.2, which is the preparation of steady-state operation gaining operational experience with the island divertor and developing and testing suitable monitoring and protection schemes. This goal requires already moderately high plasma densities. Using ECRH, the focus will be on 2nd harmonic X-mode (X2) heating, because this scheme has a single pass absorption of effectively 100%. Thus, the X2 cut-off density of 1.2×10^{20} m^{-3} defines the upper limit of the density range of OP 1.2.

---

[2] First plasma was achieved on December 10th, 2015, and OP 1.1 has been successfully completed by March 10th, 2016.

For OP 1.2 the ECRH system will be extended from six to ten gyrotrons, extending its capability from about 5 to 9 MW. In addition two remote steering launchers (with two launch positions) will be installed [18]. Such launchers have very attractive properties for a fusion power plant. They have no movable parts near the plasma and exhibit a very high power density (~ 400 MW/m^2) requiring only little space to deliver high power levels. In W7-X their launch direction is from the high field side. As a result preferentially supra-thermal electrons will be heated, allowing the energy dependence of electron confinement to be studied, and also improving the current drive efficiency.

In addition to ECRH, neutral beam injection (NBI) [11] and ion-cyclotron-resonance heating (ICRH) [19] will become available. These heating systems will allow only pulsed operation with pulse durations of around 10 s. Applying NBI and ICRH, fast-ion populations can be generated, allowing first fast-ion confinement studies. Since the total heating power will be limited to about 10 MW (by the availability of power supplies), the achievable β-values will limit the exploitation of the quasi-isodynamic optimization and also the possibility to study β-limiting stability phenomena.

C. Devlepment of integrated steady-state plasmas (OP 2)

For OP2 and subsequent operational phases W7-X will have reached its full steady-state capability. The TDU will be replaced by the actively cooled high heat-flux (HHF) divertor. In addition, the water cooling of all plasma-facing components will be completed. Steady-state heating will be provided by ECRH. To reach plasma densities beyond the X2 cut-off ($n_e > 1.2\times10^{20}$ m^{-3}) second harmonic O-mode heating has to be applied. For this purpose the W7-X ECRH system has been equipped with dedicated polarization optics to change from X2 to O2 heating when the cut-off density is reached. Since single pass absorption of O2 heating, depending also on plasma temperature, is on the order of 80%, W7-X is equipped with special in-vessel mirrors to facilitate efficient multi-pass absorption. Plasma densities beyond the O2 cut-off ($n_e > 2.4\times10^{20}$ m^{-3}) will require Bernstein wave heating.

The main objective of W7-X will be development of an integrated steady-state scenario which demonstrates the reactor capability of the concept. This involves several aspects which combine the verification of the optimization criteria and issues not directly covered by the optimization such as density control and viable divertor performance:

Confinement and stability. A central task is the verification of the neoclassical confinement optimization. According to theoretical predictions β-values of 4% can be reached with 15 MW of heating power [16]. A very interesting question is how neoclassical optimization of ε_{eff} affects turbulent transport. 3D-calculations of ion temperature gradient (ITG) driven turbulence suggest a critical gradient similar to tokamaks, but with much reduced temperature profile stiffness [20, 21]. An interesting question, which the W7-X results will have to answer, is whether an H-mode transport barrier [22] at the plasma edge will be required to achieve sufficiently good confinement. Regarding MHD stability, W7-X plasmas are predicted to be stable against pressure driven modes up to

volume averaged β-values of $<\beta> \approx 5\%$ [23]. To investigate this, however, the most recent numerical predictions show that the upgrades of the heating power including power supplies must have been completed.

Fast ion confinement. With the availability of fast ion producing heating systems (NBI and ICRH), first fast ion studies can be started. However, to fully exploit the isodynamic effects on fast-ion confinement, β-values above 3% and the corresponding heating power to reach those β-values are required. Using NBI for fast-ion production has the intrinsic problem that with increasing density the NBI deposition moves to larger radii shifting the fast ion orbits into regions where they are less confined [24]. Because high β requires improved neoclassical confinement which in turn implies high density, NBI is not ideal to study fast-ion confinement. In contrast, the power deposition of ion-cyclotron minority heating is independent of the plasma density. However, at high plasma densities the production of a sufficiently large fast ion tail becomes more difficult. Here, dedicated studies are ongoing. A possibility to increase the efficiency of the ion-cyclotron resonance frequency absorption might be a new three-ion-species plasma heating scheme which has been recently proposed [25]. While the problem to produce a fast-ion tail makes the demonstration of fast-ion confinement difficult in W7-X, this high-density feature of effective thermalization of fast-ion populations is of course a desired effect in a power plant.

Density and impurity control. As elaborated above the full exploitation of the neoclassical confinement optimization (see equation (1)) requires high density. In addition, neoclassical transport predicts hollow density profiles, if the temperature profiles are sufficiently peaked [26, 27]. Therefore, a suitable fuelling scheme will have to be established. For this purpose, first pellet injection studies will be started in OP 1.2. To avoid hollow density profiles in plasmas of several keV central temperature steady-state high speed pellet injection might become necessary. Finally, strong density gradients in combination with good neoclassical confinement show a tendency of impurity accumulation [28]. At high density a negative electric field (ion-root confinement) is expected to cause impurity accumulation. This has in the past been avoided by suitable plasma scenarios such as the high density H-mode (HDH) discovered in Wendelstein 7-AS [29]. However, up to now a clear theoretical understanding of the HDH-mode is missing which makes it impossible to predict how it will scale to W7-X.

Establishing equilibria for high power divertor operation. For its primary mode of operation the W7-X magnetic island divertor requires $\iota = 1$ and low magnetic shear at the plasma boundary. The bootstrap current is not negligible for all magnetic field configurations, which can be realized in W7-X. A finite bootstrap current has the effect that the plasma equilibrium and thus the divertor configuration and in particular the strike point positions evolve during the initial phase of a plasma pulse (on the L/R time scale which is on the order of 30 s). To avoid undue heat fluxes on the edges of the divertor tiles, which are not designed for 10 MW/m^2, mitigation schemes have been proposed. These include a so-

called scraper element protecting these edges or electron cyclotron current drive [30, 31]. To test the mitigation schemes during OP 1.2., two of the ten divertor units will be equipped with such a scraper element. A possible upgrade for a later operational phase would be actively cooled scraper elements for the HHF divertor. Another issue, related to the divertor, is the balance between the power reaching the divertor target plates by heat conduction and convection and the radiated power fraction. In particular going to power levels above 10 MW safe divertor operation is expected to require a high radiated power fraction with at least partial detachment.
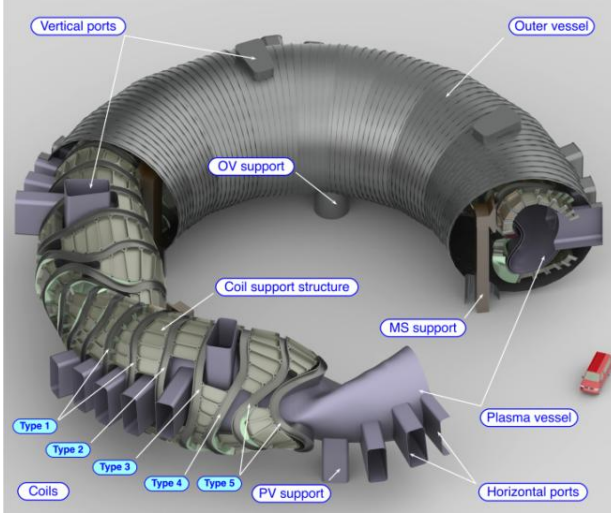

Fig. 3: Technical drawing of a HELIAS-5B power plant concept [*Schauer et al.*]. Shown are the plasma vessel, the five different coil types, the coil support structure, the magnet system support and the outer cryostat vessel. Horizontal and vertical ports are indicated to demonstrate that coils and coil support structure permit large-scale access to the plasma vessel.

An integrated steady-state plasma scenario that simultaneously addresses all these issues will have to be developed. Concerning reactor-relevant plasma facing materials an upgrade to an all-metal wall will become necessary at a later stage (after OP 2). For OP2 all plasma facing components are either made of stainless steel, amorphous carbon or CFC. This selection was chosen because experience with an all-metal wall in stellarators is missing and impurity accumulation has been an issue in previous experiments. A stepwise coverage with tungsten, similar to the approach realized in ASDEX Upgrade [32], is envisaged when sufficient experience with plasma-wall interaction and impurity transport has been gained with the OP2 first wall configuration.

Concerning further upgrades of the steady-state heating power, ECRH launchers, parts of the transmission optics and the gyrotron building already foresee two additional gyrotrons, increasing the number of microwave beams from 10 to 12. Combined with developing new gyrotrons, which, similar to the ITER gyrotrons, are designed for a power of 1.5 MW, this would increase the power level by almost a factor of two.

IV. EXTRAPOLATION TO A POWER PLANT

A direct extrapolation from W7-X to a power plant is the Helical Advanced Stellarator (HELIAS) [33, 34]. Recent studies focus on the HELIAS-5B [35, 36, 37] which like W7-X has fivefold symmetry (figure 3). The aspect ratio is similar as in W7-X, the major radius is 22 m and the average minor radius 1.8 m. The average magnetic field lies in the range of 5 to 6 T with a maximum at the coils ranging from 10 to 12 T. From the engineering point of view 6 T on axis seem feasible. However, to ease the requirements for the support structure and to save costs lower values are desirable. The size of the coils and the magnetic field are similar to the ITER values, enabling the use of the ITER coil technology [38] including the superconductor material and the magnetic field values. Bolted panels between the coils form the coil support structure [39]. For the further improvement of the fast-ion confinement stronger coil shaping might become necessary. Considering the space constraints, a possible solution could be a high temperature superconductor with a higher current density. Staying at the moderate magnetic field strength of such a stellarator, a conductor with a higher current density would result in a reduced cross-section of the coil. With regard to β no extrapolation is necessary from W7-X to the HELIAS-5B. Both are designed for $<\beta> \approx 5\%$. The fusion power is approximately 3 GW. For the blanket and shield 1.3 m between plasma and coils has been reserved. First studies of a maintenance concept indicate sufficient accessibility between the coils and the coils support structure [36]. Neutronic analysis and studies of the blanket concept have been started (in collaboration with the Karlsruhe Institute of Technology).

Considering that the HELIAS has the features of a power plant, an important question is how to bridge the gap from W7-X to such a power plant. Representing the Wendelstein line (W7-AS, W7-X and HELIAS) in dimensionless engineering parameters [40] as was done before for ITER-like tokamaks [41], it becomes clear that the gap from W7-X to a HELIAS might need to be bridged by a stellarator burning-plasma experiment. The main objective of such an experiment would be to demonstrate significant α-heating without undue α-losses, requiring a birth profile that is consistent with regions of good α-confinement. The final step to a commercial power plant would then rely on the parallel development of the tokamak line and in particular on the transfer of the technologies of a tokamak demonstration power plant (DEMO) to a HELIAS.

The decision to go forward with such an experiment will await the results of W7-X high power steady-state operation. Another factor influencing such a decision is the expected improvement of the capability to make theoretical predictions and extrapolations.

V. SUMMARY AND CONCLUSIONS

The scientific programme of W7-X is determined by the completion of the plasma facing components. Starting with a limiter configuration, plasma commissioning in 2015 is aiming at the integral commissioning of the device including plasma heating with ECRH and the first set of plasma diagnostics. The second step is a divertor configuration without water cooling. In this phase plasma pulses are limited to 10 s at 8 MW of heating power. The main goal is the preparation of the steady-state phase. Having reached the full steady-state capability in 2019, the main objective of W7-X is to demonstrate the power

plant capability of the stellarator concept. This combines high performance steady-state operation (high $nT\tau_E$) and the development of fully integrated plasma scenarios at high β for the extrapolation to a power plant. Upgrades introducing a tungsten wall and extending the steady-state heating power are envisaged.

In the European Roadmap to the Realization of Fusion Energy [40, 43], the role of W7-X is to provide the input for the decision on a burning-plasma stellarator which, in parallel to the tokamak DEMO, forms the basis for the development of a commercial fusion power plant.

REFERENCES

[1] P. Helander et al., "Stellarator and tokamak plasmas: a comparison", Plasma Phys. Control Fusion 54 (2012) 124009

[2] M. Zarnstorff et al., "Physics of the compact advanced stellarator NCSX", Plasma Phys. Control. Fusion 43 (2001) A237.

[3] M. Hirsch et al.,"Major results from the stellarator Wendelstein 7-AS", Plasma Phys. Control. Fusion 50 (2008) 053001.

[4] T. Morisaki et al.," Superdense core mode in the Large Helical Device with an internal diffusion barrier", Phys. Plasmas 14 (2007) 056113.

[5] C. D. Beidler et al., "Benchmarking of the mono-energetic transport coefficients—results from the International Collaboration on Neoclassical Transport in Stellarators (ICNTS)", Nucl. Fusion 51 (2011) 076001.

[6] W. Wobig, and S. Rehker, Proc. 7th Symp. on Fusion Techn., Grenoble, France, 1972, p. 333.

[7] C.D. Beidler et al., "Physics and engineering design for Wendelstein VII-X" , Fusion Techn. 17 (1990) 148.

[8] Grigull et al., "First island divertor experiments on the W7-AS stellarator", Plasma Phys. Control. Fusion 43 (2001) A175

[9] Y. Feng, "Up-scaling the island divertor along the W7-stellarator line", J. Nucl. Materials 438 (2013) S497.

[10] Y. Feng, M. Kobayashi, T. Lunt and D. Reiter, "Comparison between stellarator and tokamak divertor transport", Plasma Phys. Control. Fusion 53 (2011) 024009

[11] H.-S. Bosch et al., "Technical challenges in the construction of the steady-state stellarator Wendelstein 7-X",Nucl. Fusion 53 (2013) 126001.

[12] T. Rummel et al, "The Trim Coils for the Wendelstein 7-X Magnet System", IEEE Trans. on Applied Supercond. 22 (2012) 4201704

[13] F. Schauer et al., "W7-X Commissioning: Progress and Lessons Learned for Future Devices", Proceedings 26th Symposium on Fusion Engineering (2015) SX4-2.

[14] T. Sunn Pedersen et al., "Plans for first physics operation of W7-X", in preparation

[15] V. Erckmann et al., "Electron cyclotron heating for W7-X: physics and technology", Fusion Sci. Technol. 52 (2007) 291.

[16] Y. Turkin et al., "Neoclassical transport simulations for stellarators", Phys. Plasmas 18 (2011) 022505

[17] J. Geiger, C. D. Beidler, Y. Feng, H. Maaßberg, N. B. Marushchenko and Y. Turkin, "Physics in the magnetic configuration space of W7-X"; Plasma Phys. Control Fusion 57 (2015) 014004

[18] V. Erckmann, "ECRH and W7-X: An intriguing pair", AIP Conference Proceedings 1580, 542 (2014); doi: 10.1063/1.4864608.

[19] J. Ongena et al., "Study and design of the ion cyclotron resonance heating system for the stellarator Wendelstein 7-X", Phys. Plasmas 21 (2014) 061514.

[20] P. Xanthopoulos et al., "Controlling Turbulence in Present and Future Stellarators", Phys. Rev. Lett. 113 (2014) 155001

[21] P. Helander at al., "Advances in stellarator gyrokinetics ", Nucl. Fusion 55 (2015) 053030

[22] F. Wagner, M. Hirsch, H.-J. Hartfuss, H. P. Laqua, and H. Maaßberg, "H-mode and transport barriers in helical systems", Plasma Phys. Control Fusion 48 (2006) A217.

[23] C. Nührenberg, "Global ideal magnetohydrodynamic stability analysis for the configurational space of Wendelstein 7-X", Phys. Plasma 3 (1996) 2401

[24] M. Drevlak, J. Geiger, P. Helander, and Y. Turkin, "Fast particle confinement with optimized coil currents in the W7-X stellarator", Nucl. Fusion 54 (2014) 073002.

[25] Ye.O. Kazakov, D. Van Eester, R. Dumont, and J. Ongena, "On resonant ICRF absorption in three-ion component plasmas: a new promising tool for fast ion generation", Nucl. Fusion 55 (2015) 032001.

[26] H. Maaßberg, C. D. Beidler, and E. E. Simmet, "Density control problems in large stellarators with neoclassical transport", Plasma Phys. Control. Fusion 41 (1999) 1135.

[27] A. Dinklage et al., "Inter-machine validation study of neoclassical transport modelling in medium- to high-density stellarator-heliotron plasmas", Nucl. Fusion 53 (2013) 063022

[28] H. Maaßberg et al., "Transport in stellarators", Plasma Phys. Control Fusion 35 (1993) B319

[29] K. McCormick et al., "New advanced operational regime on the W7-AS stellarator", Phys. Rev. Lett. 89 (2002) 015001

[30] Lumsdaine et al., "Design and analysis of the W7-X divertor scraper element", Fusion Eng. Design 88 (2013) 1773

[31] J. Geiger et al., "Aspects of steady-state operation of the Wendelstein 7-X stellarator", Plasma Phys. Control. Fusion 55 (2013) 014006

[32] R. Neu et al., "Overview on plasma operation with a full tungsten wall in ASDEX Upgrade", Journal of Nuclear Materials 438 (2013) S34

[33] C. D. Beidler et al., "The Helias reactor HSR4/18", Nucl. Fusion 41 (2001) 1759

[34] R. C. Wolf et al., "A stellarator reactor based on the optimization criteria of Wendelstein 7-X", Fusion Eng. Design 83 (2008) 990

[35] F. Schauer et al., "Extrapolation of the W7-X Magnet System to Reactor Size", Contrib. Plasma Phys. 50 (2010) 750

[36] F. Schauer, K. Egorov and V. Bykov "HELIAS 5-B magnet structure and maintenance concept", Fusion Eng. Design 88 (2013) 1619

[37] F. Warmer et al., "HELIAS module development for systems codes", Fusion Eng. Design 91 (2015) 60

[38] F. Schauer, K. Egorov and V. Bykov, "Coil winding pack FE-analysis for a HELIAS reactor", Fusion Eng. Design 86 (2011) 636

[39] F. Schauer, K. Egorov, V. Bykov and A. Dudek, "Building block support structure for HELIAS Stellarator reactors", IEEE/INPSS 24th Symp. Fus. Eng. (SOFE), SP 1-18, 2011

[40] A. Dinklage et al., "The Initial Program of Wendelstein7-X on the Way to a HELIAS Fusion Power Plant", Proc. 25th IAEA Fusion Energy Conference (2014) FIP 3-1

[41] K. Lackner, Fusion Sci. Techn. 54 (2008) 989

[42] *www.euro-fusion.org/eurofusion/the-road-to-fusion-electricity*

Curriculum Vitae

Felix Warmer

Personal Data

Name	Felix Warmer
Date of Birth	March 9, 1988
Place of Birth	Leisnig, Germany
Nationality	German

PhD at the Max Planck Institute for Plasma Physics

Present **Responsibilities**.

- Administrative Officer for the International Stellarator-Heliotron Profile Database
- Member of the Helmholtz Initiative 'Energy 2050'
- Member of the German DEMO Working Group
- Member of the Coordinated Working Group Meeting
- Member of the PROCESS User and Development Group
- Member of the SYCOMORE User Group
- Member of the Helmholtz Graduate School for Plasma Physics

Past **Activities**.

- PhD-Representative at IPP Greifswald

Starting Date of PhD.

- 01.03.2013

Masters Thesis

Title *Reactor Extrapolation of Wendelstein 7-X*

Supervisors Prof. Dr. Dr. h.c. Bernd Rauschenbach & Priv.-Doz. Dr. Andreas Dinklage

Collaboratively carried out at the University Leipzig and the Max Planck Institute for Plasma Physics. Final Result: *With honours*

Bachelor Thesis

Title *The Riemann Mapping Theorem and its Application to Problems in Hydrodynamics*

Supervisors Prof. Dr. Hans-Peter Gittel

Carried out at the University Leipzig. Final Result: *1.3*

Academic Studies

03/2011–02/2013 **Master of Science in Physics**, *The University of Leipzig*, Leipzig, Germany.
09/2010–02/2011 **ERASMUS Student**, *Université Paul Sabatier, Toulouse III*, Toulouse, France.
10/2007–10/2010 **Bachelor of Science in Physics**, *The University of Leipzig*, Leipzig, Germany.
02/2010–02/2012 **Visiting Student**, *The University of Leipzig*, Leipzig, Germany.
Philosophy & Economics

Education

2006 **Abitur**, *Martin Luther Gymnasium Hartha*, Hartha, Germany, German university entrance qualification.
Final Result: *1.0 – With honours* (maximum: 1.0)

Experience

07/2006–03/2007 **Civil Service**, *The University Hospital of Leipzig*, Leipzig, Germany.
Responsible for patient transport

Awards

2015 Promotional Stipend from the Wilhem and Else Heraeus Foundation for the DPG Spring Meeting in Plasma Physics, Bochum, Germany

2014 Full scholarship from the Societa Italiana di Fisica & Europeen Physical Society for the International School on Energy 2014, Varenna, Italy

2010 ERASMUS Stipend

2006–2014 Full e-fellows Stipend

2007 Badge of Honour for outstanding performance in the German Abitur. Received from the Ministry of Cultural Affairs

Miscellaneous

Software Matlab, Python
Peer-reviewing for Fusion Engineering and Design, Transactions on Plasma Science
Memberships Deutsche Physikalische Gesellschaft

Languages

German **Native**
English **Professional** *Cambridge First Certificate in English, Grade A*
French **Intermediate** *ERASMUS studies in France*
Japanese **Basic** *Basic words and phrases only*

Commitments

Humanism, Martial Arts

Acknowledgements

First of all I would like to thank Prof. Robert Wolf, who employed me as a PhD at IPP giving me such a wonderful and interesting research topic and consequently put the trust in me to independently work and succeed with such a complex problem. Further I would like to thank Prof. Dieter Breitschwerdt who supported this thesis – whithout much burocratic hassle – from the TU Berlin. Also Prof. Hartmut Zohm should not go unnamed, who not only accepted to be a reviewer of this thesis, but also motivated me by his extremely friendly nature and clear overview and thoughts.

I am also extremly grateful to PD. Dr. Andreas Dinklage, from whom I could learn so much, not only scientifically but also in many different aspects of soft-skills. His outstanding clarity of thoughts helped to improve my work and myself continously.

A very special thanks goes to my colleague Dr. Craig Beidler, who I would now like to call a good friend. For me, he had – literally – always an open door and I must have asked him thousands of questions over the years and he neraly never failed to provide a reasonable answer. I could also always rely on him to provide a timely feedback on thoughts and manuscripts and his knowledge about stellarators is nearly unmatched.

I also greatly appreciate the fruitful collaboration with Dr. Pavlos Xanthopoulos. His kind and funny attitude made discussions extremely pleasant while remaining at the highest level of physics, structuring and clarity.

Further, I am thankful to Dr. Henning Maaßberg as I realised through him to be critical about scientific presentations and publications as I intially and naively believed science to be free of charlatans – I was soo wrong.

I could write a personalised appreciation to nearly every colleague in IPP, and I hope they are not offended if I express my greatest gratitude to them in the following, simply by alphabetical order:

Dr. Jürgen Baldzuhn, Dr. Sergey Bozhenkov, Dr. Victor Bykov, Dr. Michael Drevlak, Konstantin Egerov, Dr. Michael Endler, Dr. Yühe Feng, Dr. Oliver Ford, Dr. Joachim Geiger, Dr. Matthias Hirsch, Dr. Andrea Kleiber, Dr. Ralf Kleiber, Prof. Thomas Klinger, Dr. Matthias Köppen, Dr. Andreas Kus, Dr. Andreas Langenberg, Dr. Paul McNeely, Mareen Papenhagen, Dr. Ekkehard Pasch, Dr. Josephine Proll, Maria Radau, Dr. Jörg Riemann, Dr. Felix Schauer, Dr. Yuriy Turkin, and everyone else from the coffee round.

I also greatly appreciate constructive discussions and collaborations with my international colleagues, in loose order: Prof. Yokoyama, Prof. Sagara, Dr. Goto, Dr. Suzuki, Dr. Kobayashi, Prof. Ward, Dr. Kemp, Dr. Lux, Dr. Knight, Dr. Morris, Dr. Kovari.

I also want to give a special thanks to my fellow PhDs with whom I shared a office: Alexander Rodatos and Dorothea Gradic. We had many interesting discussions about

science and life in general and sometimes it was inevitable to share some sweets in order to keep the moral up. I very much enjoyed the office atmoshphere over the last years.

But there have also been other fellow PhDs who were always open for a nice discussion, a big thanks to: Holger Niemann, Hauke Hölbe, Rene Reimer, Peter Drewelow and Erik Müller.

Furthermore, I would like to thank my student Steven Torrisi. It was a very interesting and fruitful experience to be a supervisor.

It cannot be stretched enough, how important it is for the success of such a thesis to have such ingenious colleagues. Such an atmoshphere is greatly motivating to improve oneself striving to become an acknowledged scholar and colleague within the community.

I would also like to thank my friends who often provided a valve for frustration when things weren't going as smoothly as planned and consequently contributed to my mental health and moreover were good for a distraction – most noteably Johannes and Manuel. In particular I deeply thank Laura as her continous motivation significantly improved me to overcome my laziness.

Last, but no least, I would like to thank my family for their ongoing and unconditional support.

It remains to conclude this work with a quote by Albert Einstein:

'Eine Verbesserung der Bedingungen auf der Welt ist im wesentlichen nicht von wissenschaftlicher Kenntnis, sondern vielmehr von der Erfüllung humaner Traditionen und Ideale abhängig.'

Greifswald, February 10$^{\text{th}}$, 2016

150